Enhanced Air-Interfaces for Fifth Generation Mobile Broadband Communication

Yahya Jasim Harbi

Doctor of Philosophy

University of York

Department of Electronic Engineering

September 2017

Abstract

In broadband wireless multicarrier communication systems, intersymbol interference (ISI) and intercarrier interference (ICI) should be reduced. In orthogonal frequency division multiplexing (OFDM), the cyclic prefix (CP) guarantees to reduce the ISI interference. However, the CP reduces spectral and power efficiency. In this thesis, iterative interference cancellation (IIC) with iterative decoding is used to reduce ISI and ICI from the received signal in multicarrier modulation (MCM) systems. Alternative schemes as well as OFDM with insufficient CP are considered; filter bank multicarrier (FBMC/Offset QAM) and discrete wavelet transform based multicarrier modulation (DWT-MCM). IIC is applied in these different schemes. The required components are calculated from either the hard decision of the demapper output or the estimated decoded signal. These components are used to improve the received signal. Channel estimation and data detection are very important parts of the receiver design of the wireless communication systems. Iterative channel estimation using Wiener filter channel estimation with known pilots and IIC is used to estimate and improve data detection. Scattered and interference approximation method (IAM) preamble pilot are using to calculate the estimated values of the channel coefficients. The estimated soft decoded symbols with pilot are used to reduce the ICI and ISI and improve the channel estimation. The combination of Multi-Input Multi-Output MIMO and OFDM enhances the air-interface for the wireless communication system. In a MIMO-MCM scheme, IIC and MIMO-IIC-based successive interference cancellation (SIC) are proposed to reduce the ICI/ISI and cross interference to a given antenna from the signal transmitted from the target and the other antenna respectively. The number of iterations required can be calculated by analysing the convergence of the IIC with the help of EXtrinsic Information Transfer (EXIT) charts. A new EXIT approach is proposed to provide a means to define performance for a given outage probability on quasi-static channels.

Contents

List of Tables

List of Figures

Acknowledgements

I would like to show my sincere gratitude to my supervisor, Prof. Alister G. Burr, for his support and encouragement during my PhD study. I would not be able to achieve this progress, finish this thesis and complete my PhD study without his help and advise. I have learned a lot of valuable information about proper research techniques and academic writing under his supervision.

I am very grateful to my thesis advisor, Dr. Yuriy Zakharov, whose insightful discussions and suggestions have benefited me.

My deep thanks to my sponsor (Ministry of Higher Education and Scientific Research/IRAQ - University of Kufa) for offering me this great opportunity. I also would like to thank Iraqi Cultural Attache/London for the appreciated support and help throughout my PhD study.

I would also like to thank Dr. Mohammed Kashoob and other colleagues in the Communications and Signal Processing Research Group for their comments, ideas and support throughout my study.

I would like to dedicate this thesis to the memory of my late parents. Also, I would like to dedicate it to my wife, brother, sisters, friends, and my sons. I would not be able to complete this work without your support.

Declaration

I declare that this thesis is a presentation of original work and I am the sole author. This work has not previously been presented for an award at this, or any other, University. References and acknowledgements to other researchers have been given as appropriate.

Elements of the research presented in this thesis have resulted in some publications. A list of these publications can be found below.

Conference Papers

1. Yahya J. Harbi and Alister G. Burr, "IIC of the MIMO-FBMC/OQAM system using linear and SIC detection schemes in LTE channel", *IEEE Wireless and Networking Conference (WCNC 2018) Track 1:PHY and Fundamentals*, Barcelona, Spain, 2018. (Accepted)

2. Yahya J. Harbi and Alister G. Burr, "Wiener filter channel estimation for OFDM/OQAM with iterative interference cancellation in LTE channel", *19th International Conference on OFDM and Frequency Domain Technique (ICOF 2016)*, pp. 17-22, Essen, Germany, August 2016.

3. Marwa Chafii, Yahya J. Harbi and Alister G. Burr, "Wavelet-OFDM vs. OFDM: Performance Comparison", *23rd International Conference on Telecomminications (ICT 2016)*, Thessaloniki, Greece, May 2016.

4. Yahya J. Harbi and Alister G. Burr, "On ISI and ICI cancellation for FBMC/OQAM system using iterative decoding and ML detection", *IEEE Wireless and Networking Conference (WCNC 2016) Track 1:PHY and Fundamentals*, pp. 1434-1439, Doha, Qatar, April 2016.

5. Yahya J. Harbi and Alister G. Burr, "Comparison of Discrete Wavelet and FFT-OFDM under Different Channel Conditions", *The 15th Annual PostGraduate Symposium on the Convergence of Telecommunications, Networking and Broadcasting*, Liverpool, UK, 2014.

Technical Meeting Papers

1. Yahya J. Harbi and Alister G. Burr, "MIMO-FBMC/OQAM using IIC and MIMO-IIC in LTE channel", *COST IRACON* 3^{rd} *meeting*, Lisbon, Portugal, February 2017.
2. Yahya J. Harbi and Alister G. Burr, "Iterative interference cancellation for FBMC and reduced-CP OFDM", *COST IRACON* 2^{nd} *meeting*, Durham, UK, October 2016.

Chapter 1

Introduction

Contents

1.1 Overview and Motivation

Two important criteria can determine the future success of broadband wireless communications. The first is accelerating the data rate, and the second is the quality of service (QoS) available to the mobile user. This means that in the mobile communication systems, the perfect receiver should be designed to reduce the interference to achieve high spectral efficiency within the limitation of the available frequency spectrum.

The OFDM scheme has been the most popular multicarrier modulation (MCM) among the candidates for different standards to achieve high data rate transmission [1,2]. Among these standards are: digital audio broadcasting (DAB) [3], terrestrial digital video broadcasting (DVB-T) [4], wireless local area network (WLANs) IEEE 802.11a/g [5,6], World-

wide Interoperability for Microwave Access IEEE 802.16 [7–9], and Long-Term Evolution (LTE) [10, 11]. There are several advantages of OFDM schemes in broadband multicarrier communication systems [2]. One of the most important advantages is the immunity to frequency selective multipath channel [12, 13]. Due to the use of cyclic prefix (CP) and the low data rate on each of the sub-channels, OFDM is very resilient to inter-symbol interference (ISI). It efficiently employs the available spectrum by using closely-spaced overlapping sub-carriers. It requires only a simple equalisation due to the use of the multiple sub-channels. However, there are some drawbacks of the OFDM scheme. It gives rise to a high peak-to-average power ratio (PAPR) in the transmitted signal, which requires highly linear RF power amplifiers [14]. It requires a CP, which reduces spectral and power efficiency [15]. It results in relatively large out-of-band signals which again reduce spectral efficiency, especially when being used in narrowband spectral allocations. It is sensitive to Doppler shifts on time-variant channels [16, 17].

Recently, orthogonal frequency divission multiple access (OFDMA) has been proposed especially for LTE systems [18]. In OFDMA, a subset of subcarriers are allocated to each user. In LTE, to reduce ICI, the signals must be synchronized at the receiver to each user. In the network downlink, all the subcarriers are transmitted from the same point (from the base station). That means that it is easy to synchronize the signals before reaching each user. Thus OFDMA is suitable for network downlink. In the network uplink, the signals are transmitted separately from different nodes. This means that the OFDMA receiver needs additional signal processing steps with significant complexity to achieve synchronization in the received signal [19]. Hence OFDMA may not be suitable for the network uplink [20].

As we consider a new generation, it a good time to think about alternative air-interfaces. To achieve waveforms with better spectral containment per subcarrier in multiuser and massive MIMO networks, fifth generation (5G) wireless systems face significant challenges due to the limitations of OFDM in the multiuser network of future. Some research projects like 5GNOW (http://5gnow.eu/) and PHYDYAS (http://www.ict-phydyas.org/) have used filtering to improve the waveform spectral containment.

For these reasons, the research will consider some alternative proposals which may address certain defects, with a view to contributing to next generation air-interface tech-

nology. Potential approaches that will be considered for this purpose include:

- Schemes based on wavelet transforms, and variants thereof (Discrete Wavelet Transform based multicarrier modulation (DWT-MCM));
- Filter-bank multicarrier based Offset QAM (FBMC/OQAM);
- Iterative interference cancellation (IIC)/equalisation and decoding.

1.2 Aims

In the last two decades, FBMC and DWT have attracted a lot of attention and have been proposed as MCM candidates for broadband multicarrier communication systems. Many researchers have introduced different proposals to improve the performance and reduce the receiver complexity of these systems. In this thesis, design an iterative receiver is considered for these systems as well as OFDM with insufficient CP to achieve better performance and enhance the air-interface for both single-input single-output (SISO) and MIMO schemes. In addition, we are motivated to propose a bit interleaved coded modulation (BICM) based IIC scheme for quasi-static fading channel.

The aim of this work is to enhance the air-interface of broadband multicarrier communication systems. More specific objectives can then be summarised as follows:

- Using IIC to reduce the ICI/ISI interference due to the doubly-selective channel of the SISO-DWT and SISO-FBMC/OQAM systems as well SISO-OFDM with insufficient CP.
- Using IIC and MIMO-IIC to reduce the interference for MIMO scheme of the FBMC/OQAM and OFDM systems.
- To calculate the required number of IIC and decoder iterations by analysing the convergence of the IIC with the help of EXIT charts over the quasi-static fading channel.
- To improve the channel estimation of the OFDM and FBMC/OQAM systems by using an iterative IIC-based channel estimation scheme.

- To reduce the equalisation complexity for the FBMC/OQAM system by using IIC and MIMO-IIC for SISO and MIMO schemes respectively.

1.3 Contributions

The contributions of this research can be summarised as follows:

- New receivers with IIC are proposed for SISO-OFDM systems with insufficient CP, SISO-DWT based MCM, and SISO-FBMC/OQAM systems. In these receivers, the estimated decoded signal is used to improve the system performance by reducing the ICI/ISI interference. In the DWT-MCM scheme, a frequency domain equaliser is used. Low complexity equalisers are used in all these systems as in the OFDM system. The simulation results show that the error floor is significantly improved resulting in increase in the spectral efficiency. A good $Eb/N0$ gain is achieved after some IIC iterations.

- A new convergence analysis approach of the IIC scheme is proposed for the LDPC-OFDM, LDPC-DWT/MCM, and LDPC-FBMC/OQAM systems. In this scheme, the convergence of the IIC is analysed with the help of an EXIT chart. *A posteriori* information of the output of the decoder is used to analyse the convergence. Then, the required number of IIC and decoder iterations for complete interference removal is calculated. This proposal provides a means to define performance for a given outage probability on quasi-static fading channels.

- Improve the channel estimation by using iterative IIC-based channel estimation for SISO OFDM and FBMC/OQAM systems. At each IIC iteration, the ICI/ISI interference are reduced from the received signal. This means that the Least-Square (LS) vector of the channel estimation at the pilot position is updated.

- IIC and MIMO-IIC with iterative decoding are proposed for MIMO-OFDM with insufficient CP and MIMO-FBMC/OQAM systems. Successive interference cancel-

lation (SIC)-based IIC is proposed to eliminate the cross interference in the MIMO-OFDM and MIMO-FBMC/OQAM systems. In this scheme, the same equaliser is used for both systems. The error floor is significantly reduced and the performance of these systems is improved.

1.4 Thesis Outline

The structure of the thesis is as follows:

- Chapter 2: **Background**

  This chapter is devoted the introduction of the general concept of multicarrier modulation including OFDM, DWT-MCM, and FBMC/OQAM systems. The OFDM system and its implementation are described. The fundamental theory of DWT, the implementation of the typical block diagram of a DWT-MCM, decomposition and reconstruction algorithms are described. The general implementation and fundamental theory of FDMB/OQAM is given. Furthermore, the polyphase and prototype filter implementation of the filter bank are reviewed. The downlink LTE frame structure, channel profiles, and simulation parameters are described. The Clark's and Jakes' channel modelling are discussed. The SPA of the LDPC decoder is briefly described. Finally, the PAPR of DWT-MCM is described and compared with the OFDM and FBMC/OQAM systems.

- Chapter 3: **Iterative Interference Cancellation based MCM (IIC-MCM)**

  In this chapter, iterative interference cancellation receivers are proposed for OFDM, DWT-MCM, and FBNC/OQAM systems using the LDPC decoder under the effect of the LTE doubly selective channel. The IIC scheme is applied to uncoded and coded MCM systems. The bit error probability is compared with that of the conventional OFDM system with insufficient cyclic prefix (CP) under different environments.

- Chapter 4: **Wiener Filter Channel Estimation based IIC-MCM**

  In this chapter, Wiener filter based tentative channel estimation with IIC is proposed for OFDM and FBMC/OQAM systems. This means that at each IIC iteration, the Least-Square (LS) vector of the channel estimation at the pilot position is updated. The basics of one and two dimensional channel estimation using the Wiener filter are described. LTE scattered pilot-based Wiener filter channel estimation is used with OFDM and FBMC/OQAM systems. Different patterns of IAM preamble and scattered pilots are used with FBMC/OQAM. Interference Approximation Method (IAM) preambles are discussed in different scenarios. Pilot-symbol aided estimation is considered. Numerical results show that a significant BER improvement is achieved for both systems by using the IIC based tentative Wiener filter channel estimation.

- Chapter 5: **MIMO Systems based IIC-MIMO**

  In this chapter, IIC and IIC-MIMO are proposed for MIMO-OFDM and MIMO-FBMC/OQAM systems. The estimated decoded signals at the current and second streams with IIC and MIMO-IIC to reduce the ICI and ISI to a given antenna from the signal transmitted from the corresponding and other antennas respectively. An SIC-based IIC scheme is proposed to eliminate the cross interference for both MIMO OFDM and FBMC/OQAM systems. Different modulation orders, Doppler frequencies with different channel parameters are used in the numerical analysis for both systems.

- Chapter 6: **Convergence Analysis**

  In this chapter, BICM based IIC is proposed for MCM systems over the quasi-static fading channel. For both SISO and MIMO systems the required number of IIC iterations to eliminate ISI and ICI and remove them from the received signal is calculated by analysing the convergence of the IIC with the help of EXtrinsic Information Transfer (EXIT) charts. Different modulation orders, mappings, Doppler frequencies are used over different LTE channels.

- Chapter 7: **Conclusions and Future Work**

  In this chapter, the conclusions of this thesis are presented, and directions in which further research could be carried out are suggested.

1.5 Publication List

Conference Papers

1. Yahya J. Harbi and Alister G. Burr, "IIC of the MIMO-FBMC/OQAM system using linear and SIC detection schemes in LTE channel", *IEEE Wireless and Networking Conference (WCNC 2018) Track 1:PHY and Fundamentals*, Barcelona, Spain, 2018. (Accepted)

2. Yahya J. Harbi and Alister G. Burr, "Wiener filter channel estimation for OFDM/OQAM with iterative interference cancellation in LTE channel", *19th International Conference on OFDM and Frequency Domain Technique (ICOF 2016)*, pp. 17-22, Essen, Germany, August 2016.

3. Marwa Chafii, Yahya J. Harbi and Alister G. Burr, "Wavelet-OFDM vs. OFDM: Performance Comparison", *23rd International Conference on Telecomminications (ICT 2016)*, Thessaloniki, Greece, May 2016.

4. Yahya J. Harbi and Alister G. Burr, "On ISI and ICI cancellation for FBMC/OQAM system using iterative decoding and ML detection", *IEEE Wireless and Networking Conference (WCNC 2016) Track 1:PHY and Fundamentals*, pp. 1434-1439, Doha, Qatar, April 2016.

5. Yahya J. Harbi and Alister G. Burr, "Comparison of Discrete Wavelet and FFT-OFDM under Different Channel Conditions", *The 15th Annual PostGraduate Symposium on the Convergence of Telecommunications, Networking and Broadcasting*, Liverpool, UK, 2014.

Technical Meeting Papers

1. Yahya J. Harbi and Alister G. Burr, "MIMO-FBMC/OQAM using IIC and MIMO-IIC in LTE channel", *COST IRACON* 3^{rd} *meeting*, Lisbon, Portugal, February 2017.

2. Yahya J. Harbi and Alister G. Burr, "Iterative interference cancellation for FBMC and reduced-CP OFDM", *COST IRACON* 2^{nd} *meeting*, Durham, UK, October 2016.

Chapter 2

Background

Contents

2.1 Introduction

Multicarrier transmission technologies provide many advantages in broadband communication systems. Multicarrier modulation (MCM) was first used in North America in military communications in the 1950s [21].

This chapter is about MCM as broadly understood. MCM means that the data is modulated onto a set of orthogonal carriers or bearers. They can take a variety of forms: for example rectangularly pulse-shaped sine-wave for orthogonal frequency division multiplexing (OFDM), filtered sine-wave for filter bank multicarrier/offset QAM (FBMC/OQAM), and wavelet for the discrete wavelet transform based MCM (DWT-MCM).

The rest of this chapter can be organised as follows: An introduction to fundamental techniques of three different types of MCM system will be provided respectively in Sections 2.2, 2.3, and 2.4; orthogonal frequency division multiplexing (OFDM), discrete wavelet transform based multi-carrier modulation (DWT-MCM), filter bank multi-carrier based offset QAM (FBMC/OQAM). The main difference between these three types is that OFDM and FBMC/OQAM are based on a sinusoidal function whereas DWT-MCM is based on wavelets, which are the solution to a set of recursive difference equations. In Section 2.5 the downlink LTE propagation standard is used as an example of the application of these techniques and it gives a framework for comparing potential alternatives for OFDM. Clarkes and Jakes' channel model, using the power delay profile (PDP) of the LTE standard are presented in Section 2.6. LDPC codes and the sum-product decoding algorithm are presented in Section 2.7. In Section 2.8, PAPR is discussed. Finally, a summary of this chapter is given in Section 2.9.

2.2 Orthogonal Frequency Division Multiplexing (OFDM)

Nowadays, orthogonal frequency division multiplexing (OFDM) systems are employed in many different transmission standards: *WiFi*, *WiMAX*, *DVB-T*, *LTE*, and *ADSL* [4–7, 9–11]. OFDM systems are the most popular MCM. OFDM systems are robust in the presence of multipath frequency selective fading, have low complexity and achieve high data rate [2, 22]. OFDM multicarrier systems have taken on an important role in digital communication systems in order to achieve a high transmission data rate, due to its ability to solve many of the problems of wideband digital communication systems and eliminate the interference between symbols and adjacent subcarriers which occurs due to the multipath and frequency selective fading. These advantages make OFDM systems

very attractive for deployment in wireless communication systems. On the other hand, OFDM systems have high peak to average power ratio (PAPR) compared with single carrier transmission [22, 23].

The use of the discrete Fourier Transform (DFT) for modulation and demodulation was introduced in [24]. In the last two decades, DFT has been used in the implementation of OFDM systems in many commercial applications [25, 26].

Figure 2.1 illustrates a block diagram of the conventional OFDM system. The important parts of this diagram are the IFFT and FFT blocks at the transmitter and receiver respectively, which are responsible for converting the information to the discrete time domain at the transmitter and to the frequency domain at the receiver. First, a random stream of data is generated as the input symbols, with length equal to the number of bits per frame. This is processed according to the modulation techniques according to the desired constellation mapping. Next, pilots are inserted at specific locations in each OFDM symbol, which are used on the receiver side to estimate and equalise the channel. Parallel data streams are obtained by converting the modulated data plus pilots into parallel form according to the FFT size. The length of the parallel streams will then become equal to the size of the FFT (which is equal to the number of subcarriers and pilot subcarriers). After that, IFFT is used to convert the data into the time domain. Finally, to increase the symbol duration, before transmitting the OFDM signal, a specific period from the end of each symbol duration is copied and inserted at the beginning of the period as a guard interval (known as the cyclic prefix CP) which serves to avoid inter symbol interference (ISI). However, the length of the channel impulse response requires increased symbol length resulting from including this guard interval, which must be longer than the channel impulse response [27].

At the receiver, the guard interval is removed after converting the received signal into parallel streams in order to obtain data in the time domain, with the length of each symbol equal to the FFT size. Then, the FFT is applied to obtain the parallel data streams in the frequency domain. After that, the estimated values of the channel coefficients are calculated to equalise the received signal. Finally, the estimated received signal is demodulated to obtain the data, from which we calculate the bit error probability.

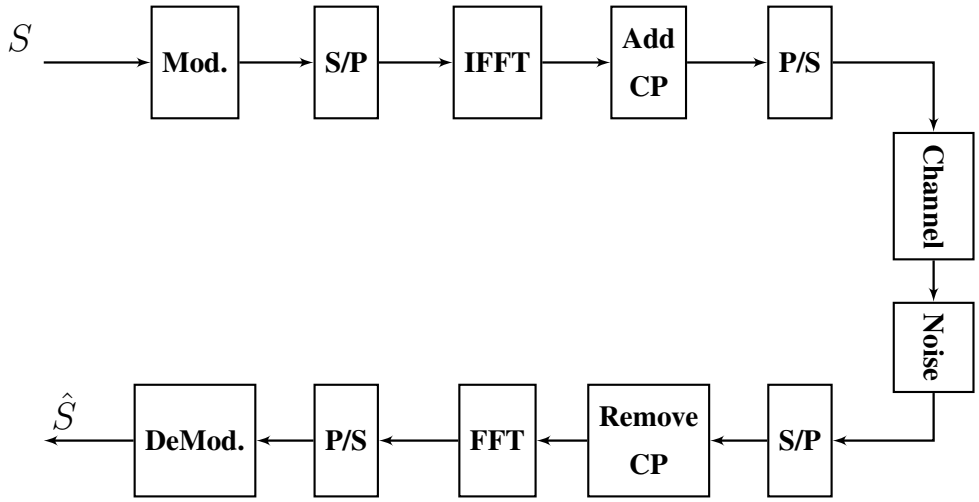

Figure 2.1: Typical block diagram of FFT-OFDM transceiver.

One of the main drawbacks of OFDM is the use of rectangular pulse shaping, which leads to large side lobes at each subcarrier. Moreover, OFDM uses the CP which reduces the maximum spectral efficiency. With insufficient CP, when the multipath delay exceeds the length of CP, the BER performance of OFDM systems is degraded due to the inter-symbol interference (ISI) and inter-carrier interference (ICI).

2.3 Discrete Wavelet Transform based MCM (DWT-MCM)

A wavelet is a mathematical function of time or space. However, unlike the Fourier transform which is structured from infinite compact support basis functions in the time domain, a wavelet has an finite compact support basis functions in the time domain. Wavelets provide different variants of the time and frequency localization properties according to its scales as will be explained in Section 2.3.2. The different mathematical properties and the flexibility to split the time-frequency plane make the wavelet basis function as a candidate for the MCM systems. The plot of typical wavelets is shown in Figure 2.4 in Section 2.3.1 for different wavelet families.

Recently, many studies have suggested DWT-MCM system as an alternative to conventional OFDM systems [28–31]. As well as the mitigating the problem of PAPR [32],

DWT-MCM holds various advantages over OFDM. It gives better time-frequency localization due to its scale nature and finite duration [33]. It also proves to be more robust to the time variability of the radio channel [34]. Better channel exploitation under different interference environments has been utilized by applying multirate wavelet based modulation techniques in both time and frequency [35]. Multirate filterbanks and wavelet transforms in channel coding and modulation have been developed and examined using different techniques such as spread-signature CDMA and spread-response precoding, fractal modulation, and lapped multitone modulation [36]. The inherent flexibility of the wavelet transform with some interesting additional advantages has made it a strong candidate for multicarrier schemes [37]. Wavelet packets as a multicarrier multiple access scheme have been extended to multiuser and cognitive radio applications [38]. The inherent orthogonality of multiwavelets has made them suitable for single and multicarrier modulation techniques in a multi user CR network and it can reduce Multiple Access Interference (MAI) [39]. Discrete wavelet multitone (DWMT) modulation is presented in 1995 [40]. This type is designed to achieve efficient bandwidth use and high spectral efficiency by the application of multi-level wavelet filters. In other words, in multicarrier modulation systems, these multi-level filters depend on the number of subcarriers where the number of levels equals $log_2(N)$, and *N* represents the number of subcarriers. Moreover, the strong point of the DWMT is its robustness to noise environments and to narrowband channel disturbance. However, high equaliser complexity is needed in the case of multipath frequency selective fading. In addition, inserting pilot symbols over data subcarriers for the normal DWMT system has not improved the system performance because it needs high equaliser complexity where each subcarrier requires more than 20 taps for equalisation [41].

The typical block diagram of the DWT-MCM scheme is the same diagram as that of the conventional OFDM system as shown in Figure 2.2. Instead of IFFT and FFT blocks in the conventional OFDM system, reconstruction algorithm or Inverse Discrete Wavelet Transform (IDWT) and decomposition algorithm or Discrete Wavelet Transform (DWT) blocks are substituted at the transmitter and the receiver respectively in the DWT-MCM scheme. IDWT and DWT will be explained in Section 2.3.2.

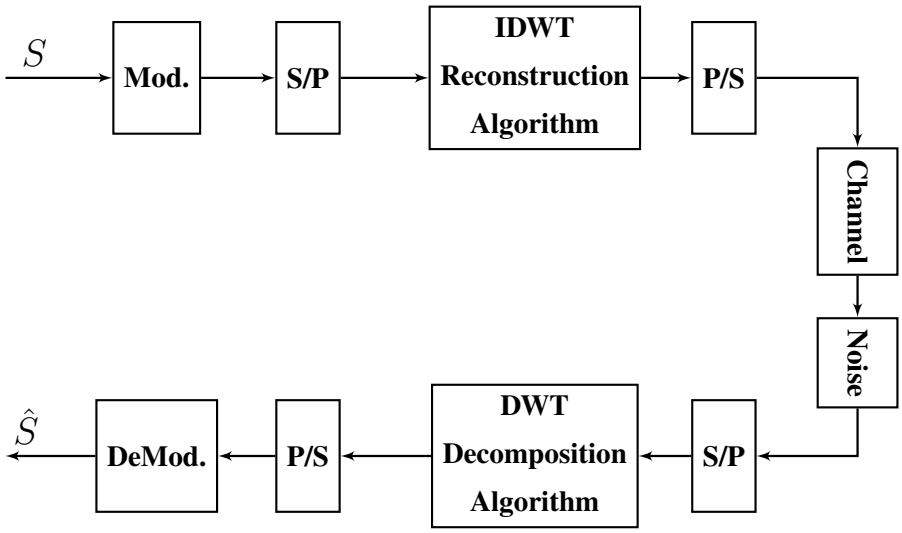

Figure 2.2: Typical block diagram of DWT-MCM transceiver.

2.3.1 Discrete Wavelet

Before delving into a discussion of data reconstruction and decomposition, it is important to present the discrete wavelet. The reason is that the discrete wavelet has a direct impact on data reconstruction and decomposition properties. The main purpose of the wavelet transform is to express signals as linear combinations of the wavelet functions at various scales and of scaling functions (which generate the wavelet function). In other words, the signal has been translated from time domain to time-frequency or time scale domain which accurately locates frequency construction with time in order to analyse signal structures of very different sizes. Moreover, from a functional point of view, the DWT is very similar to the DFT [42], in that both of them are orthogonal transforms, a signal which passes twice through the transformation, passes through transform and inverse transform, remains unchanged, and both are convolutions. In contrast, the DFT is based on a sinusoidal function while the DWT is based on wavelets, which are the solution to a set of recursive difference equations.

Let ψ and ϕ be the wavelet (mother wavelet) function and scaling function respectively. ψ is a zero average function and ϕ is an aggregation of wavelets at scales larger than one [43]. The regularity conditions state that the wavelet function should have some smoothness and concentration in both time and frequency domains [43, 44], such that:

$$\int_{-\infty}^{+\infty} \psi(t)\,\mathrm{d}t = 0 \tag{2.1}$$

$$\int_{-\infty}^{+\infty} |\psi(t)|^2\,\mathrm{d}t = \int_{-\infty}^{+\infty} |\phi(t)|^2\,\mathrm{d}t = 1 \tag{2.2}$$

The scale index (j) and time location (k) represent the important parameters for the system orthogonality which are obtained from the function $\psi(t)$ or from the scaling function $\phi(t)$.

According to Mallat [43], the contracted (recursive) versions $\psi_j(t)$ and $\phi_j(t)$ of the $\psi(t)$ and $\phi(t)$ of the DWT at dyadic scales 2^j can be defined as:

$$\psi_j(t) = 2^{-j/2}\psi(2^{-j}t) \tag{2.3}$$

$$\phi_j(t) = 2^{-j/2}\phi(2^{-j}t) \tag{2.4}$$

where $j \geq J_0$ and J_0 represents the first scale selected.

The translated forms $\psi_{j,k}$ and $\phi_{j,k}$ of the functions ψ_j and ϕ_j can be defined along the interval $[0, 2^j]$ as:

$$\begin{aligned}\psi_{j,k}(t) &= \psi(t - 2^j k) \\ &= 2^{-j/2}\psi(2^{-j}t - k)\end{aligned} \tag{2.5}$$

$$\begin{aligned}\phi_{j,k}(t) &= \phi(t - 2^j k) \\ &= 2^{-j/2}\phi(2^{-j}t - k)\end{aligned} \tag{2.6}$$

That is, $\psi_{j,k}$ and $\phi_{j,k}$ are dilated and sampled along the dyadic scale sequence 2^j and translated by k [43].

In case of IDWT, the scale parameters 2^j represent the inverse of the resolution of 2^{-j} [43]. Then, the translated forms $\psi_{j,k}$ and $\phi_{j,k}$ can be written as:

$$\psi_{j,k}(t) = 2^{j/2}\psi(2^j t - k) \tag{2.7}$$

$$\phi_{j,k}(t) = 2^{j/2}\phi(2^j t - k) \tag{2.8}$$

where the scaling index $j \in [\![J_0, J-1]\!]$ and the time location $k \in [\![0, 2^j - 1]\!]$, J represent the last scale or maximum number of decomposition levels $J = \log_2 \mathbf{N}$, and $\mathbf{N}$ represents the number of subcarriers. The case $j = J_0$ corresponds to better time localization and poorest frequency localization, whereas $j = J-1$ corresponds to poorest time localization and the best frequency resolution [43].

Then, the wavelet basis for the IDWT and DWT can be defined in (2.9) and (2.10) respectively as:

$$\{\phi_{J_0,k}\}_{k=0}^{k=2^{J_0}-1} \quad \bigcup_{j=J_0}^{J-1} \quad \{\psi_{j,k}\}_{k=0}^{k=2^j-1}, \tag{2.9}$$

$$\{\psi_{j,k}\}_{k=0}^{k=2^j-1} \quad \bigcup_{j=J-1}^{J_0} \quad \{\phi_{J_0,k}\}_{k=0}^{k=2^{J_0}-1}. \tag{2.10}$$

According to (2.7) and (2.8), the transmitted signal can be expressed as:

$$x(t) = \sum_{j=J_0}^{J-1} \sum_{k=0}^{2^j-1} w_{j,k}\psi_{j,k}(t) + \sum_{k=0}^{2^{J_0}-1} a_{J_0,k}\phi_{J_0,k}(t) \tag{2.11}$$

- $w_{j,k}$: wavelet or detail coefficients located at k-th position from scale j,
- $a_{J_0,k}$: approximation coefficients located at k-th position from the first scale J_0,
- $\psi_{j,k}$ and $\phi_{J_0,k}$ are the wavelet and the scaling functions defined in (2.6) and (2.8) respectively.

Let $h(k) = c_k$ and $g(k) = (-1)^k c_{1-k}$ be low pass filter (LPF) and high pass filter (HPF) respectively, then the scaling and wavelet coefficients at scale j are related at scale $(j+1)$ by the following relations:

$$a_j(k) = \sum_m h(m-2k)a_{j+1}(m) \tag{2.12}$$

$$w_j(k) = \sum_m g(m-2k)w_{j+1}(m) \tag{2.13}$$

There are specific parameters of the LPF and HPF filters of each wavelet family as shown in Figure 2.3. According to these filter coefficients and the contracted difference equa-

tions, the signal after each level of the reconstruction or decomposition algorithms can be calculated as in Section 2.3.2.

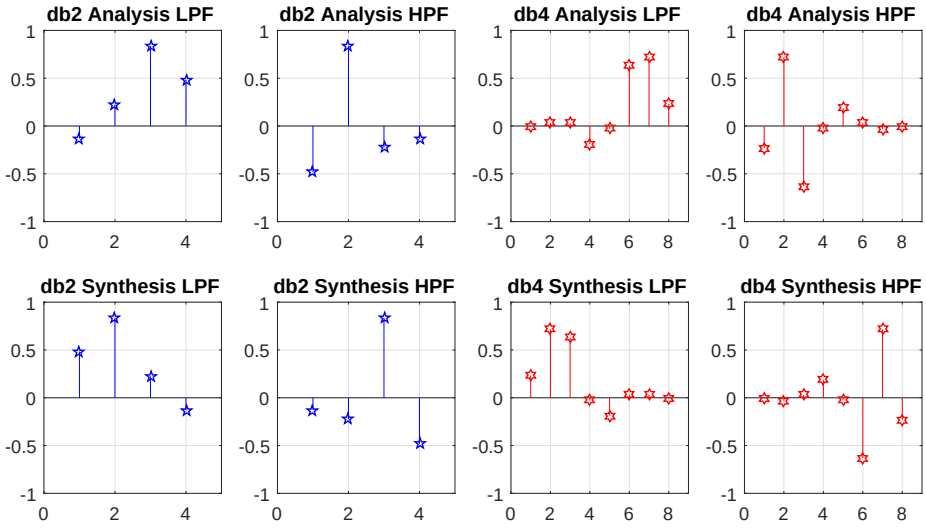

Figure 2.3: The decomposition (analysis) and reconstruction (synthesis) filters' impulse responses of the Daubechies (db2 and db4).

Figure 2.4, illustrates Scaling and Wavelet functions and expansion mode for different types of wavelet transform i.e, Haar, Daubechies (db2, db4, and db8), and DMeyer (dmey).

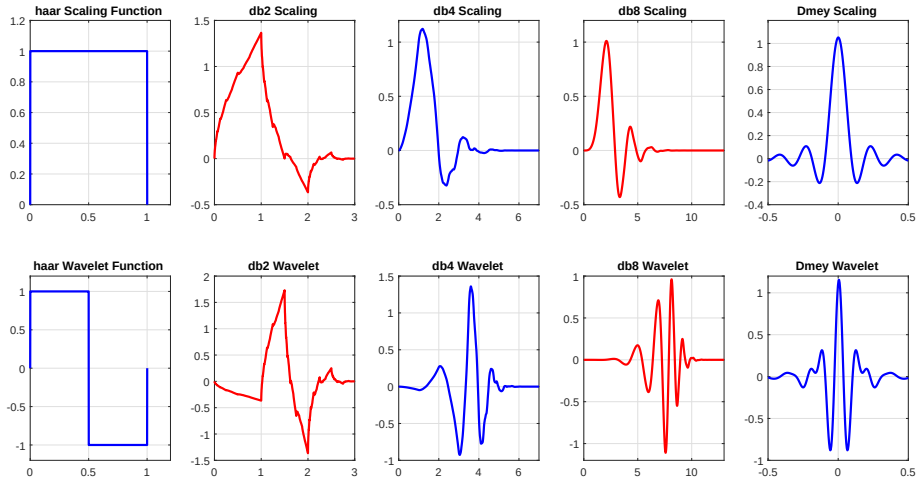

Figure 2.4: Scaling and Wavelet Functions for different types of wavelet transform.

2.3.2 Reconstruction and Decomposition Algorithms

The basic configurations for the implementation of the reconstruction (IDWT) and decomposition (DWT) algorithms of DWT-MCM are shown in Figures 2.5 and 2.6. It is clear from these figures that in the reconstruction algorithm, the approximation coefficients (scaling coefficients (a)) and the details coefficients (wavelet coefficients (w)) are upsampled by a factor of two and filtered by the LPF and HPF respectively. In contrast, in the decomposition algorithm, they are filtered by the LPF and HPF respectively and then downsampled by a factor of two.

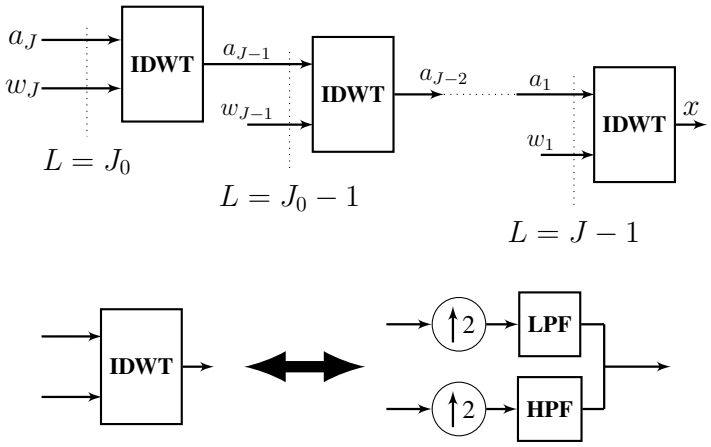

Figure 2.5: Wavelet modulation (IDWT reconstruction algorithm) implementation using filter banks.

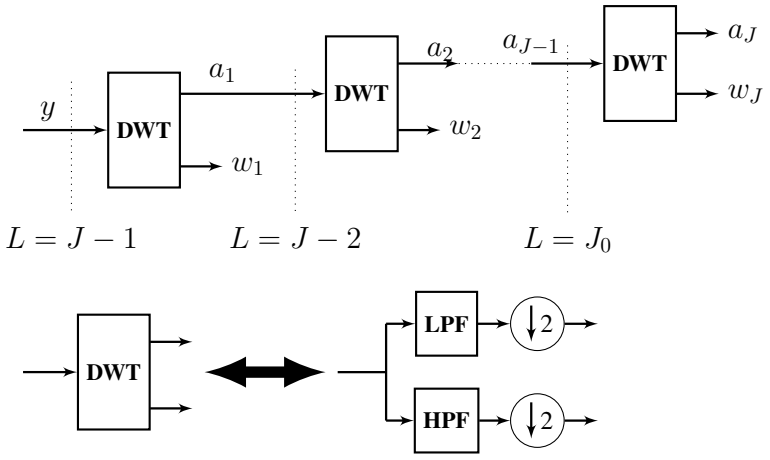

Figure 2.6: Wavelet demodulation (DWT decomposition algorithm) implementation using filter banks.

The number of reconstruction or decomposition levels L of the IDWT or DWT respectively depends mainly on the first scale selected J_0. According to the Mallat algorithm [43], $L = J - J_0$. This means that the IDWT and DWT shall be performed $J - J_0$ times in each process. For example, let C_k, X_k, and Y_k be a vector of complex symbols $C_{k,n}$, $X_{k,n}$, and $Y_{k,n}$ of the modulated, transmitted, and received signal respectively. If the number of subcarriers of each symbol equals 8, then the last scale $J = 3$ and the maximum number of decomposition levels $L = 3 - J_0$. The first scale selected J_0 varies from 0 to 2 ($[0, J-1]$) and the scaling index $j \in [\![J_0, J-1]\!]$. Then, all cases of the first scale selected can be discussed as:

- First scale selected $J_0 = 0$:
  In this case, $L = J - J_0 = 3$, which means the IDWT or DWT is performed 3 times in each process. The scale index $j = 0, 1, 2$.
  In the IDWT process, the modulated signal vector C_n can be expressed as:
  $C_n = [C_1\ C_2\ C_3\ C_4\ C_5\ C_6\ C_7\ C_8]$

  $C_{j,k}$ can be written in terms of the approximation and details components as:
  $C_{j,k} = [a_{0,0}\ w_{0,0}\ w_{1,0}\ w_{1,1}\ w_{2,0}\ w_{2,1}\ w_{2,2}\ w_{2,3}]$.

  Figure 2.7 depicts the IDWT process by using the approximation and details coefficients to generate the transmitted signal X_n.

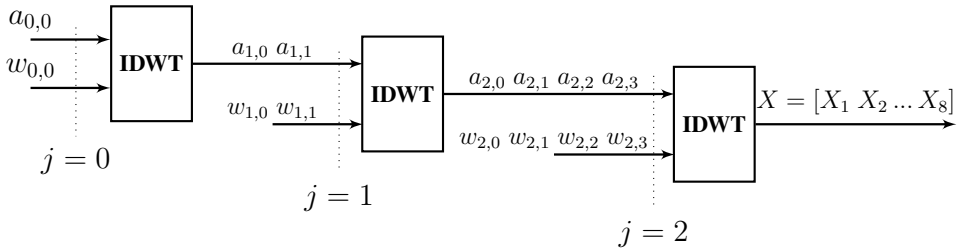

Figure 2.7: IDWT process when $J_0 = 0$, $J = 3$, $L = 3$, and scale index $j = 0, 1, 2$.

The time-frequency localization in each scale is shown in Figure 2.8 .

In the DWT process, the received signal Y_n can be defined as:
$Y_n = [Y_1\ Y_2\ Y_3\ Y_4\ Y_5\ Y_6\ Y_7\ Y_8]$

The estimated values of the $\hat{C}_{j,k}$ in terms of approximation and details coefficients $\hat{a}_{j,k}$ and $\hat{w}_{j,k}$ respectively can be shown in Figure 2.9.

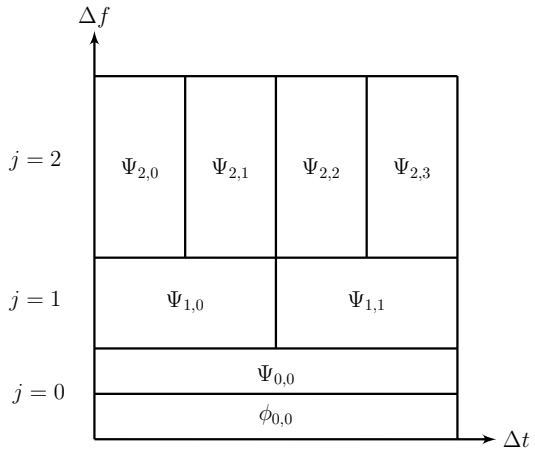

Figure 2.8: IDWT variants when $J_0 = 0$, $J = 3$, $L = 3$, and scale index $j = 0, 1, 2$.

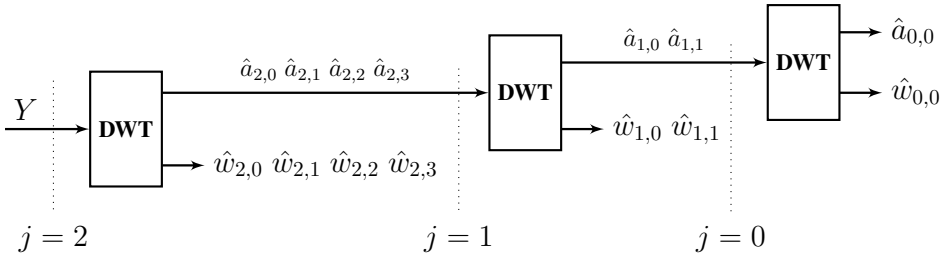

Figure 2.9: DWT process when $J_0 = 0$, $J = 3$, $L = 3$, and scale index $j = 0, 1, 2$.

Then, the estimated value of $\hat{C}_n$ can be written as:
$\hat{C}_{j,k} = [\hat{a}_{0,0}\ \hat{w}_{0,0}\ \hat{w}_{1,0}\ \hat{w}_{1,1}\ \hat{w}_{2,0}\ \hat{w}_{2,1}\ \hat{w}_{2,2}\ \hat{w}_{2,3}]$.

The time-frequency localization of the DWT in this case is shown in Figure 2.10.

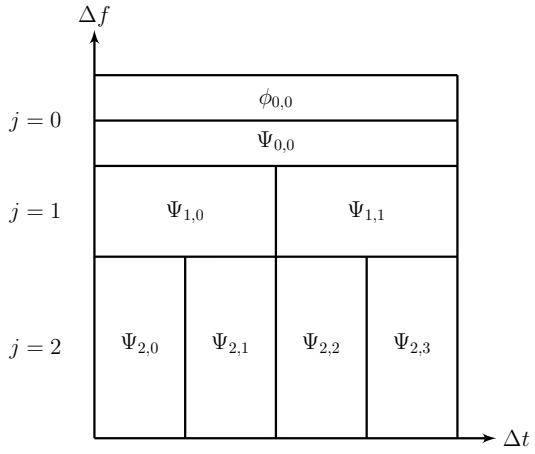

Figure 2.10: DWT variants when $J_0 = 0$, $J = 3$, $L = 3$, and scale index $j = 0, 1, 2$.

- First scale selected $J_0 = 1$:

  In this case, $L = J - J_0 = 2$, which means the IDWT or DWT is performed twice in each process. The scale index $j = 1, 2$.

  $C_{j,k}$ can be written in terms of the approximation and details components as:
  $C_{j,k} = [a_{1,0}\ a_{1,1}\ w_{1,0}\ w_{1,1}\ w_{2,0}\ w_{2,1}\ w_{2,2}\ w_{2,3}]$.

  Figure 2.11 depicts the IDWT process by using the approximation and details coefficients to generate the transmitted signal X_n.

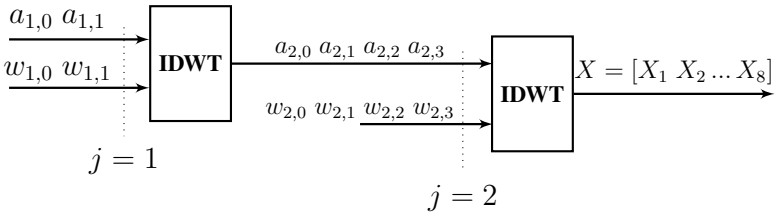

Figure 2.11: IDWT process when $J_0 = 1$, $J = 3$, $L = 2$, and scale index $j = 1, 2$.

The time-frequency localization in each scale is shown in Figure 2.12 .

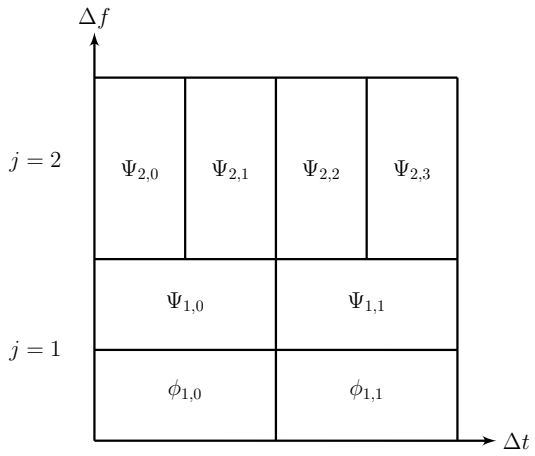

Figure 2.12: IDWT variants when $J_0 = 1$, $J = 3$, $L = 2$, and scale index $j = 1, 2$.

In the DWT process, the estimated values of the $\hat{C}_{j,k}$ in terms of approximation and detail coefficients $\hat{a}_{j,k}$ and $\hat{w}_{j,k}$ respectively is shown in Figure 2.13.

Then, the estimated value of $\hat{C_{j,k}}$ can be written as:
$\hat{C}_n = [\hat{a}_{1,0}\ \hat{a}_{1,1}\ \hat{w}_{1,0}\ \hat{w}_{1,1}\ \hat{w}_{2,0}\ \hat{w}_{2,1}\ \hat{w}_{2,2}\ \hat{w}_{2,3}]$.

The time-frequency localization of the DWT in this case is shown in Figure 2.14.

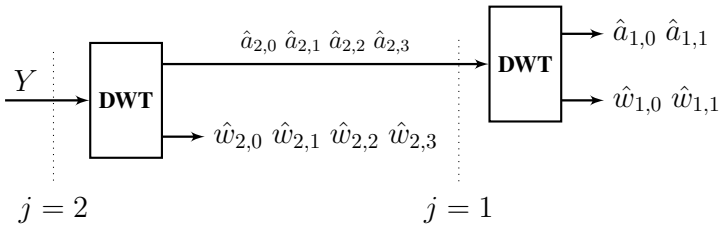

Figure 2.13: DWT process when $J_0 = 1$, $J = 3$, $L = 2$, and scale index $j = 1, 2$.

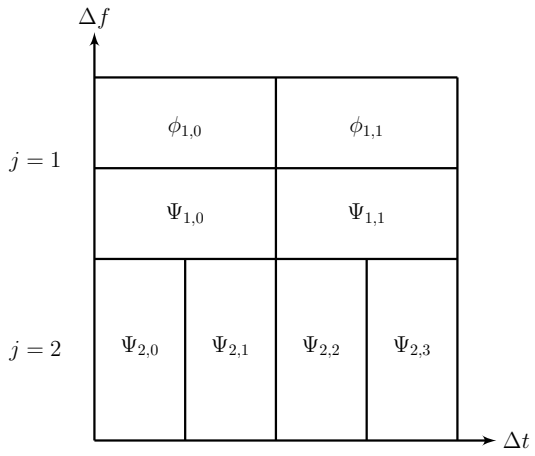

Figure 2.14: DWT variants when $J_0 = 1$, $J = 3$, $L = 2$, and scale index $j = 1, 2$.

- First scale selected $J_0 = 2$:

  In this case, $L = J - J_0 = 1$, which means the IDWT or DWT is performed twice in each process. The scale index $j = 2$.

  $C_{j,k}$ can be written in terms of the approximation and details components as:
  $C_{j,k} = [a_{2,0}\ a_{2,1}\ a_{2,2}\ a_{2,3}\ w_{2,0}\ w_{2,1}\ w_{2,2}\ w_{2,3}]$.

  Figure 2.15 depicts the IDWT process by using the approximation and detail coefficients to generate the transmitted signal X_n.

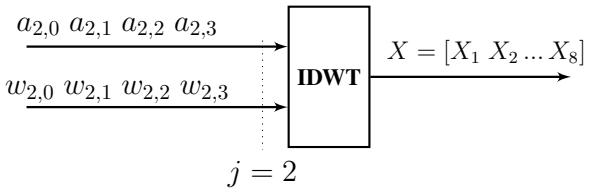

Figure 2.15: IDWT process when $J_0 = 2$, $J = 3$, $L = 1$, and scale index $j = 2$.

The time-frequency localization in each scale is shown in Figure 2.16 .

In the DWT process, the estimated values of the $\hat{C}_{j,k}$ in terms of approximation and

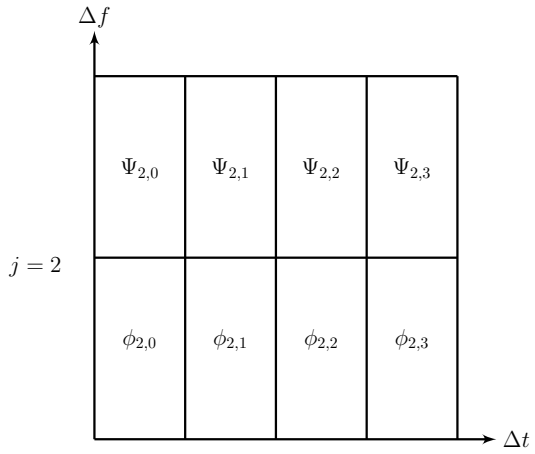

Figure 2.16: IDWT variants when $J_0 = 2$, $J = 3$, $L = 1$, and scale index $j = 2$.

detail coefficients $\hat{a}_{j,k}$ and $\hat{w}_{j,k}$ respectively is shown in Figure 2.17.

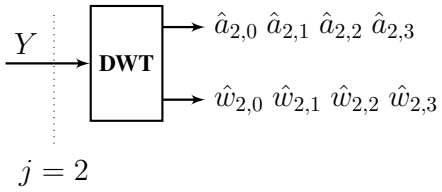

Figure 2.17: DWT process when $J_0 = 2$, $J = 3$, $L = 1$, and scale index $j = 2$.

Then, the estimated value of $\hat{C}_n$ can be written as:
$\hat{C}_{j,k} = [\hat{a}_{2,0}\ \hat{a}_{2,1}\ \hat{a}_{2,2}\ \hat{a}_{2,3}\ \hat{w}_{2,0}\ \hat{w}_{2,1}\ \hat{w}_{2,2}\ \hat{w}_{2,3}]$.

The time-frequency localization of the DWT in this case is shown in Figure 2.18.

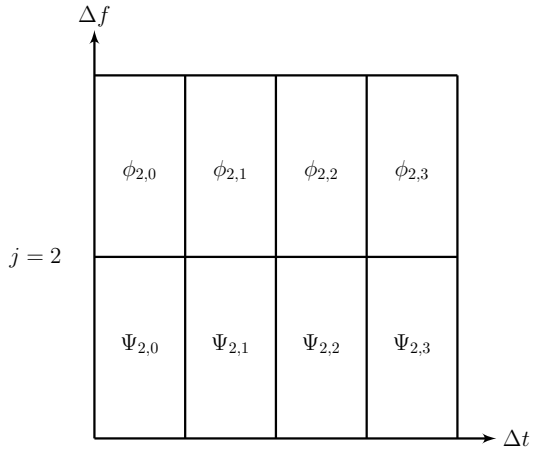

Figure 2.18: DWT variants when $J_0 = 2$, $J = 3$, $L = 1$, and scale index $j = 2$.

It is clear from the above cases that in the IDWT process, the scale index j starts from the first selected scale J_0 and is moved up until it reaches the scale $J-1$. There are 2^j and 2^{J_0} wavelet and scaling functions respectively in each scale. The wavelet function is multiplied by two in moving up from one scale to the next. At the same scale, the wavelet functions occupy the same bandwidth but are translated in time. The time-frequency localizations are changed when moving up from one scale to another. The time localization is divided by a factor of two whereas the frequency localization is multiplied by two.

On the other hand, in the DWT process, the scale index j starts from the scale $J-1$ and is moved down by steps to the scale J_0. In this case, the time and frequency localizations are multiplied and divided by a factor of two respectively in moving from the scale to the next.

In this work, if the total number of subcarriers (*N*) is 128, the number of reconstruction or decomposition levels will be varied from 1 to 7. In chapter 3, the DWT-MCM will be tested with different numbers of reconstruction and decomposition levels and different wavelet families.

2.3.3 Wavelet and Inverse Wavelet Transform Matrices

Let W and $[W]^T$ be the wavelet and inverse wavelet transform matrices respectively. Because the W matrix mainly depends on the LPF and HPF coefficients, the inverse wavelet transform is just the transpose of the wavelet matrix. For simplicity, $[W]^T$ can be used to convert the modulated signal from the wavelet domain into the time domain. In contrast, W can be used to convert the received signal from the time domain into the wavelet domain. Let $g_0, g_1, ..., g_{k-1}$ be the filter coefficients of the wavelet transform with order k (length of the filter). Then, the first level of the W matrix with size N-by-N can be represented as [45, 46]:

$$W_N^{(1)} = \begin{bmatrix} g_0 & g_1 & \cdots & \cdots & g_{k-2} & g_{k-1} & 0 & 0 & 0 & 0 & 0 & 0 \\ 0 & 0 & g_0 & g_1 & \cdots & \cdots & g_{k-2} & g_{k-1} & 0 & 0 & 0 & 0 \\ & & & & \cdots & \cdots & \cdots & \cdots & \cdots & & & \\ 0 & 0 & 0 & 0 & 0 & 0 & g_0 & g_1 & \cdots & \cdots & g_{k-2} & g_{k-1} \\ g_{k-2} & g_{k-1} & 0 & 0 & 0 & 0 & 0 & 0 & g_0 & g_1 & \cdots & \cdots \\ \cdots & \cdots & \cdots & \cdots & & & & & & & \cdots & \cdots \\ \cdots & \cdots & g_{k-2} & g_{k-1} & 0 & 0 & 0 & 0 & 0 & 0 & g_0 & g_1 \\ f_0 & f_1 & \cdots & \cdots & f_{k-2} & f_{k-1} & 0 & 0 & 0 & 0 & 0 & 0 \\ 0 & 0 & f_0 & f_1 & \cdots & \cdots & f_{k-2} & f_{k-1} & 0 & 0 & 0 & 0 \\ & & & & \cdots & \cdots & \cdots & \cdots & \cdots & & & \\ 0 & 0 & 0 & 0 & 0 & 0 & f_0 & f_1 & \cdots & \cdots & f_{k-2} & f_{k-1} \\ f_{k-2} & f_{k-1} & 0 & 0 & 0 & 0 & 0 & 0 & f_0 & f_1 & \cdots & \cdots \\ \cdots & \cdots & \cdots & \cdots & & & & & & & \cdots & \cdots \\ \cdots & \cdots & f_{k-2} & f_{k-1} & 0 & 0 & 0 & 0 & 0 & 0 & f_0 & f_1 \end{bmatrix} \tag{2.14}$$

where, $f_i = (-1)^i g_{k-1-i}$, $i = 0, 1, ..., k-1$

It is clear from (2.14) that each row contains at most k non-zero elements. This means that W_N is a sparse matrix. In general the W_N matrix at the j^{th} level can be defined as [45]:

$$W_N^{(j)} = \begin{bmatrix} W_{N/2^{j-1}}^{(1)} & \\ & I_{N-N/2^{j-1}} \end{bmatrix} \tag{2.15}$$

The pyramidal algorithm [46] is used to apply l levels $\tilde{W}_N^{(l)}$ and $[\tilde{W}]^T{}_N^{(l)}$ in the DWT and IDWT respectively. In the DWT, the process starts from the 1^{st} level and ends at the l^{th} level. The 1^{st} level is applied to the full data vector. Then the resulting vector will be processed by applying the 2^{nd} level. The algorithm continues until the l^{th} level. In contrast, during the IDWT, the process will start from the l^{th} level and continues until the 1^{st} level. In general, $\tilde{W}_N^{(l)}$ and $[\tilde{W}]^T{}_N^{(l)}$ can be expressed as:

$$\tilde{W}_N^{(l)} = W_N^{(l)} W_N^{(l-1)} \cdots W_N^{(1)} \tag{2.16}$$

$$[\tilde{W}]^{T^{(l)}}_N = [W]^{T^{(1)}}_N [W]^{T^{(2)}}_N \cdots [W]^{T^{(l)}}_N \tag{2.17}$$

2.4 Filter Bank Multi-Carrier/Offset Quadrature Amplitude Modulation (FBMC/OQAM)

The most popular filter bank scheme which is used in most multicarrier research is FBMC/OQAM. FBMC/OQAM system uses Offset QAM (OQAM) in which the in-phase and quadrature components of quadrature amplitude modulated (QAM) symbols are separated by a half symbol space delay. In addition, the prototype filter and polyphase structure are regarded as the key points to obtain an efficient system implementation and to improve the system performance by reducing the ISI and ICI will be reduced.

FBMC modulation, as an alternative to OFDM, holds various advantages over OFDM [20, 47]. First of all, better time-frequency localization. Secondly, the employment of the prototype filter, instead of a rectangular window, which provides band limited pulse-shaping filters that overlap in time and have low spectral leakage resulting in high channel capacity and reduced sensitivity to narrowband interference [48]. Furthermore, FBMC has achieved a maximum data transmission rate due to its implementation which combines filter bank and OQAM to form OFDM/OQAM [48–51].

Different types of filterbank multicarrier (FBMC) have been studied in the literature. A parallel set of pulse amplitude modulation (PAM) symbol sequences was presented by Chang [52] to form a bank of overlapping vestigial side-band (VSB) modulation filters. Maximum spectral efficiency is achieved by using half cosine roll-offs to form a perfect reconstruction FBMC system [1]. This means that a half-symbol space delay between the in-phase and the quadrature components of QAM symbol is advantageous in using a larger part of the frequency range of transmission media to avoid the degradations which gradually increase at the band edges. Efficient polyphase implementations of FBMC systems are possible [49, 50, 53]. Moreover, for both single and multicarrier, filtered multitone (FMT) systems have been proposed for VDSL standards [54].

Like any type of multicarrier modulation system, FBMC have many disadvantages; the major one is their sensitivity to carrier frequency offset (CFO) and symbol timing errors [55, 56], resulting in performance degradation which causes inter-carrier interference (ICI) between adjacent subcarriers and successive symbols. Many researchers have concentrated on estimation of FBMC systems to implement reliable and accurate synchronization schemes. Time-frequency synchronization has been discussed in [57], the transmission filter bank properties are exploited in the time domain for both blind and preamble approaches. A two stage minimum mean square error (TS-MMSE) equaliser scheme is proposed in [58], in the first stage, an MMSE equaliser has used to remove the term corresponding to ICI from the received signal, whereas, the second stage deals only with intersymbol interference (ISI). The conjugate noncircularity property of the received FBMC/OQAM signal has been used to propose a robust blind frequency offset estimator, especially for a large number of modulated signals [59]. Least square (LS) joint symbol timing and CFO estimation has been utilized to propose a new data-aided and blind estimation technique [60]. Higher bandwidth efficiency in FBMC/OQAM has achieved by using a nonlinear equaliser [61]; a Least-Mean Square (LMS) Decision Feedback Equaliser (DFE) was proposed, resulting in a significant increase in computational complexity. Different types of known preamble-based channel estimation for FBMC/OQAM systems have been used for both Single-Input Single-Output (SISO) and Multi-Input Multi-Output (MIMO) systems [62].

The basic configuration of the FBMC/OQAM transceiver model is shown in Figure 2.19. It is clear from the figure that the transmitter side consists of the OQAM Preprocessing and synthesis filter bank (SFB). The receiver side consists of an analysis filter bank (AFB), channel estimation and equalizsation, and the OQAM post-processing. Unlike the conventional OFDM system, in FBMC/OQAM, OQAM data symbols are transmitted instead of QAM. This means that the in-phase and quadrature components of the modulated signal $c_k[l]$ are offset (staggered) by a half symbol period *T/2* [63]. Baud-rate spacing is achieved between adjacent subchannels of the modulated signal. Hence information symbols free of ICI and ISI can be received.

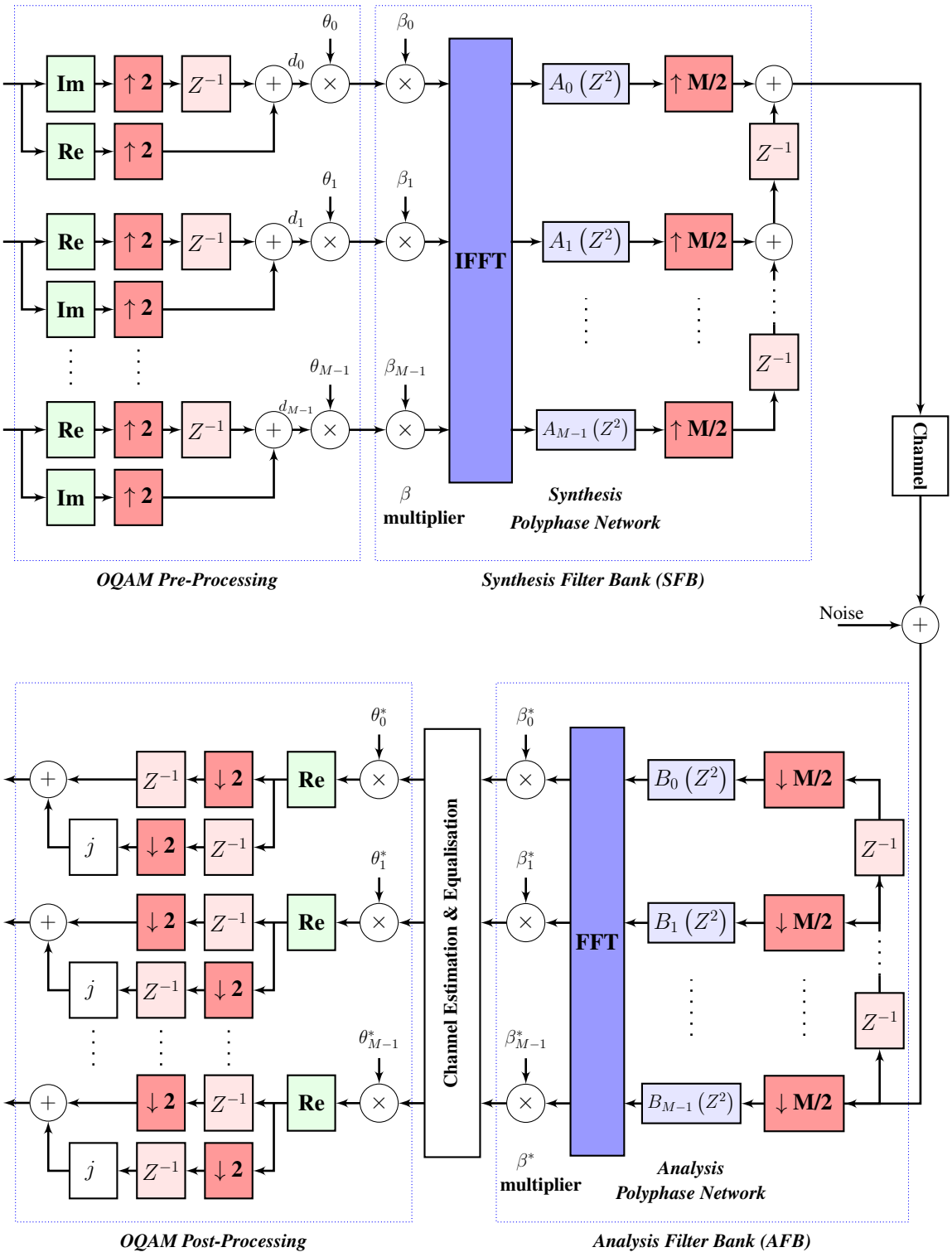

Figure 2.19: Typical block diagram of FBMC/OQAM transceiver.

2.4.1 OQAM Pre/Post-Processing

During the OQAM pre-processing, the real and the imaginary parts of a QAM complex valued symbol $c_k[l]$ are separated to form two real-valued pulse amplitude modulated (PAM) symbols $d_k[n]$ and $d_k[n+1]$:

$$d_k[n] = \begin{cases} Re(c_k[l]) & \text{if } k \text{ even} \\ Im(c_k[l]) & \text{if } k \text{ odd} \end{cases} \tag{2.18}$$

$$d_k[n+1] = \begin{cases} Im(c_k[l]) & \text{if } k \text{ even} \\ Re(c_k[l]) & \text{if } k \text{ odd} \end{cases} \tag{2.19}$$

where,

k: subcarrier index ($k = 0, 1, ..., M-1$) in which M represents the number of subcarriers.

l: time index at OQAM symbol rate.

n: time index at OQAM subsymbol rate.

After the OQAM pre-processing part, the modulated signal $x_k[n]$ can be expressed as:

$$x_k[n] = d_k[n]\,\theta_k[n] \tag{2.20}$$

where $\theta_k[n]$ represents the phase mapping between real data sequence and complex samples at the SFB input and use to maintain the orthogonality of symbols.

In general,

$$\theta_k[n] = j^{k+n} = \begin{cases} \pm 1 & \text{if } k+n \text{ even} \\ \pm j & \text{if } k+n \text{ odd} \end{cases} \tag{2.21}$$

At the receiver, the real part of the detected sequence $\hat{d}_k[n]$ can be obtained by multiplying the estimated signal $\hat{x}_k[n]$ by the conjugate of $\theta_k[n]$ as follows:

$$\hat{d}_k[n] = Re\left(\hat{x}_k[n]\,\overset{*}{\theta}_k[n]\right) \tag{2.22}$$

and then the estimated signal $\hat{c}_k[l]$ after post-processing in the QAM demodulator can be

obtained as:

$$\hat{c}_k[l] = \begin{cases} \hat{d}_k[n] + j\hat{d}_k[n+1] & \text{if } k \text{ even} \\ \hat{d}_k[n+1] + j\hat{d}_k[n] & \text{if } k \text{ odd} \end{cases} \tag{2.23}$$

2.4.2 Synthesis and Analysis Filter Bank (SFB / AFB)

The synthesis and analysis filter bank (SFB / AFB) implementation depends mainly on the design of the prototype filters and polyphase structure. However the conventional OFDM effectively uses a rectangular filter, while FBMC/OQAM uses a much longer and smoother filter response in the time domain which greatly reduces the side lobes and therefore reduces the potential for ICI and gives better frequency localization [64]. This also results in good channel capacity and reduced sensitivity to narrowband interference [65]. Figure 2.20 illustrates the normalized power spectral density (PSD) in the 8^{th} subcarrier of the transmitted signal for air-interfaces based on OFDM and FBMC/OQAM when $M = 16$ and overlapping factor $K = 4$.

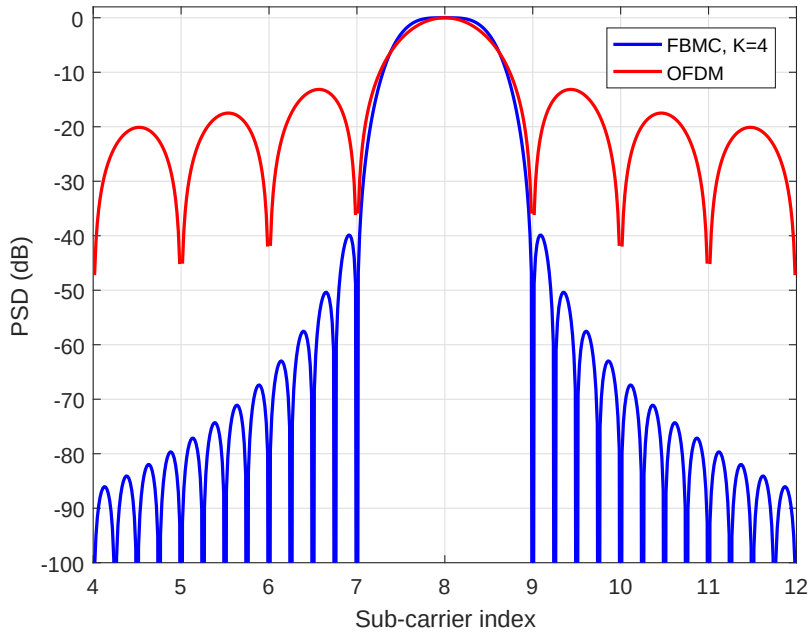

Figure 2.20: Normalized power spectral density (PSD) in the 8^{th} subcarrier of the transmitted signal for the OFDM and FBMC/OQAM systems.

The prototype filter design should meet the perfect reconstruction (PR) conditions or

provide near perfect reconstruction (NPR) characteristics [66]. However, the PR property can only be achieved under ideal transmission channel conditions. Since there is no way of avoiding interference in the wireless channel, it is impossible to get PR conditions. Thus, prototype filters are designed to satisfy NPR characteristics. In order to achieve at least NPR of the SFB and AFB, synthesis filter $g_k[m]$ and analysis filter $f_k[m]$ should be complex conjugate and time reversed versions of each other [63, 67], i.e.,

$$f_k[m] = g_k^* \left[L_p - 1 - m\right] \tag{2.24}$$

where * is the complex conjugate operator, L_p is the length of the prototype filter and *m* is the subchannel index. Complex modulated filter banks are used to achieve high spectral efficiency [63, 67]. So, the k^{th} synthesis filter $g_k[m]$ can be represented as:

$$g_k[m] = h_p[m] e^{j\frac{2\pi k}{M}\left(m - \frac{L_p - 1}{2}\right)} \tag{2.25}$$

where $h_p[m]$ is the impulse response of the prototype filter, $m = 0, 1, \cdots, L_p - 1$, ***M*** is the number of subchannels and the length of prototype filter is chosen to be $L_p = KM - 1$ where the coefficient ***K*** is an integer number and represents the overlapping factor, which controls how many multicarrier symbols overlap in the time domain.
According to (2.24), the analysis filters $f_k[m]$ can be expressed as:

$$\begin{aligned} f_k[m] &= g_k^* \left[L_p - 1 - m\right] \\ f_k[m] &= h_p^* \left[L_p - 1 - m\right] e^{j\frac{2\pi k}{M}\left(m - \frac{L_p - 1}{2}\right)} \end{aligned} \tag{2.26}$$

There are two methods to design the NPR prototype filter, the frequency sampling technique [63,66] and windowing based techniques [63,68]. A closed-form representation can be obtained to calculate the prototype filter coefficients in these two methods.

The modulation function $e_{k,m}$ used in the synthesis and analysis filters can be expressed as:

$$\begin{aligned} e_{k,m} &= e^{j\frac{2\pi k}{M}\left(m-\frac{L_p-1}{2}\right)} \\ &= e^{-j\frac{2\pi k}{M}\left(\frac{L_p-1}{2}\right)} e^{j\frac{2\pi km}{M}} \\ &= \beta_k\, \Theta_{k,m} \end{aligned} \tag{2.27}$$

where,

$$\Theta_k[m] = e^{j\frac{2\pi km}{M}} \tag{2.28}$$

$$\beta_k[n] = (-1)^{kn}\ e^{-j\frac{2\pi k}{M}\left(\frac{L_p-1}{2}\right)} \tag{2.29}$$

The term $(-1)^{kn}$ centres the output signal of each subcarrier around zero frequency [69].

The design of the polyphase filter depends on the periodicity of the modulation function [63]. To derive the expression of the k^{th} synthesis filter $G_k(z)$, suppose $m = q + tM$ where $q = 0, 1, ..., M-1$ and $t = 0, 1, ..., K-1$, also $\Theta_k[m] = \Theta_k[q + tM]$. This means that in (2.25) and (2.26), the periodicity of the modulation function $e_{k,m}$ is M. Then:

$$\begin{aligned} G_k(z) &= \sum_{m=0}^{L_p-1} h_p[m] e_{k,m} z^{-m} \\ &= \sum_{q=0}^{M-1} \sum_{t=0}^{K-1} h_p[q+tM]\beta_k \Theta_{k,q+tM} z^{-(q+tM)} \\ &= \sum_{q=0}^{M-1} \beta_k \Theta_{k,q} z^{-q} \sum_{t=0}^{K-1} h_p[q+tM] z^{-tM} \\ &= \sum_{q=0}^{M-1} \beta_k \Theta_{k,q} z^{-q} A_q\left(z^M\right) \end{aligned} \tag{2.30}$$

A joint matrix expression for all synthesis filters can be written as:

$$\mathbf{G}(z) = \boldsymbol{\beta}\,.\,\mathbf{W}\,.\,\mathbf{A}\left(z^M\right)\,.\,\mathbf{c}\,(z)\,, \tag{2.31}$$

where,

$\mathbf{G}(z) = [G_0(z)\, G_0(z) \ldots G_{M-1}(z)]^T$: synthesis filters,

$\boldsymbol{\beta} = \text{diag}\,[\beta_0\, \beta_1 \ldots \beta_{M-1}]$: β_k multipliers,

$[\mathbf{W}]_{k,q} = \Theta_{k,q}$: IDFT,

$\mathbf{A}\left(z^{M}\right) = \text{diag}\left[A_0\left(z^{M}\right)\ A_1\left(z^{M}\right)\ ...\ A_{M-1}\left(z^{M}\right)\right]$: polyphase filters,
$\mathbf{c}(z) = \left[1\ z^{-1}\ ...\ z^{-(M-1)}\right]^{T}$: delay chain.
If the all upsamplers are applied to β_k multipliers, IDFT, and polyphase filters [63], the polyphase filters can be expressed as:
$\mathbf{A}\left(z^{2}\right) = \text{diag}\left[A_0\left(z^{2}\right)\ A_1\left(z^{2}\right)\ ...\ A_{M-1}\left(z^{2}\right)\right]$
and the polyphase implementation structure is shown in Figure 2.19.

Similarly, the k^{th} analysis filter $F_k(z)$ can be expressed as:

$$\begin{aligned} F_k(z) &= \sum_{m=0}^{L_p-1} h_p[L_p-1-m]\overset{*}{e}_{k,m} z^{-m} \\ &= \sum_{q=0}^{M-1} \overset{*}{\beta}_k \overset{*}{\Theta}_{k,q} z^{-(M-1-q)} A_{M-1-q}\left(z^{2}\right) \\ &= \sum_{q=0}^{M-1} \overset{*}{\beta}_k \overset{*}{\Theta}_{k,q} z^{-(M-1-q)} B_{q}\left(z^{2}\right) \end{aligned} \tag{2.32}$$

and the matrix notation can be written as:

$$\mathbf{F}(z) = \overset{*}{\boldsymbol{\beta}} . \overset{*}{\mathbf{W}} . \mathbf{B}\left(z^{2}\right) . \mathbf{D}\left(z\right), \tag{2.33}$$

where,
$\mathbf{F}(z) = \left[F_0(z)\, F_0(z)\, ...\, F_{M-1}(z)\right]^{T}$: analysis filters,
$\overset{*}{\boldsymbol{\beta}} = \text{diag}\left[\overset{*}{\beta}_0\, \overset{*}{\beta}_1\, ...\, \overset{*}{\beta}_{M-1}\right]$: $\overset{*}{\beta}_k$ multipliers,
$[\overset{*}{\mathbf{W}}]_{k,q} = \overset{*}{\Theta}_{k,q}$: DFT,
$\mathbf{B}\left(z^{2}\right) = \text{diag}\left[B_0\left(z^{2}\right)\ B_1\left(z^{2}\right)\ ...\ B_{M-1}\left(z^{2}\right)\right]$: analysis polyphase filters,
$\mathbf{D}(z) = \left[z^{-(M-1)}\ z^{-(M-2)}\ ...\ z^{-1}\ 1\right]^{T}$: delay chain.

2.5 Long Term Evolution (LTE)

In the past two decades, Long Term Evolution (LTE) has emerged to increase the capacity and speed of wireless communication systems. LTE was first proposed by NTT DoCoMo of Japan in 2004 [70]. The LTE standard was then developed by the 3^{rd} Generation

Partnership Project (3GPP) in its release 8 document series [71, 72]. The first public implementation of the fourth-generation (4G) LTE service was in Oslo and Stockholm as a data connection with a Universal Serial Bus (USB) modem [73].

In the physical layer of the LTE system, the base-band data is transferred into a reliable signal transmission across the radio interference of the LTE system architecture. In the downlink channel (DL), data transfer between the access network of the LTE (eNodeB) and the user equipments (UE). By contrast, in the uplink channel (UL), the transformation of data from the user equipment to the eNodeB.

In general, in the DL or UL networks, the structure of transmitted data signals is the same [10, 11]. Each radio frame is 10 ms in duration and consists of a number of sub-frames up to 10 sub-frames. Each sub-frame consists of two slots with different numbers of resource blocks (RBs) for each slot with (0.5 ms) in duration as shown in Figure 2.21.

The total number of available resource blocks depends on the selected transmission bandwidth of the system. Then the total number of available subcarriers depends on the selected bandwidth. Each resource block contains 12 subcarriers of each symbol in each slot. The bandwidths parameters are defined according to the LTE specifications from 1.25MHz to 20MHz. In this work, 6 resource blocks are used with bandwidth of 1.25MHz. It is clear from Figure 2.21 that each subcarrier or resource element for one symbol period has a specific time-frequency dimension.

In this work, compared with the LTE standard, there are two differences in the parameters which are used to evaluate the MCM schemes. First, insufficient cyclic prefix (CP) is assumed to achieve high spectral efficiency. Second, Low Density Parity Check (LDPC) codes are used as a forward error correction code instead of turbo coding. For these reasons, the expression ”LTE-like” will be used instead of LTE.

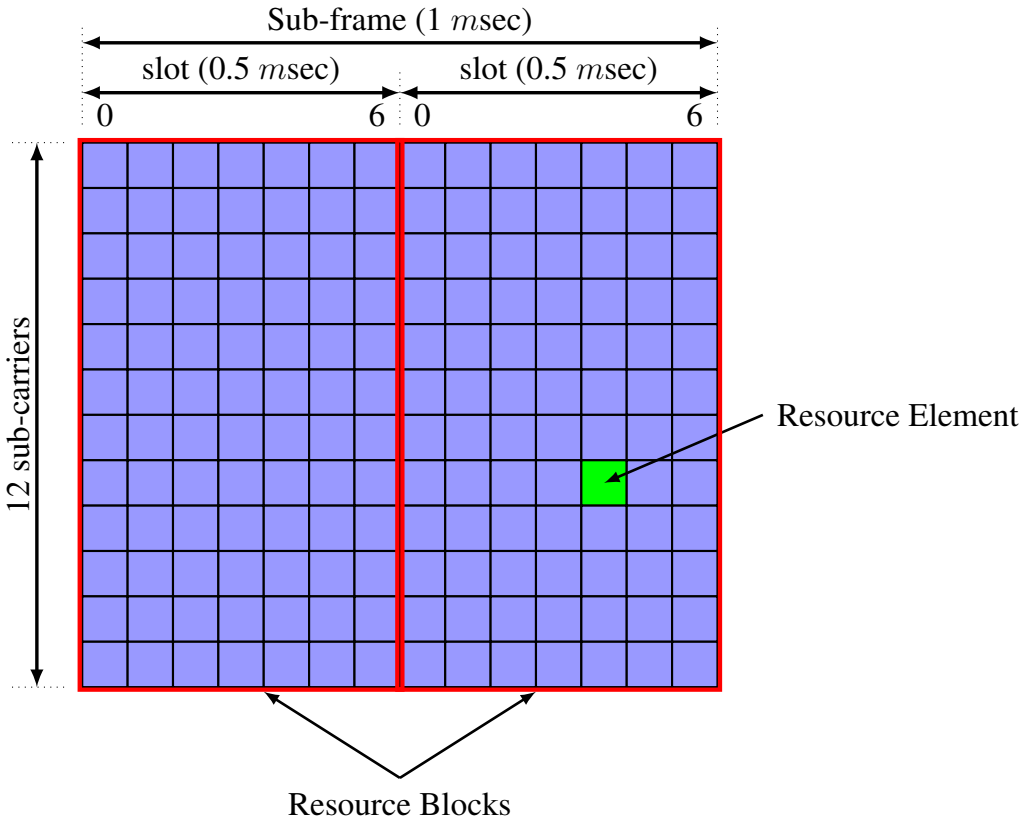

Figure 2.21: Structure of LTE sub-frame with two Resource Blocks (RBs).

2.6 Channel Modelling

The statistical representation of the physical transmission medium between the transmitter and the receiver objects (channel model) is very important to study the performance of the broadband wireless communication systems. Reflections in transmitted signal cause selectivity in the received signal. Frequency selectivity or multipath fading is caused by reflection from the physical objects between the transmitter and the receiver. Time selectivity is caused by the user's mobility and can be characterized by a Doppler spread. In general, MCM systems provide a robust solution to deal with the multipath fading channel [74–80]. However, for highly time dispersive propagation and insufficient CP, the channel destroys the orthogonality between the subcarriers. Wireless channels that are both time and frequency selective are commonly called the doubly-selective channel [81–87]. In MCM systems, channel coefficients can be estimated in both time and frequency

dimensions to achieve accurate performance as will be explained in section 4.3.

The maximum Doppler frequency f_d can be defined to describe the multipath fading channel. The Doppler frequency can be expressed as:

$$f_d = \frac{v f_c}{c} \cos(\alpha_n) = f_m \cos(\alpha_n) \tag{2.34}$$

where f_m is the maximum Doppler shift, v represents the relative motion of the moving object, f_c indicates the frequency of the propagated signal, c is the speed of light, and α_n denotes the n^{th} path arrival angle between the incident signal and the motion vector.

2.6.1 Clarke's Channel Model

In mobile communication systems, the Wide-Sense Stationary-Uncorrelated Scattering (WSSUS) channel model [88] has been used in much research to model particular mobile radio channels [89–94].The classical WSSUS channel model was derived by Clarke [95].

A theoretical reference model of isotropic scattering for narrowband cellular channels was provided by Clarke based on some assumptions [95]. First, the transmitted signal is vertically polarized. The received signal is made up of the superposition of N_{pp} propagation paths (incoming waves). The angles of arrival of these N_{pp} paths are independent and have some arbitrary probability density function (*pdf*). The N_{pp} arriving waves have constant and equal amplitudes if there is non line of sight (NLOS) propagations.

According to the above assumptions, Clarke provides a simple expression which shows the relationship between the power spectral density (PSD) of the received signal and the azimuthal bearing of the antenna's beam with respect to the azimuth angles of arrival of the N_{pp} paths. Then, the complex form of the normalized two-dimensional (2-D) frequency-flat fading channel with N_{pp} propagation paths can be expressed as [95, 96]:

$$\begin{aligned} h(t) &= \frac{1}{\sqrt{N_{pp}}} \sum_{n=1}^{N_{pp}} \exp[j(w_d t \cos(\alpha_n) + \phi_n] \\ &= h_{\Re}(t) + j h_{\Im}(t) \end{aligned} \tag{2.35}$$

where

$$h_{\Re}(t) = \frac{1}{\sqrt{N_{pp}}} \sum_{n=1}^{N_{pp}} \cos\left(w_d t \cos(\alpha_n) + \phi_n\right) \tag{2.36}$$

$$h_{\Im}(t) = \frac{1}{\sqrt{N_{pp}}} \sum_{n=1}^{N_{pp}} \sin\left(w_d t \cos(\alpha_n) + \phi_n\right) \tag{2.37}$$

where w_d denotes the radian Doppler shift with $w_d = 2\pi f_d$, and α_n and ϕ_n represent the n^{th} propagation path of the angle of arrival and initial phase respectively and they are uniformly distributed over $[-\pi, \pi]$.

The auto-correlation function of the complex envelope and the auto-correlation and cross-correlation functions of the quadrature components associated with Clarke's model can be expressed as [95, 96]:

$$R_{h_{\Re}h_{\Re}} = \mathbb{E}_{\alpha,\phi}\left[h_{\Re}(t)h_{\Re}(t+\tau)\right] = \frac{1}{2}J_0(w_d\tau), \tag{2.38}$$

$$R_{h_{\Im}h_{\Im}} = \frac{1}{2}J_0(w_d\tau), \tag{2.39}$$

$$R_{h_{\Re}h_{\Im}} = R_{h_{\Im}h_{\Re}} = 0, \tag{2.40}$$

$$R_{hh} = \mathbb{E}_{\alpha,\phi}\left[h^*(t)h(t+\tau)\right] = J_0(w_d\tau), \tag{2.41}$$

where $\mathbb{E}_{\alpha,\phi}[\cdot]$ is the expectation with respect to α and ϕ, and $J_0(\cdot)$ denotes the zero-order Bessel function of the first kind.

2.6.2 Jakes' Channel Model

Clarke's channel model has been simplified to Jakes' model [97] by using a sum of sinusoids modelling approach. Because Jakes' model does not satisfy some of the statistical properties of Clarke's model, Jakes' model does not represent wide-sense stationary (WSS) [98, 99]. To improve its statistical properties, many modifications were proposed [96, 98–102]. However, Jakes' reference model (and its modifications) is more computationally efficient than Clarke's simulator, having a smaller number of low-frequency oscillators. Hence it is often used for fading channel simulation [96, 103].

Jakes proposed some assumptions to simplify Clarke's model and provide a deterministic simulator [104]. These assumptions can be expressed as:

$$\alpha_n = \frac{2\pi n}{N_{pp}} , \qquad n = 1, 2, \ldots, N_{pp} \tag{2.42}$$

$$\phi_n = 0 , \qquad n = 1, 2, \ldots, N_{pp} \tag{2.43}$$

$$N_{pp} = 4N_o + 2 \tag{2.44}$$

where N_o represents the number of low-frequency oscillators. The number of distinct Doppler shifts is reduced from N_{pp} to $N_o + 1$.

According to the above assumptions, the normalized quadrature and in-phase components of Jakes' channel model can be given by

$$h_{\Re}(t) = \frac{2}{\sqrt{N_{pp}}} \sum_{n=1}^{N_o+1} a_n \cos(w_n t), \tag{2.45}$$

$$h_{\Im}(t) = \frac{2}{\sqrt{N_{pp}}} \sum_{n=1}^{N_o+1} b_n \sin(w_n t), \tag{2.46}$$

where

$$a_n = \begin{cases} 2\cos(\beta_n) , & n = 1, 2, \ldots, N_o \\ \sqrt{2}\cos(\beta_n) , & n = N_o + 1 \end{cases} \tag{2.47}$$

$$b_n = \begin{cases} 2\sin(\beta_n) , & n = 1, 2, \ldots, N_o \\ \sqrt{2}\sin(\beta_n) , & n = N_o + 1 \end{cases} \tag{2.48}$$

$$\beta_n = \begin{cases} \frac{\pi n}{N_o+1} , & n = 1, 2, \ldots, N_o \\ \frac{\pi}{4} , & n = N_o + 1 \end{cases} \tag{2.49}$$

$$w_n = \begin{cases} w_d \cos(\alpha_n) , & n = 1, 2, \ldots, N_o \\ w_d , & n = N_o + 1 \end{cases} \tag{2.50}$$

Table 2.1: LTE Channel Delay and Power Profile

Discrete delay (ns)			Average path gain (dB)		
EPA	EVA	ETU	EPA	EVA	ETU
0	0	0	0	0	-1.0
30	30	50	-1.0	-1.5	-1.0
70	150	120	-2.0	-1.4	-1.0
90	310	200	-3.0	-3.6	0
110	370	230	-8.0	-0.6	0
190	710	500	-17.2	-9.1	0
410	1090	1600	-20.8	-7.0	-3.0
	1730	2300		-12.0	-5.0
	2510	5000		-16.9	-7.0

2.6.3 LTE Channel Profiles

There are three types of LTE multipath channel profile: low, moderate, and high multipath delay spread values and Doppler frequencies [10, 11]. Extended Pedestrian A model (EPA) is the low spread channel to simulate the urban environment. Extended Vehicular A model (EVA) is the medium spread channel. The large spread channel is the Extended Typical Urban model (ETU) and simulates the extreme urban, suburban and rural environments. Table 2.1 represents the LTE channel power delay profile (PDP) for EPA, EVA, and ETU types. In some simulations, the channel is assumed to be perfectly known at the receiver. Otherwise, the coefficients of the channel are estimated using Wiener filter channel estimation as will be explained in section 4.3.

2.7 Low-Density Parity-Check (LDPC) Code

Low Density Parity Check (LDPC) codes are linear error correcting codes. LDPC codes were first introduced by Gallager in the 1960s [105, 106]. LDPC codes provide a performance close to the Shannon bound with less decoding complexity than other iterative decoding schemes [107]. LDPC codes can be represented by either sparse parity check matrices or the bipartite graph (Tanner graph) introduced by Tanner in the 1980s [108] as shown in Figure 2.22. In the 1990s, when iterative turbo decoding emerged, LDPC codes

were rediscovered as an iteratively decoded coding scheme for long codes [109, 110].

The sparse parity check matrices of the LDPC codes introduced by Gallager were regular matrices. This means that the ratio of the number of ones in each row or column to the length of that row or column is constant for all rows/columns. In other words, the density of each row or column is equal, and by using large block length the low density condition can be satisfied. To improve the performance of LDPC codes, irregular LDPC codes have been proposed in [111]. In this type, the number of ones in each row or column is not constant, leading to different row or column densities across the matrix. Furthermore, irregular LDPC codes achieve a better performance than that obtained with regular LDPC codes [112].

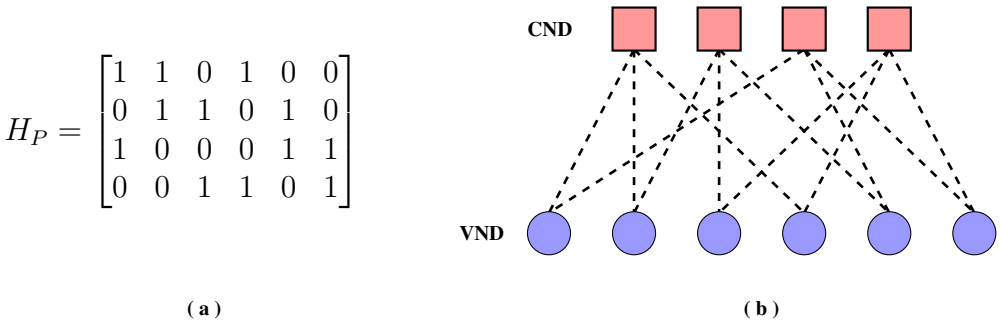

Figure 2.22: LDPC code representation, (a) H_P matrix representation, (b) Tanner graph.

2.7.1 LDPC Code Representation

For most purposes, LDPC codes can be represented by their sparse parity check matrices (H_P) or the corresponding Tanner graph as shown in Figure 2.22. If N_c and N_r represent the number of columns and rows of the matrix H_P respectively, then they represent *a parity check node decoder* or (check node decoder (CND)) and *codeword node decoder* or (bit node or variable node decoder (VND)) in the bipartite graph respectively. There is a connection (that is, an edge in the Tanner graph joins the two nodes) between bit node (*i*) and check node (*j*) when the element (*ij*) in H_P equals 1.

It is clear from Figure 2.22 that for this code there are 4-CND and 6-VND. The number of ones in each column (w_c) and row (w_r) are 2 and 3 respectively in H_P. That means

the parity-check matrix represents a regular LDPC code with constant *degree distribution* (the fraction of ones in columns and rows).

In general, the codewords in an LDPC code are generated directly by using row and column permutations by transforming the parity-check matrix into upper form and using back substitution [113]. Alternatively the encoded signal can be obtained by multiplying the data bit stream with a generator matrix G_{LDPC}. The parity-check and generator matrices are orthogonal and satisfy:

$$G_{LDPC} H_P^T = 0 \tag{2.51}$$

Gauss-Jordan elimination can be used to construct the generator matrix [114]:

$$H_P = \begin{bmatrix} A & I_{N_r - N_c} \end{bmatrix} \tag{2.52}$$

$$G_{LDPC} = \begin{bmatrix} I_{N_c} & A^T \end{bmatrix} \tag{2.53}$$

where *A* is a $(N_r - N_c) \times N_c$ binary matrix and *I* is the identity matrix.

2.7.2 Sum-Product Decoding Algorithm (SPA)

There are different types of decoding algorithms for LDPC codes; the *bit-flipping* (or hard-decision message-passing) algorithm and the sum-product algorithm (SPA) (or soft decision message-passing algorithm). The capacity of the additive white Gaussian noise (AWGN) channel can be approached by using the SPA [105, 115, 116]. Moreover, the required quantization levels can be reduced by using *log-likelihood ratios* (LLRs) with the SPA [117]. In this work, SPA is used for LDPC codes.

Figure 2.23 represents the LDPC decoder. By exchanging the extrinsic information between variable and check nodes, an approximation of the *maximum a posteriori probability* (MAP) can be obtained by using the SPA. The input message L_{in} to the decoder comes from de-interleaving the LLRs output from the de-mapper of the coded MCM system. L_{out} represents the soft output of the decoder. E_{vc} and E_{cv} are the exchanged

extrinsic information between VND and CND respectively.

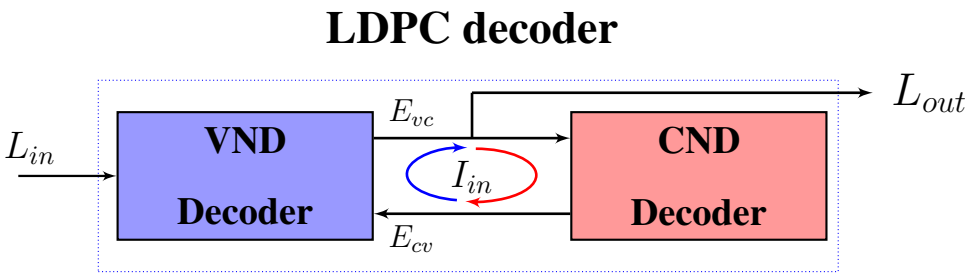

Figure 2.23: Block diagram of LDPC decoder.

Figure 2.24 shows the iterative exchange of extrinsic information between variable and check nodes. At the first iteration, L_{in} represents an initial value of the extrinsic variable node message $E_{v_{ij}}$ from bit node i to check node j. The algorithm of the k^{th} iteration can be summed up as follows:

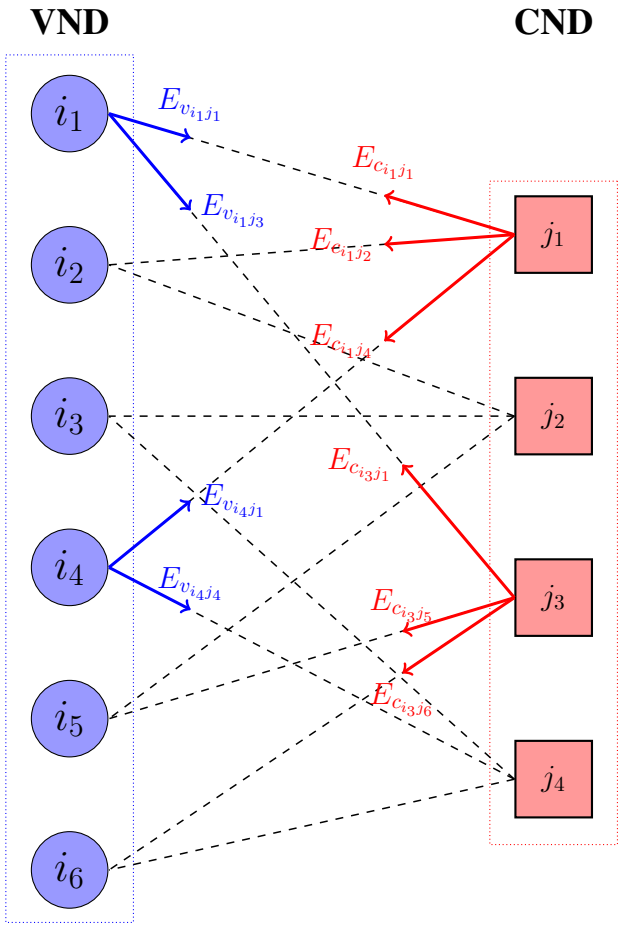

Figure 2.24: Tanner graph of iterative decoding between VND and CND.

- Calculate the extrinsic information $E_{c_{ji}}$ between check node j and bit node i. Each check node j uses the received extrinsic message from the corresponding bit node $i^{'}$ using the message $E_{v_{ij}}$ to compute the extrinsic message to the variable node i:

$$E_{c_{ji}} = 2\tanh^{-1}\left(\prod_{i' \in V_j, i' \neq i} \tanh\left(\frac{E_{v_{i'j}}}{2}\right)\right) \tag{2.54}$$

- Each bit node i uses the received message $E_{c_{ji}}$ from the corresponding check node j to update its extrinsic information which is used as extrinsic information between the variable node i and check node j in the next iteration:

$$E_{v_{ij}} = L_{in}(i) + \sum_{j' \in C_i, j' \neq j} E_{c_{j'i}} \tag{2.55}$$

- The output of the decoder L_{out} can be calculated for the current iteration as *a posteriori* LLRs:

$$L_{out}(i) = L_{in}(i) + \sum_{j' \in C_i} E_{c_{j'i}} \tag{2.56}$$

where V_i and C_j represent a set of bits from the i^{th} and j^{th} variable node and check node which are passed to the corresponding check node and variable node respectively. The extrinsic information alternates between check nodes and variable nodes using the SPA until it satisfies the condition of the MAP or reaches the maximum number of iterations I_{in}.

2.8 PAPR

Since many waveforms have been added together to form the MCM signal, it can have significant envelope variations. The ratio between the maximum power and the average power of the complex passband signal $s(t)$ is called the Peak Average Power Ratio (PAPR) [118], which is defined in **dB** as follows:

$$\text{PAPR}(dB) = 10\log_{10}\left[\frac{\max\left[|s(t)|^2\right]}{\mathbb{E}\left[|s(t)|^2\right]}\right], \qquad t \in [0, T_s] \tag{2.57}$$

In the OFDM and FBMC/OQAM systems, the IFFT output equals the sum of all components resulting from its subcarrier input signals. This lead to high PAPR, which represents one of the drawbacks of OFDM that affect the communication system performance. In DWT-MCM, the PAPR depends on the filter coefficients of the wavelet type and the number of scales L (decomposition level). At each level, the DWT-MCM system works as a single carrier system where the waveforms have the same bandwidth and they are only shifted in time.

The efficient way to characterize the PAPR is the Complementary Cumulative Distribution Function (CCDF) which can be evaluated by estimating the probability that the PAPR exceeds a particular threshold level. Figures 2.25, 2.26, and 2.27 illustrate the PAPR performance of the OFDM, FBMC/OQAM and DWT-MCM for QPSK, 16-QAM, and 64-QAM constellation respectively.

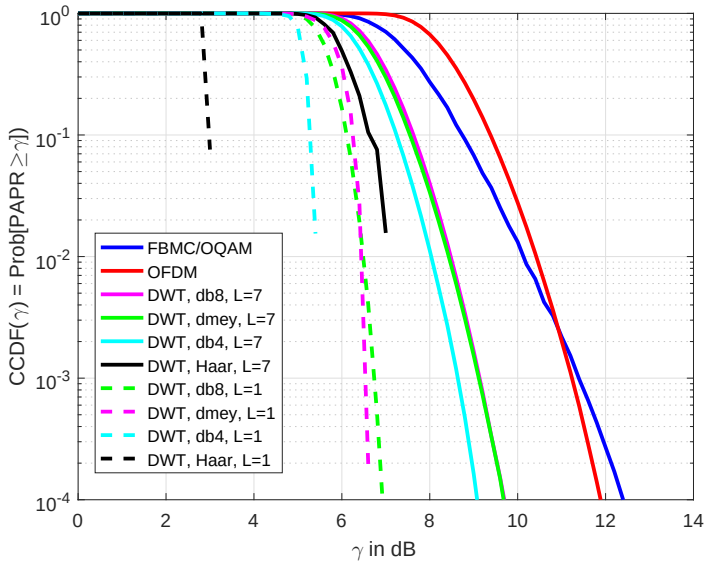

Figure 2.25: PAPR performance of the OFDM, FBMC/OQAM, and DWT-MCM with different variants and different wavelet families using QPSK constellation.

Haar, Daubechies (db4 and db8), and Dmey wavelet families are used to illustrate the PAPR performance of the DWT-MCM system with the number of scales $L = 1$ and $L = 7$

(maximum decomposition level). It is clear from these figures that the PAPR performance of the OFDM and FBMC/OQAM systems is not significantly affected by the modulation order. By contrast, the PAPR of the DWT-MCM system is increased by increasing the number of scales L and the modulation order.

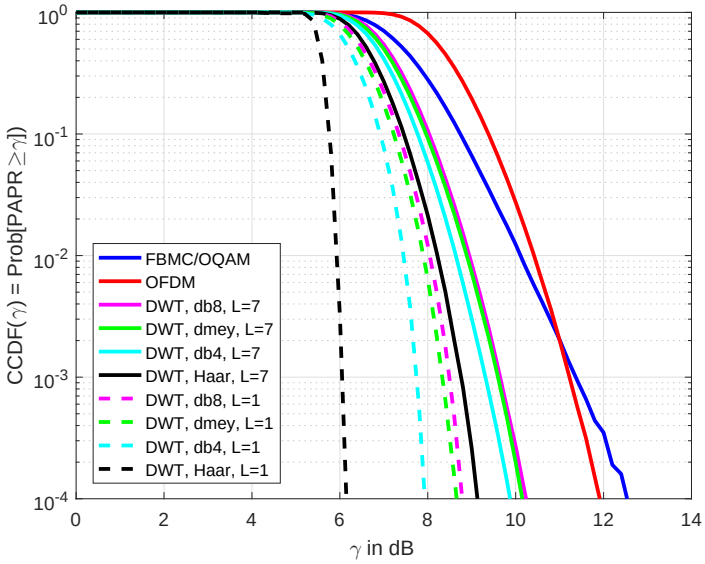

Figure 2.26: PAPR performance of the OFDM, FBMC/OQAM, and DWT-MCM with different variants and different wavelet families using 16-QAM constellation.

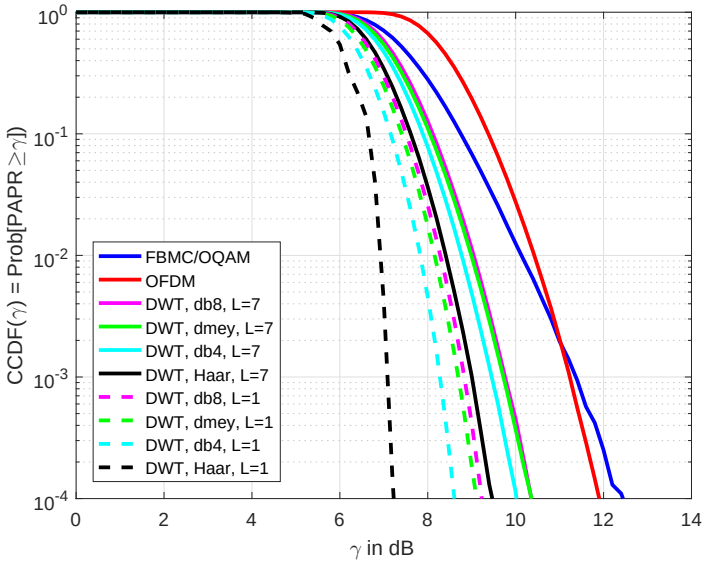

Figure 2.27: PAPR performance of the OFDM, FBMC/OQAM, and DWT-MCM with different variants and different wavelet families using 64-QAM constellation.

Figure 2.28 show the PAPR performance of the DWT-MCM system with different wavelet families using different modulation orders at scale L=1. The Daubechies (db4), Dmey, and Haar wavelet are used in this figure with 4-QAM, 16-QAM, and 64-QAM modulation. The change in the PAPR is noticeable by using different modulation orders with specific wavelet type with the same scale.

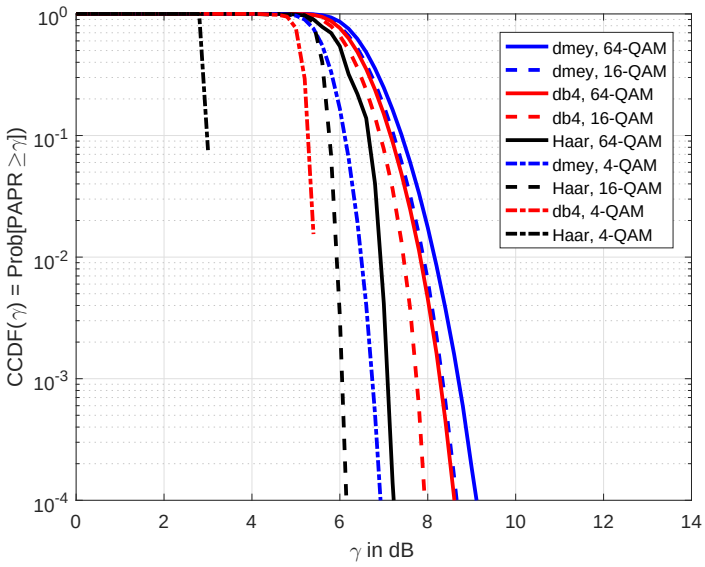

Figure 2.28: PAPR performance of the DWT-MCM system with different wavelet families using different modulation orders at L=1

2.9 Summary

This chapter can be summarised as follows:

- An overview of the theory relevant to this thesis has been presented. Some background knowledge and applications which are required for the following chapters of this thesis have been introduced.
- Three types of the MCM systems have been described: The basic concept of OFDM schemes, decomposition and reconstruction algorithms of DWT based MCM, and OQAM pre/post processing and synthesis/analysis prototype filters for FBMC/OQAM systems.

- The structure of the downlink LTE system with its specifications and parameters has been presented.
- Time-frequency selectivity with channel model characteristics have been presented. Mathematical expressions of Clark's and Jakes' simulators were introduced.
- Channel coding and decoding using LDPC codes was presented. LDPC code representations and the SPA have been studied.
- Peak to average power ratio (PAPR) was discussed for the three systems with different modulation orders and different number of scales in the case of the DWT/MCM system. A smaller PAPR is obtained for DWT-MCM than that for OFDM and FBMC/OQAM. The PAPR performance of the OFDM and FBMC/OQAM systems is not significantly affected by the modulation order, while it is increased by increasing the number of scale L and the modulation order in DWT-MCM system.

Chapter 3

Iterative Interference Cancellation based MCM (IIC-MCM)

Contents

3.1 Introduction

Iterative decoding has been widely used to achieve reliable high data rate transmission for broadband multi-carrier communication systems. However, in OFDM systems with insufficient CP, there are significant challenges for efficient receiver design under the effect of doubly-selective channels. As mentioned in Section 2.2, OFDM suffers from some drawbacks. The first is the large side lobes at each subcarrier due to the use of rectangular pulse shaping. The second limitation is the reduction in spectral efficiency due to the CP. It also

has high PAPR and synchronisation problems. Moreover, in some applications like cognitive radio and uplink network, OFDM may need additional signal-processing steps which add a significant complexity to the receiver. IIC based iterative decoding is proposed to reduce the interference and to improve the channel estimation [119–127]. In [119], iterative convolutional decoding is proposed to reduce the multiple-access interference (MAI) and ISI in code-division multiple-access (CDMA) systems. IIC is presented to reduce the interference in evolved multimedia broadcast multicast systems (eMBMSs) using FBMC/QAM scheme with diferent prototype filters [120]. An iterative decision feedback equaliser (DFE) with derivative of the channel amplitude has been introduced to cancel the ICI interference of the OFDM scheme in the DVB-T system [121]. Serial-interference-cancellation (SIC) and parallel-interference-cancellation based iterative decoding are proposed to reduce the error floor in OFDM systems [124].

In this chapter, an IIC based iterative LDPC decoder is proposed for SISO DWT-MCM, FBMC/OQAM systems as well OFDM systems with insufficient CP. At the receiver, in each iteration, the estimated decoded signal is used to calculate the estimated values of the lost components from the transmitted signal due to the effect of the multipath channel. A ZF or MMSE equaliser is used in all systems. In OFDM and FBMC/OQAM systems, the received signal is equalised in the frequency domain directly. In the DWT-MCM system, the received signal is converted from time domain into frequency domain, and a ZF or MMSE equaliser is used to equalise it. After that, it is converted into the time domain again. Furthermore, uncoded IIC will be tested for these systems in order to reduce the receiver complexity. In this case, the hard decision of the demapper is used to calculate the estimated value of the components lost due to the effect of the channel.

The rest of this chapter is organised as follows: In Section 3.2 a system model is introduced. IIC based MCM is described in Section 3.3. Simulation results are given in Section 3.5. Finally, a summary of this chapter is presented in Section 3.6.

3.2 System Model

Consider a SISO-OFDM system with N subcarriers over a multipath doubly-selective channel. The channel impulse response (CIR) can be represented as $\mathbf{h} = [h(0), h(1), ..., h(L-1)]^T$, where the length of the CIR is L. The k^{th} vector of transmitted symbols is written as $\mathbf{x} = [x_k^o, x_k^1, ..., x_k^{N-1}]^T$. In the case of an OFDM system with CP length N_{cp}, the k^{th} transmitted vector can be written as $\mathbf{x} = [x_k^{N-N_{cp}}, x_k^{N-N_{cp}+1}, ..., x_k^{N-1}, x_k^0, x_k^1, ..., x_k^{N-1}]^T$. The k^{th} vector of the received signal $\mathbf{y}$ results from linearly convolving the transmitted signal with the CIR:

Before delving into a discussion of the proposed model, it is necessary to explain the effect of the multipath propagation on the transmitted symbols. Let $\mathbf{x} = [x_0\ x_1\ x_2\ x_3]$ be the transmitted data sequence with the number of subcarriers ($N = 4$), and $\mathbf{h} = [h_0\ h_1\ h_2\ h_3]$ be the CIR with length $L = 4$.

In the case of SISO-OFDM with sufficient CP ($N_{cp} \geq L - 1$), Figure 3.1-a represents the linear convolution between $\mathbf{x}[n]$ and $\mathbf{h}[n]$ ($\mathbf{x}[n] * \mathbf{h}[n]$). Figure 3.1-b introduces the result of the linear convolution after removing the CP.

It is clear from Figure 3.1 that with sufficient CP ($N_{cp} = L - 1 = 3$), and after removing the CP, the received signal can be represented in the frequency domain as:

$$\mathbf{y}_k = \mathbf{H}\mathbf{x}_k + \tilde{\eta}_k \tag{3.1}$$

where $\mathbf{H}$ is a circulant channel matrix of size $N \times N$ and $\tilde{\eta}_k$ is a zero-mean independent and identically distributed (i.i.d.) AWGN vector at the k_{th} time instant with σ_n^2 variance ($N_0 = \sigma_n^2$). Then, the effect of the multipath channel can be easily removed during equalisation.

In the case of insufficient CP ($N_{cp} < L - 1$), $N_{cp} = 0$ in this example, ICI/ISI interference are introduced due to the effect of the multipath frequency-selective fading channel. The orthogonality property has been lost. This means that the multicarrier data symbols are overlapped at the receiver input as shown in Figure 3.2.

(a)

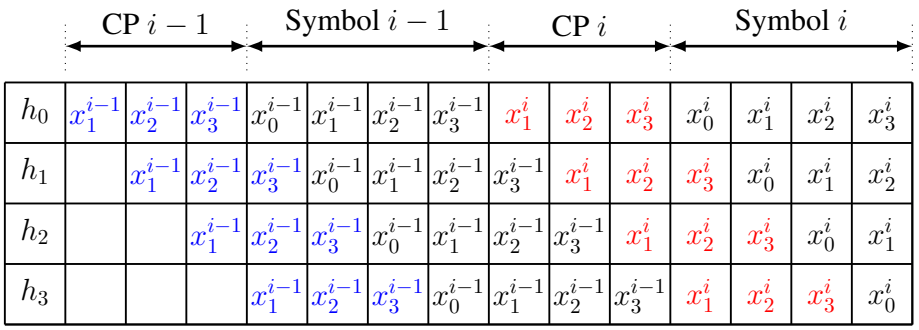

(b)

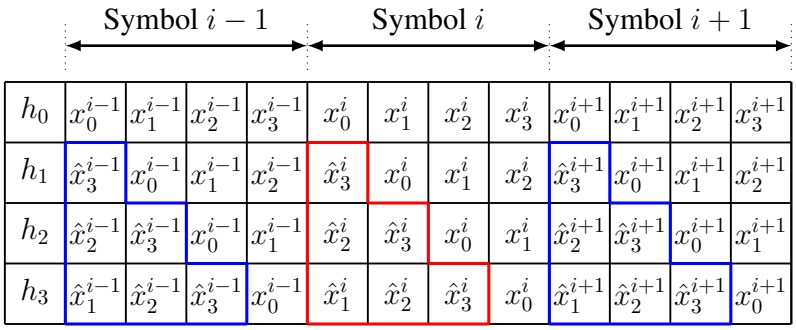

Figure 3.1: Effect of the multipath propagation on the received data symbols with sufficient CP: (a) linear convolution with CP, (b) after CP removal.

Figure 3.2-a shows the effect of the channel, while Figure 3.2-b shows the effect of cancelling the ISI from the previous signal and adding the estimated signal to create the circulant form. In this case, the time domain received signal can be expressed as follows (see, for example [128–131]):

$$\mathbf{y}_k = \mathbf{H}\mathbf{F}_N\mathbf{x}_k - \mathbf{A}\mathbf{F}_N\mathbf{x}_k + \mathbf{B}\mathbf{F}_N\mathbf{x}_{k-1} + \tilde{\eta}_k \tag{3.2}$$

where $\mathbf{F}_N$ is the normalized IFFT matrix of size $N \times N$, matrices $\mathbf{A}$ and $\mathbf{B}$ denote the ICI and ISI components of the channel respectively and will be described in Section 3.3.

(a)

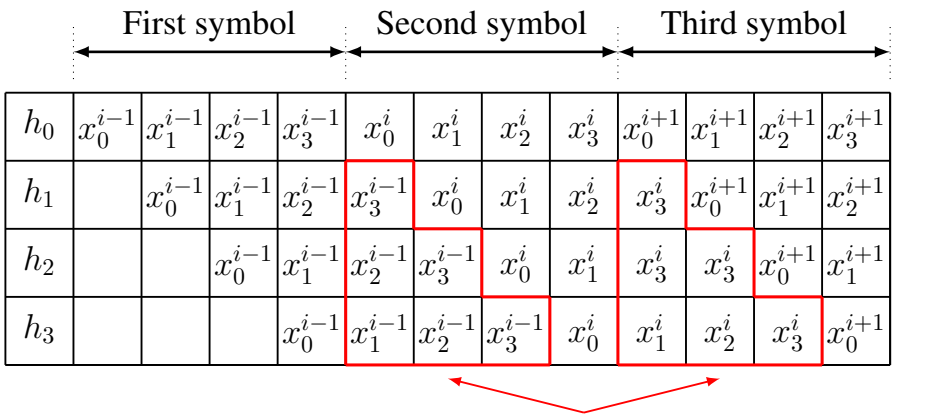

(b)

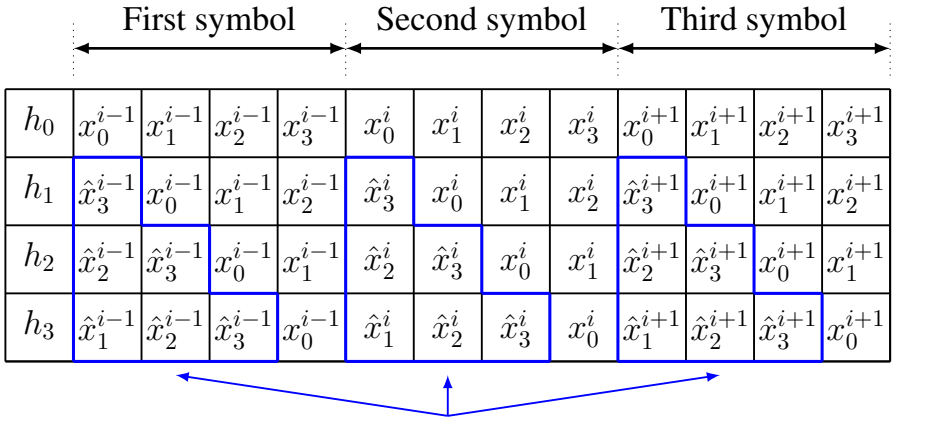

Figure 3.2: Effect of the multipath propagation on the received data symbols with no CP: (a) linear convolution with ISI to be removed, (b) estimated signal to be added.

3.3 IIC-MCM

Starting from (3.2), the received data symbol $\mathbf{y}_k$ can be expressed as:

$$\mathbf{y}_k = \mathbf{H}_{CIRC}\mathbf{x}_k - \mathbf{H}_{ICI}\mathbf{x}_k + \mathbf{H}_{ISI}\mathbf{x}_{k-1} + \tilde{\eta}_k \tag{3.3}$$

where channel matrices $\mathbf{H}_{CIRC}$, $\mathbf{H}_{ICI}$, and $\mathbf{H}_{ISI}$ correspond respectively to the circulant matrix with all coefficients and the residual matrices that lead to ICI and ISI, and $\tilde{\eta}_k$ represents Gaussian noise at the k^{th} time instant, and the matrices $\mathbf{H}_{CIRC}, \mathbf{H}_{ICI}, \mathbf{H}_{ISI} \in$

$\mathbb{C}^{N\times N}$ [128–131].

In this chapter, to reduce the ICI and ISI, the undesirable terms containing $\mathbf{H}_{ICI}$ and $\mathbf{H}_{ISI}$ must be removed from the received data symbols. First we calculate the channel matrices $\mathbf{H}_{ICI}$ and $\mathbf{H}_{ISI}$. Next we multiply them by the current and previous values of the estimated transmitted data symbols $\hat{\mathbf{x}}_k$ and $\hat{\mathbf{x}}_{k-1}$ respectively to obtain $\mathbf{H}_{ICI}\hat{\mathbf{x}}_k$ and $\mathbf{H}_{ISI}\hat{\mathbf{x}}_{k-1}$. Finally, we add and subtract the obtained components from the multicarrier symbols which overlap at the receiver input as shown in Figure 3.4. After some iterations, the estimated received signal can be expressed as:

$$\hat{\mathbf{y}}_k = \mathbf{H}_{CIRC}\hat{\mathbf{x}}_k + \tilde{\eta}_k \tag{3.4}$$

The received signal in the frequency domain can be represented as:

$$\hat{\mathbf{Y}}_k = F\mathbf{H}_{CIRC}F^{\mathbf{H}}\hat{\mathbf{X}}_k + F\tilde{\eta}_k \tag{3.5}$$

According to the eigenvalue decomposition (EVD) of the circulant matrix [132] i.e. $\mathbf{H}_{CIRC} = F^{\mathbf{H}}\mathbf{H}F$, the estimated received signal in the frequency domain can be expressed as:

$$\hat{\mathbf{Y}}_k = \mathbf{H}\hat{\mathbf{X}}_k + \eta_k \tag{3.6}$$

where $\mathbf{H} \in \mathbb{C}^{N\times N}$ constitutes a diagonal matrix that comprises the Channel Frequency Response (CFR) along its diagonal components.

Let N_{cp}, L_c, and E respectively represent the number of cyclic prefix samples, the length of the LTE channel, and the excess channel length over the cyclic prefix. Then $E = L_c - N_{cp} - 1$. Channel matrices $\mathbf{H}_{ICI}$, $\mathbf{H}_{ISI}$ can be expressed as:

$$\mathbf{H}_{ISI} = \begin{bmatrix} 0_{E\times(N-E)} & \mathbf{H}_1 \\ 0_{(N-E)\times(N-E)} & 0_{(N-E)\times E} \end{bmatrix} \tag{3.7}$$

$$\mathbf{H}_{ICI} = \begin{bmatrix} 0_{E\times(N-E-N_{cp})} & \mathbf{H}_1 & 0_{E\times N_{cp}} \\ 0_{(N-E)\times(N-E-N_{cp})} & 0_{(N-E)\times E} & 0_{(N-E)\times N_{cp}} \end{bmatrix} \tag{3.8}$$

where the interference originating with matrix $\mathbf{H}_1 \in \mathbb{C}^{E\times E}$ depends mainly on the value of the channel impulse response $\mathbf{h}$ and can be represented as:

$$\mathbf{H}_1 = \begin{bmatrix} h_{L_c-1} & \cdots & \cdots & h_{N_{cp}-1} \\ 0 & \ddots & & \vdots \\ \vdots & \ddots & \ddots & \vdots \\ 0 & \cdots & 0 & h_{L_c-1} \end{bmatrix} \tag{3.9}$$

in the case of $N_{cp} = 0$, $\mathbf{H}_{ICI} = \mathbf{H}_{ISI}$. Also, $\mathbf{H}_{ICI} = \mathbf{H}_{ISI} = 0$ with sufficient CP.

In coded MCM systems, the IIC scheme is applied in two scenarios:

- *Case I*: In this scenario, the hard decision of the demapper output is used to calculate the ICI/ISI interference components as explained in Section 3.3. This information is used to cancel these components from the received signal. Hard decisions on the coded data are obtained directly (without passing through the decoder), and this is repeated a fixed number of times, then the soft output of the demapper is passed to the decoder, which is applied only once, as shown in Figure 3.3.
- *Case II*: In this scenario, the soft decisions are passed to the decoder (without any iterations using the hard decisions of the coded data), then the soft output of the decoder is used to estimate and cancel the interference, and this process is iterated multiple times. as shown in Figures 3.4 and 3.5.

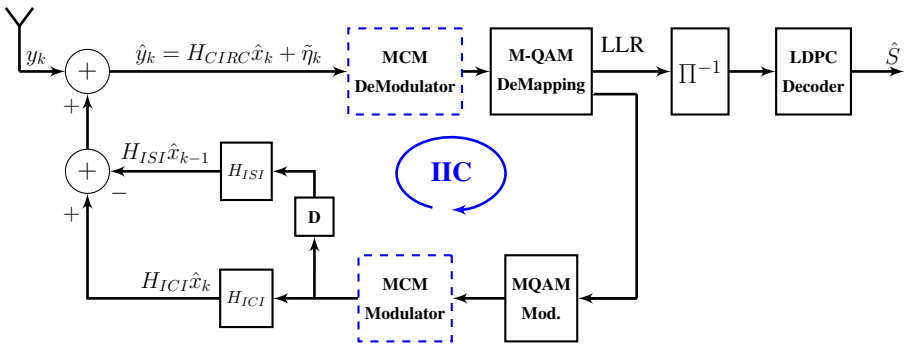

Figure 3.3: Receiver side of the proposed IIC scheme of the LDPC-MCM systems using hard decisions of the demaper output.

In the SISO-DWT-MCM system, two cases for channel equalisation are considered:

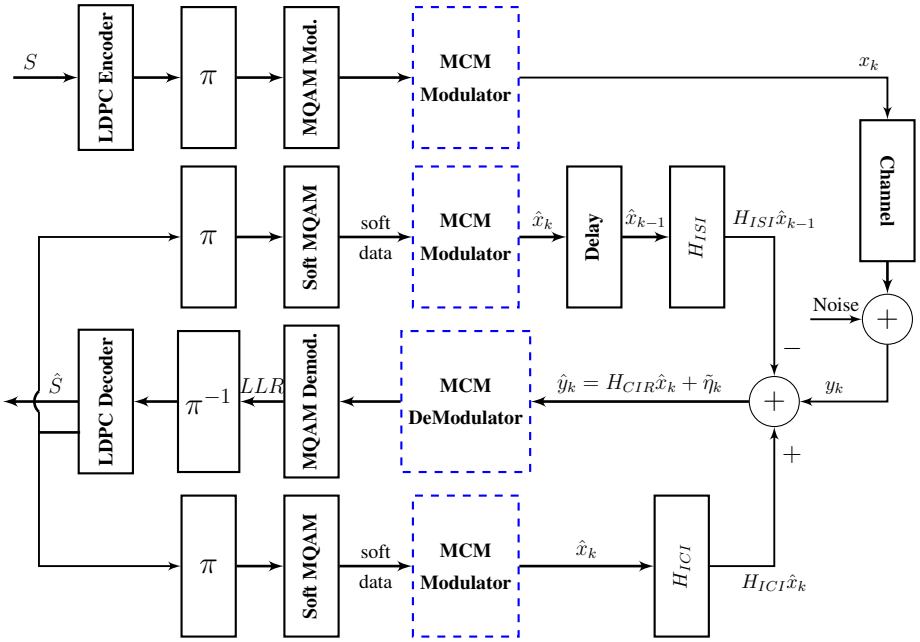

Figure 3.4: Basic configuration diagram of the iterative interference cancellation of FBMC/OQAM system.

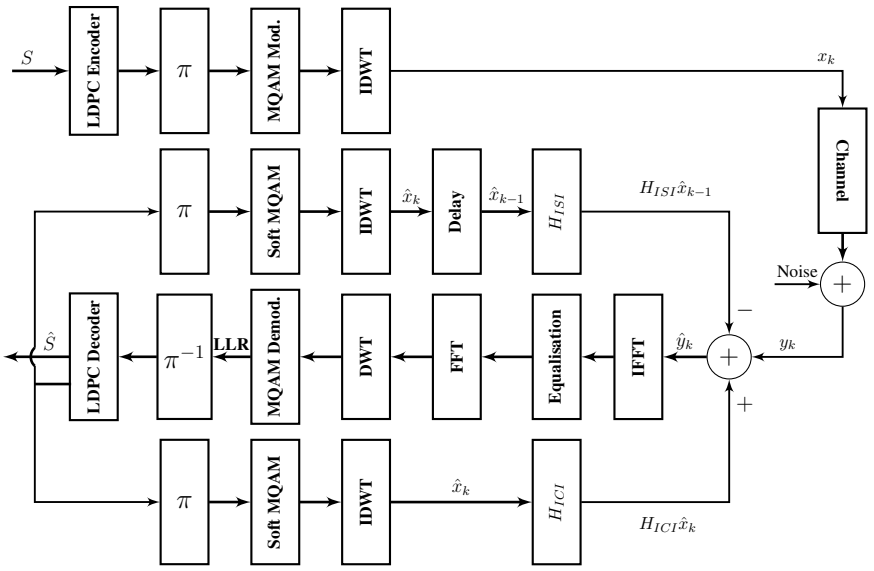

Figure 3.5: Basic configuration diagram of the iterative interference cancellation of DWT-MCM system.

- *Case I* using a frequency domain equaliser: In this case, the channel detection will be performed in the frequency domain. This means that the time domain received signal is first converted into the frequency domain and channel equalisation is applied. After that the detected signal is converted into the time domain again as shown in Figure 3.5.

- *Case II* using wavelet domain equaliser: In this case, the channel must first be represented as an N-by-N circulant matrix $\mathbf{H}_c$. Let $\mathbf{h}$ be the CIR with length L and $\mathbf{h} = [h(0), h(1), ..., h(L-1)]^T$. $\mathbf{H}_c$ can be represented as:

$$\mathbf{H}_c = \begin{bmatrix} h_0 & h_1 & \cdots & \cdots & h_{L-2} & h_{L-1} & 0 & \cdots & 0 \\ 0 & h_0 & h_1 & \cdots & \cdots & h_{L-2} & h_{L-1} & 0 & \cdots \\ & & \cdots & & \cdots & \cdots & \cdots & \cdots & \cdots \\ 0 & \cdots & 0 & h_0 & h_1 & \cdots & \cdots & h_{L-2} & h_{L-1} \\ h_{L-1} & 0 & \cdots & 0 & h_0 & h_1 & \cdots & \cdots & h_{L-2} \\ & \cdots & \cdots & & & \cdots & \cdots & & \\ & & \cdots & \cdots & & & \cdots & \cdots & \\ \cdots & \cdots & h_{L-2} & h_{L-1} & 0 & \cdots & 0 & h_0 & h_1 \\ h_1 & \cdots & \cdots & h_{L-2} & h_{L-1} & 0 & \cdots & 0 & h_0 \end{bmatrix} \tag{3.10}$$

  After that, apply $\tilde{W}_N^{(l)}$ and $[\tilde{W}]^T{}_N^{(l)}$ which are given in (2.16) and (2.17) respectively, to generate an equivalent wavelet domain channel:

$$\tilde{\mathbf{H}}_N^{(l)} = \tilde{W}_N^{(l)} \mathbf{H}_c [\tilde{W}]^T{}_N^{(l)} \tag{3.11}$$

  Finally, multiply each received data symbol in the wavelet domain by $[\tilde{\mathbf{H}}_N^{(l)}]^{-1}$ to detect the received data signal.

3.4 Computational Complexity

The computational complexity of the MCM systems can be evaluated by calculating the number of real multiplications. The OFDM system only consists of IFFT and FFT. This

means that the complexity can be expressed as:

$$\mathcal{O}_{OFDM} = 2Nlog_2(N) \tag{3.12}$$

Since DWT-MCM system with frequency domain equaliser needs two more blocks IDWT and DWT compared with OFDM system. This means that its complexity is higher than OFDM. According to Mallat algorithm [43], DWT and IDWT consist of down-sampling and up-sampling by a factor of two respectively and filtering the approximation coefficients $a_{j,k}$ and the detail coefficients $w_{j,k}$ respectively by a LPF and HPF with G non-zero coefficient length. Therefore the complexity of the DWT can be expressed as:

$$\sum_{j=J_0+1}^{J} 2^j G \leq \sum_{j=1}^{J} 2^j G = 2NG \tag{3.13}$$

The complexity of the DWT-MCM system with frequency domain equaliser can be written as:

$$\mathcal{O}_{DWT-MCM} = 2NG + 2Nlog_2(N) \tag{3.14}$$

According to (3.14), the complexity increase is a factor of about $\mathcal{O}(\frac{G}{log_2(N)} + 1)$ compared with that of OFDM, which is affordable since G is bounded and the number of bearers N is usually large.

In FBMC/OQAM system, the total number of real multiplications for the transmitter side is the sum of the multiplications of each SFB processing block; β-multipliers, IFFT, and N-branch polyphase filtering. During the OQAM pre-processing, the complex-valued QAM is separated into its in-phase and quadrature components. Therefore, the complexity of the transmitter side will be multiplied by 2 and can be written as:

$$\mathcal{O}_{FBMC/OQAM_{TX}} = 2(2N + Nlog_2(N) + 2KN) \tag{3.15}$$

where K represents the overlapping factor.

At the receiver side, similar processing blocks are used but in reverse order to that of transmitter side. This means that the overall complexity of the FBMC/OQAM system can be written as:

$$\mathcal{O}_{FBMC/OQAM} = 4(2N + Nlog_2(N) + 2KN) \tag{3.16}$$

After $N_{IIC-Itrs}$ IIC iterations, the number of the real multiplications of the three systems can be written as:

$$\mathcal{O}_{OFDM_{IIC}} = N_{IIC-Itrs} \times 2Nlog_2(N) \tag{3.17}$$

$$\mathcal{O}_{DWT-MCM_{IIC}} = N_{IIC-Itrs} \times (2NG + 2Nlog_2(N)) \tag{3.18}$$

$$\mathcal{O}_{FBMC/OQAM_{IIC}} = N_{IIC-Itrs} \times 4(2N + Nlog_2(N) + 2KN) \tag{3.19}$$

The comparison of the computational complexity among the three systems with and without IIC is shown in Figure 3.6. This figure shows the number of real multiplications against the number of subcarriers.

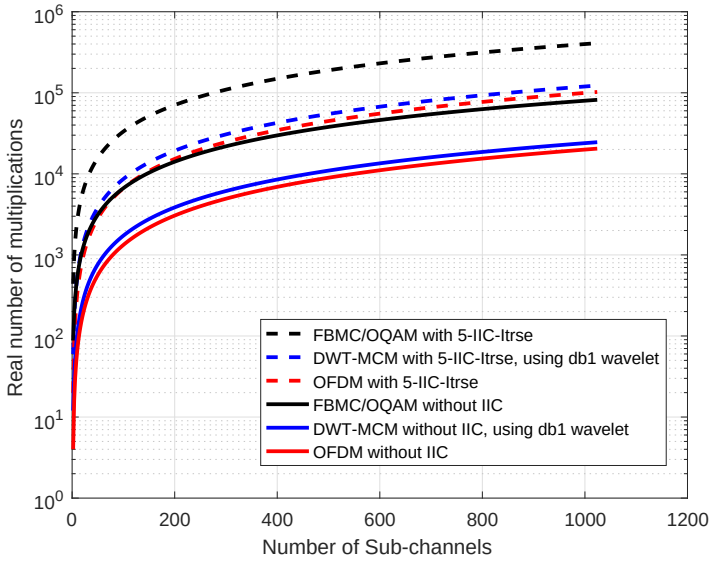

Figure 3.6: Number of real multiplications vs the number of subcarriers for MCM systems.

3.5 Simulation Results

In this chapter, a signal format based on the LTE downlink standard for SISO-OFDM is used but with insufficient CP and with the channel perfectly known at the receiver. The abbreviations which are used in this simulation are defined in Table 3.1. The simulation performance of DWT, OFDM and FBMC systems is evaluated using the simulation parameters which are defined and illustrated in Table 3.2. The PDPs for the EPA, EVA, and ETU types of the LTE channel are presented in Table 2.1.

In the SISO system, the signal-to-noise ratio (SNR) can be calculated in terms of the ratio of bit energy to noise power spectral density (E_b/N_0) as:

$$SNR = (E_b/N_0)\left(\frac{N_{Sc}}{N+N_{cp}}\right)(R_c N_{bps}) \tag{3.20}$$

where R_c is the coding rate and N_{bps} represents the number of bits per symbol, $N_{bps} = log_2(M)$ and M is the constellation order.

Table 3.1: Abbreviations

Abbreviations	Definitions
N_{Fig}	Figure number
Eq.	Equalisation type
IIC-Itrs	Number of IIC iterations
R_k	Error floor reduction factor after some IIC iterations
Gap	The gap from the PCIC simulation results in dB

Table 3.2: Simulation Parameters Definition

Parameters	Definitions	Specifications
N	Total number of sub-carriers (used & unused)	128
N_{RB}	Number of resource blocks	6
N_{Sc-RB}	Number of sub-carriers per resource block	12
N_{Sc}	Number of used sub-carriers	$N_{Sc-RB} \times N_{RB}$
N_{slot}	Number of slots per resource block	2
N_{sym}	Number of symbols per slot	7 (OFDM and DWT) 14 (FBMC/OQAM)
N_s	Total number of symbols per resource block	$N_{sym} \times N_{slot}$
N_{cp}	Length of cyclic prefix (in samples)	0 10
M-QAM	Modulation type	4-QAM 16-QAM 64-QAM
S_s	Sub-carrier spacing (KHz)	15 KHz
F_s	Sampling frequency	$S_s \times N$
LTE	Type of LTE channel	EPA, EVA, and ETU
H_{LDPC}	Parity check matrix of LDPC code	$[1008, 2016]$ (4-QAM) $[2016, 4032]$ (16-QAM) $[3042, 6048]$ (64-QAM)

3.5.1 Uncoded Systems

In this case, to reduce the receiver complexity, the three systems are tested without using iterative decoding. In this case, the output of the demapper is used to process the received signal by calculating the required components lost due to the effect of the multipath channel. First, the estimated values of the current and previous data symbols $\hat{\mathbf{x}}_k$ and $\hat{\mathbf{x}}_{k-1}$ will be calculated from the hard output of the demapper. Then we multiply them by the resid-

ual matrices that lead to ICI and ISI $\mathbf{H}_{ICI}$, and $\mathbf{H}_{ISI}$ to obtain the components $\mathbf{H}_{ICI}\hat{\mathbf{x}}_k$, and $\mathbf{H}_{ISI}\hat{\mathbf{x}}_{k-1}$ which are then used to reduce the interference specifically by cancelling it.

First, the performance of the three systems will be compared with sufficient CP. Figures 3.7 and 3.8 illustrate the bit error probability for the three systems over the EVA-LTE channel and using the ZF equaliser with 4-QAM and 16-QAM modulations respectively. It is clear from these figures that the BER curve is noticeably improved for the DWT-MCM at high $Eb/N0$.

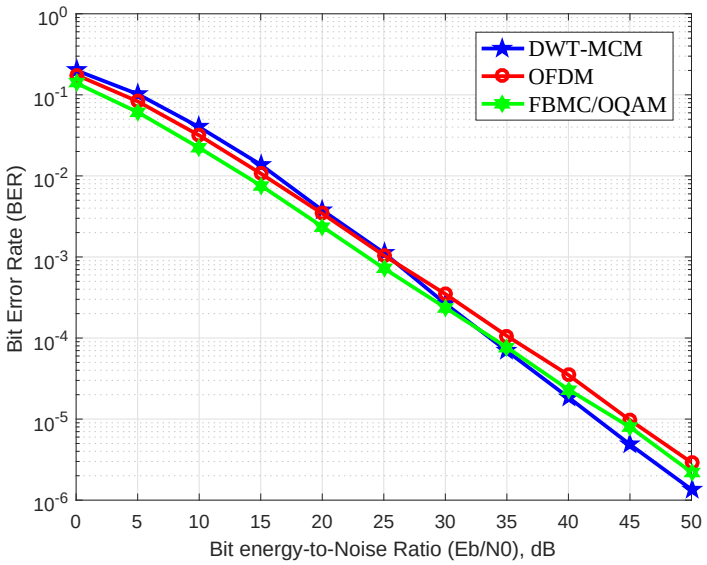

Figure 3.7: BER curves for SISO-OFDM, SISO-FBMC/OQAM, and SISO-DWT-MCM systems using ZF equaliser with 4-QAM modulation over (EVA) LTE channel.

Figures 3.9 and 3.10 show the simulation results of the three systems over the EVA-LTE channel using the MMSE equaliser with 4-QAM and 16-QAM modulations respectively. These figures show that the BER for DWT-MCM is significantly improved compared with OFDM and FBMC/OQAM systems with the MMSE equaliser. This is because the signal spectrum of all wavelet bearers is distributed across the whole channel bandwidth in a similar way to single carrier frequency domain equalisation (SC-FDE) [133], which provides a large diversity advantage on a frequency-selective channel.

Simulation results for the frame error rate (FER) of the three systems can be found in Appendix A.

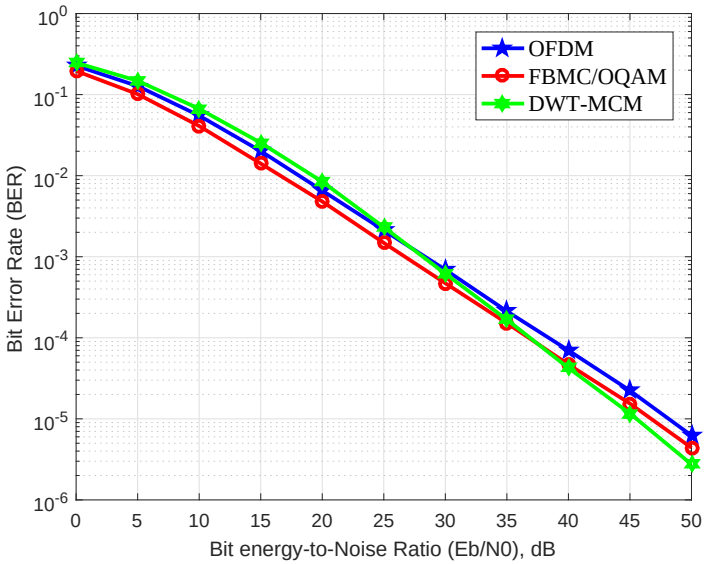

Figure 3.8: Bit error probability curves for SISO-OFDM, SISO-FBMC/OQAM, and SISO-DWT-MCM systems using ZF equaliser with 16-QAM modulation over (EVA) LTE channel.

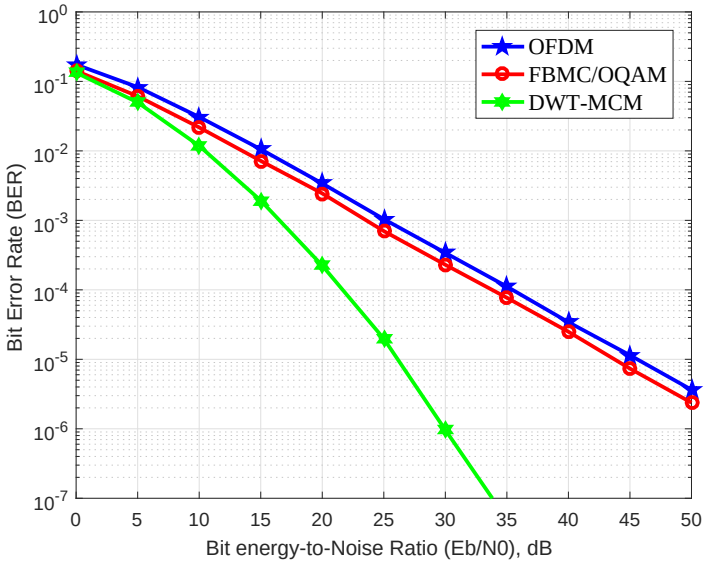

Figure 3.9: BER curves for SISO-OFDM, SISO-FBMC/OQAM, and SISO-DWT-MCM systems using MMSE equaliser with 4-QAM modulation over (EVA) LTE channel.

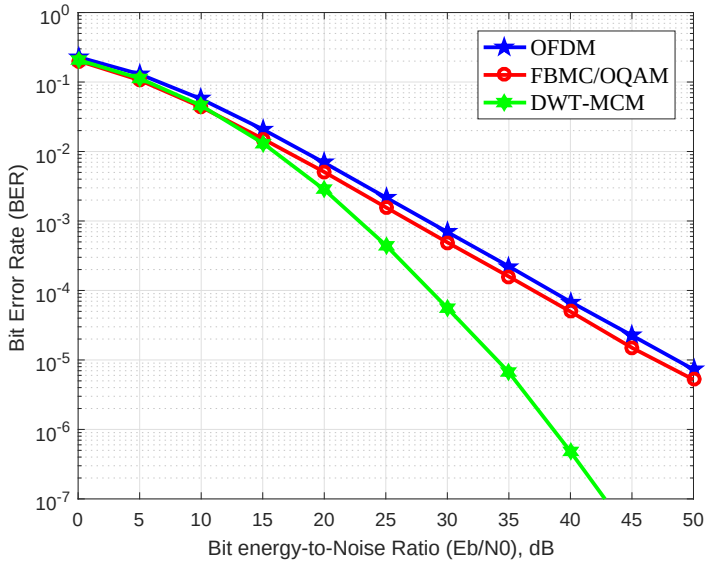

Figure 3.10: BER curves for SISO-OFDM, SISO-FBMC/OQAM, and SISO-DWT-MCM systems using MMSE equaliser with 16-QAM modulation over (EVA) LTE channel.

Figure 3.11 illustrates the simulation results of the bit error probability using 16-QAM and 4-QAM modulation over the EVA channel with wavelet domain equaliser (WDE) and ZF-FDE.

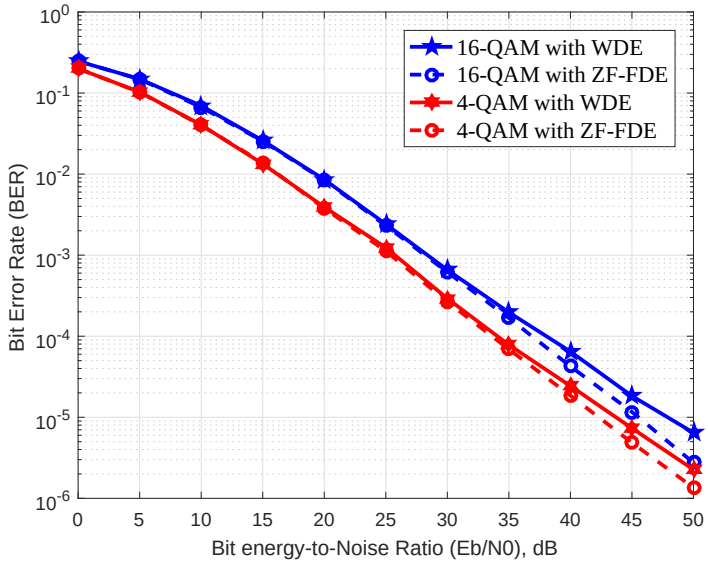

Figure 3.11: BER curves for SISO-DWT-MCM system using WDE and ZF-FDE with 16-QAM and 4-QAM modulation over (EVA) LTE channel.

Figure 3.12 shows the BER performance of the SISO-DWT-MCM system with different levels of Haar wavelet. In this case, MMSE equaliser and 16-QAM modulation over EVA channel. It is clear from this figure that the BER performance is better in the low levels than in high wavelet levels because the higher level wavelets have lower bandwidth, and hence less frequency diversity.

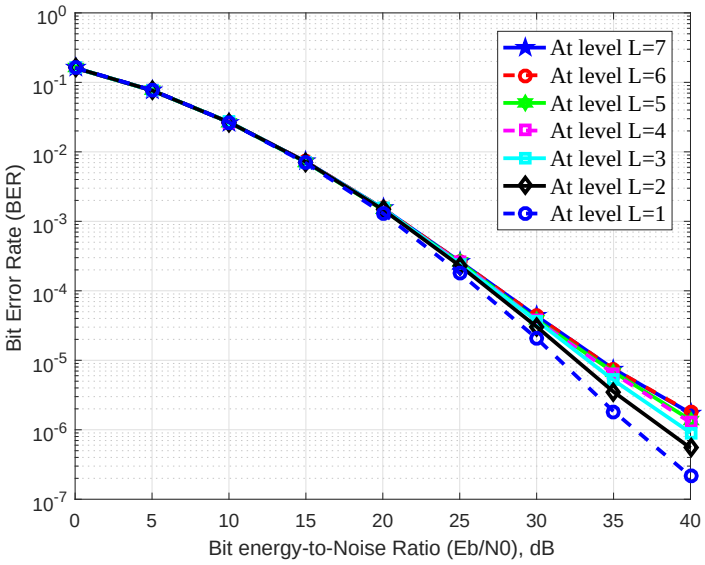

Figure 3.12: BER curves for SISO-DWT-MCM system with different scales levels of Haar wavelet using MMSE equaliser with 16-QAM modulation over (EVA) LTE channel.

Now the IIC scheme is used to improve the performance of these systems with insufficient CP (CP=0). The hard output decisions of the demapper are used to calculate the estimated values of the undesirable components in the received signal. After removing these components, EVD is applied to the resulting signal in the frequency domain. After some iterations, the resulting signal will be improved, giving lower error floor in the BER curves. The results have been obtained with the EPA, EVA, and ETU LTE channels, different values of the Doppler frequency and modulation order as well as with different levels of the decomposition and reconstruction algorithms and different wavelet families in the case of DWT-MCM. For space reasons, some of these results are not included in this chapter.

Figure 3.13 shows the BER simulation results for the uncoded SISO-OFDM system using ZF and MMSE equalisation. Different parameters are used in this figure. 4-QAM

and 16-QAM modulation, 5 Hz and 70 Hz Doppler frequencies, and over the EVA/ETU LTE channel. In this figure, the BER simulation results are compared with the result with perfect channel state information (PCSI). In PCSI, the actual transmitted data is assumed to be known, and used to calculate the interference components and subtract them from the received signal. This means that the PCSI assumes not only perfect channel state knowledge, but also perfect interference cancellation. However, due to the Doppler shift, the resulting time-variant channel is not perfectly known at the receiver. This means that an error floor will appear at high $Eb/N0$ when the Doppler frequency is 70 Hz.

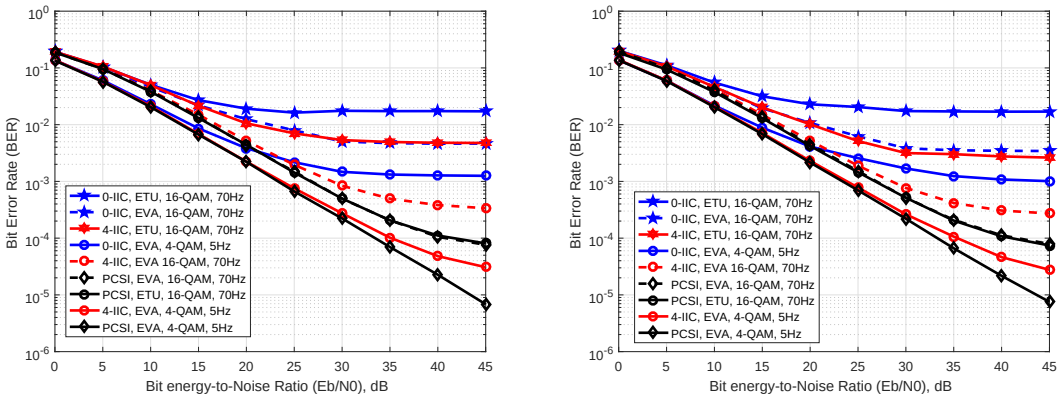

(a) ZF-Equaliser (b) MMSE-Equaliser

Figure 3.13: BER curves for SISO-OFDM system with different modulation orders and Doppler frequencies over EVA/ETU channel. (a) ZF-Equaliser (b) MMSE-Equaliser.

It is clear from this figure that the BER performance have improved after some IIC iterations. The error floor is reduced but not completely removed. The improvements in the BER simulation results of the OFDM system are reduced with the increase of the modulation order, Doppler shift, and the spread of the channel. As shown in Figure 3.13, there remains an error floor in the BER simulation results, though it is reduced by a factor of approximately 41, 14, and 4 with ZF equaliser and by 36, 13, and 6 with MMSE equaliser after four IIC iterations by using 4-QAM with 5 HZ Doppler over EVA channel, 16-QAM with 70 Hz Doppler over EVA channel, and 16-QAM with 70 Hz Doppler over ETU channel respectively, measured at 45 dB $Eb/N0$.

Figures 3.14 and 3.15 show the BER simulation results of the uncoded SISO-FBMC/OQAM and SISO-DWT/MCM respectively. In this part, the Daubechies (db4) wavelet is used with decomposition and reconstruction levels $L = 1$ in the DWT-MCM

system.

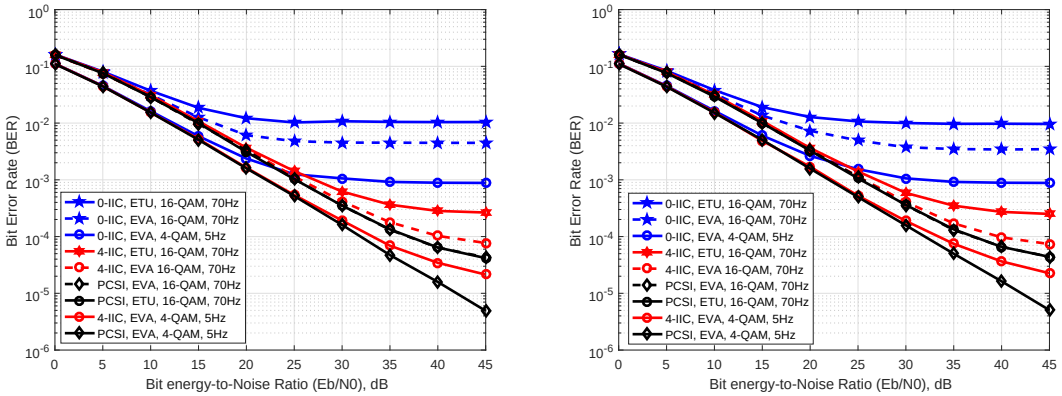

(a) ZF-Equaliser (b) MMSE-Equaliser

Figure 3.14: BER curves for SISO-FBMC/OQAM system with different modulation orders and Doppler frequencies over EVA/ETU channel. (a) ZF-Equaliser (b) MMSE-Equaliser.

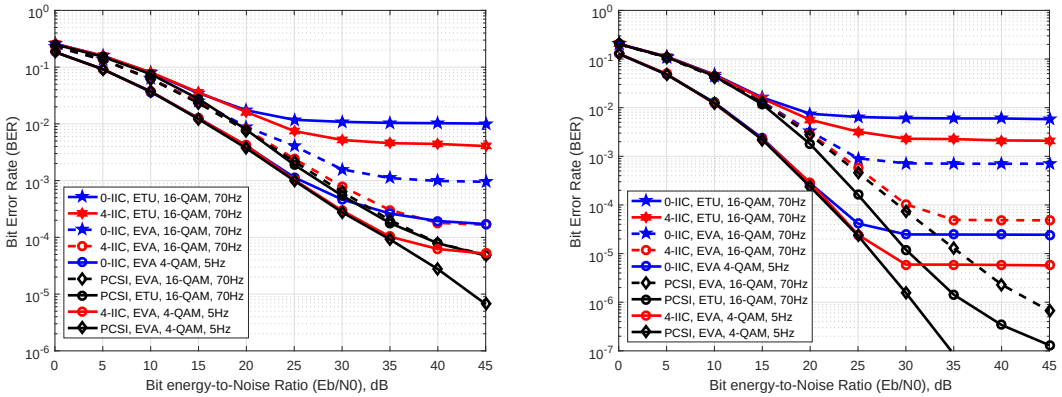

(a) ZF-Equaliser (b) MMSE-Equaliser

Figure 3.15: BER curves for SISO-DWT/MCM system with different modulation orders and Doppler frequencies over EVA/ETU channel using Daubechies (db4) wavelet with L=1. (a) ZF-Equaliser (b) MMSE-Equaliser.

The simulation results of the uncoded OFDM, FBMC/OQAM, and DWT-MCM systems are illustrated in Table 3.3.

Table 3.3: Simulation results for uncoded systems based IIC

System	N_{Fig}	Eq.	IIC-Itrs	R_k	$Eb/N0$ dB	Channel	Doppler Hz	M-QAM
OFDM	3.13	ZF	4	41	45	EVA	5	4-QAM
		ZF	4	14	45	EVA	70	16-QAM
		ZF	4	4	45	ETU	70	16-QAM
		MMSE	4	36	45	EVA	5	4-QAM
		MMSE	4	13	45	EVA	70	16-QAM
		MMSE	4	6	45	ETU	70	16-QAM
FBMC/ OQAM	3.14	ZF	4	41	45	EVA	5	4-QAM
		ZF	4	58	45	EVA	70	16-QAM
		ZF	4	39	45	ETU	70	16-QAM
		MMSE	4	39	45	EVA	5	4-QAM
		MMSE	4	47	45	EVA	70	16-QAM
		MMSE	4	39	45	ETU	70	16-QAM
DWT/ MCM	3.15	ZF	4	3	45	EVA	5	4-QAM
		ZF	4	6	45	EVA	70	16-QAM
		ZF	4	3	45	ETU	70	16-QAM
		MMSE	4	4	45	EVA	5	4-QAM
		MMSE	4	15	45	EVA	70	16-QAM
		MMSE	4	3	45	ETU	70	16-QAM

3.5.2 Coded Systems

Figures 3.16 and 3.17 show the BER simulation results of the LDPC-OFDM and LDPC-FBMC/OQAM systems respectively (*Case I*). In these figures, different modulation orders and Doppler frequency values are used over EVA channel. The error floors are completely removed and significant improvement is noticeable in these figures. In LDPC-OFDM, the $Eb/N0$ gap from the PCSI simulation result becomes approximately 2.5 dB

and 1.2 dB after four IIC iterations with the ZF and MMSE equaliser respectively. By contrast, in the LDPC-FBMC/OQAM, the gap becomes 0.7 dB and 1.2 dB with ZF equaliser and 0.5 dB and 0.75 dB with MMSE equaliser after the fourth IIC iteration by using 4-QAM with 5Hz Doppler, 16-QAM with 70 Hz Doppler respectively over EVA channel, measured at 10^{-6} BER.

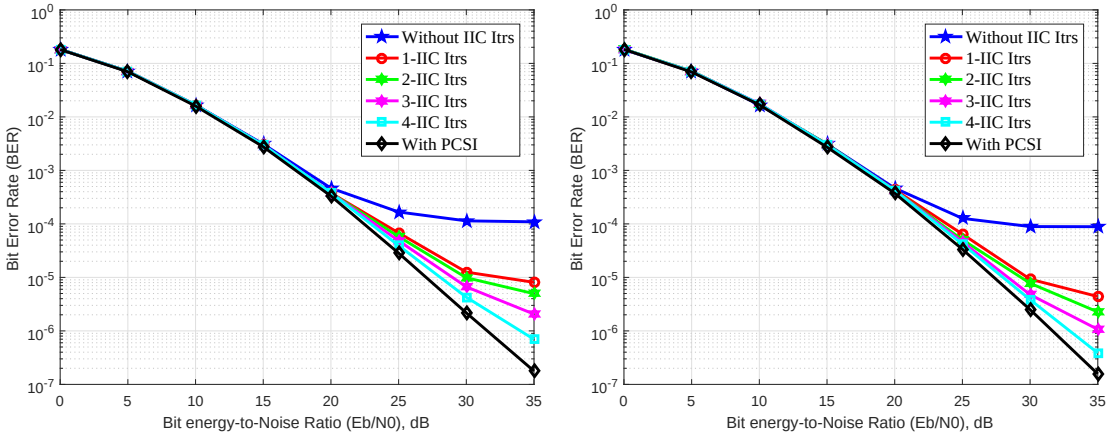

(a) ZF equaliser (b) MMSE equaliser

Figure 3.16: BER performance of the LDPC-OFDM system *Case I* using demapping hard decision output with QPSK at 5Hz Doppler frequency over EVA LTE (a) ZF equaliser (b) MMSE equaliser.

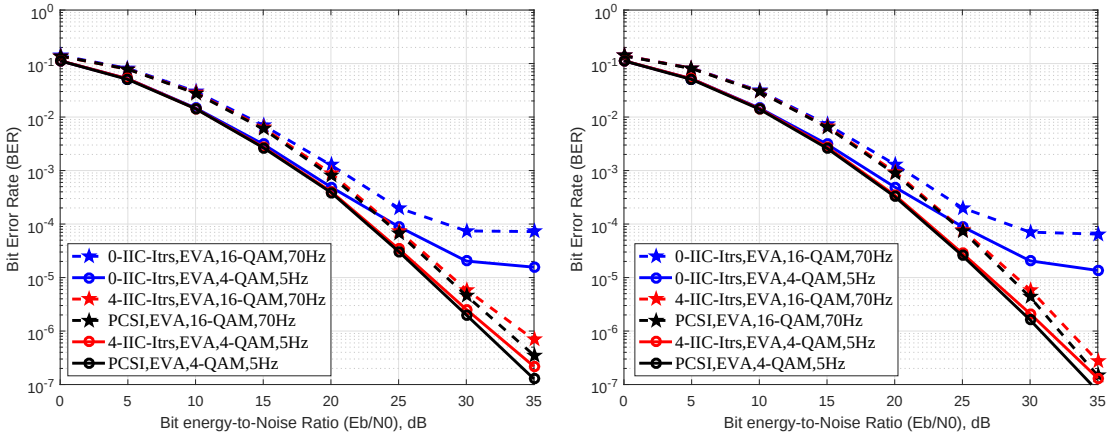

(a) ZF equaliser (b) MMSE equaliser

Figure 3.17: BER performance of the LDPC-FBMC/OQAM system *Case I* using demapping hard decision output with 4-QAM/16-QAM at 5Hz/70Hz Doppler frequency over EVA LTE (a) ZF equaliser (b) MMSE equaliser.

Figures 3.18, 3.19, and 3.20 show the simulation results of the LDPC-OFDM, LDPC-FBMC/OQAM, and LDPC-DWT/MCM systems (*Case I*) with different parameters. In the LDPC-DWT/MCM system, the Daubechies (db4) wavelet is used with decomposition and reconstruction levels $L = 6$. The results and parameters are illustrated in Table 3.4.

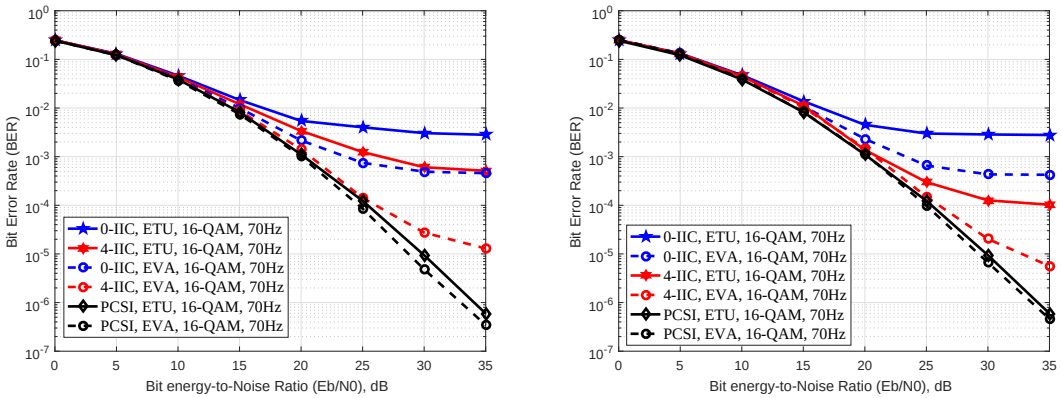

(a) ZF-Equaliser (b) MMSE-Equaliser

Figure 3.18: BER curves for LDPC-OFDM (*Case I*) system with different modulation orders and Doppler frequencies over EVA/ETU channel. (a) ZF-Equaliser (b) MMSE-Equaliser.

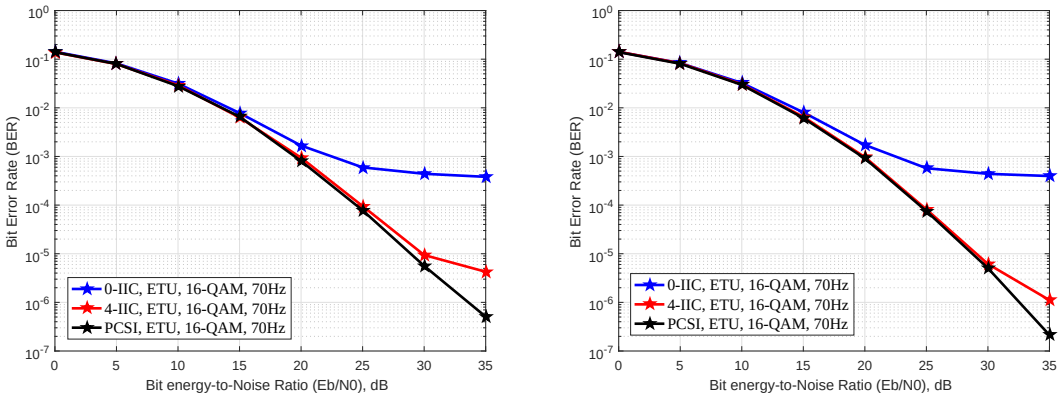

(a) ZF-Equaliser (b) MMSE-Equaliser

Figure 3.19: BER curves for LDPC-FBMC/OQAM (*Case I*) system with different modulation orders and Doppler frequencies over EVA/ETU channel. (a) ZF-Equaliser (b) MMSE-Equaliser.

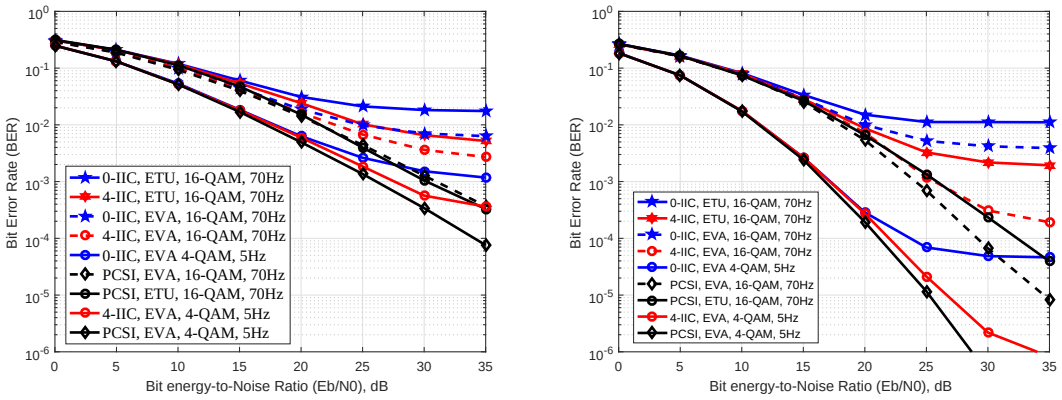

(a) ZF-Equaliser (b) MMSE-Equaliser

Figure 3.20: BER curves for LDPC-DWT/MCM (*Case I*) system with different modulation orders and Doppler frequencies over EVA/ETU channel using Daubechies (db4) wavelet with L=6. (a) ZF-Equaliser (b) MMSE-Equaliser.

Table 3.4: Simulation results for LDPC-MCM systems (*Case I*) based IIC

System	N_{Fig}	Eq.	IIC-Itrs	R_k	$Eb/N0$ dB	Channel	Doppler Hz	M-QAM
OFDM	3.18	ZF	4	35	35	EVA	70	16-QAM
		ZF	4	6	35	ETU	70	16-QAM
		MMSE	4	75	35	EVA	70	16-QAM
		MMSE	4	72	35	ETU	70	16-QAM
FBMC/ OQAM	3.19	ZF	4	90	35	ETU	70	16-QAM
		MMSE	4	356	35	ETU	70	16-QAM
DWT/ MCM	3.20	ZF	4	3	35	EVA	5	4-QAM
		ZF	4	2	35	EVA	70	16-QAM
		ZF	4	3	35	ETU	70	16-QAM
		MMSE	4	56	35	EVA	5	4-QAM
		MMSE	4	20	35	EVA	70	16-QAM
		MMSE	4	6	35	ETU	70	16-QAM

As a conclusion of the first scenario of coded OFDM, DWT/MCM, and FBMC/OQAM systems, according to the above figures, the error floors are reduced by using iterative interference cancellation. With the MMSE equaliser, a significantly better performance is obtained for all systems compared with the ZF equaliser. This is because the main feature with the MMSE equaliser is a considerable increase in diversity order. This occurs because of the combination of coding and MMSE.

In the second scenario of the coded OFDM, DWT/MCM, and FBMC/OQAM systems, the soft output decoded symbols are used to calculate the ICI/ISI interference components in each IIC iteration. Figures 3.21 and 3.22 show the simulation results of the LDPC-OFDM and LDPC-FBMC/OQAM systems (*Case II*). In Figure 3.21, 4-QAM and 16-QAM are used respectively with 5 Hz and 70 Hz Doppler frequency over the EVA channel with the ZF and MMSE equaliser. In Figure 3.22, 4-QAM and 16-QAM are used respectively with 5 Hz and 70 Hz Doppler frequency over the EVA channel and 16-QAM with 70 Hz Doppler shift over ETU channel with use the ZF and MMSE equaliser. As shown in these figures, the error floors are completely removed after four IIC iterations. The simulation results of these figures are discussed in Table 3.5. Where the **Gap** in Table 3.5 refers to the gap from the PCSI simulation results measured in dB at specific BER value.

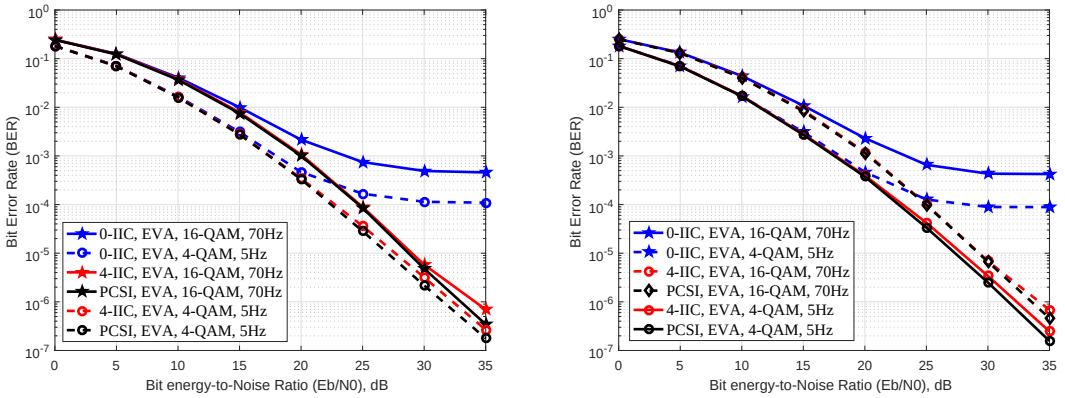

(a) ZF-Equaliser (b) MMSE-Equaliser

Figure 3.21: BER curves for LDPC-OFDM (*Case II*) system with different modulation orders and Doppler frequencies over EVA channel. (a) ZF-Equaliser (b) MMSE-Equaliser.

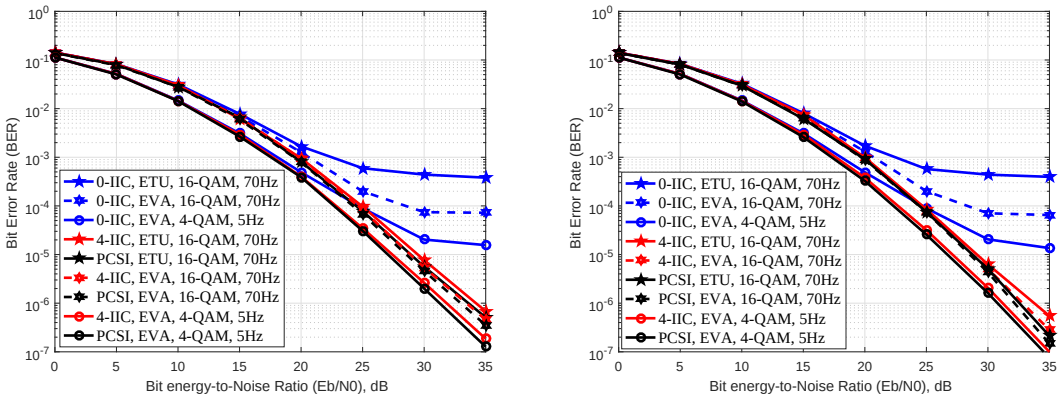

(a) ZF-Equaliser (b) MMSE-Equaliser

Figure 3.22: BER curves for LDPC-FBMC/OQAM (*Case II*) system with different modulation orders and Doppler frequencies over EVA/ETU channel. (a) ZF-Equaliser (b) MMSE-Equaliser.

Table 3.5: Simulation results for LDPC OFDM and FBMC/OQAM systems (*Case II*)

System	N_{Fig}	Eq.	IIC-Itrs	**Gap** dB	BER	Channel	Doppler Hz	M-QAM
OFDM	3.21	ZF	4	0.75	10^{-6}	EVA	5	4-QAM
		ZF	4	1.2	10^{-6}	EVA	70	16-QAM
		MMSE	4	0.6	10^{-6}	EVA	5	4-QAM
		MMSE	4	0.7	10^{-6}	EVA	70	16-QAM
FBMC/ OQAM	3.22	ZF	4	0.5	10^{-6}	EVA	5	4-QAM
		ZF	4	0.6	10^{-6}	EVA	70	16-QAM
		ZF	4	0.8	10^{-6}	ETU	70	16-QAM
		MMSE	4	0.4	10^{-6}	EVA	5	4-QAM
		MMSE	4	0.5	10^{-6}	EVA	70	16-QAM
		MMSE	4	0.8	10^{-6}	ETU	70	16-QAM

Figures 3.23 and 3.24 show the simulation results of the LDPC-OFDM and LDPC-DWT/MCM (*Case II*). In Figure 3.23, the more severe LTE channel is used with 16-QAM and 70 Hz Doppler shift and using the ZF and MMSE equaliser. The simulation results

and parameters of these figures are shown in Table 3.6.

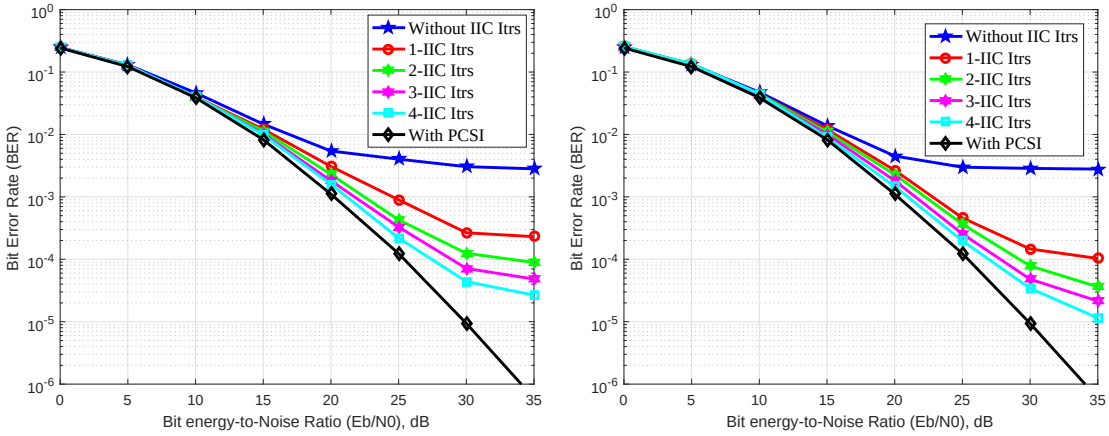

(a) ZF equaliser (b) MMSE equaliser

Figure 3.23: BER performance of the LDPC-OFDM system using soft decoding output with 16QAM at 70Hz Doppler frequency over ETU LTE (a) ZF equaliser (b) MMSE equaliser.

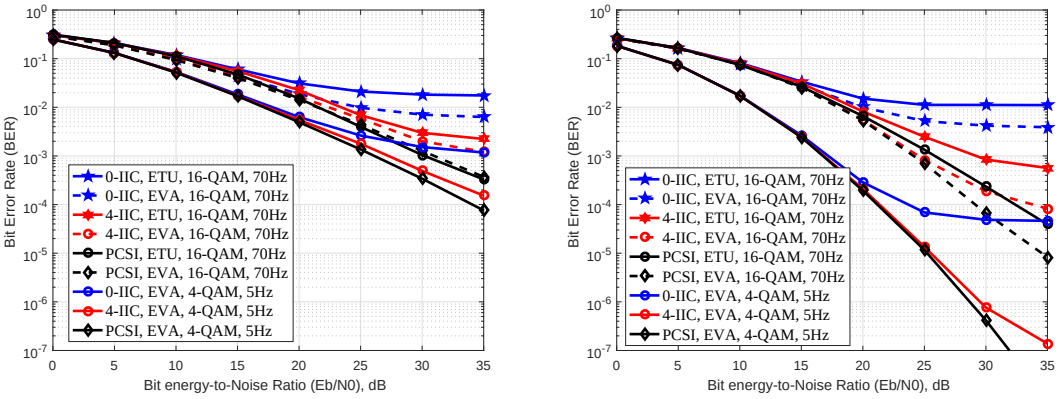

(a) ZF-Equaliser (b) MMSE-Equaliser

Figure 3.24: BER curves for LDPC-DWT/MCM (*Case II*) system with different modulation orders and Doppler frequencies over EVA/ETU channel using Daubechies (db4) wavelet with L=6. (a) ZF-Equaliser (b) MMSE-Equaliser.

Table 3.6: Simulation results for LDPC OFDM and DWT/MCM systems (*Case II*)

System	N_{Fig}	Eq.	IIC-Itrs	R_k	$Eb/N0$ dB	Channel	Doppler Hz	M-QAM
OFDM	3.23	ZF	4	106	35	ETU	70	16-QAM
		MMSE	4	243	35	ETU	70	16-QAM
DWT/ MCM	3.24	ZF	4	8	35	EVA	5	4-QAM
		ZF	4	5	35	EVA	70	16-QAM
		ZF	4	8	35	ETU	70	16-QAM
		MMSE	4	334	35	EVA	5	4-QAM
		MMSE	4	47	35	EVA	70	16-QAM
		MMSE	4	20	35	ETU	70	16-QAM

As a conclusion of the second scenario of coded-MCM systems, and based on the above figures and tables, the simulation results were significantly improved through using the iterative interference cancellation. The error floors were completely removed over the EVA channel in the LDPC-OFDM system. However, with the use of the ETU channel the error floors were reduced but not completely removed. In the LDPC-DWT/MCM, the error floors were reduced but not completely removed. In contrast, in the LDPC-FBMC/OQAM systems, the error floors were completely removed over the EVA and ETU channels. The error floors have been removed more easily (with fewer iterations) in FBMC compared with that of OFDM. This is probably because in OFDM, the spectrum of each modulated subcarrier is much wider. Thus the ICI extends over many subcarriers. In FBMC, however, the filtering greatly reduces the bandwidth of the subcarriers. This means that the ICI only extends over the adjacent subcarrier. This seems to make it easier for the iterative process to correct symbol errors by exploiting *a priori* information from the adjacent subcarriers.

3.6 Summary

This chapter can be summarised as follows:

- The effect of the multipath propagation on the transmitted signal was explained for SISO-OFDM system with sufficient and insufficient CP.
- An iterative interference cancellation (IIC) scheme has been presented for SISO OFDM, FBMC/OQAM, and DWT/MCM systems. The undesirable components in the received signal were calculated in different scenarios to reduce the ICI/ISI interference. IIC can reduce or remove the error floor with insufficient CP for all the three systems. In FBMC/OQAM systems, more significant improvement can be achieved than that for the other systems due to the use of a much longer and smoother filter response in the time domain which greatly reduces the side lobes and therefore reduces the potential for ICI. In general, we may conclude that a significant improvement can be achieved by using IIC.
- In uncoded SISO OFDM, FBMC/OQAM, and DWT/MCM systems, the ICI/ISI interference components have been calculated directly from the hard output of the de-mapper. In contrast, in coded systems, the simulation results have been discussed in two scenarios. First, the ICI/ISI interference components have been calculated from the hard decision output of the de-mapper and on the last IIC iteration the soft decision de-mapper output is interleaved and used as an input to the LDPC decoder.

Chapter 4

Wiener Filter Channel Estimation based IIC-MCM

Contents

4.1 Introduction

In wireless communication systems, the retrieving of the information with great accuracy is very challenging and is highly dependent on the precision of the estimated value of the CSI. In the previous chapter, it is assumed that CSI is known at the receiver. However, in practice, it is very important to obtain the accurate value of the CSI by means of channel estimation. IIC based iterative decoding is used to achieve better channel estimation [119–

124]. SISO and MIMO-OFDM system performance is significantly improved by using a parametric model (PM) channel estimation based LDPC iterative receiver [134]. In Bluetooth time division duplex (TDD) frame (short frame), one dimensional (1-D) Wiener filter channel estimation is used for OFDM based cognitive radio (CR) transmission [135]. However, in long frames, the 1-D Wiener filter channel estimation lost its robustness against the time-variant channel. In single and multi-channel, the Wiener filter is used to estimate the coefficients of the complex short-time Fourier transform (STFT) to achieve noise reduction in the STFT domain [136]. 2-D Wiener filter channel estimation is used to improve the estimated coefficients of the channel when the spaced-frequency and spaced-time correlation function is known [137–140].

In OFDM systems, blind and data/pilot-aided channel estimation techniques have been proposed [141–143]. In the FBMC/OQAM scheme, the channel estimation issue is different due to the intrinsic imaginary interference where the orthogonality conditions only depend on the real components [48]. Preamble-based channel estimation [62, 144, 145] and scattered pilot-based channel estimation [69, 146, 147] have been presented for FBMC/OQAM system. There are different structures of preamble based channel estimation; Pairs of Pilots (POP), Real Interference Approximation Method (IAM-R), Complex IAM (IAM-C), and Extended IAM-C (E-IAM-C) techniques. In each scheme, different structures for used and unused pilots (zero subcarriers) are inserted at known positions at the receiver as shown in Figure 4.1.

In this chapter, pilot-aided Wiener filter channel estimation will be used for both SISO OFDM and FBMC/OQAM systems. Scattered pilots are used to calculate the coefficients of the Wiener filter to estimate the channel for both OFDM and FBMC/OQAM systems. Furthermore, the IAM preamble is used to estimate the coefficients of the channel of the FBMC/OQAM system.

The rest of this chapter is organised as follows: In Section 4.2 a system model of IIC based channel estimation is introduced. In Section 4.3 Wiener filter channel estimation is introduced. Scattered and preamble pilots based Wiener filter channel estimation is described in Section 4.4. Simulation results are given in Section 4.6. Finally, a summary of this chapter is presented in Section 4.7.

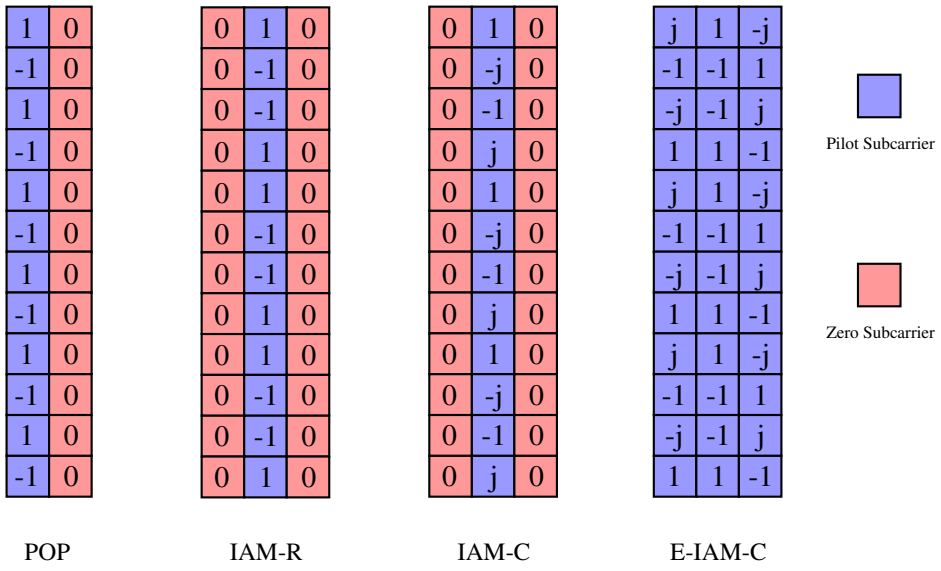

Figure 4.1: POP, IAM-R, IAM-C, and E-IAM-C preamble structures.

4.2 System Model

The IIC scheme is presented in Section 3.2 of Chapter 3 where the CSI is assumed to be known at the receiver. However, in practice the CSI is unknown at the receiver, the channel estimation is crucial at the receiver of the broadband communication systems. As in Chapter 3, the received signal can be represented as in (3.3). The estimated values of the undesirable components $\hat{\mathbf{H}}_{ICI}\hat{\mathbf{x}}_k$ and $\hat{\mathbf{H}}_{ISI}\hat{\mathbf{x}}_{k-1}$ can be calculated from the estimated decoded signal and estimated value of the coefficients of the channel. In this chapter, the channel estimation is repeated after each IIC iteration as shown in Figure 4.2. Figure 4.2 shows the receiver side of the iterative channel estimation of the LDPC-FBMC/OQAM system using Wiener filter channel estimation. AFB, SFB, and WF represent respectively the analysis filter bank, synthesis filter bank, and Wiener filter channel estimation. After some iterations, the estimated received signal can be expressed as:

$$\hat{\mathbf{y}}_k = \hat{\mathbf{H}}_{CIRC}\hat{\mathbf{x}}_k + \tilde{\eta}_k \tag{4.1}$$

The received signal in the frequency domain can be represented as:

$$\hat{\mathbf{Y}}_k = F\hat{\mathbf{H}}_{CIRC}F^{\mathbf{H}}\hat{\mathbf{X}}_k + F\tilde{\eta}_k \tag{4.2}$$

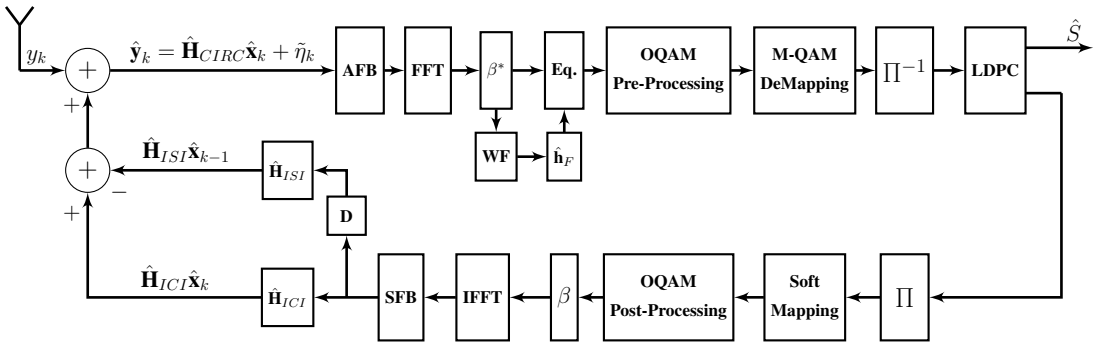

Figure 4.2: Receiver side of the iterative channel estimation of the LDPC-FBMC/OQAM system using Wiener filter channel estimation.

According to the eigenvalue decomposition (EVD) of the circulant matrix [132] i.e. $\hat{\mathbf{H}}_{CIRC} = F^{\mathbf{H}}\hat{\mathbf{H}}F$, the estimated received signal in the frequency domain can be expressed as:

$$\hat{\mathbf{Y}}_k = \hat{\mathbf{H}}\hat{\mathbf{X}}_k + \eta_k \tag{4.3}$$

where $\hat{\mathbf{H}} \in \mathbb{C}^{N\times N}$ constitutes a diagonal matrix that comprises the estimated values of the CFR along its diagonal components.

Channel matrices $\hat{\mathbf{H}}_{ICI}$, $\hat{\mathbf{H}}_{ISI}$ can be expressed as:

$$\hat{\mathbf{H}}_{ISI} = \begin{bmatrix} 0_{E\times(N-E)} & \hat{\mathbf{H}}_1 \\ 0_{(N-E)\times(N-E)} & 0_{(N-E)\times E} \end{bmatrix} \tag{4.4}$$

$$\hat{\mathbf{H}}_{ICI} = \begin{bmatrix} 0_{E\times(N-E-N_{cp})} & \hat{\mathbf{H}}_1 & 0_{E\times N_{cp}} \\ 0_{(N-E)\times(N-E-N_{cp})} & 0_{(N-E)\times E} & 0_{(N-E)\times N_{cp}} \end{bmatrix} \tag{4.5}$$

where E represents the excess channel length over the CP, $E = L_c - N_{cp} - 1$ and L_c and N_{cp} respectively represent the length of the channel and the number of the CP samples. The interference originating with matrix $\hat{\mathbf{H}}_1 \in \mathbb{C}^{E\times E}$ depends mainly on the estimated channel value $\hat{\mathbf{h}}$ and can be represented as:

$$\hat{\mathbf{H}}_1 = \begin{bmatrix} \hat{\mathbf{h}}_{L_c-1} & \cdots & \cdots & \hat{\mathbf{h}}_{N_{cp}-1} \\ 0 & \ddots & & \vdots \\ \vdots & \ddots & \ddots & \vdots \\ 0 & \cdots & 0 & \hat{\mathbf{h}}_{L_c-1} \end{bmatrix} \tag{4.6}$$

in the case of $N_{cp} = 0$, $\hat{\mathbf{H}}_{ICI} = \hat{\mathbf{H}}_{ISI}$. Also, $\hat{\mathbf{H}}_{ICI} = \hat{\mathbf{H}}_{ISI} = 0$ with sufficient CP.

4.3 Wiener Filter Channel Estimation

The Wiener filter is a filter or channel interpolation method which is used to estimate a desired signal from an unknown signal. Due to the strong correlation of the channel in both time and frequency not all sub-carriers need be exploited for channel estimation: hence pilot QAM symbols are spaced at intervals in time and frequency. Exploiting both time and frequency correlation provides a smoothing and prediction filter [148, 149].

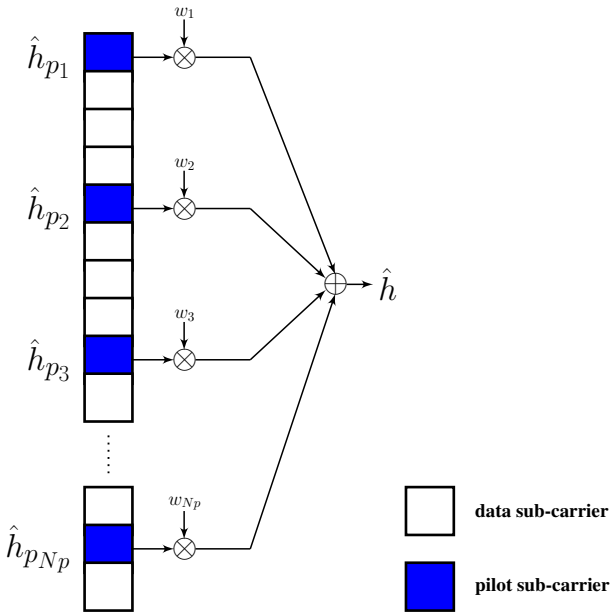

Figure 4.3: Wiener filtering.

In general, the number of taps of the Wiener filter depends on the number of pilot symbols N_p as shown in Figure 4.3. The estimated channel vector $\hat{\mathbf{h}}$ can be obtained as follows:

$$\hat{\mathbf{h}} = \mathbf{W}\hat{\mathbf{h}}_p \tag{4.7}$$

where $\mathbf{W}$ and $\hat{\mathbf{h}}_p$ represent respectively the $N_d \times N_p$ Wiener filter interpolation matrix, and the $N_p \times 1$ LS vector of the N_p channel estimates at the pilot positions, where N_d is

the number of data positions in the frame. $\hat{\mathbf{h}}_p$ and $\mathbf{W}$ are given by

$$\hat{\mathbf{h}}_p = \begin{bmatrix} \frac{Y_1}{X_1} & \frac{Y_2}{X_2} & \dots & \frac{Y_{N_p}}{X_{Np}} \end{bmatrix} \tag{4.8}$$

$$\mathbf{W} = \mathbf{R}_{dp}\mathbf{R}_{\hat{p}\hat{p}}^{-1} \tag{4.9}$$

where Y and X represent the received and transmitted pilots respectively; $\mathbf{R}_{dp}$ is a $N_d \times N_p$ matrix containing cross correlations between data symbol positions and pilot symbol positions; $\mathbf{R}_{\hat{p}\hat{p}}$ is a $N_p \times N_p$ matrix containing auto-correlations between pilot symbol positions. According to [137], $\mathbf{R}_{\hat{p}\hat{p}}$ can be written as:

$$\mathbf{R}_{\hat{p}\hat{p}} = \mathbf{R}_{pp} + \frac{\beta}{\mathbf{SNR}_p}\mathbf{I}_{N_p} \tag{4.10}$$

where $\mathbf{R}_{pp}$ is a $N_p \times N_p$ matrix containing auto-correlations between pilot symbol positions; $\mathbf{I}_{N_p}$ is a $N_p \times N_p$ identity matrix and β is a constant depending on the signal constellation (β equals 1 and 17/9 for 4-QAM and 16-QAM respectively); $\mathbf{SNR}_p$ denotes the pilot symbol power E_s versus the noise power σ_n^2.

From (4.9) and (4.10), $\mathbf{W}$ and $\hat{\mathbf{h}}$ can be expressed as:

$$\mathbf{W} = \mathbf{R}_{dp}\left(\mathbf{R}_{pp} + \frac{\beta}{\mathbf{SNR}_p}\mathbf{I}_{N_p}\right)^{-1} \tag{4.11}$$

$$\hat{\mathbf{h}} = \mathbf{R}_{dp}\left(\mathbf{R}_{pp} + \frac{\beta}{\mathbf{SNR}_p}\mathbf{I}_{N_p}\right)^{-1}\hat{\mathbf{h}}_p \tag{4.12}$$

In 2D estimation, the cross and auto-correlation matrices are calculated using the product of the channel time and frequency correlations R_{hh}^t and R_{hh}^f

$$R_{hh}^t = E\{h(t_1)h^*(t_2)\} \tag{4.13}$$

$$R_{hh}^f = E\{h(f_1)h^*(f_2)\} \tag{4.14}$$

The autocorrelation matrices in frequency and time are defined by the power delay profile of the LTE channel [150] and Jakes' model [97] respectively.

4.4 FBMC/OQAM Channel Estimation

In SISO-OFDM, scattered pilot based channel estimation is used to estimate the coefficients of the channel. Figure 4.4 represents the scattered pilots according to LTE standard and shows the pilots and data symbol positions for each subframe. According to these positions, the Wiener filter interpolation matrix $\mathbf{W}$ will be calculated as in Eq. 4.11. In OFDM systems, pilots are inserted after the M-QAM modulation. At the receiver, the received pilots are extracted from the received signal in the frequency domain. The estimated value of the LS vector $\hat{\mathbf{h}}_p$ can be calculated using the received pilots as in Eq. 4.8. The Wiener filter interpolation matrix $\mathbf{W}$ and LS vector $\hat{\mathbf{h}}_p$ are used to calculated the coefficients of the channel before the M-QAM demodulator as in Eq. 4.12.

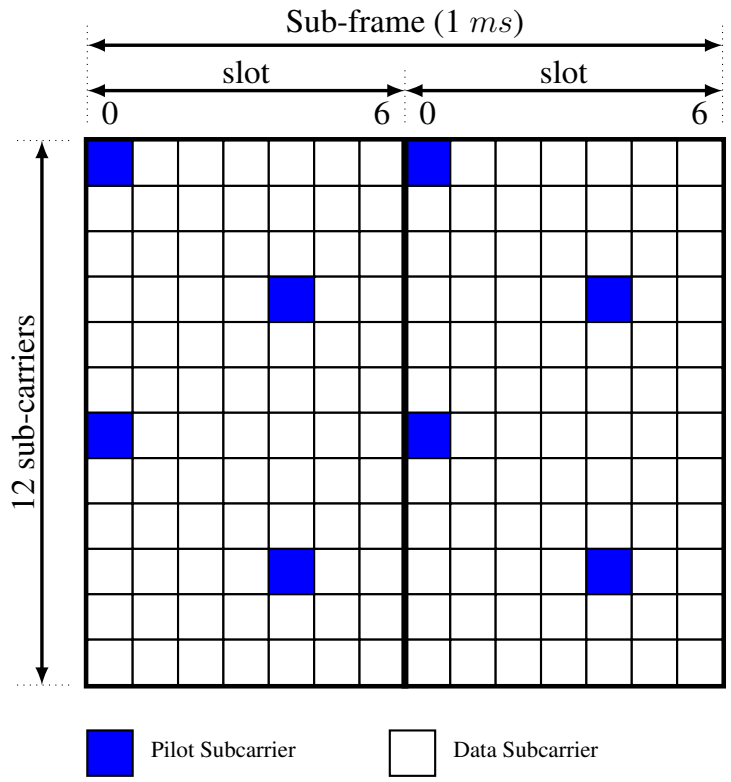

Figure 4.4: Pilot and data symbols positions for each subframe in SISO-OFDM-FFT system.

In the case of data-aided channel estimation, the Wiener filter interpolation matrix $\mathbf{W}$

and the estimated value of the coefficients of the channel $\hat{\mathbf{h}}$ can be calculated as:

$$\mathbf{W} = \mathbf{R}_{(N_p+N_d)\times(N_p+N_d)} \left(\mathbf{R}_{(N_p+N_d)\times(N_p+N_d)} + \frac{\beta}{\mathbf{SNR}_{p+d}} \mathbf{I}_{N_p+N_d} \right)^{-1} \tag{4.15}$$

$$\hat{\mathbf{h}} = \mathbf{W}\hat{\mathbf{h}}_{p+d} \tag{4.16}$$

where $\mathbf{R}_{(N_p+N_d)\times(N_p+N_d)}$ represents the autocorrelation matrix between all pilot and data positions and $\hat{\mathbf{h}}_{p+d}$ are the channel LS estimator at all pilots and data positions.

In this case, a large number of taps in the Wiener filter in the iterative process lead to high receiver complexity. For that reason, pilot-aided channel estimation will be used in this chapter.

In SISO-FBMC/OQAM systems, scattered and preamble pilots are used to estimate the channel coefficients. Figure 4.5 represents the scattered pilots and shows the pilots and data symbol positions for each subframe in the SISO-FBMC/OQAM system.

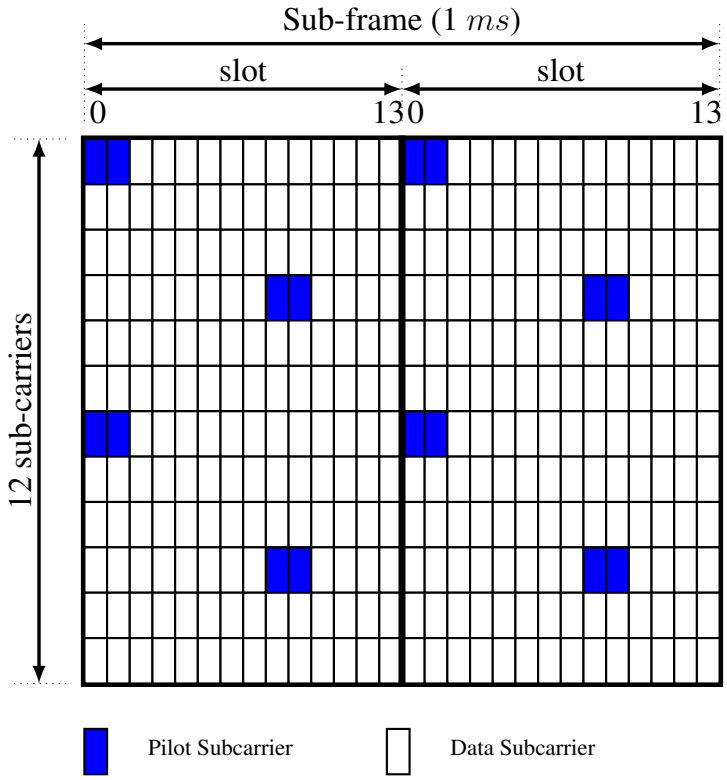

Figure 4.5: Pilot and data symbols positions for each subframe in FBMC/OQAM system.

In the case of scattered pilots, pilots are inserted after M-QAM modulation as in the OFDM system. Each pilot is separated into its in-phase and quadrature components due to OQAM pre-processing as shown in Figure 4.5. To reduce the effect of the intrinsic interference, the locations of in-phase and quadrature components of each pilot are used to calculate the Wiener filter interpolation matrix $\mathbf{W}$ and LS vector $\hat{\mathbf{h}}$. $\mathbf{W}$ and $\hat{\mathbf{h}}$ are used to calculate the estimated value of the coefficients of the channel before the OQAM post-processing. Therefore, the OQAM symbols can be detected by taking the real value after the channel estimation and equalisation.

In the case of preamble pilots, known preamble based channel estimation has been studied [62], and different preamble structures have been demonstrated for both single-antenna and multiple antenna FBMC/OQAM systems. In [144], two preamble-based methods for channel estimation have been introduced for the FBMC/OQAM system, and the performance of the system has been analysed in the absence of Doppler spread and synchronization errors.

The IAM preamble is used in the SISO-FBMC/OQAM system as shown in Figure 4.6. Pilot preambles are inserted directly after the OQAM pre-processing and the channel coefficients are calculated before OQAM post-processing and then take the real values of the estimated signal to detect the QAM symbols. In this case, the channel estimation with IAM preambles will be discussed in different scenarios with different values of the MDS.

- *Case I:* One IAM preamble pilot is inserted in each slot of the FBMC sub-frame as shown in Figure 4.6. In this case, the symbol duration is (0.5/17 *m*sec) with the duration between the pilot symbols (0.5×16/17 *m*sec - 14-FBMC data symbols and 2-unused symbols).
- *Case II:* Two IAM preambles are inserted in each slot of the FBMC sub-frame. In this case, the symbol duration is (0.5/20 *m*sec) and the duration between the pilot symbols is (0.5×9/20 *m*sec - 7-FBMC data symbols and 2-unused symbols).
- *Case III:* Three IAM preambles are inserted in each slot of the FBMC sub-frame. In this case, the symbol duration is (0.5/23 *m*sec) and the duration between the pilot symbols is (0.5×6/23 *m*sec - 4-FBMC data symbols and 2-unused symbols).

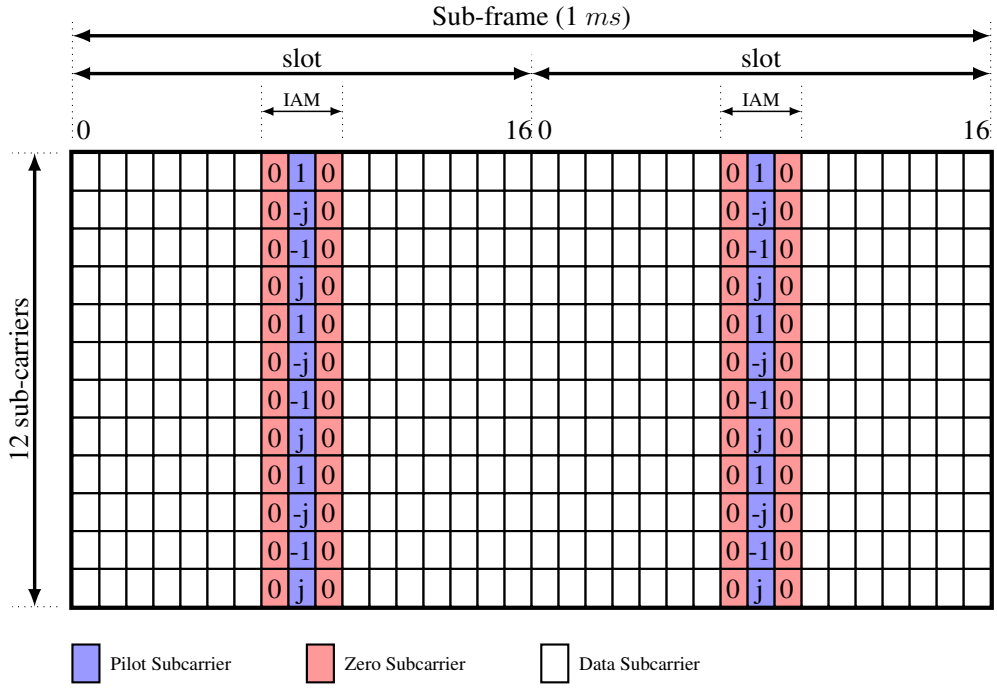

Figure 4.6: Pilot and data symbols positions for each subframe in SISO-FBMC/OQAM system using 1-IAM preamble per slot.

In the channel estimation, the average error within the transmitted block is called a mean square error (MSE). The MSE of the above channel estimation is calculated by

$$MSE = E\{|\mathbf{h} - \hat{\mathbf{h}}|^2\} \tag{4.17}$$

where $\mathbf{h}$ and $\hat{\mathbf{h}}$ contains the actual and estimated channel coefficients respectively.

4.5 Computational Complexity

To calculate the computational complexity of the Wiener filter channel estimation with scattered pilots, it is necessary to calculate the number of real multiplications and additions. However the additions operation is cheaper to implement than multiplications, and hence the complexity analysis will be based on the number of multiplication operations in this chapter. The Wiener filter interpolation matrix $\mathbf{W}$ needs to be calculated only once per block. This means that the complexity of $\mathbf{W}$ does not change with the IIC

scheme. In (4.11), the dimensions of $\mathbf{R}_{dp}$, $\mathbf{R}_{pp}$, and $\frac{\beta}{\mathbf{SNR}_p}\mathbf{I}_{Np}$ are $N_d \times N_p$, $N_p \times N_p$, and $N_p \times N_p$ respectively. Consider one multiplication operation between $\frac{\beta}{\mathbf{SNR}_p}$ and $\mathbf{I}_{Np}$, one inverse operation $(\mathbf{R}_{pp} + \frac{\beta}{\mathbf{SNR}_p}\mathbf{I}_{Np})^{-1}$, and one multiplication operation between $\mathbf{R}_{dp}$ and $(\mathbf{R}_{pp} + \frac{\beta}{\mathbf{SNR}_p}\mathbf{I}_{Np})^{-1}$. Then, the complexity of the multiplication between $\frac{\beta}{\mathbf{SNR}_p}$ and $\mathbf{I}_{Np}$ is $\mathcal{O}(N_P)$ operations, the inverse operation is $\mathcal{O}(N_P^3)$, and the matrix multiplication between $\mathbf{R}_{dp}$ and $(\mathbf{R}_{pp} + \frac{\beta}{\mathbf{SNR}_p}\mathbf{I}_{Np})^{-1}$ is $\mathcal{O}(N_P N_{dp}^2)$. Therefore, the complexity of the Wiener filter interpolation matrix of the OFDM system can be written as:

$$\mathcal{O}_{\mathbf{W}-OFDM} = N_p^3 + N_p(N_{dp}^2 + 1) \tag{4.18}$$

In FBMC/OQAM system, each data and pilot symbol is separated into its in-phase and quadrature components. Then, the complexity of the Wiener filter interpolation matrix compared with OFDM system can be expressed as:

$$\mathcal{O}_{\mathbf{W}-FBMC/OQAM} = 8N_p^3 + 2N_p(2N_{dp}^2 + 1) \tag{4.19}$$

With tentative Wiener filter channel estimation, the coefficients of the channel need to be calculated in each IIC iteration. This means that the complexity will be increased with uses of the IIC scheme. In (4.12), the dimensions of $\mathbf{W}$ and $\hat{\mathbf{h}}_p$ are $N_d \times N_p$ and $N_p \times 1$ respectively. There is one multiplication operation between $\mathbf{W}$ and $\hat{\mathbf{h}}_p$ whose complexity is $\mathcal{O}(N_d N_P)$. Therefore, after $N_{IIC-Itrs}$ IIC iterations, the complexity of the Wiener filter channel estimation for both systems can be written as:

$$\mathcal{O}_{OFDM} = \mathcal{O}_{\mathbf{W}-OFDM} + N_{IIC-Itrs}(N_d N_p) \tag{4.20}$$

$$\mathcal{O}_{FBMC/OQAM} = \mathcal{O}_{\mathbf{W}-FBMC/OQAM} + N_{IIC-Itrs}(4N_d N_p) \tag{4.21}$$

4.6 Simulation Results

The simulation performance of the Wiener filter channel estimation based scattered/preamble pilots of the LDPC-OFDM and LDPC-FBMC/OQAM systems is evaluated using the simulation parameters which are defined and illustrated in Table 4.1. The PDPs for the EPA, EVA, and ETU types of the LTE channel are presented in Table 2.1.

Table 4.1: Simulation Parameters Definition

Parameters	Definitions	Specifications
N	Total number of sub-carriers (used & unused)	128
N_{RB}	Number of resource blocks	6
N_{Sc-RB}	Number of sub-carriers per resource block	12
N_{Sc}	Number of used sub-carriers	$N_{Sc-RB} \times N_{RB}$
N_{slot}	Number of slots per resource block	2
N_{sym}	Number of symbols per slot	7 (OFDM) 14 (FBMC/OQAM) 17 (IAM case I) 20 (IAM case II) 23 (IAM case II)
N_s	Total number of symbols per resource block	$N_{sym} \times N_{slot}$
N_{cp}	Length of cyclic prefix (in samples)	0
M-QAM	Modulation type	4-QAM 16-QAM
S_s	Sub-carrier spacing (KHz)	15 KHz
F_s	Sampling frequency	$S_s \times N$
LTE	Type of LTE channel	EVA
H_{LDPC}	Parity check matrix of LDPC code	$[960, 1920]$ (4-QAM) $[1920, 3840]$ (16-QAM) $[1008, 2016]$ (4-QAM-IAM) $[2016, 4032]$ (4-QAM-IAM)

Figures 4.7 and 4.8 show BER simulation results for the LDPC-OFDM and LDPC-FBMC/OQAM systems using scattered pilot based Wiener filter channel estimation. In these figures, different modulation orders, Doppler frequencies are used for both systems over EVA/ETU LTE channel using ZF equaliser.

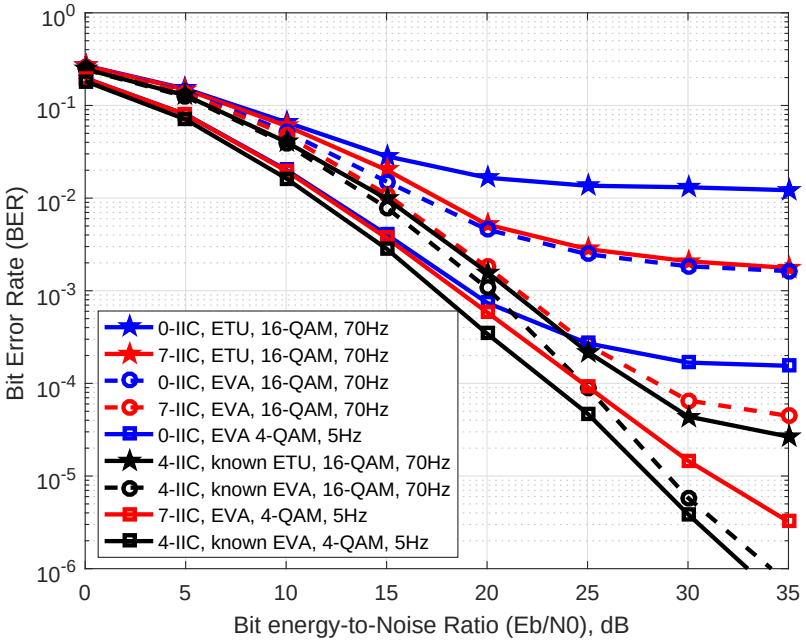

Figure 4.7: BER curves for LDPC-OFDM system with different modulation orders and Doppler frequencies over EVA/ETU channel using scattered pilot based Wiener filter channel estimation with ZF equaliser.

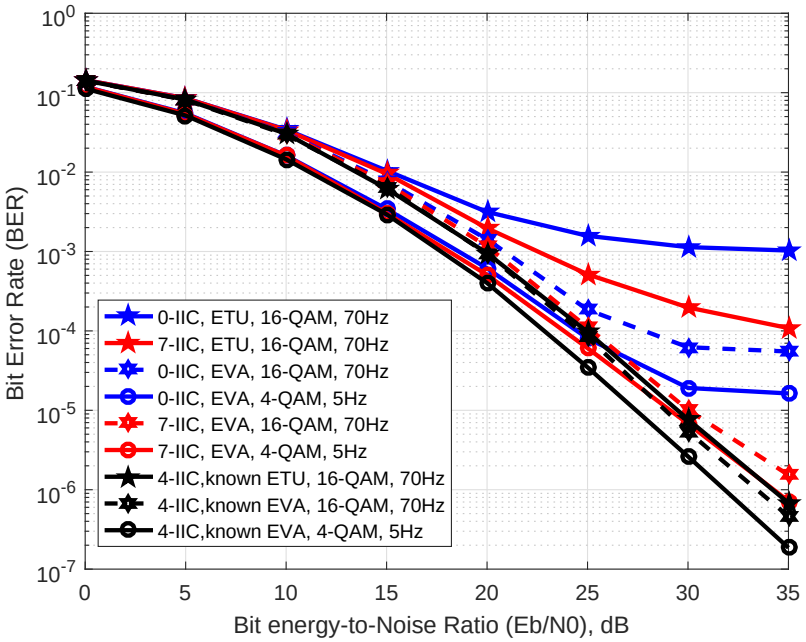

Figure 4.8: BER curves for LDPC-FBMC/OQAM system with different modulation orders and Doppler frequencies over EVA/ETU channel using scattered pilot based Wiener filter channel estimation with ZF equaliser.

Figures 4.9 and 4.10 show simulation results for the LDPC-OFDM and LDPC-FBMC/OQAM systems using an MMSE equaliser with scattered pilot based Wiener filter channel estimation with the same parameters which are used with the ZF equaliser.

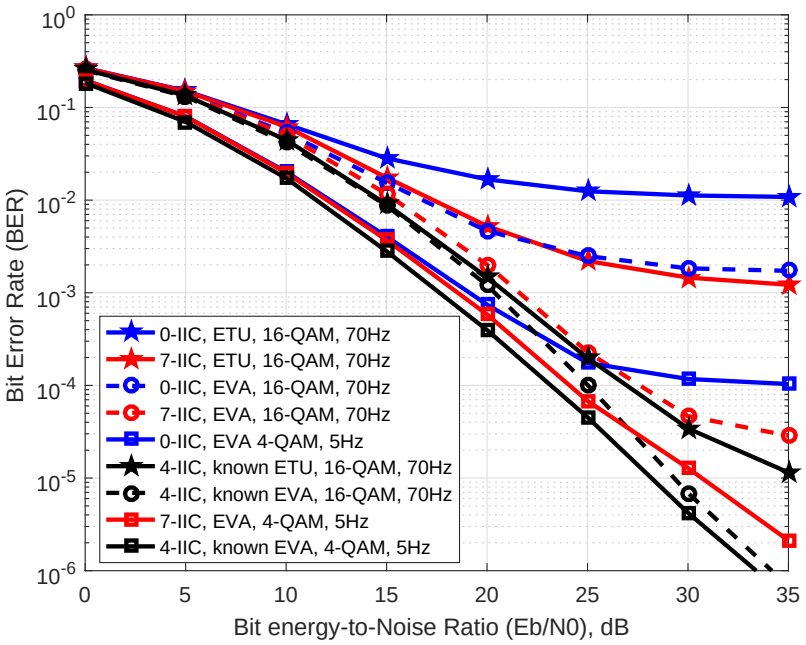

Figure 4.9: BER curves for LDPC-OFDM system with different modulation orders and Doppler frequencies over EVA/ETU channel using scattered pilot based Wiener filter channel estimation with MMSE equaliser.

As shown in these figures, the performance of both systems is significantly improved after 7-IIC iterations using Wiener filter channel estimation. However, the error floors are eliminated in LDPC-OFDM system with 4-QAM and the EVA channel, while the use of high modulation order and severe channels lead to an irreducible error floor in the simulated BER. In LDPC-FBMC/OQAM systems, the error floors are removed with EVA channel, while it still exist with the use of ETU channel. Furthermore, the simulation results are compared with the case of using 4-IIC iteration with perfectly known channel at the receiver. With perfectly known channel at the receiver, we have done less IIC iteration than that with the channel estimation. In the perfect knowledge case, It is converge by 4 IIC iterations and any more iterations do not make any difference. In contrast, up tp 7-IIC iterations are required with the case of channel estimation. In OFDM system, these is a significant difference between the simulations results of the case of perfect knowledge and channel estimation. In case of perfect knowledge, with 4-IIC iterations, the error

floors are reduced by a factor larger than that of using 7-IIC iteration channel estimation. With use 4-QAM over the EVA channel, the error floors are completely removed in both cases with significant significant improvement with perfect channel knowledge. In LDPC-FBMC/OQAM system, the simulation results approximately same in both cases over the EVA channel and there is a significant difference over ETU channel. With use the EVA channel, the error floors are completely removed with the same factor in both cases. In general, the error floor of OFDM system is larger than that of the FBMC/OQAM system. The comparison between these figures is illustrated in Table 4.2.

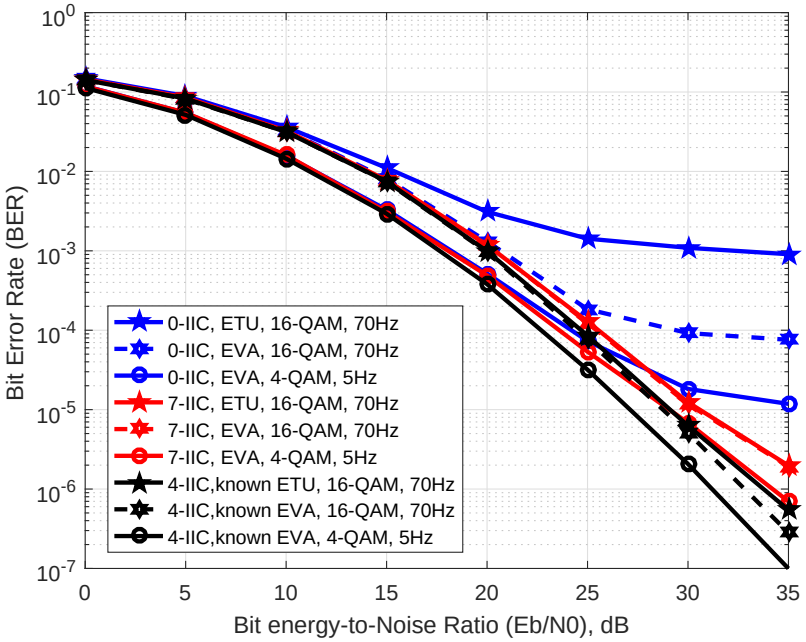

Figure 4.10: BER curves for LDPC-FBMC/OQAM system with different modulation orders and Doppler frequencies over EVA/ETU channel using scattered pilot based Wiener filter channel estimation with MMSE equaliser.

In Table 4.2, 4-QAM and 16-QAM with 5 Hz and 70 Hz Doppler frequency respectively are used in the simulation results for both systems. In the OFDM system, the error floors are reduced by a factor R_k 37 and 60 over EVA channel and 7 and 9 over the ETU channel with the ZF and MMSE equaliser respectively. With the use of 4-QAM, the error floors are completely removed and the gap from the perfect knowledge with 4-IIC iterations simulation results is approximately of 3.2 dB and 2.5 dB with the ZF and MMSE equaliser respectively, measured at 10^{-5} BER .In contrast, in FBMC/OQAM system, over the ETU channel, the error floors are reduced by a factor of 9 with ZF equaliser, measured

at 35 dB $Eb/N0$ and completely removed with MMSE equaliser. Over the EVA channel, the error floors are removed with the gap from the perfect knowledge with 4-IIC iterations simulation results is approximately of 1.7 dB and 1.6 dB with the ZF and MMSE equaliser respectively, measured at 10^{-5}.

Table 4.2: Simulation results for LDPC OFDM and FBMC/OQAM systems using scattered pilots channel estimation with 7 IIC-Itrs

System	N_{Fig}	**Gap** (dB)	BER	R_k	$Eb/N0$ dB	Channel	Doppler Hz	M-QAM
	4.7	-	-	37	35	EVA	70	16-QAM
	4.7	-	-	7	35	ETU	70	16-QAM
OFDM	4.7	3.2	10^{-5}	-	-	EVA	5	4-QAM
	4.9	-	-	60	35	EVA	70	16-QAM
	4.9	-	-	9	35	ETU	70	16-QAM
	4.9	2.5	10^{-5}	-	-	EVA	5	4-QAM
	4.8	-	-	9	35	ETU	70	16-QAM
	4.8	1.7	10^{-5}	-	-	EVA	70	16-QAM
FBMC/	4.8	1.7	10^{-5}	-	-	EVA	5	4-QAM
OQAM	4.10	2	10^{-5}	-	-	ETU	70	16-QAM
	4.10	1.6	10^{-5}	-	-	EVA	70	16-QAM
	4.10	1.6	10^{-5}	-	-	EVA	5	4-QAM

Figure 4.11 and 4.12 show the MSE simulation results for the OFDM and FBMC/OQAM systems using 4-QAM and 16-QAM with the MMSE equaliser over the EVA channel. We note that the Wiener filter-based channel estimation for the FBMC/OQAM system provides a smaller MSE than that of OFDM. In this chapter, IIC is used to improve the channel estimation. At each IIC iteration, estimated decoded signal is used to calculate the ICI/ISI components. After remove these components, the channel LS estimator is repeated to improve the estimated values of the channel coefficients as shown in Figure 4.2. After 7 IIC iterations the error floors in the MMSE simulation are reduced by a factor of 12 and 10.5 for the OFDM system and by 2.6 and 2.5 for the

FBMC/OQAM using 4-QAM and 16-QAM respectively, measured at 40 dB $Eb/N0$.

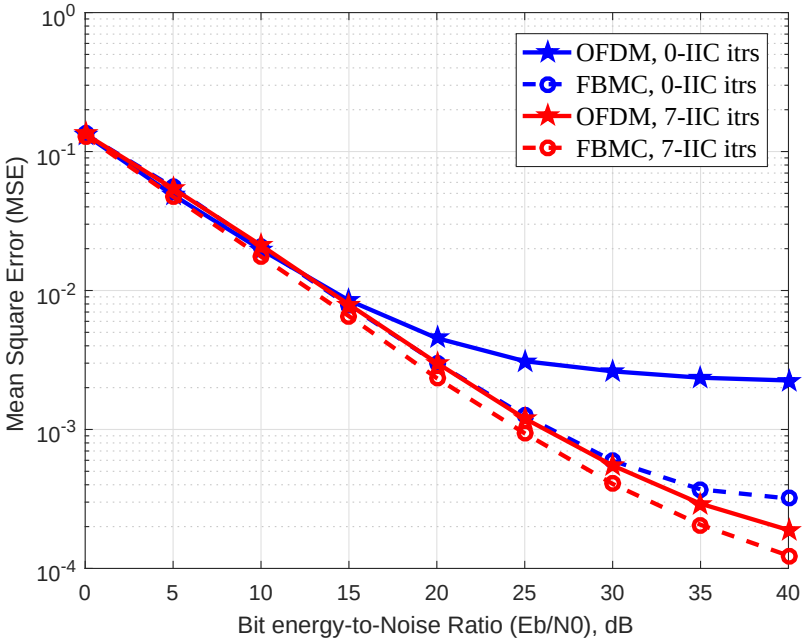

Figure 4.11: MSE curves for LDPC OFDM and FBMC/OQAM systems using 4-QAM and 5 Hz Doppler frequencies over EVA channel with MMSE equaliser.

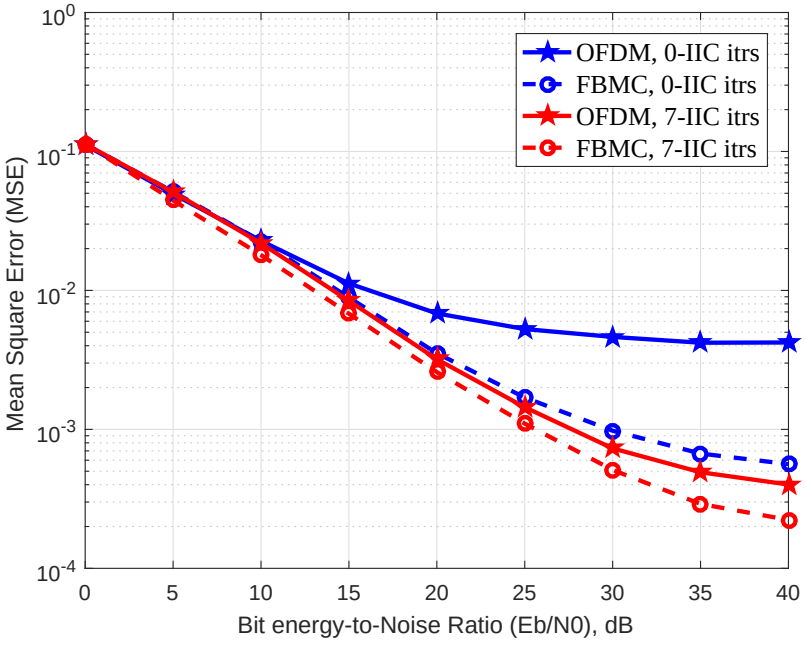

Figure 4.12: MSE curves for LDPC OFDM and FBMC/OQAM systems using 16-QAM and 70 Hz Doppler frequencies over EVA channel with MMSE equaliser.

In the case of IAM preamble based Wiener filter channel estimation, the EVA channel is used in the simulation of the LDPC-FBMC/OQAM system. 4-QAM and 16-QAM modulation orders are used with 5 Hz and 70 Hz Doppler frequencies respectively with ZF equaliser. In this case, the error floors are eliminated. Figures 4.13, 4.14, and 4.15 show the simulation results of the LDPC-FBMC/OQAM system using IAM preamble with 1-IAM, 2-IAM, and 3-IAM preambles per each slot of the FBMC sub-frame respectively.

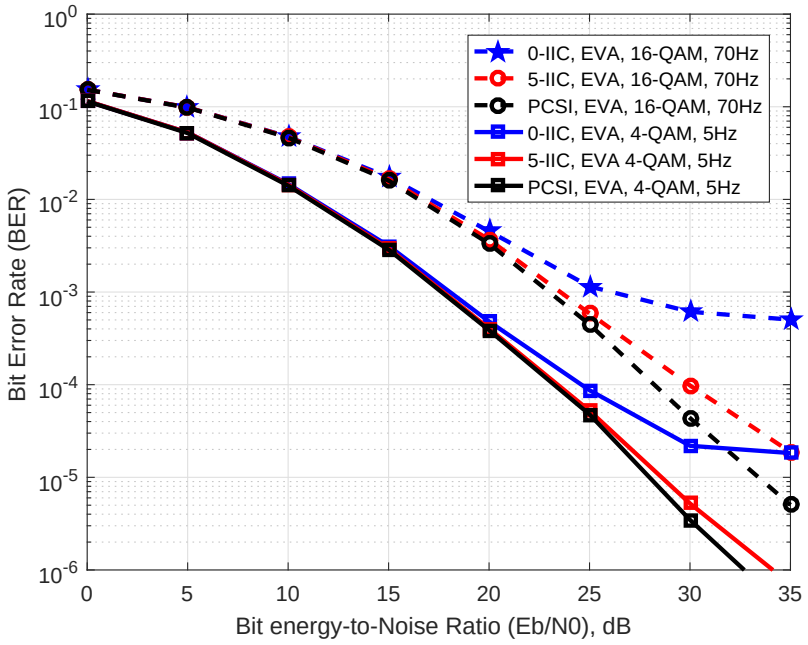

Figure 4.13: BER curves for LDPC-FBMC/OQAM system with different modulation orders and Doppler frequencies over EVA channel using 1-IAM preamble per slot Wiener filter channel estimation with ZF equaliser.

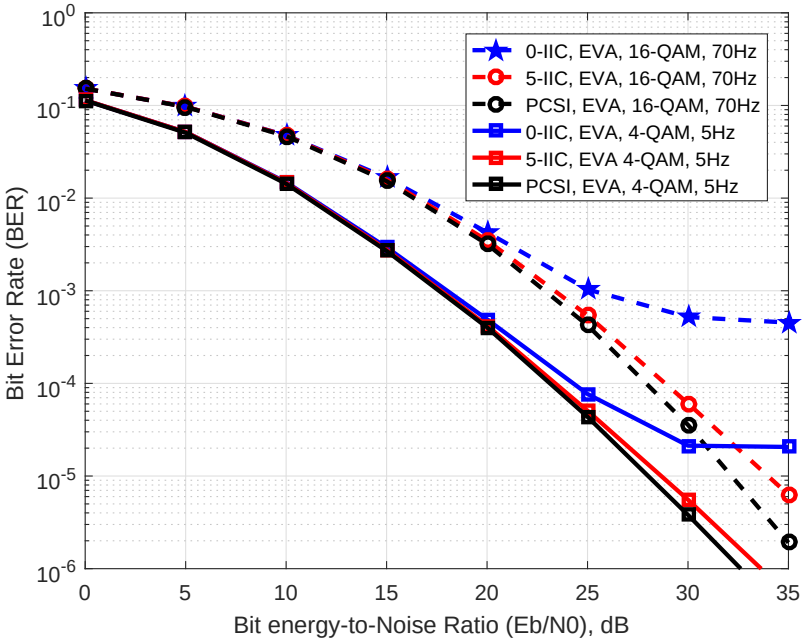

Figure 4.14: BER curves for LDPC-FBMC/OQAM system with different modulation orders and Doppler frequencies over EVA channel using 2-IAM preamble per slot Wiener filter channel estimation with ZF equaliser.

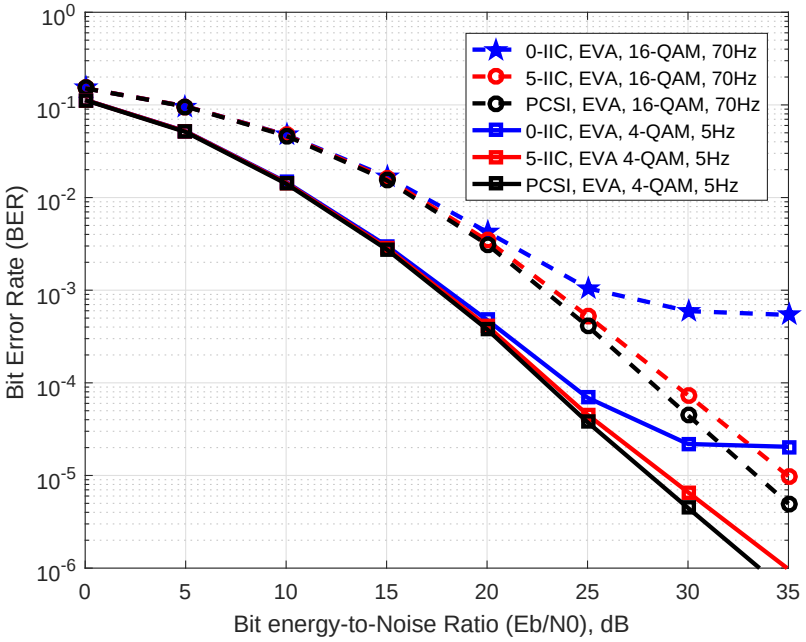

Figure 4.15: BER curves for LDPC-FBMC/OQAM system with different modulation orders and Doppler frequencies over EVA channel using 3-IAM preamble per slot Wiener filter channel estimation with ZF equaliser.

It is clear from these figures that with 1-IAM preamble in each slot, the gap from the PCSI simulation result is approximately 0.6 dB and 3.5 dB using 4-QAM and 16-QAM respectively. With 2-IAM preambles per each slot, the gaps become 0.6 dB and 1.6 dB with 4-QAM and 16-QAM respectively. With 3-IAM preambles, the gap is reduced to 1.5 dB with 16-QAM compared with the use of 2-IAM preambles. As in scattered pilot channel estimation, in the IAM preamble, the 2-D Wiener filter channel estimation is used. This means that the time and frequency correlations are exploited. The time correlations depend on the time interval between the IAM preambles in each sub-frame. With use IAM preambles, the time interval is reduced and strong time correlations is achieved. This reduces the gap from the PCSI simulation results as shown in the above figures.

To compare the proposed IIC scheme with Wiener filter channel estimation with related work, the simulation parameters in [120] will be used. An un-coded FBMC/QAM system is used with 4-QAM, single tap equaliser and LS estimator with linear interpolation over the COST 207 Typical Urban Reception (TU6) channel [151]. Figure 4.16

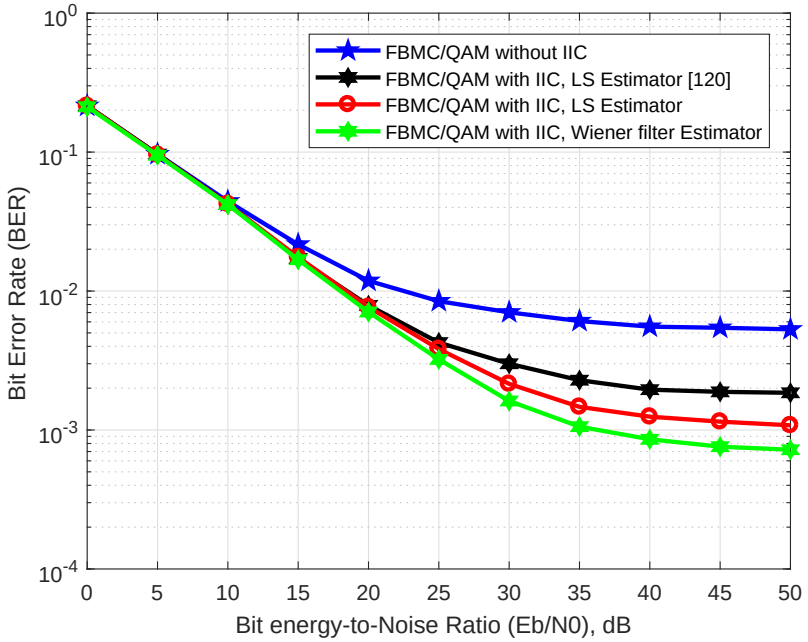

Figure 4.16: BER curves for Un-coded FBMC/QAM system with 4-QAM over COST207-TU6 channel using LS estimator with linear and Wiener filter interpolations.

shows the BER simulation results of the proposed system using LS and Wiener filter estimators with and without IIC. In [120], with IIC, the reduction factor of the error floors was approximately 3. In contrast, with the proposed IIC scheme, the error floors are re-

duced by a factor of approximately 5 and 7 with LS estimator with linear and Wiener filter interpolations respectively, measured at 50 dB $Eb/N0$ as shown in Figure 4.16.

4.7 Summary

This chapter can be summarised as follows:

- An iterative interference cancellation (IIC) based Wiener filter channel estimation using scattered pilots has been presented for LDPC-OFDM and LDPC-FBMC/OQAM systems with insufficient CP. In both systems, the error floors are significantly reduced after some IIC iteration. In general, the error floors of the LDPC-FBMC/OQAM system are lower than those of the OFDM system.
- Wiener filter channel estimation was introduced. One and two dimension channel estimation based on scattered pilots were explained using channel time and frequency correlations.
- Different modulation orders with different Doppler frequencies are used in both systems over the EVA and ETU channels. After 7-IIC iterations, the error floors are removed in the OFDM system using 4-QAM over the EVA channel, but it still exists with 16-QAM over the EVA channel. In LDPC-FBMC/OQAM system, the error floors are completely removed with 4-QAM and 16-QAM over the EVA channel.
- Iterative channel estimation based IIC is used in this chapter with scattered pilot and Wiener filter channel estimation. A significant improvement in MSE simulation results is achieved for both OFDM and FBMC/OQAM systems. FBMC/OQAM system provides less MSE than that of OFDM.
- IAM-preamble pilot based Wiener filter channel estimation of the LDPC-FBMC/OQAM system has been presented in three scenarios, using 1-IAM, 2-IAM, and 3-IAM preambles in each slot of the FBMC sub-frame. The error floors are substantially eliminated after 5-IIC iterations for all three cases.
- 4-QAM and 16-QAM are used with IAM preamble based Wiener filter channel estimation over EVA channel. As the number of IAM preambles per slot increases,

a significant improvement is noticeable in the simulation result using high order modulation.

Chapter 5

MIMO systems based on IIC-MCM

Contents

5.1 Introduction

OFDM system has become a very popular multicarrier modulation scheme, used in many wireless systems due to its attractive features. OFDM systems are employed in different standards over different channel conditions. On the other hand, Multiple-Input Multiple-Output (MIMO) [152] is used to enhance link capacity and spectral efficiency: hence the combination MIMO-OFDM can improve the overall system performance and achieve higher throughput. However, there are significant challenges for efficient receiver design for a time-variant multipath channel. Such a channel adds undesirable components to the received signal from the signal transmitted from the other antennas.

To improve the performance of MIMO systems, it is necessary to reduce the interference resulting from the effect of the channel as well the interference due to the signal transmitted from other antennas. This means that the channel equalisation and detection should be improved. In [153], two hybrid stages are proposed for the uplink MIMO-OFDM systems for interference cancellation and equalisation framework. In these stages, time and frequency domain equalization are used to reduce the ICI and channel distortion respectively. Wind-Flex and Ubiquitous Antenna are used to increase the number of users, data rate, and the capacity of MIMO-OFDM systems [154]. In [155], dynamic pilot allocation (DPA) for DFT is used to improve the channel estimation for MIMO-OFDM systems. In this approach, MIMO iterative pilot search (MIPS) algorithm is used with successive interference cancellation (SIC) and ML to reduce the DPA complexity.

As in the SISO OFDM and FBMC/OQAM systems, an IIC based iterative receiver is used to reduce the interference and improve the channel estimation in MIMO systems [156–162]. To reduce the interference and minimize the sum MSE of the MIMO-FBMC/OQAM systems, two techniques have been presented in [163]. A suboptimal solution and an alternating optimization method with iterative processing are used in the first and second technique respectively. A coordinated transmit beamforming iterative technique is presented to reduce the intrinsic and multi-user interference for the MIMO-FBMC/OQAM system [164].

On the other hand, there are several new technical problems of the FBMC/OQAM system. Equalisation complexity is one of the more important of these. The FBMC/OQAM system performance is not satisfactory when a one tap Minimum-Mean Square Error (MMSE) equaliser is used [165]. An equalisation technique based on frequency sampling (FS) is introduced in [166] and extended in [167]. In this approach, the equaliser is designed for each subchannel in the frequency domain. To reduce the effect of the intrinsic interference in MIMO-FBMC systems, a widely linear MMSE equaliser is proposed with a two-step receiver in [168].

Our emphasis in this contribution is to propose iterative interference cancellation (IIC) and MIMO-IIC schemes to eliminate ISI/ICI interference without increasing the equaliser complexity. IIC and MIMO-IIC are used with linear detection to reduce the effect of channels on the transmitted signal from the current and other streams respectively. Further-

more, SIC detection is used to reduce the cross interference due to the transmitted signal from the other antennas. The combination SIC-IIC is proposed to improve the overall system performance and achieve high throughput in the wireless communication system. SIC-IIC is used in different scenarios. Two receiver schemes (SIC-IIC and MIMO-SIC-IIC) are used and developed for both MIMO-FBMC/OQAM and MIMO-OFDM systems with an insufficient cyclic prefix (CP). An LDPC iterative decoder is used with M-QAM modulation in different environments for the time-variant multipath LTE channel.

The remainder of this chapter is outlined as follows: An introduction to fundamental techniques of spatial multiplexing in the 2×2 MIMO system will be given in Section 5.2. In Section 5.2.2 a SIC scheme is introduced for the 2×2 MIMO system. The proposed IIC and MIMO-IIC schemes for both MIMO-OFDM and MIMO-FBMC/OQAM systems are discussed in Section 5.3. Two scenarios applying SIC based IIC to MIMO-OFDM and MIMO-FBMC/OQAM systems are introduced in Section 5.3.2. Simulation results are given in Section 5.5. Finally, this chapter is summarised in Section 5.6.

5.2 MIMO Detection

5.2.1 Linear MIMO Detection

Spatial multiplexing is a transmission technique which has been used in MIMO systems in order to provide high data rates by providing additional data bandwidth in wireless communication systems [169]. Different portions of independent information (data streams) are transmitted across different propagation paths. In general, in MIMO spatial multiplexing, the number of the receive antennas (N_R) must be greater than or equal to the number of the transmit antennas (N_T). In this case, the spatial multiplexing gain (N_S) (or maximum spatial multiplexing order, or degrees of freedom) can be expressed as:

$$N_S = \min(N_T, N_R) \tag{5.1}$$

ZF MIMO detection

One of the popular MIMO detection technique is a ZF MIMO detection which presents a low computational complexity. However, the system performance may be degraded due to the introduced noise enhancement. In this detector, the received symbol vector is multiplied by the pseudo inverse of the channel matrix. The ZF MIMO detection filtering (equalisation) matrix $\mathbf{G}_{ZF}$ can be expressed as [170, 171]:

$$\mathbf{G}_{ZF} = \left(\mathbf{H}_i^{\mathbf{H}}\mathbf{H}_i\right)^{-1}\mathbf{H}_i^{\mathbf{H}} \tag{5.2}$$

where $\mathbf{H}_i$ ia an *i*th $N_R \times N_T$ MIMO channel matrix given by

$$\mathbf{H}_i = \begin{bmatrix} h_{1,1}^{(i)} & \cdots & h_{1,k}^{(i)} & \cdots & h_{1,N_T}^{(i)} \\ \vdots & \ddots & \vdots & & \vdots \\ h_{r,1}^{(i)} & \cdots & h_{r,k}^{(i)} & \cdots & h_{r,N_T}^{(i)} \\ \vdots & \ddots & \vdots & & \vdots \\ h_{N_R,1}^{(i)} & \cdots & h_{N_R,k}^{(i)} & \cdots & h_{N_R,N_T}^{(i)} \end{bmatrix} \tag{5.3}$$

where $h_{r,k}^{(i)}$ represents the *i*th element of a channel vector $\mathbf{h}_{r,k}$ that describe the CFR between the *r*th receive and *k*th transmit antennas.

MMSE MIMO detection

To alleviate the noise which is introduced by the ZF MIMO detector, MMSE MIMO detector was introduced. In this detector, the MMSE MIMO filtering (equalisation) matrix $\mathbf{G}_{MMSE}$ can be expressed as [171]:

$$\mathbf{G}_{MMSE} = \left(\mathbf{H}_i^{\mathbf{H}}\mathbf{H}_i + \sigma_n^2\mathbf{I}_{NT}\right)^{-1}\mathbf{H}_i^{\mathbf{H}} \tag{5.4}$$

5.2.2 Successive Interference Cancellation (SIC) Detection

In MIMO systems, SIC is a sequential detection algorithm which is used to detect the transmitted symbols [170]. At the first layer, the estimated symbol vector is detected by using a ZF or MMSE MIMO detector. Then the estimated detected vector is subtracted from the received signal vector. The resulting signal is used in the next layer to calculate the estimated symbol vector. The algorithm is continued until all symbols are detected. For that reason, this algorithm is known as a layered detector.

In MIMO-OFDM systems, due to the effect of the multipath propagation, especially with insufficient CP, and the cross interference due to the transmitted signal from the other antenna, there will be some erronrous decisions in the first layer estimated detected symbols. This means that error propagation will occur in the next layers. To improve the decision of the first layer detected symbols, the Vertical Bell labs LAyered Space Time (V-BLAST) or ordered SIC (OSIC) detection algorithm is utilized [172, 173]. In this approach, in every layer, each estimated detected symbol is calculated from the symbol with highest signal to interference noise ratio (SINR).

Figure 5.1 represents the basic configuration diagram of the (2×2) MIMO channel system. In this figure, $\mathbf{x}_1$ and $\mathbf{x}_2$ represent the transmitted data streams from the transmitting antennas N_{T1} and N_{T2} respectively, $\mathbf{h}_{11}$, $\mathbf{h}_{12}$, $\mathbf{h}_{21}$, and $\mathbf{h}_{22}$ are the different propagation paths, and $\mathbf{y}_1$ and $\mathbf{y}_2$ are the received data streams at the receiver antennas N_{R1} and N_{R2} respectively. Such that:

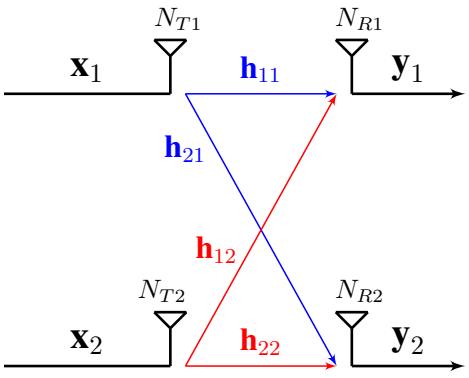

Figure 5.1: (2×2) MIMO channel system.

$$\mathbf{y}_1 = \mathbf{h}_{11}\mathbf{x}_1 + \mathbf{h}_{12}\mathbf{x}_2 + \tilde{\eta}_1, \tag{5.5}$$

$$\mathbf{y}_2 = \mathbf{h}_{21}\mathbf{x}_1 + \mathbf{h}_{22}\mathbf{x}_2 + \tilde{\eta}_2 \tag{5.6}$$

where $\tilde{\eta}_1$ and $\tilde{\eta}_2$ are the Gaussian noise on the received antennas N_{R1} and N_{R2}, respectively.

Equations (5.5) and (5.6) can be expressed in matrix notation as:

$$\begin{bmatrix} \mathbf{y}_1 \\ \mathbf{y}_2 \end{bmatrix} = \begin{bmatrix} \mathbf{h}_{11} & \mathbf{h}_{12} \\ \mathbf{h}_{21} & \mathbf{h}_{22} \end{bmatrix} \begin{bmatrix} \mathbf{x}_1 \\ \mathbf{x}_2 \end{bmatrix} + \begin{bmatrix} \tilde{\eta}_1 \\ \tilde{\eta}_2 \end{bmatrix} \tag{5.7}$$

Then,

$$\mathbf{y} = \mathbf{H}\mathbf{x} + \tilde{\eta} \tag{5.8}$$

In the case of SIC based ZF detection, the ZF filter $\mathbf{G}_{ZF}$ which is given in (5.2) is used. Then, the estimated symbols $\hat{\mathbf{x}}_1$ and $\hat{\mathbf{x}}_2$ must be first calculated to apply them in the first layer of the SIC algorithm:

$$\begin{bmatrix} \hat{\mathbf{x}}_1 \\ \hat{\mathbf{x}}_2 \end{bmatrix} = \mathbf{G}_{ZF} \begin{bmatrix} \mathbf{y}_1 \\ \mathbf{y}_2 \end{bmatrix} \tag{5.9}$$

In the case of the SIC based MMSE detection, the MMSE filtering matrix $\mathbf{G}_{MMSE}$ given in (5.4) is used. Again the estimated symbols $\hat{\mathbf{x}}_1$ and $\hat{\mathbf{x}}_2$ must be first calculated to use them in the first layer of the SIC algorithm.

$$\begin{bmatrix} \hat{\mathbf{x}}_1 \\ \hat{\mathbf{x}}_2 \end{bmatrix} = \mathbf{G}_{MMSE} \begin{bmatrix} \mathbf{y}_1 \\ \mathbf{y}_2 \end{bmatrix} \tag{5.10}$$

To avoid error propagation in the next layers, the estimated value of the symbol with the highest SINR will be selected to calculate the resulting signal at each received antenna. If symbol $\mathbf{x}_2$ has a high enough SINR, the estimated value $\hat{\mathbf{x}}_2$ is assumed to be equal to $\mathbf{x}_2$. Then, the effect of symbol $\mathbf{x}_2$ will be subtracted from the received signals $\mathbf{y}_1$ and $\mathbf{y}_2$, $i.e.$

$$\begin{bmatrix}\mathbf{r}_1\\ \mathbf{r}_2\end{bmatrix} = \begin{bmatrix}\mathbf{y}_1 - \mathbf{h}_{12}\hat{\mathbf{x}}_2\\ \mathbf{y}_2 - \mathbf{h}_{22}\hat{\mathbf{x}}_2\end{bmatrix} = \begin{bmatrix}\mathbf{h}_{11}\mathbf{x}_1 + \tilde{\eta}_1\\ \mathbf{h}_{21}\mathbf{x}_1 + \tilde{\eta}_2\end{bmatrix} = \begin{bmatrix}\mathbf{h}_{11}\\ \mathbf{h}_{21}\end{bmatrix}\mathbf{x}_1 + \begin{bmatrix}\tilde{\eta}_1\\ \tilde{\eta}_2\end{bmatrix} \tag{5.11}$$

Equation (5.11) can be expressed as:

$$\mathbf{r} = \mathbf{h}_1\mathbf{x}_1 + \tilde{\eta} \tag{5.12}$$

where $\mathbf{h}_1 = \begin{bmatrix}\mathbf{h}_{11}\\ \mathbf{h}_{21}\end{bmatrix}$ and $\tilde{\eta} = \begin{bmatrix}\tilde{\eta}_1\\ \tilde{\eta}_2\end{bmatrix}$.

If the symbol $\mathbf{x}_1$ has the highest SINR, the effect of symbol $\hat{\mathbf{x}}_1$ will be subtracted from the received signals $\mathbf{y}_1$ and $\mathbf{y}_2$, $i.e.$

$$\begin{bmatrix}\mathbf{r}_1\\ \mathbf{r}_2\end{bmatrix} = \begin{bmatrix}\mathbf{y}_1 - \mathbf{h}_{11}\hat{\mathbf{x}}_1\\ \mathbf{y}_2 - \mathbf{h}_{21}\hat{\mathbf{x}}_1\end{bmatrix} = \begin{bmatrix}\mathbf{h}_{12}\mathbf{x}_2 + \tilde{\eta}_1\\ \mathbf{h}_{22}\mathbf{x}_2 + \tilde{\eta}_2\end{bmatrix} = \begin{bmatrix}\mathbf{h}_{12}\\ \mathbf{h}_{22}\end{bmatrix}\mathbf{x}_2 + \begin{bmatrix}\tilde{\eta}_1\\ \tilde{\eta}_2\end{bmatrix} \tag{5.13}$$

Equation (5.13) can be expressed as:

$$\mathbf{r} = \mathbf{h}_2\mathbf{x}_2 + \tilde{\eta} \tag{5.14}$$

where $\mathbf{h}_2 = \begin{bmatrix}\mathbf{h}_{12}\\ \mathbf{h}_{22}\end{bmatrix}$ and $\tilde{\eta} = \begin{bmatrix}\tilde{\eta}_1\\ \tilde{\eta}_2\end{bmatrix}$.

At the next layer of the SIC algorithm, the estimated symbols $\hat{x}_1$ and $\hat{x}_2$ can be calculated from (5.12) and (5.14) respectively. In this case, (5.11) represents a new channel model with one transmitting antenna and two received antennas. This means that the estimated symbol value $\hat{x}_1$ can be optimally detected by using Maximal Ratio Combining (MRC) algorithm as:

$$\hat{\mathbf{x}}_1 = \frac{(\mathbf{h}_1)^{\mathbf{H}}\,\mathbf{r}}{(\mathbf{h}_1)^{\mathbf{H}}\mathbf{h}_1} \tag{5.15}$$

Similarly,

$$\hat{\mathbf{x}}_2 = \frac{(\mathbf{h}_2)^{\mathbf{H}}\,\mathbf{r}}{(\mathbf{h}_2)^{\mathbf{H}}\mathbf{h}_2} \tag{5.16}$$

5.3 System Model

5.3.1 Using Linear MIMO Detection

The MIMO 2×2 system is the simplest and most widely used of the spatial multiplexing systems. The received signal at each receive antenna contains residual and previous data symbol components which lead to ICI and ISI respectively. Furthermore, these two pairs of undesirable components result from the effect of the multipath channels on the signals transmitted from the corresponding and other antennas respectively as shown in Figure 5.2.

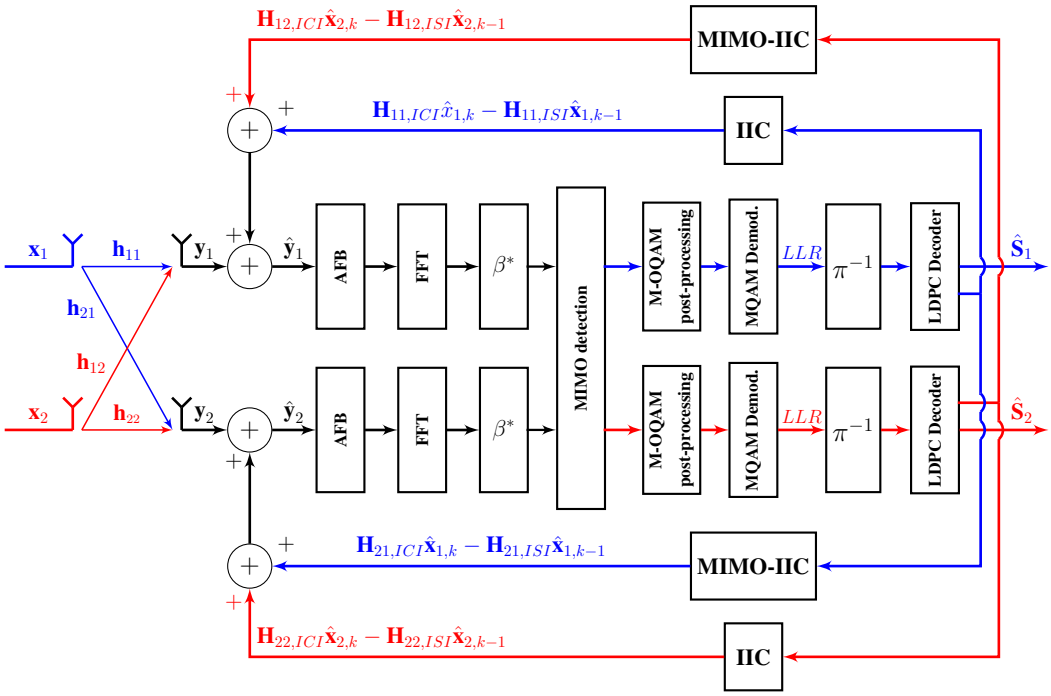

Figure 5.2: Basic configuration diagram of proposed IIC and MIMO-IIC of LDPC-MIMO-FBMC/OQAM system.

In general, the received data symbols $\mathbf{y}_{1,k}$ and $\mathbf{y}_{2,k}$ at the receive antennas N_{R1} and

N_{R2}, respectively, at time instant k can be expressed as:

$$\begin{aligned}\mathbf{y}_{1,k} &= \mathbf{x}_{1,k}\mathbf{h}_{11} + \mathbf{x}_{2,k}\mathbf{h}_{12} + \tilde{\eta}_k \\ &= \mathbf{H}_{11,\text{CIRC}}\mathbf{x}_{1,k} + \mathbf{H}_{12,\text{CIRC}}\mathbf{x}_{2,k} \\ &- \mathbf{H}_{11,\text{ICI}}\mathbf{x}_{1,k} + \mathbf{H}_{11,\text{ISI}}\mathbf{x}_{1,k-1} \\ &- \mathbf{H}_{12,\text{ICI}}\mathbf{x}_{2,k} + \mathbf{H}_{12,\text{ISI}}\mathbf{x}_{2,k-1} + \tilde{\eta}_k\end{aligned} \tag{5.17}$$

$$\begin{aligned}\mathbf{y}_{2,k} &= \mathbf{x}_{1,k}\mathbf{h}_{21} + \mathbf{x}_{2,k}\mathbf{h}_{22} + \tilde{\eta}_k \\ &= \mathbf{H}_{22,\text{CIRC}}\mathbf{x}_{2,k} + \mathbf{H}_{21,\text{CIRC}}\mathbf{x}_{1,k} \\ &- \mathbf{H}_{22,\text{ICI}}\mathbf{x}_{2,k} + \mathbf{H}_{22,\text{ISI}}\mathbf{x}_{2,k-1} \\ &- \mathbf{H}_{21,\text{ICI}}\mathbf{x}_{1,k} + \mathbf{H}_{21,\text{ISI}}\mathbf{x}_{1,k-1} + \tilde{\eta}_k\end{aligned} \tag{5.18}$$

where channel matrices $\mathbf{H}_{11,\text{CIRC}}$, $\mathbf{H}_{11,\text{ICI}}$, $\mathbf{H}_{11,\text{ISI}}$, $\mathbf{H}_{12,\text{ICI}}$, and $\mathbf{H}_{12,\text{ISI}}$ correspond respectively to the circulant matrix with all coefficients and the residual matrices that lead to ICI and ISI due to the effect of the channel on transmitted signals $\mathbf{x}_1$ and $\mathbf{x}_2$, and $\tilde{\eta}_k$ represents Gaussian noise at the k^{th} time instant, with $\mathbf{H}_{\text{CIRC}}, \mathbf{H}_{\text{ICI}}, \mathbf{H}_{\text{ISI}} \in \mathbb{C}^{N\times N}$ [128–131] and N is the number of subcarriers.

To reduce the ICI and ISI from the received signals $\mathbf{y}_{1,k}$ and $\mathbf{y}_{2,k}$, the undesirable terms containing $\mathbf{H}_{11,\text{ICI}}$, $\mathbf{H}_{11,\text{ISI}}$, $\mathbf{H}_{12,\text{ICI}}$, and $\mathbf{H}_{12,\text{ISI}}$ must be removed from the received data symbols $\mathbf{y}_{1,k}$ and $\mathbf{H}_{22,\text{ICI}}$, $\mathbf{H}_{22,\text{ISI}}$, $\mathbf{H}_{21,\text{ICI}}$, and $\mathbf{H}_{21,\text{ISI}}$ must be removed from the received data symbols $\mathbf{y}_{2,k}$. In this chapter, we propose a two-step receiver using IIC and MIMO-IIC to remove these undesirable components, as follows:

- *First step:* In IIC, the channel matrices $\mathbf{H}_{11,\text{ICI}}$, $\mathbf{H}_{11,\text{ISI}}$, $\mathbf{H}_{22,\text{ICI}}$, and $\mathbf{H}_{22,\text{ISI}}$ are calculated. Next, the estimated decoded signal is used to calculate the current and previous values of the estimated transmitted data symbols ($\hat{\mathbf{x}}_{1,k}$ and $\hat{\mathbf{x}}_{2,k}$) and ($\hat{\mathbf{x}}_{1,k-1}$ and $\hat{\mathbf{x}}_{2,k-1}$) respectively. Then, multiply them by the channel matrices to get ($\mathbf{H}_{11,\text{ICI}}\hat{\mathbf{x}}_{1,k}$ and $\mathbf{H}_{11,\text{ISI}}\hat{\mathbf{x}}_{1,k-1}$) and ($\mathbf{H}_{22,\text{ICI}}\hat{\mathbf{x}}_{2,k}$ and $\mathbf{H}_{22,\text{ISI}}\hat{\mathbf{x}}_{2,k-1}$) to remove them from the received signals $\mathbf{y}_{1,k}$ and $\mathbf{y}_{2,k}$ respectively.
- *Second step:* In MIMO-IIC, the channel matrices $\mathbf{H}_{12,\text{ICI}}$, $\mathbf{H}_{12,\text{ISI}}$, $\mathbf{H}_{21,\text{ICI}}$, and $\mathbf{H}_{21,\text{ISI}}$ are calculated. Next, the estimated decoded signal is used to calculate the current and previous values of the estimated transmitted data symbol ($\hat{\mathbf{x}}_{1,k}$ and $\hat{\mathbf{x}}_{2,k}$) and ($\hat{\mathbf{x}}_{1,k-1}$ and $\hat{\mathbf{x}}_{2,k-1}$) respectively. Then, multiply them by the channel matrices to get

$\mathbf{H}_{21,\text{ICI}}\hat{\mathbf{x}}_{1,k}$, $\mathbf{H}_{12,\text{ICI}}\hat{\mathbf{x}}_{2,k}$, $\mathbf{H}_{21,\text{ISI}}\hat{\mathbf{x}}_{1,k-1}$, and $\mathbf{H}_{12,\text{ISI}}\hat{\mathbf{x}}_{2,k-1}$.

- Finally, the components which are calculated in the first and second steps are removed from the multicarrier symbols which overlap at the receiver input.

After some iterations, the ICI and ISI terms are cancelled, and the estimated received signal at the received antenna N_{R1} can be expressed as:

$$\hat{\mathbf{y}}_{1,k} = \mathbf{H}_{11,\text{CIRC}}\hat{\mathbf{x}}_{1,k} + \mathbf{H}_{12,\text{CIRC}}\hat{\mathbf{x}}_{2,k} + \tilde{\eta}_k \tag{5.19}$$

The received signal in the frequency domain can be represented as:

$$\hat{\mathbf{Y}}_{1,k} = F\mathbf{H}_{11,\text{CIRC}}F^{\mathbf{H}}\hat{\mathbf{X}}_{1,k} + F\mathbf{H}_{12,\text{CIRC}}F^{\mathbf{H}}\hat{\mathbf{X}}_{2,k} + F\tilde{\eta}_k \tag{5.20}$$

According to the eigenvalue decomposition (EVD) of the circulant matrix [132] i.e. $\mathbf{H}_{11,\text{CIRC}} = F^{\mathbf{H}}\mathbf{H}_{11}F$, the estimated received signal in the frequency domain can be expressed as:

$$\hat{\mathbf{Y}}_{1,k} = \mathbf{H}_{11}\hat{\mathbf{X}}_{1,k} + \mathbf{H}_{12}\hat{\mathbf{X}}_{2,k} + \eta_k \tag{5.21}$$

where $\mathbf{H}_{11}$ and $\mathbf{H}_{12} \in \mathbb{C}^{N\times N}$ are diagonal matrices that contain the Channel Frequency Responses (CFR), $\mathbf{hF}_{11}$ and $\mathbf{hF}_{12}$ respectively, along their diagonals.

Let N_{cp}, L_c, and E respectively represent the number of cyclic prefix samples, the length of the LTE channel, and the excess channel length over the cyclic prefix. Then $E = L_c - N_{cp} - 1$. Channel matrices $\mathbf{H}_{11,\text{ICI}}$, $\mathbf{H}_{11,\text{ISI}}$, $\mathbf{H}_{12,\text{ICI}}$, and $\mathbf{H}_{12,\text{ISI}}$ can be expressed as:

$$\mathbf{H}_{11,\text{ISI}} = \begin{bmatrix} 0_{E\times(N-E)} & \mathbf{H}_1 \\ 0_{(N-E)\times(N-E)} & 0_{(N-E)\times E} \end{bmatrix} \tag{5.22}$$

$$\mathbf{H}_{11,\text{ICI}} = \begin{bmatrix} 0_{E\times(N-E-N_{cp})} & \mathbf{H}_1 & 0_{E\times N_{cp}} \\ 0_{(N-E)\times(N-E-N_{cp})} & 0_{(N-E)\times E} & 0_{(N-E)\times N_{cp}} \end{bmatrix} \tag{5.23}$$

$$\mathbf{H}_{12,\text{ISI}} = \begin{bmatrix} 0_{E\times(N-E)} & \mathbf{H}_2 \\ 0_{(N-E)\times(N-E)} & 0_{(N-E)\times E} \end{bmatrix} \tag{5.24}$$

$$\mathbf{H}_{12,\text{ICI}} = \begin{bmatrix} 0_{E\times(N-E-N_{cp})} & \mathbf{H}_2 & 0_{E\times N_{cp}} \\ 0_{(N-E)\times(N-E-N_{cp})} & 0_{(N-E)\times E} & 0_{(N-E)\times N_{cp}} \end{bmatrix} \tag{5.25}$$

where the interference originating with matrix $\mathbf{H}_1$ and $\mathbf{H}_2 \in \mathbb{C}^{E\times E}$ depends mainly on the channel values $\mathbf{h}_{11}$ and $\mathbf{h}_{12}$ respectively and can be represented as:

$$\mathbf{H}_1 = \begin{bmatrix} h_{11,L_c-1} & \cdots & \cdots & h_{11,N_{cp}-1} \\ 0 & \ddots & & \vdots \\ \vdots & \ddots & \ddots & \vdots \\ 0 & \cdots & 0 & h_{11,L_c-1} \end{bmatrix} \tag{5.26}$$

$$\mathbf{H}_2 = \begin{bmatrix} h_{12,L_c-1} & \cdots & \cdots & h_{12,N_{cp}-1} \\ 0 & \ddots & & \vdots \\ \vdots & \ddots & \ddots & \vdots \\ 0 & \cdots & 0 & h_{12,L_c-1} \end{bmatrix} \tag{5.27}$$

in the case of $N_{cp} = 0$, $\mathbf{H}_{\text{ICI}} = \mathbf{H}_{\text{ISI}}$.

Similarly, we use the two-step receiver with IIC and MIMO-IIC to reduce the ICI/ISI interference from the received signal $\mathbf{y}_{2,k}$ in the second stream,

$$\begin{aligned} \mathbf{y}_{2,k} &= \mathbf{x}_{1,k}\mathbf{h}_{12} + \mathbf{x}_{2,k}\mathbf{h}_{22} \\ &= \mathbf{H}_{21,\text{CIRC}}\mathbf{x}_{1,k} + \mathbf{H}_{22,\text{CIRC}}\mathbf{x}_{2,k} \\ &- \mathbf{H}_{22,\text{ICI}}\mathbf{x}_{2,k} + \mathbf{H}_{22,\text{ISI}}\mathbf{x}_{2,k-1} \\ &- \mathbf{H}_{21,\text{ICI}}\mathbf{x}_{1,k} + \mathbf{H}_{21,\text{ISI}}\mathbf{x}_{1,k-1} + \tilde{\eta}_k \end{aligned} \tag{5.28}$$

Channel matrices $\mathbf{H}_{22,\text{ICI}}$, $\mathbf{H}_{22,\text{ISI}}$, $\mathbf{H}_{21,\text{ICI}}$, and $\mathbf{H}_{21,\text{ISI}}$ can be expressed as:

$$\mathbf{H}_{22,\text{ISI}} = \begin{bmatrix} 0_{E\times(N-E)} & \mathbf{H}_3 \\ 0_{(N-E)\times(N-E)} & 0_{(N-E)\times E} \end{bmatrix} \tag{5.29}$$

$$\mathbf{H}_{22,\text{ICI}} = \begin{bmatrix} 0_{E\times(N-E-N_{cp})} & \mathbf{H}_3 & 0_{E\times N_{cp}} \\ 0_{(N-E)\times(N-E-N_{cp})} & 0_{(N-E)\times E} & 0_{(N-E)\times N_{cp}} \end{bmatrix} \tag{5.30}$$

$$\mathbf{H}_{21,\text{ISI}} = \begin{bmatrix} 0_{E\times(N-E)} & \mathbf{H}_4 \\ 0_{(N-E)\times(N-E)} & 0_{(N-E)\times E} \end{bmatrix} \tag{5.31}$$

$$\mathbf{H}_{21,\text{ICI}} = \begin{bmatrix} 0_{E\times(N-E-N_{cp})} & \mathbf{H}_4 & 0_{E\times N_{cp}} \\ 0_{(N-E)\times(N-E-N_{cp})} & 0_{(N-E)\times E} & 0_{(N-E)\times N_{cp}} \end{bmatrix} \tag{5.32}$$

$$\mathbf{H}_3 = \begin{bmatrix} h_{22,L_c-1} & \cdots & \cdots & h_{22,N_{cp}-1} \\ 0 & \ddots & & \vdots \\ \vdots & \ddots & \ddots & \vdots \\ 0 & \cdots & 0 & h_{22,L_c-1} \end{bmatrix} \tag{5.33}$$

$$\mathbf{H}_4 = \begin{bmatrix} h_{21,L_c-1} & \cdots & \cdots & h_{21,N_{cp}-1} \\ 0 & \ddots & & \vdots \\ \vdots & \ddots & \ddots & \vdots \\ 0 & \cdots & 0 & h_{21,L_c-1} \end{bmatrix} \tag{5.34}$$

After some iterations, the estimated value of the received signal $\mathbf{y}_{2,k}$ becomes:

$$\hat{\mathbf{y}}_{2,k} = \mathbf{H}_{21,\text{CIRC}}\hat{\mathbf{x}}_{1,k} + \mathbf{H}_{22,\text{CIRC}}\hat{\mathbf{x}}_{2,k} + \tilde{\eta}_k \tag{5.35}$$

In the frequency domain and according to the eigenvalue decomposition (EVD), $\hat{\mathbf{y}}_{2,k}$ can be represented as:

$$\hat{\mathbf{Y}}_{2,k} = F\mathbf{H}_{21,\text{CIRC}}F^{\mathbf{H}}\hat{\mathbf{X}}_{1,k} + F\mathbf{H}_{22,\text{CIRC}}F^{\mathbf{H}}\hat{\mathbf{X}}_{2,k} + F\tilde{\eta}_k \tag{5.36}$$

$$\hat{\mathbf{Y}}_{2,k} = \mathbf{H}_{21}\hat{\mathbf{X}}_{1,k} + \mathbf{H}_{22}\hat{\mathbf{X}}_{2,k} + \eta_k \tag{5.37}$$

The MIMO detector with ZF or MMSE equaliser is used to equalise the signals $\hat{\mathbf{Y}}_{1,k}$ and $\hat{\mathbf{Y}}_{2,k}$. The equalised signals obtained will be processed by the other parts of the system to get the estimated decoded signals $\hat{\mathbf{S}}_1$ and $\hat{\mathbf{S}}_2$ as shown in Figure 5.2. For both MIMO-OFDM and MIMO-FBMC/OQAM systems, one full iteration of the LDPC decoder, using the sum-product algorithm [114], is performed per outer IIC iteration.

5.3.2 Using SIC Detection

SIC is used to reduce the cross interference from the signal at the receive antennas due to the propagation paths from different transmitting antennas. In this chapter, the IIC with SIC will be discussed in different scenarios:

- *Case I:* In this case, SIC is applied after all the desired IIC iterations as shown in Figure 5.3. First, IIC and MIMO-IIC are applied as explained in Section 5.3. The soft estimated decoded signal is used to calculate the ICI and ISI components. M-QAM soft mapping is used to modulate the interleaved signal. Then an OFDM or FBMC/OQAM modulator is used to calculate the estimated symbols $\hat{x_1}$ and $\hat{x_2}$ which are used in turn to calculate the undesirable components in the received signal. Then, we remove these components from the received signals y_1 and y_2 at each received antenna N_{R1} and N_{R2} respectively. After the desired number of IIC iterations, the estimated received signal $\hat{y}_1$ and $\hat{y}_2$ will be obtained as shown in Figure 5.2. After that, the estimated symbols $\hat{x}_1$ and $\hat{x}_2$ are used in the SIC algorithm to improve the system performance by reducing the cross interference from the received signals as explained in Section 5.2.2. Hence estimated symbols free of ICI, ISI, and cross interference can be obtained. The OFDM or FBMC/OQAM demodulator is applied with an MRC detector. Finally, the estimated data symbols are calculated by applying the soft M-QAM demapper, de-interleaver, and LDPC decoder on the detected signal.
- *Case II:* In this case, at the first IIC iteration, the estimated symbols $\hat{x}_1$ and $\hat{x}_2$ after LDPC decoder are directly used in the SIC algorithm. $\hat{x}_1$ and $\hat{x}_2$ are calculated as explained in *Case I*. After that, the SIC is used to improve the estimated symbols $\hat{x}_1$ and $\hat{x}_2$ as explained in Section 5.2.2. The improved estimated signals are used to calculate the ICI and ISI component. These components will be removed from the received signals y_1 and y_2 to obtain the estimated received signal $\hat{y}_1$ and $\hat{y}_2$. This process will be repeated until the desired number of the IIC iterations is satisfied as shown in Figure 5.4.

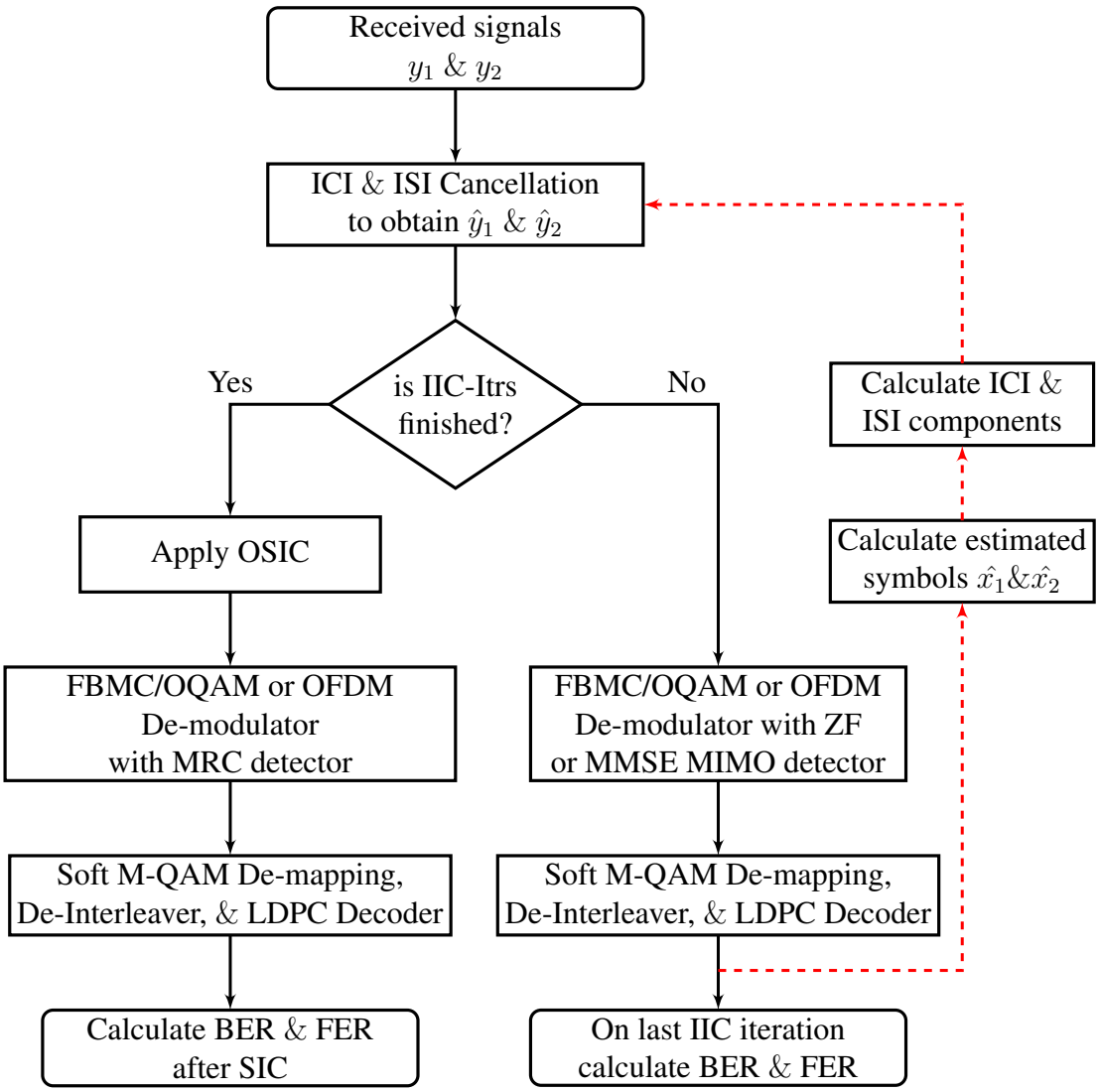

Figure 5.3: SIC based IIC flowchart (case-I).

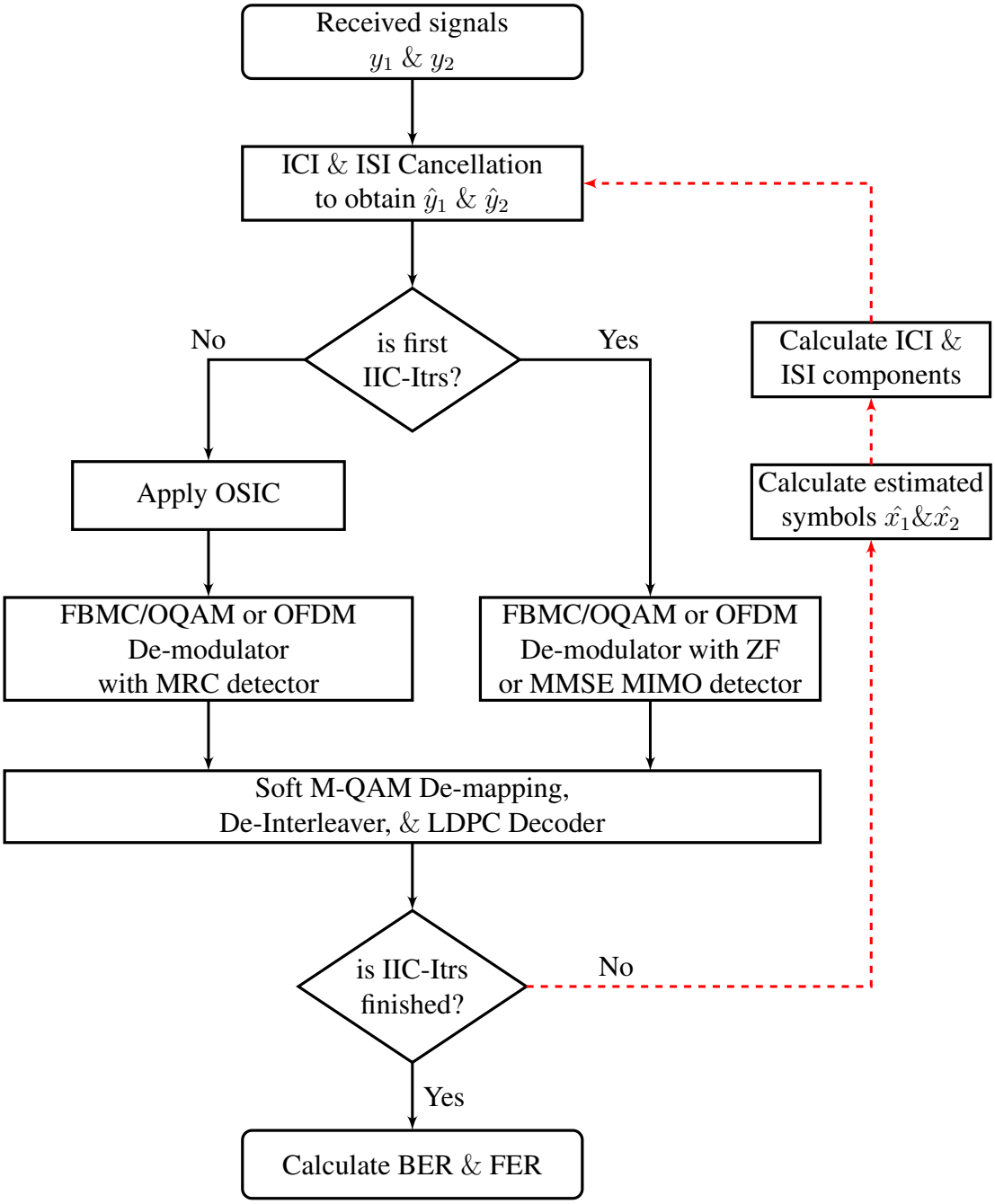

Figure 5.4: SIC based IIC flowchart (case-II).

5.4 Computational Complexity

The computational complexity of the MIMO-MCM systems can be evaluated by calculating the complexity of the linear and SIC detectors. In this chapter, the MIMO-MCM systems are operating in a quasi-static environment. This means that the channel transfer matrix $\mathbf{H}$ is constant during each transmitted frame. Therefore, the linear MIMO detection filtering matrices $\mathbf{G}_{ZF}$ and $\mathbf{G}_{MMSE}$ and SIC MIMO detection need to be calculated once per transmitted frame.

5.4.1 Complexity of ZF MIMO Detection

To calculate the complexity of the linear ZF-MIMO detection, start from (5.2) the expression of the ZF-MIMO detection equalisation matrix $\mathbf{G}_{ZF}$. The matrix-vector multiplication to calculate the estimated vector $\mathbf{s}_{est}$ from the transmitted vector $\mathbf{x}$ is given by

$$\mathbf{s}_{est} = \mathbf{G}_{ZF}\mathbf{x} \tag{5.38}$$

According to [174], the complexity of this complex matrix product is equal to $N_T(N_R - 1)$ complex additions and $N_T N_R$ complex multiplications. The complexity of slicing $N_T M - ary$ constellation points equals $N_T \log_2(M)$ real additions. Then, the complexity in terms of real additions and real multiplications [174] is equal $2N_T N_R + 2N_T(N_R - 1) + N_T \log_2(M)$ real additions and $4N_T N_R$ real multiplications.

In this chapter, each transmitted frame consists of 14 OFDM transmitted symbols or 28 FBMC/OQAM transmitted symbols with N subcarriers length. Therefore, the complexity of the ZF detection of each OFDM transmitted frame is equal $14\times N(2N_T N_R+2N_T(N_R-1) + N_T \log_2(M))$ real additions and $14 \times N \times 4N_T N_R$ real multiplications and the complexity of the ZF detection of each FBMC/OQAM transmitted frame is equal $28 \times N(2N_T N_R + 2N_T(N_R - 1) + N_T \log_2(M))$ real additions and $28 \times N \times 4N_T N_R$ real multiplications

5.4.2 Complexity of ZF with SIC MIMO Detection

As mentioned in 5.2.2, the SIC algorithm is iterative. After each SIC iteration, the dimension of the matrices used is reduced. This means that the complexity per SIC iteration is therefore reduced. The minimum squared of row of the ZF-MIMO detection filtering matrix represents the weight vector. These weighting vectors are used in the first SIC iteration to find the first estimate element of the transmitted data symbols. After that, the values of the transmitted constellation symbols are calculated which are used to calculate the next estimated element. Then, the effect of estimated symbol is subtracted from the received signal as explained in (5.11). The SIC iterative process continues N_T times. The complexity of the weight vector iterative process equals $N_R - 1$ complex additions, $\log_2(M)$ real additions, and N_R complex multiplications. Scale-vector product are a vector subtraction can be noticed in (5.11). Then, the complexity of the scale-vector product equals N_R complex multiplications and the complexity of the vector subtraction is N_R complex additions. The complexity of the ZF with SIC detection of each OFDM transmitted symbol in terms of real additions and real multiplications equals $14 \times N(2N_T(4N_R - 1) + N_T \log_2(M))$ real additions and $14 \times N(8N_T N_R)$ real multiplications and the complexity of each FBMC/OQAM transmitted symbol is $28 \times N(2N_T(4N_R - 1) + N_T \log_2(M))$ real additions and $28 \times N(8N_T N_R)$ real multiplications. More information about the efficient low-complexity of the SIC algorithm can be found in [175–177].

5.4.3 Complexity of MMSE Linear Detection and MMSE with SIC MIMO Detection

In MMSE-MIMO linear detection, the MMSE filtering matrix G_{MMSE} has the same dimension as the ZF filtering matrix G_{ZF}. This means that the complexity of MMSE detection and MMSE with SIC detection equals the complexity of the ZF detection and ZF with SIC detection which is calculated in 5.4.1 and 5.4.2.

5.4.4 Complexity of Linear and SIC Detections based IIC

As noted in 5.4.3, the complexity of the linear MMSE and ZF MIMO detections are equal, so the complexity of IIC will be discussed in the general situation. To discuss the complexity of the linear and SIC detection MIMO systems with IIC, it is necessary to calculate the complexity of the cases of using linear and SIC detectors which are explained in 5.3.2. The flow charts of the algorithm of these cases are shown in Figures 5.3 and 5.4. It is clear from these figures the IIC process of the *case-I* is only applied with linear MIMO detection. After the desired number of IIC iterations ($N_{IIC-Itrs}$), the SIC-MIMO detection is used. In *case-II*, $N_{IIC-Itrs}$ iterations of the IIC process are used with both linear and SIC MIMO detections. Therefore the complexity of the linear and SIC MIMO detections of these cases can be summarised:

$$\mathcal{O}_{case-I} = N_{IIC-Itrs} \times \mathcal{O}_{Linear-detection} + \mathcal{O}_{SIC-detection} \tag{5.39}$$

$$\mathcal{O}_{case-II} = N_{IIC-Itrs} \times (\mathcal{O}_{Linear-detection} + \mathcal{O}_{SIC-detection}) \tag{5.40}$$

According to (5.39) and (5.40), the complexity of the *case-II* of the MIMO system with linear and SIC detection is higher than that of the *case-I*.

5.5 Simulation Results

The simulated performance of the LDPC-MIMO-OFDM and LDPC-MIMO-FBMC/OQAM systems is evaluated using the simulation parameters which are given in Table 5.1. The PDPs for the EVA type of the LTE channel are presented in Table 2.1.

Table 5.1: Simulation Parameters Definition for the MIMO-MCM

Parameters	Definitions	Specifications
N_T	Number of transmitting antennas	2
N_R	Number of receive antennas	2 and 4
N	Total number of sub-carriers (used & unused)	128
N_{RB}	Number of resource blocks	6
N_{Sc-RB}	Number of sub-carriers per resource block	12
N_{Sc}	Number of used sub-carriers	$N_{Sc-RB} \times N_{RB}$
N_{slot}	Number of slots per resource block	2
N_{sym}	Number of symbols per slot	7 (OFDM) 14 (FBMC/OQAM)
N_s	Total number of symbols per resource block	$N_{sym} \times N_{slot}$
N_{cp}	Length of cyclic prefix (in samples)	0
M-QAM	Modulation type	4-QAM 16-QAM
S_s	Sub-carrier spacing (KHz)	15 KHz
F_s	Sampling frequency	$S_s \times N$
LTE	Type of LTE channel	EVA
H_{LDPC}	Parity check matrix of LDPC code	$[1008, 2016]$ (4-QAM) $[2016, 4032]$ (16-QAM)

Figure 5.5 shows the BER simulation results of the coded 2×2 MIMO-OFDM and MIMO-FBMC/OQAM systems using linear MMSE detection with 4-QAM and 16-QAM with 5 Hz and 70 Hz Doppler frequency over the EVA channel. After 5 IIC iterations, it is clear from this figure that the error floors are completely removed in both systems. The gaps from the PCIC simulation results are approximately of 0.9 dB and 1.6 dB for FBMC/OQAM system and 1.2 dB and 3.5 dB for OFDM system using 4-QAM with 5 Hz Doppler and 16-QAM with 70 Hz Doppler shift respectively, measured at 10^{-6} BER.

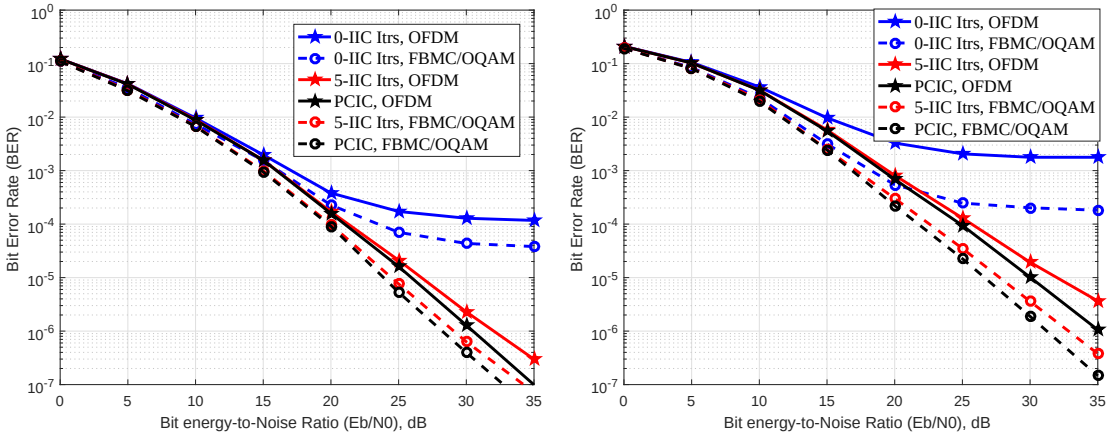

(a) 4-QAM and 5 Hz Doppler frequency (b) 16-QAM and 70 Hz Doppler frequency

Figure 5.5: BER performance of a 2×2 LDPC-MIMO-OFDM and LDPC-MIMO-FBMC/OQAM systems using linear MMSE detection over the EVA channel (a) 4-QAM and 5 Hz Doppler frequency (b) 16-QAM and 70 Hz Doppler frequency.

Figure 5.6 shows the BER simulation results of both coded 2×2 MIMO-OFDM and MIMO-FBMC/OQAM systems using linear MMSE detection with *case-I* and *case-II*SIC detection with 4-QAM and 5Hz Doppler frequency over the EVA channel. In MIMO-

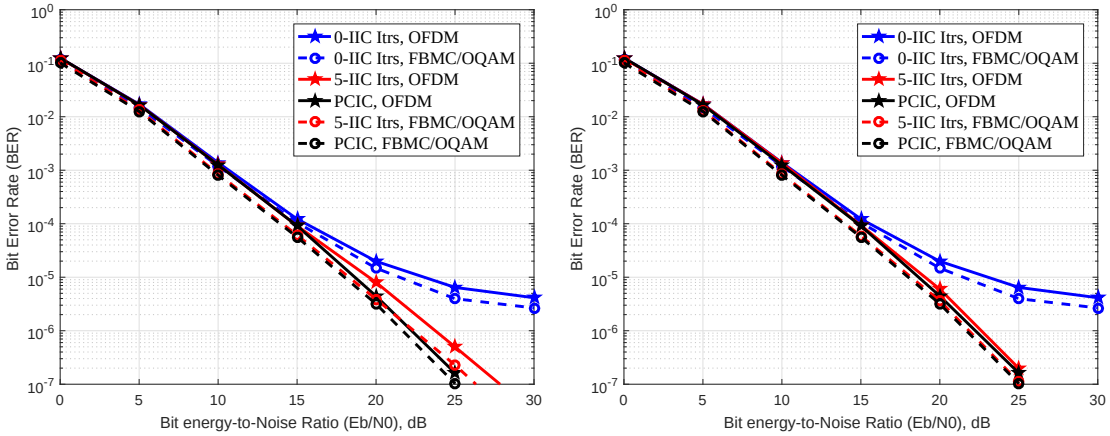

(a) SIC *case-I* (b) SIC *case-II*

Figure 5.6: BER performance of a 2×2 LDPC-MIMO-OFDM and LDPC-MIMO-FBMC/OQAM systems using linear MMSE and SIC detections with 4-QAM and 5 Hz Doppler frequency over the EVA channel (a) SIC *case-I* (b) SIC *case-II*.

OFDM systems, after 5 IIC iterations, the gap from the PCIC simulation result is approximately of 1 dB and 0.35 dB with using SIC *case-I* and *case-II* respectively, measured

at 10^{-6} BER. Using the SIC algorithm, the $Eb/N0$ gain between the PCIC simulation results becomes approximately 8.25 dB, measured at 10^{-6} BER. In contrast, in MIMO-FBMC/OQAM systems, the gap becomes 0.7 dB and 0.15 dB with SIC *case-I* and *case-II* respectively. 6.6 dB $Eb/N0$ gain is achieved with using SIC algorithm. In both cases, the transmitted signals are used directly to calculate the ICI/ISI components. After removing these components, the PCIC simulation results are obtained. There is a significant improvement in the PCIC simulation results with SIC detection compared to that without SIC. That because of the diversity which is achieved with SIC as explained in Section 5.3.2.

Figure 5.7 shows the simulation results of the LDPC-MIMO-OFDM and LDPC-MIMO-FBMC/OQAM systems using MMSE linear and SIC detection *case I* and *case II* with 16-QAM and 70 Hz Doppler frequency over the EVA channel. It is clear from this figure that the error floors are completely removed after 5 IIC iterations in both systems with both cases of the SIC detections. After 5 iterations, the gap from the PCIC simulation results is approximately of 1.6 dB and 0.7 dB for the OFDM system and 0.7 dB and 0.45 dB for FBMC/OQAM using *case I* and *case II* SIC detection respectively, measured at 10^{-6} BER.

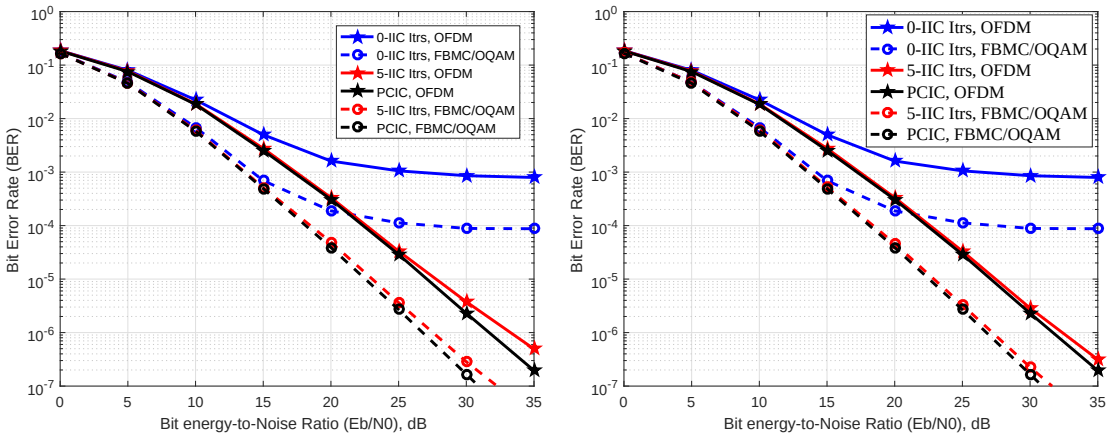

(a) SIC *case-I* (b) SIC *case-II*

Figure 5.7: BER performance of a 2×2 LDPC-MIMO-OFDM and LDPC-MIMO-FBMC/OQAM systems using linear MMSE and SIC detections with 4-QAM and 5 Hz Doppler frequency over the EVA channel (a) SIC *case-I* (b) SIC *case-II*.

For more scalability, 2×4 MIMO scheme is used for both OFDM and FBMC/OQAM systems. Figures 5.8 and 5.9 show respectively that the BER and FER simulation results

for both LDPC-OFDM and FBMC/OQAM systems using 2×4 MIMO scheme and linear MMSE with SIC detection and 16QAM over EVA channel. The comparison between both LDPC-OFDM and LDPC-FBMC/OQAM systems with 2×2 MIMO and 2×4 MIMO schemes is summarised in Table 5.2.

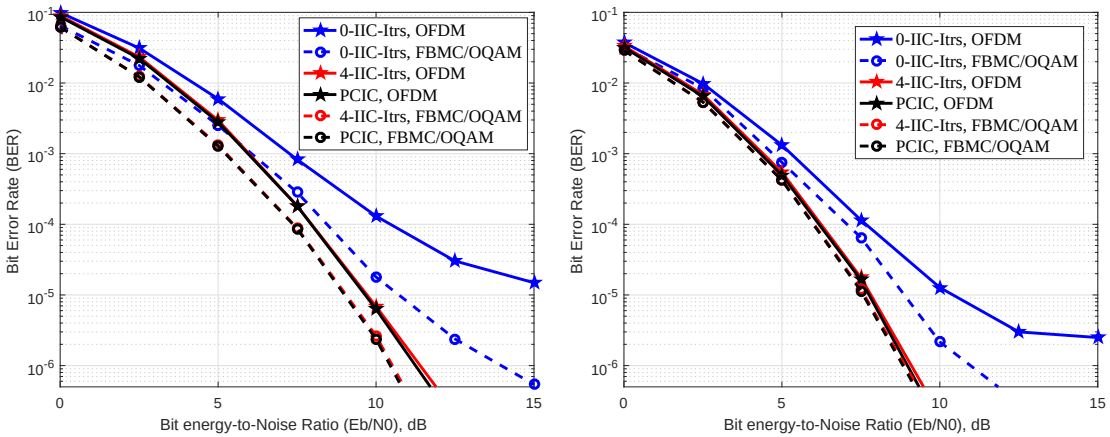

(a) Without SIC (b) With SIC *case-I*

Figure 5.8: BER performance of a 2×4 LDPC-MIMO-OFDM and LDPC-MIMO-FBMC/OQAM systems using linear MMSE and with and without SIC detections with 16-QAM and 70 Hz Doppler frequency over the EVA channel (a) Without SIC (b) With SIC *case-I*.

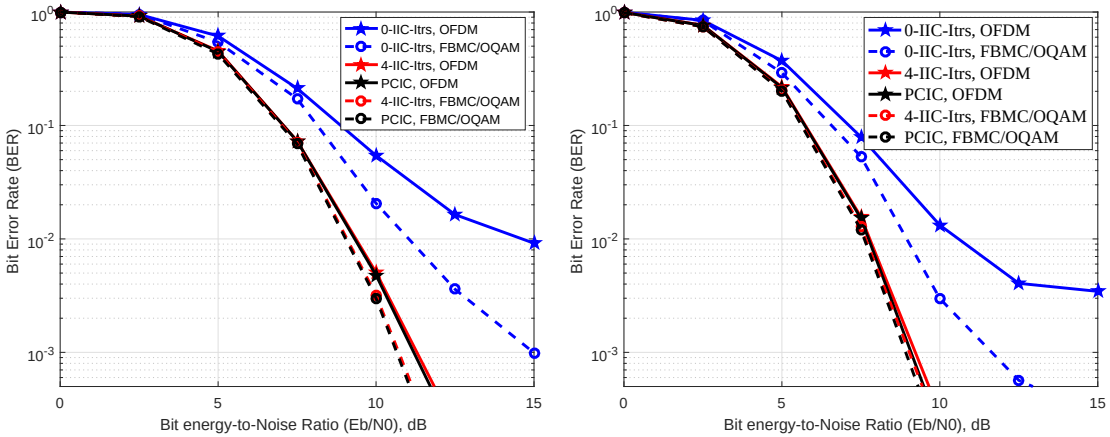

(a) Without SIC (b) With SIC *case-I*

Figure 5.9: FER performance of a 2×4 LDPC-MIMO-OFDM and LDPC-MIMO-FBMC/OQAM systems using linear MMSE and with and without SIC detections with 16-QAM and 70 Hz Doppler frequency over the EVA channel (a) Without SIC (b) With SIC *case-I*.

Table 5.2: Simulation results for 2×2 and 2×4 MIMO-OFDM and MIMO-FBMC/OQAM systems using linear and SIC detections with 4-QAM and 16-QAM over EVA channel.

System	Figure	Use SIC	IIC-Itrs	**Gap** from PCIC (dB)	Gain after SIC (dB)	BER/ FER	M-QAM
OFDM	5.5(a)	-	5	1.2	-	10^{-6}	4-QAM
	5.5(b)	-	5	3.5	-	10^{-6}	16-QAM
	5.6(a)	*case-I*	5	1	8.25	10^{-6}	4-QAM
	5.6(b)	*case-II*	5	0.35	8.25	10^{-6}	4-QAM
	5.7 (a)	*case-I*	5	1.6	8.25	10^{-6}	16-QAM
	5.7 (b)	*case-II*	5	0.7	8.25	10^{-6}	16-QAM
	5.8(a)	-	5	0.15	-	10^{-6}	16-QAM
	5.8(b)	*case-I*	5	0.12	2.3	10^{-6}	16-QAM
	5.9(a)	-	5	0.1	-	10^{-3}	16-QAM
	5.9(b)	*case-I*	5	0.1	2.1	10^{-3}	16-QAM
FBMC/ OQAM	5.5(a)	-	5	0.9	-	10^{-6}	4-QAM
	5.5(b)	-	5	1.6	-	10^{-6}	16-QAM
	5.6(a)	*case-I*	5	0.7	6.6	10^{-6}	4-QAM
	5.6(b)	*case-II*	5	0.15	6.6	10^{-6}	4-QAM
	5.7 (a)	*case-I*	5	0.7	6.6	10^{-6}	16-QAM
	5.7 (b)	*case-II*	5	0.45	6.6	10^{-6}	16-QAM
	5.8(a)	-	5	0.08	-	10^{-6}	16-QAM
	5.8(b)	*case-I*	5	0.06	1.7	10^{-6}	16-QAM
	5.9(a)	-	5	0.06	-	10^{-3}	16-QAM
	5.9(b)	*case-I*	5	0.06	1.8	10^{-3}	16-QAM

It is clear from the above figures that the error floors are completely removed after 5 IIC iterations with both linear and SIC detections. With IIC only and with *case I* of SIC, after five IIC iterations, the gap from the PCIC simulation results is smaller in FBMC/OQAM simulation than that of OFDM with both 4-QAM and 16-QAM as shown in Table 5.2.

However, the $Eb/N0$ gain after applying *case I* of the SIC in the OFDM system is better than that of FBMC/OQAM. With the *case II* of the SIC detection, the performance of the FBMC/OQAM systems is better than that of OFDM after five IIC iteration as shown in Table 5.2. In general, with used SIC detection, the second order diversity is approximately achieved.

5.6 Summary

This chapter can be summarised as follows:

- IIC and MIMO-IIC schemes have been applied to MIMO-OFDM and MIMO-FBMC/OQAM systems with linear detection to reduce ICI/ISI interference without increasing the equaliser complexity. IIC and MIMO-IIC have been used to reduce the ICI/ISI interference of the transmitted signal from the target and the other antenna respectively. After some iterations, the error floors have been completely removed in both systems. A more significant improvement has been achieved for the MIMO-FBMC/OQAM system than for the MIMO-OFDM.
- SIC detection has been applied using two approaches. In the first, after the desired number of IIC and MIMO-IIC iterations, the SIC algorithm has been used to improve the system performance by reducing the cross interference between data streams. In the second, at the first iteration, IIC and MIMO-IIC have been used to calculate the ICI/ISI components from the estimated decoded signals and remove them from the received signals. After that SIC detection has been applied for the desired number of iterations. With both approaches, a significant improvement has been achieved for both MIMO-OFDM and MIMO-FBMC/OQAM systems. In both cases, a second order diversity has been approximately achieved.

Chapter 6

Convergence Analysis

Contents

6.1 Introduction

In iterative decoding systems, the important parameters to analyse the system convergence are: the required number of iterations, the start of the waterfall region (convergence threshold), and the trajectory of the iterative process. These parameters can be determined by describing the exchange of the mutual information by using the so-called the EXtrinsic Information Transfer (EXIT) chart [178].

To reduce the complexity of the iterative receiver, Bit Interleaved Coded Modulation (BICM) was introduced in [179], using a bit interleaver between an encoder and

a mapper. To improve the performance, Gray mapping is used with the BICM system [180]. To achieve a better performance for iterative decoding, BICM based iterative decoding (BICM-ID) or iterative demapping and decoding (IDEM) were introduced in [181, 182]. Different constellation mappings are used instead of Gray mapping because it does not perform well with these systems [183]. In broadband communication systems, BICM was studied for SISO-OFDM systems in [184] and for MIMO-OFDM in [184, 185]. Furthermore, Fast-Than-Nyquist OFDM/OQAM (FTN-OFDM/OQAM) system has been proposed to switch between FTN and Nyquist modes without increasing the system complexity [186].

In this chapter, an iterative interference cancellation based BICM (BICM-IIC) scheme is proposed for the OFDM, DWT/MCM and FBMC/OQAM systems to study the performance of these systems and calculate the required number of iterations to eliminate ISI and ICI and remove them from the received signal. Compensation schemes are developed for these three systems with an insufficient CP. ISI and ICI are eliminated for LDPC-OFDM, LDPC-DWT/MCM and LDPC-FBMC/OQAM systems in all but the most severe multipath channels. An LDPC iterative decoder is used with different mapping M-QAM modulation in different environments for different channel conditions. The convergence of the iterative interference cancellation (IIC) for these systems is analysed with the help of EXIT charts when the channel is assumed to be known at the receiver. This proposal provides a means to define performance for a given outage probability on quasi-static fading channels.

The rest of this chapter is organized as follows: In Section 6.2 a system model of the BICM-IIC scheme for SISO-MCM systems is introduced. Simulation results for SISO-MCM are given in Section 6.4. In Section 6.5, a system model of the BICM-IIC for LDPC-MIMO-OFDM and LDPC-MIMO-FBMC/OQAM systems with the simulation results are presented. Finally, a summary of this chapter is presented in Section 6.6.

6.2 Convergence Analysis of SISO Systems

To study the performance of the LDPC-FBMC/OQAM and LDPC-OFDM systems with BICM-IIC, there are two iterative processes convergence analyses are performed. First, the iterative process of the LDPC decoding (Dec_2) between the variable node decoding (VND) and check node decoding (CND), which is denoted by inner iteration (I_{in}) [187–189]. Second, the iterative process of the iterative interference cancellation between the interference cancellation part with demapping (Dec_1) and the LDPC decoding (Dec_2) which is denoted by outer iteration (I_{out}) as shown in the proposed model of BICM-IIC in Figure 6.1. Furthermore, the effect of the iterative process I_{in} on the convergence analysis of the iterative process I_{out} will be studied. In Figure 6.1, I_{A1} and I_{A2} represent the *a priori* mutual information input of the interference cancellation part (Dec_1) and the LDPC decoder (Dec_2) respectively, and I_{E1} and I_{E2} represent their corresponding extrinsic mutual information output.

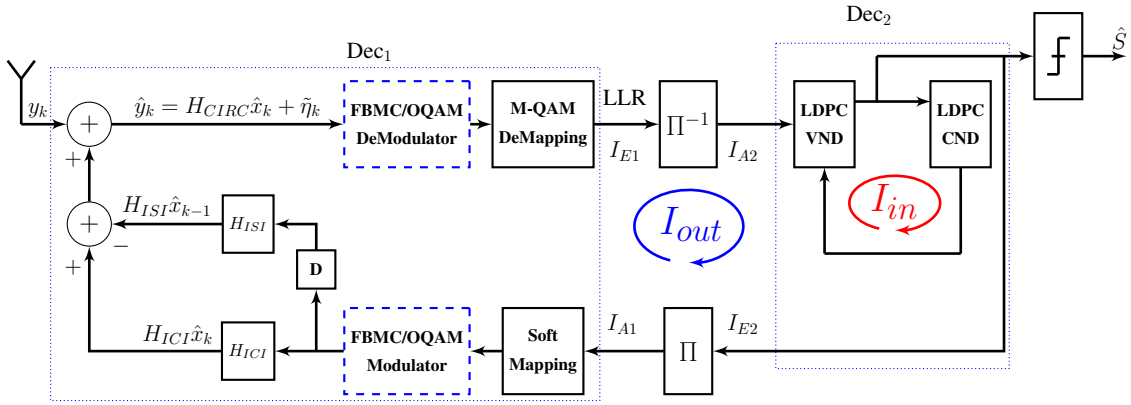

Figure 6.1: Receiver side of the proposed BICM-IIC scheme of the LDPC-FBMC/OQAM system.

Instead of using the probability density function of the transmitted bit $x \in \{-1, +1\}$ [178], a simple approximation is used to calculate the mutual information I (*a priori* or extrinsic) [190].

$$I \approx 1 - \frac{1}{N_t} \sum_{n=1}^{N_t} log_2 \left(1 + e^{-x_n L_n}\right) \tag{6.1}$$

where N_t is the length of transmitted signal and L_n is the LLR associated with the trans-

mitted bit x.

According to [178], to calculate the *a priori* mutual information I_A, first, the prior $A(x_n)$ of the known transmitted information x can be calculated by applying an independent random variable u_x with zero mean and variance σ_x^2 as:

$$A(x_n) = \frac{\sigma_x^2}{2} x_n + u_x \tag{6.2}$$

According to [191], for the random variable x, the variance σ_x^2 for each given mutual information value $I_x \in \{0, 1\}$ can be approximately calculated as:

$$\sigma_x \approx \left(-\frac{1}{G_1} \log_2 \left(1 - (I_a)^{1/G_3} \right) \right)^{1/2G_2} \tag{6.3}$$

where $G_1 = 0.3070$, $G_2 = 0.8935$, and $G_3 = 1.1064$.

The EXIT curves for Dec_1 and Dec_2 can be obtained by drawing the mutual information (I_{A1}, I_{E2}) against (I_{E1}, I_{A2}) where they are placed on the abscissa and the ordinate of the graph respectively as shown in Figure 6.2. The tunnel between these two curves describes the convergence analysis of the iterative system. If the EXIT tunnel is open, a minimum BER will be achieved. By contrast, the system performance is become closer to the channel capacity at the narrower EXIT tunnel.

To draw the EXIT curves for Dec_1 and Dec_2, the *a priori* mutual information I_{A1} and I_{A2} are calculated directly from the known interleaved and encoded signals respectively by using equations (6.1) to (6.3). Then, extrinsic mutual information I_{E1} and I_{E2} are calculated by applying (6.1) to the extrinsic outputs of Dec_1 and Dec_2 respectively as shown in Figure 6.1. The tunnel between these two curves must be open. In other words, these two curves must be intersect across the EXIT chart. The IIC and decoding iterations (I_{out} and I_{in}) can be represented by exchanging of extrinsic information from one curve to the other as a *zig-zag* trajectory in EXIT chart. The convergence point is achieved when the extrinsic output of the decoder, I_{E2}, reaches one, that is, when the trajectory reaches the right hand side of the diagram.

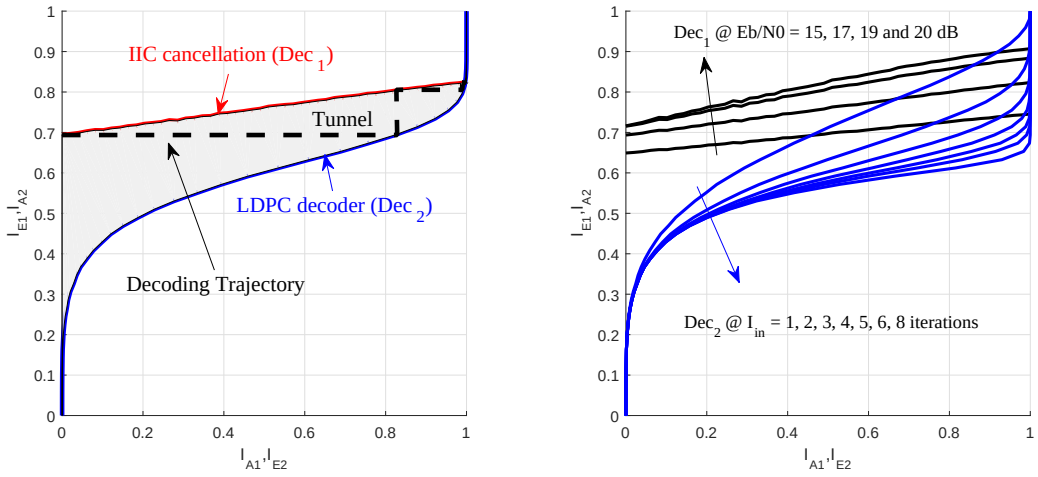

(a) (b)

Figure 6.2: (a) EXIT chart and the decoding trajectory of two concatenated decoders (b) EIXT curves of Dec_1 and Dec_2 with different E_b/N_0 and I_{in} values.

6.3 Convergence Analysis of MIMO Systems

Figure 6.3 shows the block diagram of the receiver side of the proposed BICM-IIC model of the 2×2 MIMO-MCM system. In this section, the convergence analysis will be discussed in two scenarios. First, the number of MIMO-IIC iterations will be predicted by drawing the EXIT chart with linear detection and without SIC detection. Second, at the first iteration MIMO-IIC will be applied with linear detection. Then SIC detection will be used to improve the system performance. In this case, the number of MIMO-IIC iterations will be predicted with SIC detection. In this figure, the outer iteration I_{out} represents the iterative process between the MIMO-IIC detector with detection and demapping (Dec_1) and the LDPC decoder (Dec_2). The first part Dec_1 represents the 2×2 MCM demodulator with linear and SIC detection and M-QAM demapper. First, after ICI/ISI cancellation, the received signals are equalised using linear or SIC detection as explained in Section 5.3. Then the equalised signals for each stream are demodulated using M-QAM demapping. The second part Dec_2 represent the iterative process between the VND and CND of the LDPC decoder. The convergence analysis of the outer iteration I_{out} can be obtained by drawing the extrinsic mutual information (I_{E11} or I_{E12}) against the *a priori* mutual information (I_{A11} or I_{A12}) respectively.

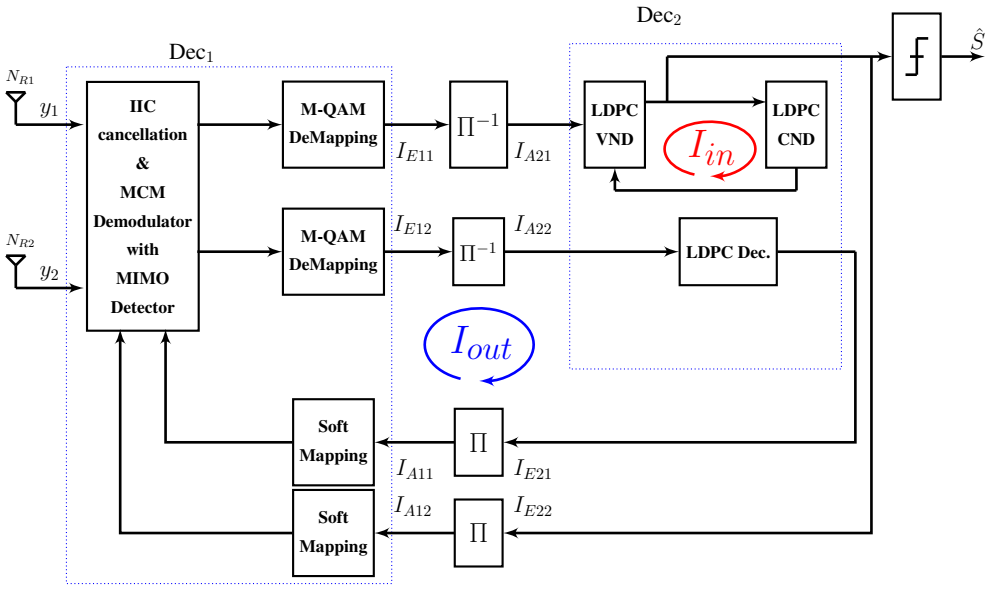

Figure 6.3: Receiver side of the proposed BICM-IIC scheme of the 2×2 MIMO-MCM systems.

6.4 Simulation results of SISO systems

In SISO LDPC-OFDM, LDPC-DWT/MCM, and LDPC-FBMC/OQAM systems based BICM-IIC scheme, the simulation parameters which are defined in Table 3.2 will be used in this section with different mapping for 16-QAM.

Figure 6.2-(a) shows the EXIT chart with the decoding trajectory of interference cancellation with demapper (Dec_1) and LDPC decoder (Dec_2). The decoding trajectory shows the required number of the IIC iterations to reduce ISI and ICI from the received signal. The EXIT curves of the Dec_1 and Dec_2 depend mainly on the E_b/N_0 and the I_{in} respectively as shown in Figure 6.2-(b). At low $Eb/N0$, the transfer characteristics of the Dec_1 are shifted downward. This means that transfer characteristics of the Dec_1 and Dec_2 are intersected at low mutual information. Therefore, the ICI and ISI cannot be reduced resulting in an error floor in BER curve. As I_{in} and $Eb/N0$ increase, the tunnel between the Dec_1 and Dec_2 transfer characteristics open as shown in Figure 6.2-(a). Then, the performance of the system will be improved and the error floor will be reduced with fewer IIC iterations.

Table 6.1: EVA/ETU-LTE downlink channel impulse response h_t

Channel impulse response h_t	
EVA	ETU
-0.4276 + 0.3073i	-0.2257 + 0.2603i
-0.2341 - 0.1383i	0.3498 + 0.7665i
0.0983 + 0.4364i	0
0.0424 - 0.0076i	-0.0891 - 0.3977i
0	0.1920 - 0.1698i
0.0668 + 0.0655i	0
	0
	0
	0
	0
	-0.0692 - 0.2294i

As mentioned in the literature, different mappings are used in the BICM-ID system where with gray mapping the demapper curve (I_{E_1} vs. I_{A_1}) is almost flat. This means that there is no significant gain with increasing *a priori* mutual information and the iterations of the iterative process. The *a priori* information which is calculated directly from the encoded signal (to draw the demapper curve) or obtained from the estimated decoded signal (to draw the trajectory) is fed directly to the demapper to improve the detection of the current bits. In this section, the *a priori* information (I_{A_1}) is only used to improve the received signal by reducing the interference which occurs due to the effect of the multipath channel.

In addition to the $Eb/N0$ value, the transfer characteristic of the Dec_1 also depends on the CIR. For each transmitted frame, a specific CIR is randomly generated. This means that a specific transfer characteristic is obtained for each transmitted frame. From the sampling frequency (the subcarrier spacing multiply by the number of subcarriers), the sample period is calculated. Then, the powers of taps within one sample period are aggregated. A new sampled power delay profile is thereby created and then following that power delay profile, new randomly chosen tap weights are generated. After that, this new power delay profile and tap weights are used with the Jakes' model to generate the CIR. Now, to study the transfer characteristics of Dec_1 and Dec_2 of the LDPC-OFDM, LDPC-DWT/MCM, and LDPC-FBMC/OQAM based IIC, a specific CIR (h_t) of the EVA and ETU LTE downlink is generated as shown in Table 6.1.

Figure 6.4 shows the EXIT chart transfer characteristics of the LDPC-OFDM system based BICM-IIC using 64-QAM over the EVA/ETU-LTE channels. It is clear from this figure that with low $Eb/N0$ (14 or 15 dB), the transfer characteristics of the two decoders intersect at low mutual information. With increased $Eb/N0$ (17dB or more) and more LDPC decoder iterations, the tunnel is opened and low BER can be achieved with fewer I_{out} iterations as shown in Figure 6.5.

In the case of the EVA channel, with 1 decoder iteration, the two curves intersect at mutual information between 0.3 and 0.9 at $Eb/N0$ between 15 dB and 20 dB. This means that the tunnel is blocked and the system performance cannot be improved through IIC iterations as shown in Figure 6.5. With more decoder iterations ($I_{in} \geq 3$) and with high $Eb/N0$ (≥ 19), the tunnel between these two curves is open. These $Eb/N0$ values correspond to the waterfall region (turbo cliff position) as verified in Figure 6.5.

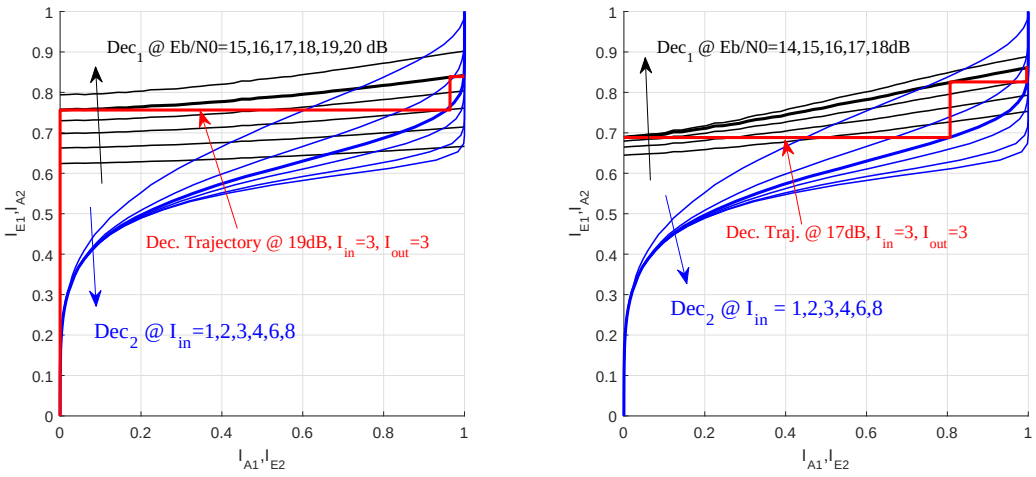

(a) EVA channel (b) ETU channel

Figure 6.4: EXIT chart and the decoding trajectory of the LDPC-OFDM system based BICM-IIC using 64QAM and MMSE equaliser (a) EVA channel (b) ETU channel.

Figure 6.5 shows the BER curves of the LDPC-OFDM based BICM-IIC scheme using 64-QAM over the EVA/ETU-LTE channel impulse response given in Table 6.1. The sold blue curves show the BER performance at 1 LDPC decoder iteration and without IIC iteration. As shown in the EXIT chart, in this case, the two curves intersect at various values of mutual information (≥ 0.9), depending on the $Eb/N0$ values. This means that the tunnel is blocked and the system performance cannot be improved even with more I_{out}

iterations as shown in the dashed blue curve. When the $Eb/N0$ increases, the EXIT curve of $Dec1$ is moved up. With more decoder iterations $I_{in} = 3$, according to the EXIT chart, the tunnel is open and more than 3 outer iterations are required to reach the intersection point between the two curves at mutual information equal to 1 when $Eb/N0 \geq 19$ dB with the EVA channel. This means that the turbo cliff (or waterfall region) will be observed in BER simulations. The red curves show the BER simulation result for this case. When the $Eb/N0 \leq 16$ dB, the two EXIT curves are intersected at mutual information (≤ 0.7) and the tunnel is blocked. The result of that so-called low $Eb/N0$ region as shown in the red curve in Figure 6.4. Similarly when the number of LDPC decoder iteration increases, the EXIT curve becomes flatter. The result of that is that with more LDPC decoder iterations, the tunnel opens more quickly. This means that a steeper BER curve is obtained.

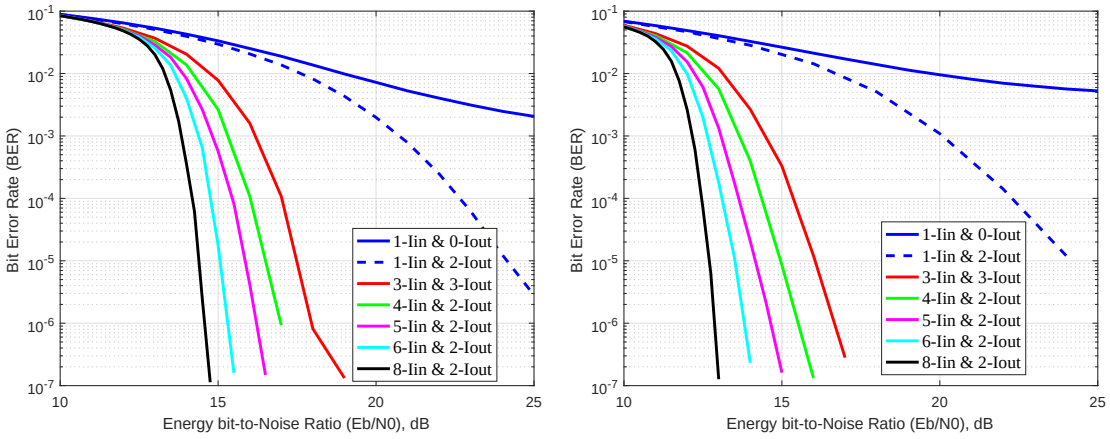

(a) EVA channel (b) ETU channel

Figure 6.5: BER performance of the LDPC-OFDM system based BICM-IIC scheme using 64QAM and MMSE equaliser (a) EVA channel (b) ETU channel.

In this section, in addition to the use of Gray mapped 16-QAM, the optimized mapping $M16^r$ and maximum squared Euclidian weight (MSEW) mapping are used [192, 193]. Binary switching is used to design the $M16^r$ mapping [192].

Figures 6.6 and 6.7 show the BER simulation results and EXIT curves with decoding trajectory of the LDPC-OFDM based BICM-IIC using $M16^r$ and MSEW mappings respectively with a ZF equaliser over the EVA channel. The CIR of the EVA-LTE channel which is given in Table 6.1 is used. We notice in these figures that with $Eb/N0 \leq 13$ dB and $I_{in} = 1$, the two curves intersect at low mutual information (≤ 0.25) and the tunnel

is blocked. Again, the IIC iterations cannot improve the system performance, resulting in a high BER. The result of that simulation as shown in solid and dashed blue curves in Figures 6.6-b and 6.7-b. With increase $Eb/N0 \geq 14$ dB, the tunnel is open. This means

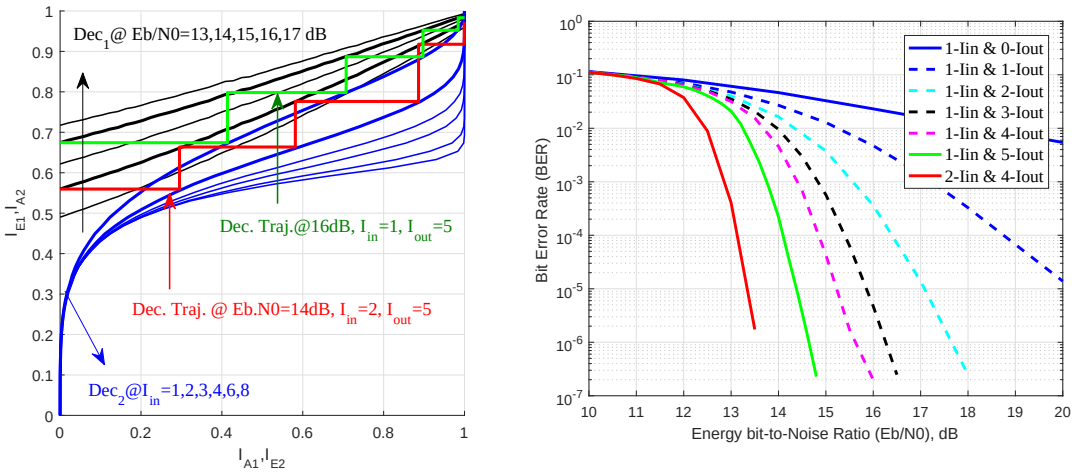

(a) EXIT chart

(b) BER

Figure 6.6: BER and EXIT chart with the decoding trajectory of the LDPC-OFDM system based BICM-IIC scheme using $M16^r$ mapping with a ZF equaliser over the EVA channel (a) EXIT chart (b) BER.

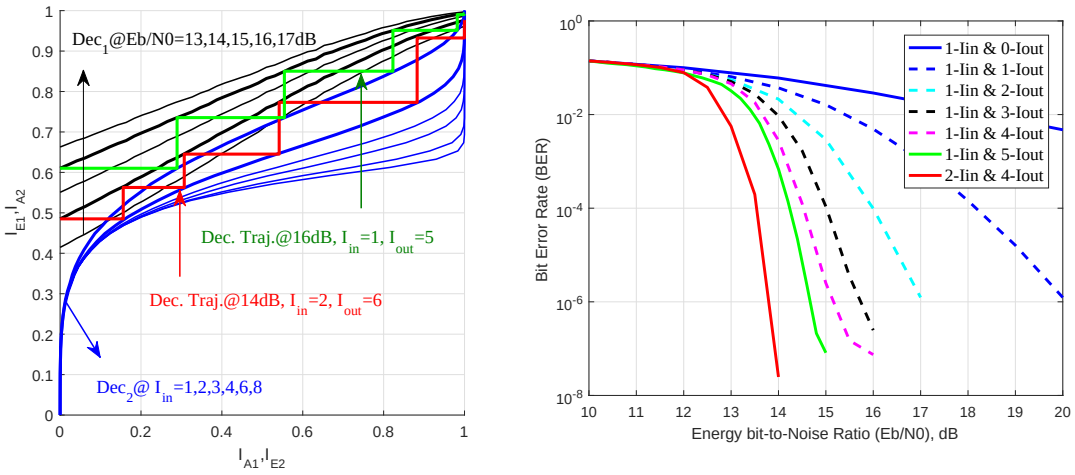

(a) EXIT chart

(b) BER

Figure 6.7: BER and EXIT chart with the decoding trajectory of the LDPC-OFDM system based BICM-IIC scheme using MSEW mapping with a ZF equaliser over the EVA channel (a) EXIT chart (b) BER.

that with an increasing number of IIC iterations, the system performance is improved and

the waterfall region is obtained at the corresponding $Eb/N0$ value as shown in the sold green curves in the BER simulation results. As the number of decoder iterations increases ($I_{in} = 2$), the tunnel becomes wider and the turbo cliff position is achieved at lower $Eb/N0$ values as shown in the solid red curve in the BER simulations. Furthermore, these mappings change the slope of the EXIT curve to better match the decoder EXIT curve, for smaller numbers of inner iterations.

Figure 6.8 shows the BER performance and EXIT chart characteristics of the LDPC-DWT/MCM based BICM-IIC system using an MMSE equaliser and Gray mapped 64-QAM over the ETU-LTE channel given in Table 6.1. In this figure, for one decoder iteration I_{in} and $Eb/N0 \leq 20$ dB, the two curves intersect at a mutual information ≤ 0.8. This means that more IIC iterations cannot improve the system performance and high BER simulation will be obtained as shown in the sold blue BER curve. With increase the decoder iteration, the tunnel becomes wider and the turbo cliff position is achieved at low $Eb/N0$ values.

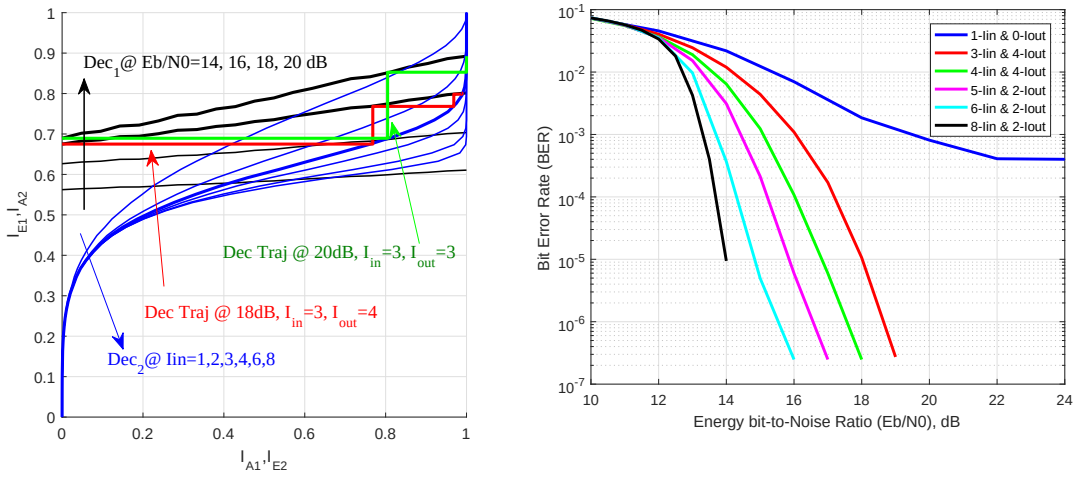

(a) EXIT chart

(b) BER

Figure 6.8: BER performance and EXIT chart characteristics of the LDPC-DWT/MCM system based BICM-IIC scheme using MMSE equaliser over ETU channel (a) EXIT chart (b) BER.

Figure 6.9 shows the BER performance and EXIT chart characteristics of the LDPC-DWT/MCM based BICM-IIC system using an MMSE equaliser and MSEW mapped 16-QAM over the EVA-LTE channel given in Table 6.1. Using MSEW mapped 16-QAM,

an open tunnel is obtained when the $EbN0 \geq 16$ dB regardless of the number of decoder iterations. A the number of decoder iterations increases, fewer IIC iterations are required to achieve low BER simulation results as shown in Figure 6.9-b.

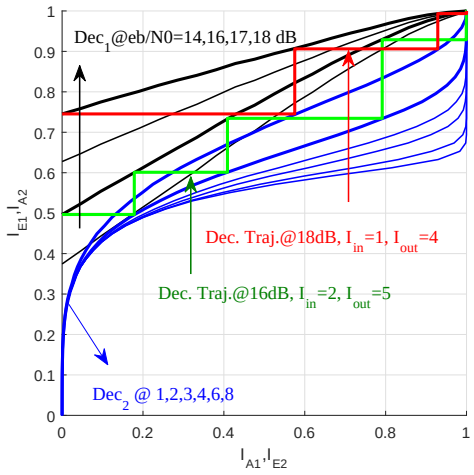

(a) EXIT chart

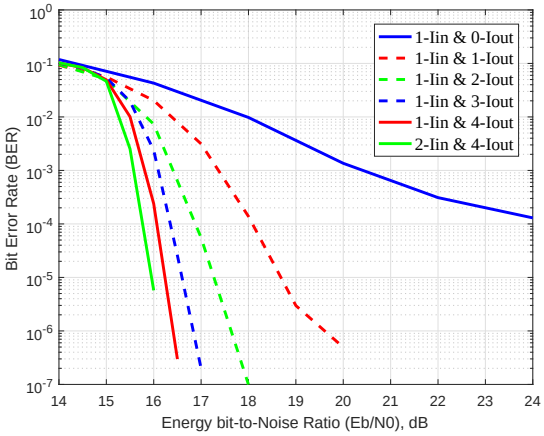

(b) BER

Figure 6.9: BER performance and EXIT chart characteristics of the LDPC-DWT/MCM system based BICM-IIC scheme using MMSE equaliser with MSEW mapped 16-QAM over EVA channel (a) EXIT chart (b) BER.

Figures 6.10 and 6.11 show the EXIT chart transfer characteristic and the corresponding BER simulation results respectively of the LDPC-FBMC/OQAM system using Gray mapped 64-QAM with MMSE equaliser over the EVA/ETU-LTE channels. As in previous figures, with Gray mapping, with one decoder iteration ($I_{in} = 1$), the tunnel is closed when $Eb/N0 \leq 20$ dB. This means that more IIC iterations cannot improve the system performance, resulting in high BER. As the number of decoder iterations increases $I_{in} \geq 3$, low BER is achieved and the $Eb/N0$ values corresponding to the turbo cliff area have to be reduced as shown in Figures 6.12 and 6.13.

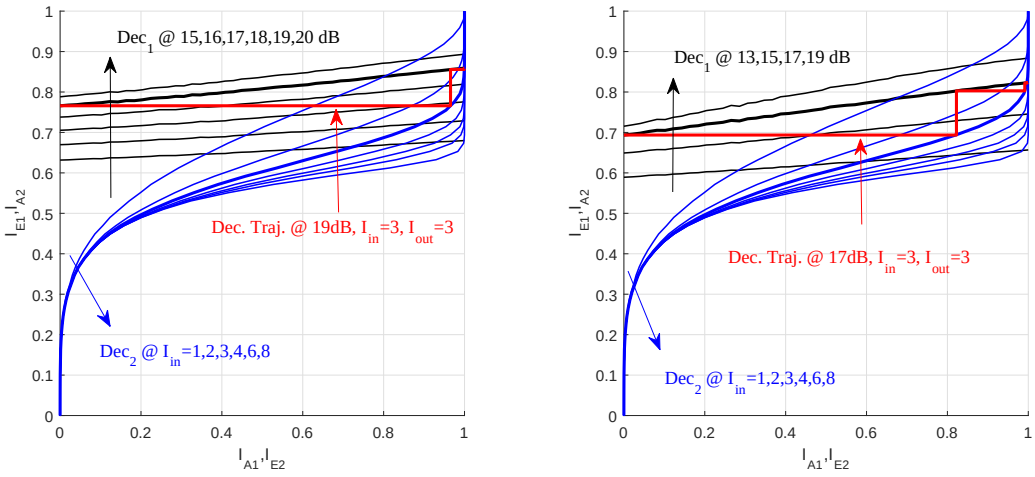

(a) EVA channel (b) ETU channel

Figure 6.10: EXIT chart transfer characteristics of the LDPC-FBMC/OQAM system based BICM-IIC scheme using MMSE equaliser with Gray mapping 64-QAM (a) EVA channel (b) ETU channel.

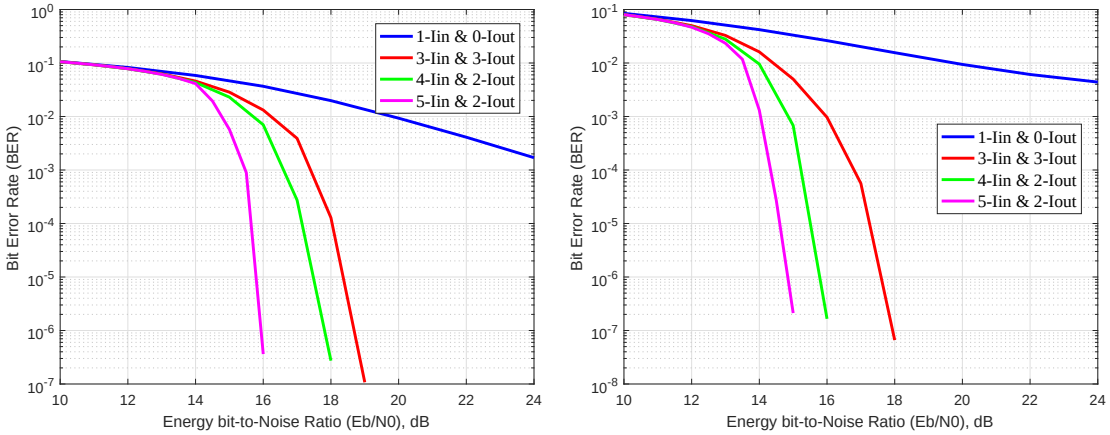

(a) EVA channel (b) ETU channel

Figure 6.11: BER curves of the LDPC-FBMC/OQAM system based BICM-IIC scheme using MMSE equaliser with Gray mapping 64-QAM (a) EVA channel (b) ETU channel.

Figures 6.12 and 6.13 show the EXIT chart transfer characteristic and its corresponding BER simulation results for the LDPC-FBMC/OQAM system using $M16^r$ and MSEW mapped 16-QAM respectively with ZF equaliser over EVA channel. We notice in these figures that using $M16^r$ and MSEW mapped 16-QAM, the tunnel remains open even with 1 decoder iteration if $Eb/N0 \geq 13$ dB. This means that low BER can be achieved after

some IIC iterations as shown in the BER simulation curves. With more decoder iterations, the tunnel becomes wider and the turbo cliff position can be noticed corresponding to this $Eb/N0$ value, and a steeper BER simulation curve is obtained.

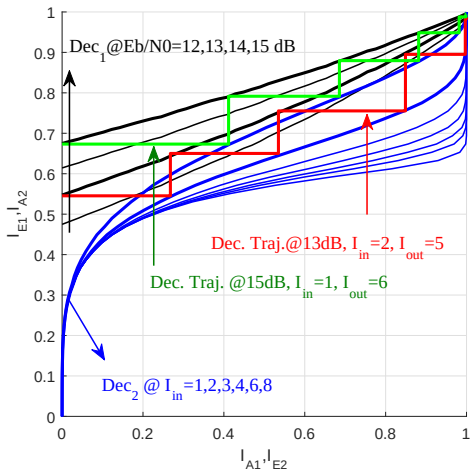

(a) EXIT chart

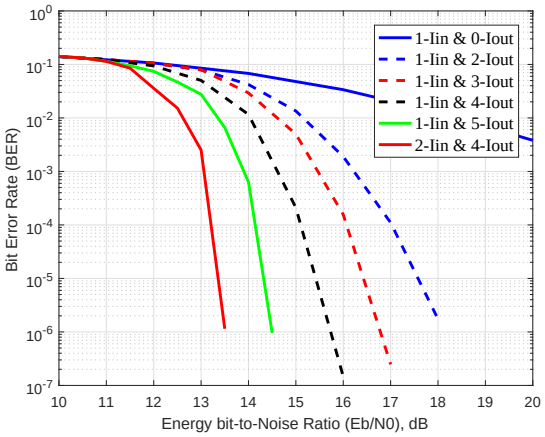

(b) BER

Figure 6.12: EXIT chart characteristic and BER simulation of the LDPC-FBMC/OQAM system based BICM-IIC scheme $M16^r$ mapped 16-QAM with ZF equaliser over EVA channel (a) EXIT chart (b) BER.

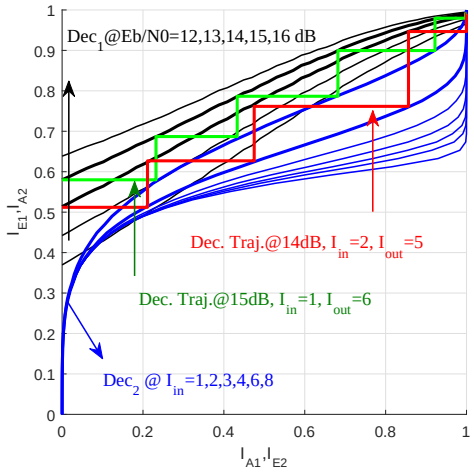

(a) EXIT chart

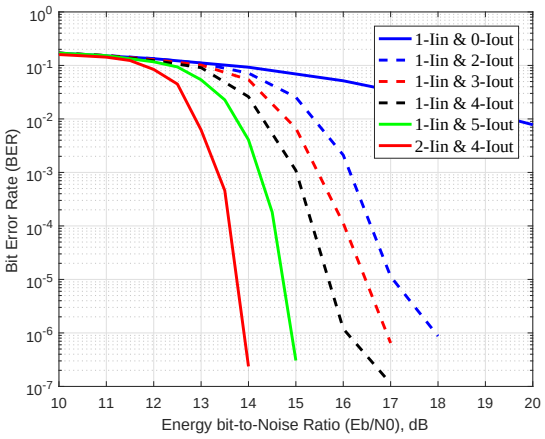

(b) BER

Figure 6.13: BER performance of the LDPC-FBMC/OQAM system based BICM-IIC scheme using MSEW mapped 16-QAM with ZF equaliser over EVA channel (a) EXIT chart (b) BER.

The problem with the above set of EXIT charts is that they are for one specific channel

out of a random set, and therefore do not describe the statistics of the performance of the decoder on random channels. The EXIT chart as originally defined can be used on fading channels only in the limit of ergodic fading with very long codes [178], but as they stand they cannot be used with quasi-static fading. This proposal provides a means to define performance for a given outage probability on quasi-static fading channels. The idea here is to consider 90% of the cases, so the EXIT curve is the mutual information achieved in 90% of the cases. We assume 100 randomly chosen channels. For each channel, a different EXIT curve is obtained. This means that 100 detector lines are obtained and we could find a position on the graph such that 90% lie above and 10% below this position. That means that this amount of mutual information is achieved in 90% of those random channels. This means that at each *a priori* mutual information I_{A1}, we take the 90^{th} line down from the top. The line which is drawn across these points indicates that in 90% of the channels, the mutual information would at least be satisfied. If this line does not intersect with the decoder transfer characteristic curve, that means in 90% of the channels the iterations will proceed. Figure 6.14 shows the EXIT curves between the mutual information I_{E1} and I_{A1} of the interference cancellation part Dec_1 using 50 randomly generated instances of the ETU channel with 16-QAM at 15 dB $Eb/N0$. The red line represents the selected EXIT curve and there are 45 (90% of 50) of the corresponding EXIT curves which lie above it. The same approach can be used with different availability figures depending on the requirements of the application.

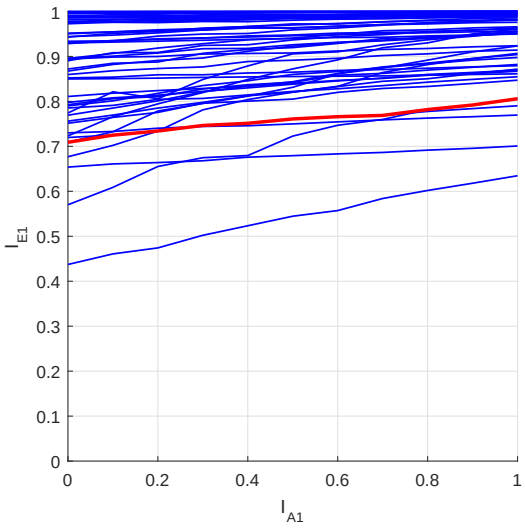

Figure 6.14: Convergence analysis for the Dec_1 part of the OFDM system using 50 random ETU channel with 16-QAM at 15 dB $Eb/N0$.

In the remainder of this section, 1000 cases are used. This means that 900 of the corresponding EXIT curves should lie above the selected line. In this case, Figures 6.15 and 6.16 show the EXIT chart curves and BER performance of the LDPC-OFDM and LDPC-FBMC/OQAM systems with the BICM-IIC scheme using Gray mapped 16-QAM with ZF equaliser over the ETU channel. We notice in these figures that in the EXIT

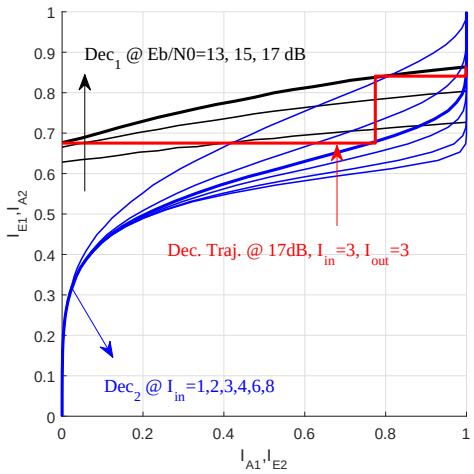

(a) EXIT chart

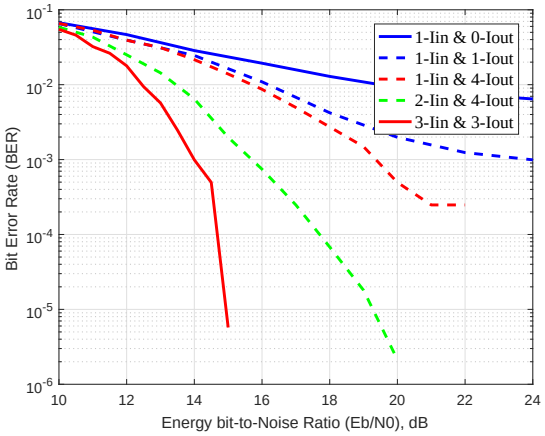

(b) BER

Figure 6.15: EXIT chart curves and BER performance of the LDPC-OFDM system based BICM-IIC scheme using 90% of all cases with Gray mapped 16-QAM and ZF equaliser over ETU channel (a) EXIT chart (b) BER.

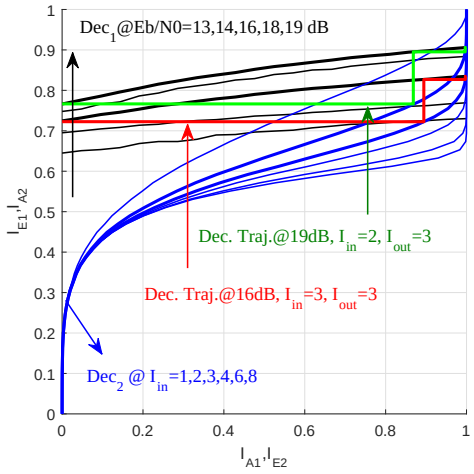

(a) EXIT chart

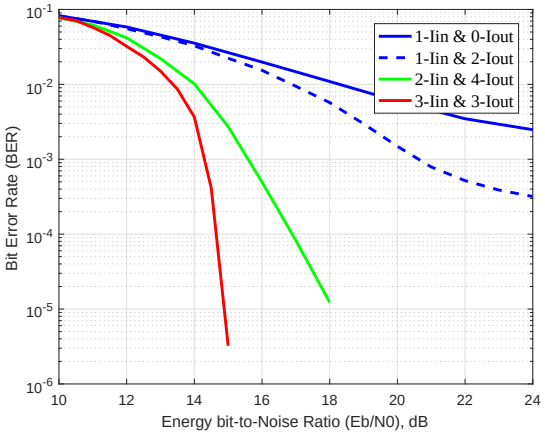

(b) BER

Figure 6.16: EXIT chart curves and BER performance of the LDPC-FBMC/OQAM system based BICM-IIC scheme using 90% of all cases with Gray mapped 16-QAM and ZF equaliser over ETU channel (a) EXIT chart (b) BER.

chart for both systems the tunnel is blocked with one decoder iteration. This means that the system performance cannot be improved with IIC iterations and high BER is obtained as shown by the BER simulation curves. As the number of decoder iterations increases to $I_{in} = 2$, the tunnel will open at high $Eb/N0$ (≥ 18 dB) and the system performance will be improved resulting in low BER as shown in the green curves in the BER simulation results. With more decoder iterations, the tunnel becomes wider and the BER simulation result becomes steeper as shown in the red BER simulation curves.

6.5 Simulation results of MIMO systems

As in SISO systems, the EXIT characteristic curves will first be drawn with specific CIR. Random CIRs are generated for the specified sampling frequency, using the approach described in Section 6.4. The CIRs used are listed in Table 6.2.

Table 6.2: EVA-LTE downlink channel impulse response (h_t) for MIMO systems

Channel impulse response using the EVA-LTE channel			
h_{11}	h_{21}	h_{12}	h_{22}
0.1936 - 0.5404i	0.2699 + 0.3722i	0.9454 + 0.0294i	-0.7712 + 0.6355i
-0.4388 - 0.2040i	-0.3912 - 0.3374i	-0.6683 - 0.1928i	-0.8779 + 0.0331i
0.1087 - 0.0203i	-0.2805 - 0.2007i	-0.0457 + 0.0876i	-0.1649 - 0.0589i
-0.0230 + 0.0275i	0.1061 + 0.0138i	0.1244 + 0.0402i	0.1696 - 0.00157i
0	0	0	0
-0.0190 + 0.0375i	-0.1482 - 0.0682i	-0.0572 - 0.0645i	-0.0368 + 0.0935i

Figures 6.17 and 6.18 show the EXIT chart transfer characteristic with the corresponding BER simulation results of the LDPC-MIMO-OFDM systems using linear and SIC detection respectively with Gray mapped 16-QAM over the EVA channel.

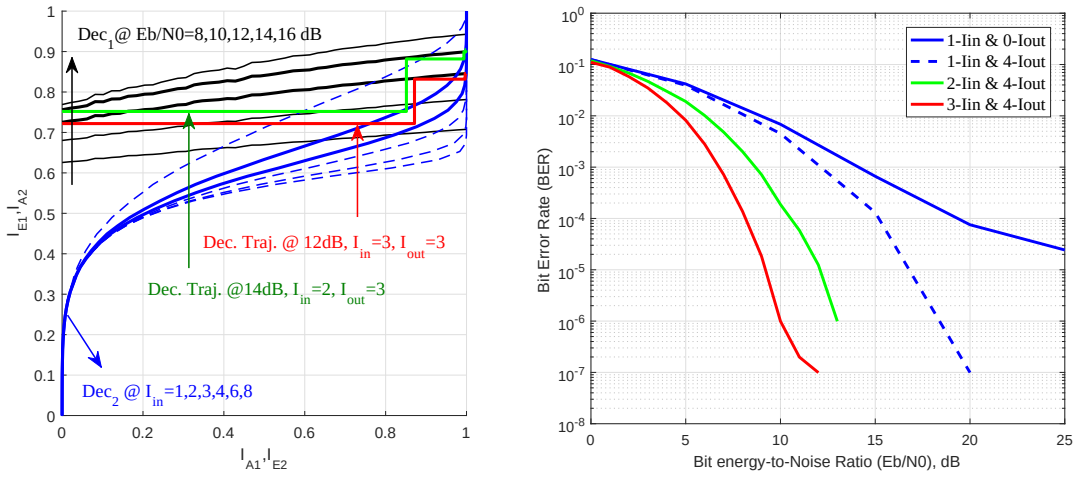

(a) EXIT chart

(b) BER

Figure 6.17: EXIT chart curves and BER performance of the LDPC-MIMO-OFDM system based BICM-IIC scheme using linear detection with Gray mapped 16-QAM and MMSE equaliser over EVA channel (a) EXIT chart (b) BER.

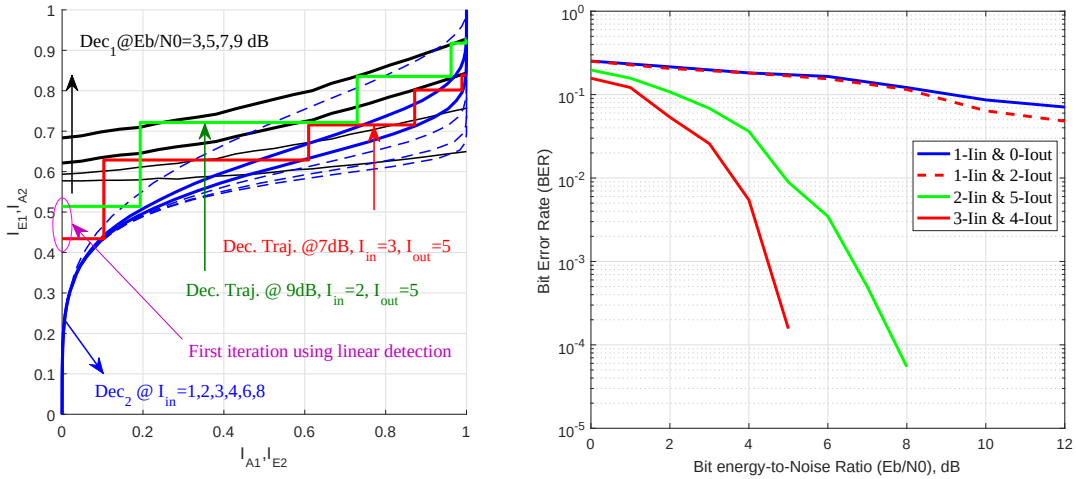

(a) EXIT chart

(b) BER

Figure 6.18: EXIT chart curves and BER performance of the LDPC-MIMO-OFDM system based BICM-IIC scheme using SIC detection with Gray mapped 16-QAM over EVA channel (a) EXIT chart (b) BER.

It is clear from these figures that as the number of decoder iterations (I_{in}) increases, the tunnel opens and the performance of the system will improve. This results in the BER simulation results shown in the green and red curves, giving low BER. In the case of

SIC detection, the decoding trajectory in the first iteration does not meet the upper EXIT curve, because of the linear detection in the first iteration.

Figure 6.19 shows the EXIT chart and BER simulation results of the LDPC-MIMO-FBMC/OQAM system using linear detection with Gray mapped 16-QAM and MMSE equaliser over the EVA channel. We notice in this figure that the tunnel opens with more decoder iterations. With the number of decoder iterations increases, low BER simulation results are obtained as shown in the green and red curves.

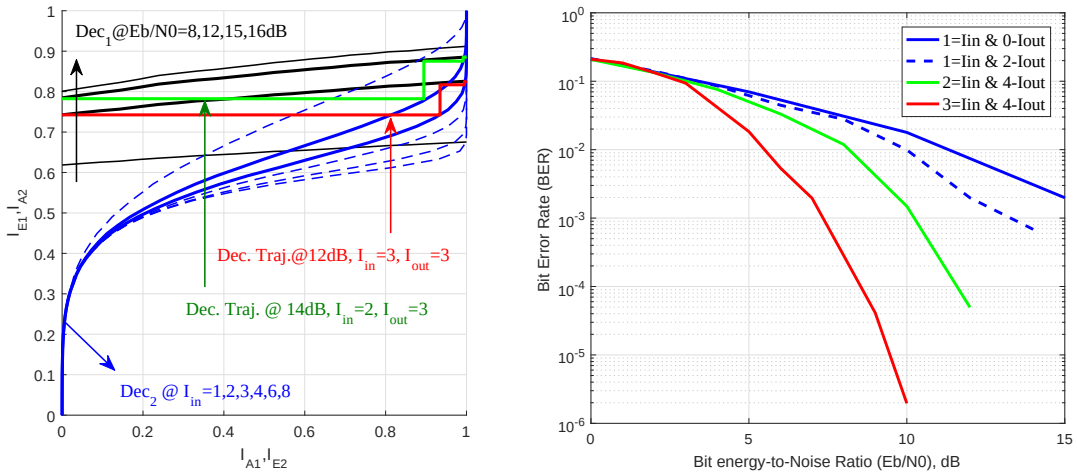

(a) EXIT chart

(b) BER

Figure 6.19: EXIT chart curves and BER performance of the LDPC-MIMO-FBMC/OQAM system based BICM-IIC scheme using linear detection with Gray mapped 16-QAM and MMSE equaliser over EVA channel (a) EXIT chart (b) BER.

As in the SISO systems, an EXIT chart for 90% of channels has been drawn and compared with the corresponding BER simulation results of the MIMO systems. In this case, Figures 6.20 and 6.21 show the EXIT chart and the BER simulation results of the MIMO-OFDM and MIMO-FBMC/OQAM systems using linear detection with MMSE equaliser and Gray mapped 16-QAM over the EVA channel.

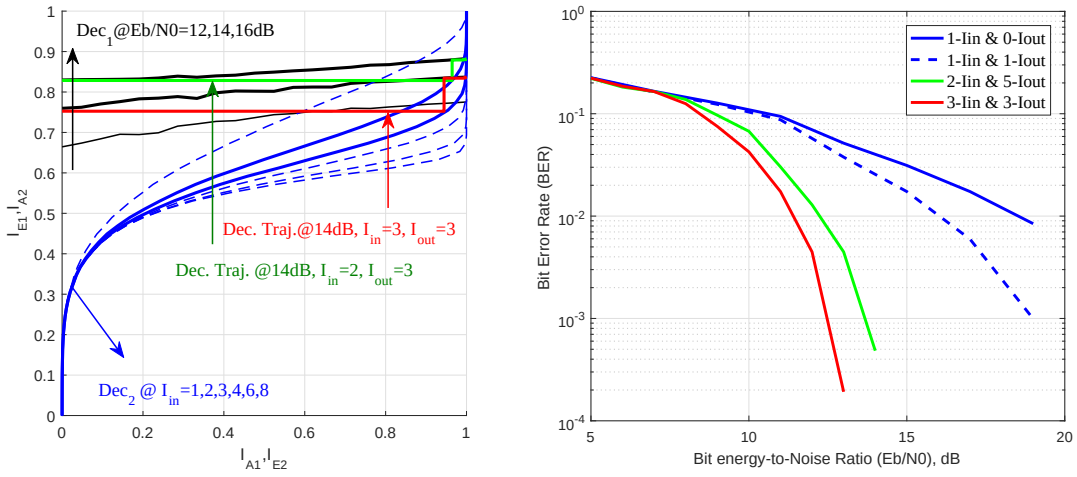

(a) EXIT chart

(b) BER

Figure 6.20: EXIT chart curves and BER performance of the LDPC-MIMO-OFDM system based BICM-IIC scheme using linear detection with Gray mapped 16-QAM and MMSE equaliser over EVA channel (a) EXIT chart (b) BER.

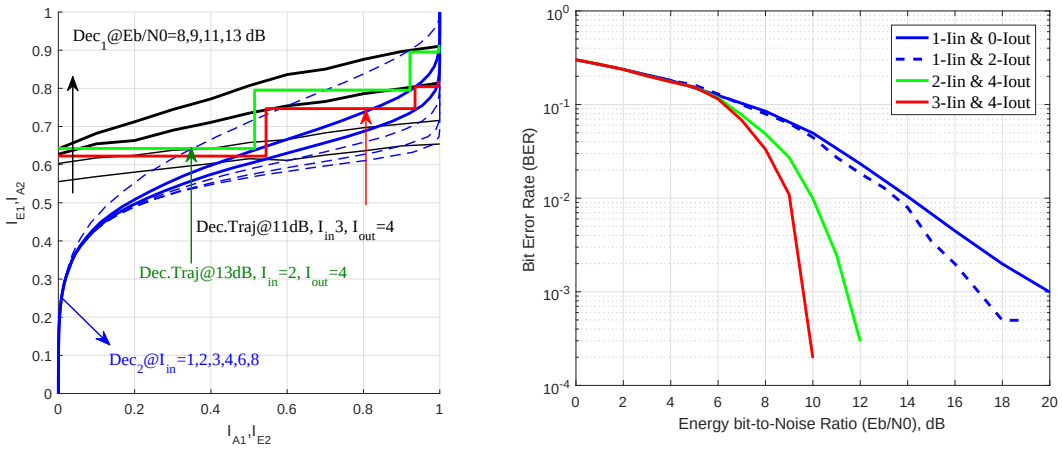

(a) EXIT chart

(b) BER

Figure 6.21: EXIT chart curves and BER performance of the LDPC-MIMO-FBMC/OQAM system based BICM-IIC scheme using linear detection with Gray mapped 16-QAM and MMSE equaliser over EVA channel (a) EXIT chart (b) BER.

6.6 Summary

This chapter can be summarised as follows:

- IIC based BICM has been proposed for SISO-MCM systems with different modulation orders, and mappings for 16-QAM, over the EVA/ETU channels. The required number of IIC iterations has been calculated by considering the exchange of the mutual information using the EXIT chart. The convergence threshold has been noted with its corresponding $Eb/N0$ values in the BER simulation results.
- IIC and MIMO-IIC based BICM have been used with linear and SIC detection for both MIMO-OFDM and MIMO-FBMC/OQAM systems. The required number of the MIMO-IIC iterations and the turbo cliff area have been calculated with the help of the EXIT chart in different scenarios. First, linear detection only is used: In this case, the required number of the IIC and MIMO-IIC iterations have been calculated. Second, SIC detection has been used: In this case, the linear detection has been used in the first iteration and the SIC detection for the rest.
- The performance of the decoder has been described on random channels by using an EXIT chart defined for 90% of the cases which is used through the simulation. In this case, the performance of the systems on quasi-static channels has been defined for a given outage probability.

Chapter 7

Conclusions and Future Work

Contents

7.1 Summary of the Work

The conclusions of this thesis can be summarised as follows:

- Chapter 1 was devoted to an introduction to the research topic; Aims of this work; Contributions; Outline of thesis and list of publications.
- Chapter 2 provided the literature review of previous work that we used throughout this thesis, and which includes: the general concept of multicarrier modulation (MCM) including OFDM, DWT-MCM, and FBMC/OQAM systems; The decomposition and reconstruction implementation algorithms for the DWT-MCM system; The fundamental theory of the FBMC/OQAM system with its polyphase and prototype filter implementation; Downlink LTE frame structure, channel profiles, and its simulation parameters; The Clark's and Jakes' channel modelling; Sum-product

algorithm for LDPC decoding.

- In Chapter 3, the performance of iterative interference cancellation (IIC) with iterative decoding of OFDM, DWT-MCM, and FBMC/OQAM was investigated in a time-frequency selective channel. Different modulation orders, different Doppler frequencies, and different environments were used to study the systems' performance. Different approaches were applied to calculate the ICI/ISI interference to delete them from the received signal. We may conclude that the significantly better performance is obtained for all systems by using iterative interference cancellation. However, after some IIC iterations, the simulation results of the FBMC/OQAM systems were closest to the PCSI simulation results than the other systems.

- In Chapter 4, a tentative channel estimation-based IIC and Wiener filter was proposed for the LDPC-OFDM and LDPC-FBMC/OQAM systems. Scattered pilots and IAM preamble were used in this chapter. Pilot-aided Wiener filter was applied to estimate the channel coefficients for both systems. Different distributions of the IAM preambles Wiener filter channel estimation were used with FBMC/OQAM system. The IIC scheme was used to improve the received signal by calculating the ICI/ISI interference and removing it from the received signal. A significant improvement was obtained in the simulation result for both systems. Better results were achieved with FBMC/OQAM system than of OFDM compared with the PCSI simulation results.

- In Chapter 5, a MIMO-IIC scheme using successive interference cancellation (SIC) was proposed for MIMO-OFDM and MIMO-FBMC/OQAM systems. IIC and MIMO-IIC are used to reduce the effect of channels of the transmitted signal from the current and other streams respectively. SIC is used to reduce the cross interference. The simulation results were obtained with different modulation orders, different Doppler frequencies, and different channel statistics. The performance of both systems with the combination of IIC and SIC was found to be close to that of PCSI simulation result.

- In Chapter 6, the important parameters to analyse the iterative system convergence were determined by describing the exchange of the mutual information by using the EXIT chart. These parameters are: the required number of IIC iteration, the start of the turbo cliff area, and the trajectory of the iterative process. Different

mappings of the 16-QAM and different LTE channels were used in the simulations; The simulation results were discussed for both SISO and MIMO systems; With Gray mappings, more decoder iterations were required to achieve low BER while with $M16^r$ and MSEW mapped 16-QAM, an open tunnel was obtained with one decoder iteration; A new EXIT chart technique was proposed in this chapter which can be used to define performance for a given outage probability on quasi-static fading channels.

7.2 General conclusion

The context of the work is the predominance of orthogonal frequency-division multiplexing (OFDM) in the physical layer of wireless standards, including fourth generation mobile. The benefit of OFDM has been that it allows high rate broadband data transmission on highly frequency-selective wireless channels, without requiring complex equalisation. However it has a number of deficiencies as explained in the literature. The research has considered some alternative proposals which may address certain of these defects, with a view to contributing to next generation air-interface technology. Potential approaches that were considered for this purpose include: DWT-MCM; FBMC/OQAM; IIC for SISO systems; MIMO-IIC with linear and SIC detection for MIMO systems.

In general, with sufficient cyclic prefix (CP), the simulation results obtained for DWT-MCM are significantly better than those of the other systems especially with an MMSE equaliser. This is because the signal spectrum for all wavelet bearers is distributed across the whole bandwidth, which provides a large diversity on a frequency selective channel. IIC is a useful technique for the OFDM system with insufficient CP, DWT-MCM, and FBMC/OQAM. IIC can remove some of the problems of equalization in FBMC/OQAM systems. The simulation results were significantly improved in the FBMC/OQAM system compared with the other systems. With the MMSE equaliser and IIC, a significantly better performance was obtained in all systems compared with the ZF equaliser. That is because of the combination of coding and MMSE which increases the diversity order. With the EVA channel, after the desired number of IIC iterations, the error floors are completely removed in the OFDM system with insufficient CP, resulting in simulation results close

to the results of the PCSI. This means that with IIC, the ICI and ISI can be avoided without using the CP. The ICI and ISI components are accurately calculated using the forward error correction. The soft decoded symbols of the LDPC decoder are used to calculate these components and then remove them from the received signal during the IIC scheme. Iterative channel estimation was proposed with IIC and 2-D Wiener filter for both OFDM with insufficient CP and FBMC/OQAM systems. After some IIC iterations, the error floor were drastically reduced in both systems. Linear and SIC detection methods were used with IIC in both 2×2 MIMO OFDM and FBMC/OQAM systems. The error floors were completely removed by using IIC in both systems. A significant improvement was achieved by using SIC detection with IIC in different cases. A new strategy for the convergence analysis was proposed to provide an approach that can be used on quasi-static fading channels.

7.3 Future Work

Based on the proposed strategies, algorithms details, analysis, and results obtained in this thesis, the further work of relevant research are suggested and summarised as below:

- In Chapter 4, iterative channel estimation based IIC with 2-D Wiener filter was proposed for both OFDM and FBMC/OQAM systems. Hence further work is proposed to develop iterative channel estimation based IIC with 1-D Wiener filter and preamble pilot to calculate the estimated coefficients of the channel for DWT-MCM. In the wavelet domain, there are time-scale variations. This means that the coefficients of the Wiener filter will be calculated using the interpolation in time domain only.
- In Chapter 5, the linear and SIC MIMO detection schemes with IIC and MIMO-IIC that were proposed for both LDPC-MIMO-OFDM and LDPC-MIMO-FBMC/OQAM systems could be extended to MIMO-DWT/MCM.
- In Chapter 5, 2×2 and 2×4 MIMO schemes were used for both OFDM and FBMC/OQAM systems. This could be extended to larger numbers of antennas.
- In Chapter 5, SIC detection based IIC was proposed for both LDPC OFDM and FBMC/OQAM systems:different detection algorithms, such as PIC, SQRD, list

sphere decoding, and K-Best detection could be investigated, for use with the IIC scheme for MIMO-MCM systems.

- In Chapter 6, 2×2 MIMO was used to discuss the convergence analysis for both OFDM and FBMC/OQAM system. The convergence analysis could also be extended to larger numbers of antennas.

- In Chapter 6, the convergence analysis for 2×2 MIMO was discussed with linear and SIC detection. We propose further work to use different detection algorithms, such as ML, PIC, SQRD, list sphere decoding, and K-Best detection to obtain the EXIT chart characteristic for MIMO systems.

Glossary

3GPP	3^{rd} **G**eneration **P**artnership **P**roject
AFB	**S**nalysis **F**ilter **B**ank
APP	**A P**osteriori **P**robability
AWGN	**A**dditive **W**hite **G**aussian **N**oise
BPSK	**B**inary **P**hase **S**hift **K**eying
BER	**B**it **E**rror **R**ate
BICM	**B**it **I**interleaved **C**oded **M**odulation
CCDF	**C**omplementary **C**umulative **D**istribution **F**unction
CDMA	**C**ode **D**ivision **M**ultiple **A**ccess
CFO	**C**arrier **F**requency **O**ffset
CFR	**C**hannel **F**requency **R**esponse
CIR	**C**hannel **I**mpulse **R**esponse
CND	**C**heck **N**ode **D**ecoder
CP	**C**yclic **P**refix
CSI	**C**hannel **S**tate **I**nformation
DAB	**D**igital **A**udio **B**roadcasting
DFE	**D**ecision **F**eedback **E**qualizer
DFT	**D**iscrete **F**ourier **T**ransformt
DL	**D**own**L**ink
DPA	**D**ynamic **P**ilot **A**llocation
DVB-T	**T**errestrial **D**igital **V**ideo **B**roadcasting
DWMT	**D**iscrete **W**avelet **M**ulti**T**one
DWT	**D**iscrete **W**avelet **T**ransformt
EPA	**E**xtended **P**edestrian **A** model

ETU	**E**xtended **T**ypical **U**rban model
E-UTRA	**E**volved **U**niversal **T**errestrial **R**adio **A**ccess
EVA	**E**xtended **V**ehicular **A** model
EVD	**E**igen**V**alue **D**ecomposition
EXIT	**EX**trinsic **I**nformation**T**ransfer
FBMC	**F**ilter **B**ank **M**ulti**C**arrier
FEC	**F**orward **E**rror **C**orrection
FER	**F**rame **E**rror **R**ate
FFT	**F**ast **F**ourier **T**ransform
FMT	**F**iltered **M**ulti**T**one
FTN	**F**ast-**T**han **N**yquist
HPF	**H**igh-**P**ass **F**ilter
IAM	**I**nterference **A**pproximation **M**ethod
ICI	**I**nter **C**arrier **I**nterference
IDWT	**I**nverse **D**iscrete **W**avelet **T**ransform
IFFT	**I**nverse **F**ast **F**ourier **T**ransform
IIC	**I**terative **I**nterference **C**ancellation
ISI	**I**nter **S**ymbol **I**nterference
LDPC	**L**ow-**D**ensity **P**arity-**C**heck
LLR	**L**og **L**ikelihood **R**atio
LMMSE	**L**inear **M**inimum **M**ean **S**quare **E**rror
LMS	**L**east-**M**ean **S**quare
LPF	**L**ow-**P**ass **F**ilter
LS	**L**east **S**quares
LTE	**L**ong **T**ermd **E**volution
MAI	**M**ultiple **A**ccess **I**nterference
MAP	**M**aximum **A** **P**osteriori
MCM	**M**ulti**C**arrier **M**odulation
MDS	**M**aximum **D**oppler **S**hift
MIMO	**M**ulti **I**iput **M**ulti **O**utput
MIPS	**M**ulti-input-multiple-output **I**terative **P**ilot **S**earch
ML	**M**aximum **L**ikelihood
MMSE	**M**inimum **M**ean **S**quare **E**rror

MSE	**M**ean **S**quare **E**rror
NLOS	**N**on **L**ine of **S**ight
NPR	**N**ear **P**erfect **R**econstruction
OFDM	**O**rthogonal **F**requency **D**ivision **M**ultiplexing
OFDMA	**O**rthogonal **F**requency **D**ivision **M**ultiple **A**ccess
OQAM	**O**ffset **Q**uadrature **A**mplitude **M**odulation
PAM	**P**ulse **A**mplitude **M**odulation
PAPR	**P**eak-to-**A**verage **P**ower **R**atio
PCI	**P**erfect **C**hannel **I**iformation
PCIC	**P**erfect **C**hannel **I**nterference **C**ancellation
PCSI	**P**erfect **C**hannel **S**tate **I**iformation
PDF	**P**robability **D**ensity **F**unction
PDP	**P**ower **D**elay **P**rofile
PR	**P**erfect **R**econstruction
PSD	**P**ower **S**pectral **D**ensity
QAM	**Q**uadrature **A**mplitude **M**odulation
QPSK	**Q**uadrature **P**hase **S**hift **K**eying
QoS	**Q**uality of **S**ervice
RBs	**R**esource **B**locks
RE	**R**esource **E**lement
RF	**R**adio **F**requency
SC-FDE	**S**ingle **C**arrier **F**requency **D**omain **E**qualizer
SFB	**S**ynthesis **F**ilter **B**ank
SIC	**S**uccessive **I**nterference **C**ancellation
SINR	**S**ignal-to-**I**nterference **N**oise **R**atio
SISO	**S**ingle **I**nput **S**ingle **O**utpute
SNR	**S**ignal-to-**N**oise **R**atio
SPA	**S**um-**P**roduct **A**lgorithm
TS-MMSE	**T**wo **S**tage **MMSE**
UE	**U**ser **E**quipment
UL	**U**p**L**ink
UMTS	**U**niversal **M**obile **T**elecommunications **S**ystem
USB	**U**niversal **S**erial **B**us

VDSL	**V**ery-high-bit-rate **D**igital **S**ubscriber **L**ine
VND	**V**ariable **N**ode **D**ecoder
VSB	**V**stigial **S**ide-**B**and
Wi-Fi	**Wi**reless-**Fi**delity
Wi-Max	**W**orldwide **I**nteroperability for **M**icrowave **A**ccess
WLAN	**W**ireless **L**ocal **A**rea **N**etwork
WSS	**W**ide **S**ense **S**tationary
WSSUS	**W**ide **S**ense **S**tationary **U**ncorrelated **S**cattering
ZF	**Z**ero **F**orcing

Bibliography

[1] B. Saltzberg, "Performance of an efficient parallel data transmission system," *IEEE Transactions on Communication Technology*, vol. 15, no. 6, pp. 805–811, December 1967.

[2] J. A. C. Bingham, "Multicarrier modulation for data transmission: an idea whose time has come," *IEEE Communications Magazine*, vol. 28, no. 5, pp. 5–14, May 1990.

[3] "ETSI ETS 300 401, Radio Broadcasting Systems; Digital Audio Broadcasting (DAB) to mobile, portable and fixed receivers.," *European Standard (Telecommunications series) , Valbonne, France*, February 1995.

[4] European Telecommunications Standards Institute, "Digital Video Broadcasting (DVB); Framing structure, channel coding and modulation for digital terrestrial television (ETSI ETS 300 744, V1.6.1)," January 2009.

[5] "Information technology–Telecommunications and information exchange between systems Local and metropolitan area networks–Specific requirements Part 11: Wireless LAN Medium Access Control (MAC) and Physical Layer (PHY) Specifications," *ISO/IEC/IEEE 802-11:2012(E) (Revison of ISO/IEC/IEEE 802-11-2007)*, pp. 1–2793, March 2012.

[6] "Information technology–Telecommunications and information exchange between systems Local and metropolitan area networks–Specific requirements Part 11: Wireless LAN Medium Access Control (MAC) and Physical Layer (PHY) Specifications," *ISO/IEC/IEEE 802-11:2012(E) (Revison of ISO/IEC/IEEE 802-11-2005 and Amendments)*, pp. 1–2798, November 2012.

[7] "IEEE Standard for Air Interface for Broadband Wireless Access Systems," *IEEE Std 802.16-2012 (Revision of IEEE Std 802.16-2009)*, pp. 1–2542, August 2012.

[8] "IEEE Standard for WirelessMAN-Advanced Air Interface for Broadband Wireless Access Systems," *IEEE Std 802.16.1-2012*, pp. 1–1090, September 2012.

[9] "IEEE Standard for Air Interface for Broadband Wireless Access Systems (Amendment 2: Higher Reliability Networks)," *IEEE Std 802.16n-2013*, pp. 1–168, March 2013.

[10] ETSI-TS-36.211, "Technical Specification. LTE; Evolved Universal Terrestrial Radio Access (E-UTRA); Physical Channels and Modulation (3GPP TS 36.211 version 10.5.0 Release 10)," 2012.

[11] 3GPP-TS-36.101, "Technical Specification. LTE; Evolved Universal Terrestrial Radio Access (E-UTRA); User Equipment (UE) radio transmission and reception (3GPP TS 36.101 version 11.8.0 Release 11)," 2014.

[12] L. Cimini, "Analysis and Simulation of a Digital Mobile Channel Using Orthogonal Frequency Division Multiplexing," *IEEE Transactions on Communications*, vol. 33, no. 7, pp. 665–675, July 1985.

[13] M. Alard and R. Lassalle, "principle of modulation and channel coding for digital broadcasting for mobile receivers," *EBU Review Technical*, , no. 224, pp. 168–190, August 1987.

[14] T. Jiang and Y. Wu, "An Overview: Peak-to-Average Power Ratio Reduction Techniques for OFDM Signals," *IEEE Transactions on Broadcasting*, vol. 54, no. 2, pp. 257–268, June 2008.

[15] L. Dai, J. Wang, Z. Wang, P. Tsiaflakis, and M. Moonen, "Spectrum- and Energy-Efficient OFDM Based on Simultaneous Multi-Channel Reconstruction," *IEEE Transactions on Signal Processing*, vol. 61, no. 23, pp. 6047–6059, December 2013.

[16] A. G. Armada and M. Calvo, "Phase noise and sub-carrier spacing effects on the performance of an OFDM communication system," *IEEE Communications Letters*, vol. 2, no. 1, pp. 11–13, January 1998.

[17] P. Robertson and S. Kaiser, "Analysis of the effects of phase-noise in orthogonal frequency division multiplex (OFDM) systems," *IEEE International Conference on Communications, 1995. ICC '95 Seattle, 'Gateway to Globalization', Washington, USA*, vol. 3, pp. 1652–1657, June 1995.

[18] T. A. Weiss and F. K. Jondral, "Spectrum pooling: an innovative strategy for the enhancement of spectrum efficiency," *IEEE Communications Magazine*, vol. 42, no. 3, pp. S8–S14, March 2004.

[19] M. Morelli, C. C. J. Kuo, and M. O. Pun, "Synchronization Techniques for Orthogonal Frequency Division Multiple Access (OFDMA): A Tutorial Review," *Proceedings of the IEEE*, vol. 95, no. 7, pp. 1394–1427, July 2007.

[20] B. Farhang-Boroujeny, "OFDM Versus Filter Bank Multicarrier," *IEEE Signal Processing Magazine*, vol. 28, no. 3, pp. 92–112, May 2011.

[21] R. R. Mosier and R. G. Clabaugh, "Kineplex, a bandwidth-efficient binary transmission system," *Transactions of the American Institute of Electrical Engineers, Part I: Communication and Electronics*, vol. 76, no. 6, pp. 723–728, January 1958.

[22] S. Ahmed and M. Kawai, "Dynamic null-data subcarrier switching for OFDM PAPR reduction with low computational overhead," *Electronics Letters*, vol. 48, no. 9, pp. 498–499, April 2012.

[23] Y. Jiang, "New companding transform for PAPR reduction in OFDM," *IEEE Communications Letters*, vol. 14, no. 4, pp. 282–284, April 2010.

[24] S. Weinstein and P. Ebert, "Data transmission by frequency-division multiplexing using the discrete Fourier transform," *IEEE Transactions on Communication Technology*, vol. 19, no. 5, pp. 628–634, October 1971.

[25] R. Van Nee, G. Awater, M. Morikura, H. Takanashi, M. Webster, and K. W. Halford, "New high-rate wireless LAN standards," *IEEE Communications Magazine*, vol. 37, no. 12, pp. 82–88, December 1999.

[26] R. Van Nee, "A new OFDM standard for high rate wireless LAN in the 5 GHz band," in *Gateway to 21st Century Communications Village. VTC 1999-Fall. IEEE VTS 50th Vehicular Technology Conference, Amsterdam, Netherlands*, September 1999, vol. 1, pp. 258–262.

[27] A. Bahai, B. Saltzberg, and M. Ergen, *Multi-carrier digital communications theory and applocations of OFDM*, Springer Science and Business Media, Inc., Boston, 2004.

[28] B. G. Negash and H. Nikookar, "Wavelet based OFDM for wireless channels," in *IEEE VTS 53rd Vehicular Technology Conference (VTS SPRING 2001) - Rhodes, Greece*, May 2001, vol. 1, pp. 688–691.

[29] Z. Youbing and C. Shijie, "A novel Multicarrier Signal Transmission System over Multipath Channel of Low-voltage Power Line," *IEEE Transactions on Power Delivery*, vol. 19, no. 4, pp. 1668–1672, October 2004.

[30] M. Gautier and J. Lienard, "Efficient wavelet packet modulation for wireless communication," in *The Third Advanced International Conference on Telecommunications, AICT 2007, Mauritius*, May 2007, pp. 19–24.

[31] G. Stefano and L. Oleg, "Recent Developments in the Standardization of Power Line Communications within the IEEE," *Communications Magazine, IEEE*, vol. 46, no. 7, pp. 64–71, July 2008.

[32] B. G. Negash and H. Nikookar, "Wavelet-based multicarrier transmission over multipath wireless channels," *Electronics Letters*, vol. 36, no. 21, pp. 1787–1788, October 2000.

[33] M. Oltean and A. Isar, "On the time-frequency localization of the wavelet signals, with application to orthogonal modulations," in *International Symposium on Signals, Circuits and Systems (ISSCS 2009), USA*. IEEE, July 2009, pp. 1–4.

[34] M. Oltean, "Wavelet OFDM performance in flat fading channels," *Scientific Bulletin of University Politehnica Timisoara, ETC Series*, vol. 52, no. 66, pp. 167–172, 2007.

[35] A. R. Lindsey and J. C. Dill, "Wavelet packet modulation: a generalized method for orthogonally multiplexed communications," in *Proceedings of the Twenty-Seventh Southeastern Symposium on System Theory*. IEEE, March 1995, pp. 392–396.

[36] G. W. Wornell, "Emerging applications of multirate signal processing and wavelets in digital communications," *Proceedings of the IEEE*, vol. 84, no. 4, pp. 586–603, April 1996.

[37] A. Jamin and P. Mähönen, "Wavelet packet modulation for wireless communications," *Wireless Communications and Mobile Computing*, vol. 5, no. 2, pp. 123–137, March 2005.

[38] M. Mathew, A. B. Premkumar, and C. Tong Lau, "Multiple access scheme for multi user Cognitive Radio based on wavelet transforms," in *IEEE 71st Vehicular Technology Conference (VTC2010-Spring), Taipei, Taiwan*, May 2010, pp. 1–5.

[39] M. Mathew, A. B. Premkumar, and C. Tong Lau, "Multiwavelets based multi-user cognitive radio network," in *IEEE 12th International Conference on Communication Systems (ICCS), Singapore*, November 2010, pp. 772–776.

[40] S. D. Sandberg and M. A. Tzannes, "Overlapped discrete multitone modulation for high speed copper wire communications," *IEEE Journal on selected areas in communications*, vol. 13, no. 9, pp. 1571–1585, December 1995.

[41] B. Farhang-Boroujeny and L. Lin, "Cosine modulated multitone for very high-speed digital subscriber lines," in *Proceedings.(ICASSP'05). IEEE International Conference on Acoustics, Speech, and Signal Processing, Philadelphia, PA, United States*, March 2005, vol. 3, pp. 345–348.

[42] T. Edwards, *Discrete wavelet transforms: Theory and implementation. Technical report*, Stanford University, 1991.

[43] S. Mallat, *A Wavelet Tour of Signal Processing*, Laurent Demanet, 3rd edition, 2008.

[44] M. Pollicott and H. Weiss, "How smooth is your wavelet? wavelet regularity via thermodynamic formalism," *Communications in Mathematical Physics*, vol. 281, no. 1, pp. 1–21, 2008.

[45] L. Fu-Rong, C. Wai-Ki, and M. Ng, "Discrete wavelet transforms for Toeplitz matrices," *Linear algebra and its applications*, vol. 370, pp. 269–285, January 2003.

[46] I. Daubechies, "Orthonormal bases of compactly supported wavelets," *Communications on pure and applied mathematics*, vol. 41, no. 7, pp. 909–996, 1988.

[47] H. Zhang, D. Le Ruyet, D. Roviras, Y. Medjahdi, and H. Sun, "Spectral efficiency comparison of OFDM/FBMC for uplink cognitive radio networks," *EURASIP Journal on Advances in Signal Processing*, , no. 1, pp. 92–112, 2010.

[48] P. Siohan, C. Siclet, and N. Lacaille, "Analysis and design of OFDM/OQAM systems based on filterbank theory," *IEEE Transactions on Signal Processing*, vol. 50, no. 5, pp. 1170–1183, May 2002.

[49] B. Hirosaki, "An Orthogonally Multiplexed QAM System Using the Discrete Fourier Transform," *IEEE Transactions on Communications*, vol. 29, no. 7, pp. 982–989, July 1981.

[50] B. Hirosaki, "A Maximum Likelihood Receiver for an Orthogonally Multiplexed QAM System," *IEEE Journal on Selected Areas in Communications*, vol. 2, no. 5, pp. 757–764, September 1984.

[51] D. Lacroix, N. Goudard, and M. Alard, "OFDM with guard interval versus OFDM/offsetQAM for high data rate UMTS downlink transmission," *IEEE 54th Vehicular Technology Conference. VTC Fall 2001. Proceedings, Atlantic City, NJ, USA*, vol. 4, pp. 2682–2686, October 2001.

[52] R. W. Chang, "Synthesis of band-limited orthogonal signals for multichannel data transmission," *The Bell System Technical Journal*, vol. 45, no. 10, pp. 1775–1796, December 1966.

[53] B. Hirosaki, "An Analysis of Automatic Equalizers for Orthogonally Multiplexed QAM Systems," *IEEE Transactions on Communications*, vol. 28, no. 1, pp. 73–83, January 1980.

[54] G. Cherubini, E. Eleftheriou, S. Oker, and J. M. Cioffi, "Filter bank modulation techniques for very high speed digital subscriber lines," *IEEE Communications Magazine*, vol. 38, no. 5, pp. 98–104, May 2000.

[55] P. K. Remvik and N. Holte, "Carrier frequency offset robustness for OFDM systems with different pulse shaping filters," in *IEEE Global Telecommunications Conference, GLOBECOM 97, Phoenix, AZ, USA*. IEEE, November 1997, vol. 1, pp. 11–15.

[56] T. Fusco, A. Petrella, and M. Tanda, "Sensitivity of multi-user filter-bank multicarrier systems to synchronization errors," in *3rd International Symposium on Communications, Control and Signal Processing, ISCCSP, Malta*. IEEE, March 2008, pp. 393–398.

[57] A. Assalini and A. M. Tonello, "Time-frequency synchronization in filtered multitone modulation based systems," *presented at the IEEE WPMC03, Yokosuka, Kanagawa, Japan*, pp. 19–22, October 2003.

[58] A. Ikhlef and J. Louveaux, "An enhanced MMSE per subchannel equalizer for highly frequency selective channels for FBMC/OQAM systems," in *IEEE 10th Workshop on Signal Processing Advances in Wireless Communications, IEEE-SPAWC09, Perugia*. IEEE, June 2009, pp. 186–190.

[59] P. Ciblat and E. Serpedin, "A fine blind frequency offset estimator for OFDM/OQAM systems," *IEEE Transactions on Signal Processing*, vol. 52, no. 1, pp. 291–296, January 2004.

[60] T. Fusco, A. Petrella, and M. Tanda, "Data-aided symbol timing and CFO synchronization for filter bank multicarrier systems," *IEEE Transactions on Wireless Communications*, vol. 8, no. 5, pp. 2705–2715, May 2009.

[61] D. S. Waldhauser, L. G. Baltar, and J. A. Nossek, "Adaptive decision feedback equalization for filter bank based multicarrier systems," in *IEEE International Symposium on Circuits and Systems, IEEE ISCAS, Taipei, Taiwan*. IEEE, May 2009, pp. 2794–2797.

[62] E. Kofidis, D. Katselis, A. Rontogiannis, and S. Theodoridis, "Preamble-based channel estimation in OFDM/OQAM systems: a review," *Signal Processing*, vol. 93, no. 7, pp. 2038–2054, March 2013.

[63] A. Viholainen, M. Bellanger, and M. Huchard, "Prototype filter and filter bank structure," *Technical Report, PHYDYAS Project, PHYsical layer for DYnamic AccesS and cognitive radio*, , no. ICT - 211887, PHYDYAS- 007, D5-1, January 2009.

[64] J. Bazzi, P. Weitkemper, and K. Kusume, "Power Efficient Scattered Pilot Channel Estimation for FBMC/OQAM," in *Proceedings of 10th International ITG Confer-*

ence on Systems, Communications and Coding; (SCC 2015), Hamburg, Germany. VDE, February 2015, pp. 1–6.

[65] A. Petrella, *Synchronization algorithms for FBMC systems*, Ph.D. thesis, Università degli Studi di Napoli Federico II, 2009.

[66] M. G. Bellanger, "Specification and design of a prototype filter for filter bank based multicarrier transmission," *IEEE International Conference on Acoustics, Speech, and Signal Processing. Proceedings, Salt Lake City, USA*, vol. 4, pp. 2417–2420, May 2001.

[67] T. Hidalgo Stitz, "Filter Bank Techniques for the Physical Layer in Wireless Communications," *Tampere University of Technology publications*, vol. 919, 2010.

[68] P. Martin, R. Bregovic, A. Martin-Marcos, F. Cruz-Roldan, and T. Saramaki, "A generalized window approach for designing transmultiplexers," *IEEE Transactions on Circuits and Systems I: Regular Papers*, vol. 55, no. 9, pp. 2696–2706, October 2008.

[69] T. H. Stitz, T. Ihalainen, A. Viholainen, and M. Renforsv, "Pilot-Based Synchronization and Equalization in Filter Bank Multicarrier Communications," *EURASIP Journal on Advances in Signal Processing*, February 2010.

[70] T Nakamura and S Abeta, "Super 3G Technology Trends/Part 1: Super 3G Overview and Standardization Activities," *NTT DoCoMo Technical Journal*, vol. 8, no. 2, pp. 52–56, 2006.

[71] E. Dahlman, S. Parkvall, J. Skold, and P. Beming, *3G evolution: HSPA and LTE for mobile broadband*, Academic Press, Oxford, UK, 2nd edition, 2008.

[72] D. Astely, E. Dahlman, A. Furuskr, Y. Jading, M. Lindstrm, and S. Parkvall, "LTE: the evolution of mobile broadband," *IEEE Communications Magazine*, vol. 47, no. 4, pp. 44–51, April 2009.

[73] J. Gozalvez, "First Commercial LTE Network [Mobile Radio]," *IEEE Vehicular Technology Magazine*, vol. 5, no. 2, pp. 8–16, June 2010.

[74] A. Gorokhov and J. P. Linnartz, "Robust OFDM receivers for dispersive time-varying channels: Equalization and channel acquisition," *IEEE Transactions on Communications*, vol. 52, no. 4, pp. 572–583, April 2004.

[75] A. B. Awoseyila, C. Kasparis, and B. G. Evans, "Robust time-domain timing and frequency synchronization for OFDM systems," *IEEE Transactions on Consumer Electronics*, vol. 55, no. 2, pp. 391–399, May 2009.

[76] S. M. Phoong, Y. Chang, and C. Y. Chen, "DFT-modulated filterbank transceivers for multipath fading channels," *IEEE Transactions on Signal Processing*, vol. 53, no. 1, pp. 182–192, January 2005.

[77] M. Wen, X. Cheng, L. Yang, Y. Li, X. Cheng, and F. Ji, "Index modulated OFDM for underwater acoustic communications," *IEEE Communications Magazine*, vol. 54, no. 5, pp. 132–137, May 2016.

[78] C.l Esli, M. Koca, and H. Deliç, "Iterative joint tone-interference cancellation and decoding for MIMO-OFDM," *IEEE Transactions on Vehicular Technology*, vol. 57, no. 5, pp. 2843–2855, September 2008.

[79] T. Strohmer and S. Beaver, "Optimal OFDM design for time-frequency dispersive channels," *IEEE Transactions on Communications*, vol. 51, no. 7, pp. 1111–1122, July 2003.

[80] H. Minn, V. K. Bhargava, and K. B. Letaief, "A robust timing and frequency synchronization for OFDM systems," *IEEE Transactions on Wireless Communications*, vol. 2, no. 4, pp. 822–839, July 2003.

[81] J. Hao, J. Wang, and Y. Wu, "A new equalizer in doubly-selective channels for TDS-OFDM," *IEEE Transactions on Broadcasting*, vol. 61, no. 1, pp. 91–97, March 2015.

[82] P. Muneer and S. M. Sameer, "Pilot-aided joint estimation of doubly selective channel and carrier frequency offsets in OFDMA uplink with high-mobility users," *IEEE Transactions on Vehicular Technology*, vol. 64, no. 1, pp. 411–417, January 2015.

[83] B. Li, M. Sun, X. Li, A. Nallanathan, and C. Zhao, "Energy detection based spectrum sensing for cognitive radios over time-frequency doubly selective fading channels," *IEEE Transactions on Signal Processing*, vol. 63, no. 2, pp. 402–417, January 2015.

[84] P. Cheng, Z. Chen, Y. Rui, Y. J. Guo, L. Gui, M. Tao, and Q. T. Zhang, "Channel estimation for OFDM systems over doubly selective channels: A distributed compressive sensing based approach," *IEEE Transactions on Communications*, vol. 61, no. 10, pp. 4173–4185, October 2013.

[85] K. Zhong, Y. C. Wu, and S. Li, "Signal Detection for OFDM-Based Virtual MIMO Systems under Unknown Doubly Selective Channels, Multiple Interferences and Phase Noises," *IEEE Transactions on Wireless Communications*, vol. 12, no. 10, pp. 5309–5321, October 2013.

[86] X. Ma and G. B. Giannakis, "Maximum-diversity transmissions over doubly selective wireless channels," *IEEE Transactions on Information Theory*, vol. 49, no. 7, pp. 1832–1840, July 2003.

[87] P. Schniter, "Low-complexity equalization of OFDM in doubly selective channels," *IEEE Transactions on Signal Processing*, vol. 52, no. 4, pp. 1002–1011, April 2004.

[88] P. Bello, "Characterization of randomly time-variant linear channels," *IEEE transactions on Communications Systems*, vol. 11, no. 4, pp. 360–393, December 1963.

[89] P. Hoeher, "A statistical discrete-time model for the WSSUS multipath channel," *IEEE Transactions on Vehicular Technology*, vol. 41, no. 4, pp. 461–468, November 1992.

[90] K. W. Yip and T. S. Ng, "Efficient simulation of digital transmission over WSSUS channels," *IEEE Transactions on Communications*, vol. 43, no. 12, pp. 2907–2913, December 1995.

[91] J. S. Sadowsky and V. Kafedziski, "On the correlation and scattering functions of the WSSUS channel for mobile communications," *IEEE Transactions on Vehicular Technology*, vol. 47, no. 1, pp. 270–282, February 1998.

[92] C. Sgraja, J. Tao, and C. Xiao, "On discrete-time modeling of time-varying WSSUS fading channels," *IEEE Transactions on Vehicular Technology*, vol. 59, no. 7, pp. 3645–3651, September 2010.

[93] A. I. Prikhodko, "Optimal and suboptimal differentially coherent reception of MDPSK in time-spread WSSUS channel," *IEEE Transactions on Communications*, vol. 58, no. 9, pp. 2604–2610, September 2010.

[94] P. S. Wang and D. W. Lin, "On maximum-likelihood blind synchronization over WSSUS channels for OFDM systems," *IEEE Transactions on Signal Processing*, vol. 63, no. 19, pp. 5045–5059, October 2015.

[95] R. H. Clarke, "A statistical theory of mobile-radio reception," *The Bell System Technical Journal*, vol. 47, no. 6, pp. 957–1000, July 1968.

[96] C. Xiao, Y. R. Zheng, and N. C. Beaulieu, "Novel sum-of-sinusoids simulation models for Rayleigh and Rician fading channels," *IEEE Transactions on Wireless Communications*, vol. 5, no. 12, pp. 3667–3679, December 2006.

[97] W. C. Jakes, *Microwave mobile communications*, Wiley, New York, 1974; reissued by IEEE press, 1994.

[98] M. F. Pop and N. C. Beaulieu, "Limitations of sum-of-sinusoids fading channel simulators," *IEEE Transactions on Communications*, vol. 49, no. 4, pp. 699–708, April 2001.

[99] M. Patzold, U. Killat, F. Laue, and Y. Li, "On the statistical properties of deterministic simulation models for mobile fading channels," *IEEE Transactions on Vehicular Technology*, vol. 47, no. 1, pp. 254–269, February 1998.

[100] Y. R. Zheng and C. Xiao, "Simulation models with correct statistical properties for Rayleigh fading channels," *IEEE Transactions on Communications*, vol. 51, no. 6, pp. 920–928, June 2003.

[101] K. W. Yip and T. S. Ng, "A simulation model for Nakagami-m fading channels, m <1," *IEEE Transactions on Communications*, vol. 48, no. 2, pp. 214–221, February 2000.

[102] C. Xiao and Y. R. Zheng, "A generalized simulation model for Rayleigh fading channels with accurate second-order statistics," in *IEEE 55th Vehicular Technology Conference (VTC Spring 2002), Birmingham, Ala., United States*, May 2002, vol. 1, pp. 170–174.

[103] A. Alimohammad and B. F. Cockburn, "Modeling and hardware implementation aspects of fading channel simulators," *IEEE Transactions on Vehicular Technology*, vol. 57, no. 4, pp. 2055–2069, July 2008.

[104] P. Dent, G. E. Bottomley, and T. Croft, "Jakes fading model revisited," *Electronics letters*, vol. 29, no. 13, pp. 1162–1163, June 1993.

[105] R. Gallager, "Low-density parity-check codes," *IRE Transactions on Information Theory*, vol. 8, no. 1, pp. 21–28, January 1962.

[106] R. Gallager, "Low density parity check codes, Research Monograph series," 1963.

[107] L. R. Varshney, "Performance of LDPC Codes Under Faulty Iterative Decoding," *IEEE Transactions on Information Theory*, vol. 57, no. 7, pp. 4427–4444, July 2011.

[108] R. Tanner, "A recursive approach to low complexity codes," *IEEE Transactions on Information Theory*, vol. 27, no. 5, pp. 533–547, September 1981.

[109] D. J. MacKay and R. M. Neal, "Near shannon limit performance of low density parity check codes," *Electronics letters*, vol. 32, no. 18, pp. 1645–1646, August 1996.

[110] M. Sipser and D. A. Spielman, "Expander codes," *IEEE Transactions on Information Theory*, vol. 42, no. 6, pp. 1710–1722, November 1996.

[111] M. Luby, M. Mitzenmacher, A Shokrollah, and D. Spielman, "Analysis of low density codes and improved designs using irregular graphs," in *Proceedings of the 30th annual ACM symposium on Theory of computing*. ACM, May 1998, pp. 249–258.

[112] M. Luby, M. Mitzenmacher, M. A. Shokrollahi, and D. A. Spielman, "Improved low-density parity-check codes using irregular graphs," *IEEE Transactions on Information Theory*, vol. 47, no. 2, pp. 585–598, February 2001.

[113] T. J. Richardson and R. L. Urbanke, "Efficient encoding of low-density parity-check codes," *IEEE Transactions on Information Theory*, vol. 47, no. 2, pp. 638–656, February 2001.

[114] S. Johnson, "Iterative error correction: Turbo, low-density parity-check and repeat-accumulate codes," Cambridge University Press, 2009.

[115] D. J. MacKay, "Good error-correcting codes based on very sparse matrices," *IEEE transactions on Information Theory*, vol. 45, no. 2, pp. 399–431, March 1999.

[116] S. Y. Chung, G. D. Forney, T. J. Richardson, and R. Urbanke, "On the design of low-density parity-check codes within 0.0045 db of the shannon limit," *IEEE Communications letters*, vol. 5, no. 2, pp. 58–60, February 2001.

[117] L. Ping and W. K. Leung, "Decoding low density parity check codes with finite quantization bits," *IEEE Communications Letters*, vol. 4, no. 2, pp. 62–64, February 2000.

[118] Y. S. Cho, J. Kim, W. Y. Yang, and C. G. Kang, *MIMO-OFDM Wireless Communications With MATLAB*, Wiley, October 2010.

[119] X. Wang and H. V. Poor, "Iterative (turbo) soft interference cancellation and decoding for coded CDMA," *IEEE Transactions on Communications*, vol. 47, no. 7, pp. 1046–1061, July 1999.

[120] B. Kwon, S. Kim, D. Jeon, and S. Lee, "Iterative Interference Cancellation and Channel Estimation in Evolved Multimedia Broadcast Multicast System Using Filter-Bank Multicarrier-Quadrature Amplitude Modulation," *IEEE Transactions on Broadcasting*, vol. 62, no. 4, pp. 864–875, December 2016.

[121] S. Tomasin, A. Gorokhov, H. Yang, and J. P. Linnartz, "Iterative interference cancellation and channel estimation for mobile OFDM," *IEEE Transactions on Wireless Communications*, vol. 4, no. 1, pp. 238–245, January 2005.

[122] N. Albeanu and T. J. Lim, "Optimization of linear iterative interference-cancellation receivers for CDMA communications," *IEEE Transactions on Communications*, vol. 52, no. 3, pp. 376–379, March 2004.

[123] B. F. Beidas, H. El Gamal, and S. Kay, "Iterative interference cancellation for high spectral efficiency satellite communications," *IEEE Transactions on Communications*, vol. 50, no. 1, pp. 31–36, January 2002.

[124] A. F. Molisch, M. Toeltsch, and S. Vermani, "Iterative Methods for Cancellation of Intercarrier Interference in OFDM Systems," *IEEE Transactions on Vehicular Technology*, vol. 56, no. 4, pp. 2158–2167, July 2007.

[125] M. Mostafa, "Stability Proof of Iterative Interference Cancellation for OFDM Signals With Blanking Nonlinearity in Impulsive Noise Channels," *IEEE Signal Processing Letters*, vol. 24, no. 2, pp. 201–205, February 2017.

[126] C. H. Yih, "Iterative Interference Cancellation for OFDM Signals With Blanking Nonlinearity in Impulsive Noise Channels," *IEEE Signal Processing Letters*, vol. 19, no. 3, pp. 147–150, March 2012.

[127] M. Chen and A. G. Burr, "Low-Complexity Iterative Interference Cancellation Multiuser Detection for Overloaded MIMO OFDM IDMA System," *WSA 2013; 17th International ITG Workshop on Smart Antennas, Stuttgard, Germany*, pp. 1–5, March 2013.

[128] K. W. Cheong and J. M. Cioffi, "Precoder for DMT with insufficient cyclic prefix," in *IEEE International Conference on Communications, 1998. ICC 98. Conference Record, ATLANTA, GEORGIA, IJSA*. IEEE, June 1998, vol. 1, pp. 339–343.

[129] C. J. Park and G. H. Im, "Efficient DMT/OFDM transmission with insufficient cyclic prefix," *IEEE Communications Letters*, vol. 8, no. 9, pp. 576–578, September 2004.

[130] X. Sun, L. J. Cimini, L. J. Greenstein, and D. S. Chan, "ICI/ISI aware beamforming for MIMO-OFDM wireless system," in *43rd Annual Conference on Information Sciences and Systems, Baltimore Maryland, USA*. IEEE, March 2009, pp. 103–107.

[131] Y. Jin and X. G. Xia, "An Interference Nulling Based Channel Independent Precoding for MIMO-OFDM Systems with Insufficient Cyclic Prefix," *IEEE Transactions on Communications*, vol. 61, no. 1, pp. 131–143, January 2013.

[132] S. Stefania, T. Issam, and B. Matthew, *LTE-the UMTS long term evolution : from theory to practice*, John Wiley, 2nd edition, 2011.

[133] A. Tajer and A. Nosratinia, "Diversity order in ISI channels with single-carrier frequency-domain equalizers," *IEEE Transactions on Wireless Communications*, vol. 9, no. 3, pp. 1022–1032, March 2010.

[134] Y. Liu, Z. Tan, H. Hu, L. J. Cimini, and G. Y. Li, "Channel Estimation for OFDM," *IEEE Communications Surveys Tutorials*, vol. 16, no. 4, pp. 1891–1908, Fourthquarter 2014.

[135] I. Budiarjo, H. Nikookar, and L. P. Ligthart, "Performance Evaluation of OFDM Based Cognitive Radio System with Wiener Filter Channel Estimation Using Frequency Hopping GSM Channel Model at 900 MHz," in *European Conference on Wireless Technologies, Linz, Austria.* IEEE, October 2007, pp. 74–77.

[136] M. Parchami, W. P. Zhu, B. Champagne, and E. Plourde, "Recent Developments in Speech Enhancement in the Short-Time Fourier Transform Domain," *IEEE Circuits and Systems Magazine*, vol. 16, no. 3, pp. 45–77, Thirdquarter 2016.

[137] O. Edfors, M. Sandell, J. Beek, S. K. Wilson, and P. O. Borjesson, "OFDM channel estimation by singular value decomposition," *IEEE Transactions on Communications*, vol. 46, no. 7, pp. 931–939, July 1998.

[138] J. Kyoung Moon and S. In Choi, "Performance of channel estimation methods for OFDM systems in a multipath fading channels," *IEEE Transactions on Consumer Electronics*, vol. 46, no. 1, pp. 161–170, February 2000.

[139] M. Morelli and U. Mengali, "A comparison of pilot-aided channel estimation methods for OFDM systems," *IEEE Transactions on Signal Processing*, vol. 49, no. 12, pp. 3065–3073, December 2001.

[140] F. Shu, J. Lee, L. N. Wu, and G. L. Zhao, "Time-frequency channel estimation for digital amplitude modulation broadcasting systems based on OFDM," *IEE Proceedings on Communications*, vol. 150, no. 4, pp. 259–264, August 2003.

[141] S. Coleri, M. Ergen, A. Puri, and A. Bahai, "Channel estimation techniques based on pilot arrangement in OFDM systems," *IEEE Transactions on Broadcasting*, vol. 48, no. 3, pp. 223–229, September 2002.

[142] J. H. Manton, "Optimal training sequences and pilot tones for OFDM systems," *IEEE Communications Letters*, vol. 5, no. 4, pp. 151–153, April 2001.

[143] M. K. Ozdemir and H. Arslan, "Channel estimation for wireless OFDM systems," *IEEE Communications Surveys Tutorials*, vol. 9, no. 2, pp. 18–48, 2007.

[144] C. Lele, J. P. Javaudin, R. Legouable, A. Skrzypczak, and P. Siohan, "Channel estimation methods for preamble-based OFDM/OQAM modulations," *European Transactions on Telecommunications*, vol. 19, no. 7, pp. 741–750, September 2008.

[145] E. Kofidis and D. Katselis, "Improved interference approximation method for preamble-based channel estimation in FBMC/OQAM," in *19th European Signal Processing Conference, Barcelona, Spain*. IEEE, August 2011, pp. 1603–1607.

[146] C. Lélé, R. Legouable, and P. Siohan, "Iterative scattered pilot channel estimation in OFDM/OQAM," in *10th Workshop on Signal Processing Advances in Wireless Communications (SPAWC), Perugia, Italy*. IEEE, June 2009, pp. 176–180.

[147] C. Lélé, "Iterative scattered-based channel estimation method for OFDM/OQAM," *EURASIP Journal on Advances in Signal Processing*, , no. 1, pp. 14, 2012.

[148] P. Hoeher, S. Kaiser, and P. Robertson, "Two-dimensional pilot-symbol-aided channel estimation by Wiener filtering," *IEEE International Conference on Acoustics, Speech, and Signal Processing (ICASSP-97), Munich, Germany*, vol. 3, pp. 1845–1848, April 1997.

[149] P. Hoeher, S. Kaiser, and P. Robertson, "Pilot-symbol-aided channel estimation in time and frequency," in *Multi-carrier spread-spectrum*, pp. 169–178. Springer, 1997.

[150] Y. Li, L. Cimini, and N. Sollenberger, "Robust channel estimation for OFDM systems with rapid dispersive fading channels," *IEEE Transactions on Communications*, vol. 46, no. 7, pp. 902–915, July 1998.

[151] M Failli, *Digital Land Mobile Radio Communications. COST 207*, Luxembourg: EC, 1989.

[152] D. Gesbert, M. Shafi, D.S. Shiu, P.J. Smith, and A. Naguib, "From theory to practice: An overview of MIMO space-time coded wireless systems," *IEEE Journal on Selected Areas in Communications*, vol. 21, no. 3, pp. 281–302, April 2003.

[153] T. Tang and R. W. Heath, "Space-time interference cancellation in MIMO-OFDM systems," *EEE Transactions on Vehicular Technology*, vol. 54, no. 5, pp. 1802–1816, September 2005.

[154] L. Giangaspero, L. Agarossi, G. Paltenghi, S. Okamura, M. Okada, and S. Komaki, "Co-channel interference cancellation based on MIMO OFDM systems," *IEEE Wireless Communications*, vol. 9, no. 6, pp. 8–17, December 2002.

[155] L. Li, R. C. de Lamare, and A. G. Burr, "Dynamic pilot allocation with channel estimation in closed-loop multi-input-multi-output orthogonal frequency division multiplexing systems," *IET Communications*, vol. 8, no. 11, pp. 2017–2025, July 2014.

[156] S. Park, B. Shim, and J. W. Choi, "Iterative Channel Estimation Using Virtual Pilot Signals for MIMO-OFDM Systems," *IEEE Transactions on Signal Processing*, vol. 63, no. 12, pp. 3032–3045, June 2015.

[157] K. Y. Fan and P. Y. Tsai, "An RLS Tracking and Iterative Detection Engine for Mobile MIMO-OFDM Systems," *IEEE Transactions on Circuits and Systems I: Regular Papers*, vol. 62, no. 1, pp. 185–194, January 2015.

[158] S. Wu, L. Kuang, Z. Ni, J. Lu, D. Huang, and Q. Guo, "Low-Complexity Iterative Detection for Large-Scale Multiuser MIMO-OFDM Systems Using Approximate Message Passing," *IEEE Journal of Selected Topics in Signal Processing*, vol. 8, no. 5, pp. 902–915, October 2014.

[159] Y. Qiao, S. Yu, P. Su, and L. Zhang, "Research on an iterative algorithm of LS channel estimation in MIMO OFDM systems," *IEEE Transactions on Broadcasting*, vol. 51, no. 1, pp. 149–153, March 2005.

[160] Y. Sun, Z. Xiong, and X. Wang, "EM-based iterative receiver design with carrier-frequency offset estimation for MIMO OFDM systems," *IEEE Transactions on Communications*, vol. 53, no. 4, pp. 581–586, April 2005.

[161] H. Lee, B. Lee, and I. Lee, "Iterative detection and decoding with an improved V-BLAST for MIMO-OFDM systems," *IEEE Journal on Selected Areas in Communications*, vol. 24, no. 3, pp. 504–513, March 2006.

[162] D. N. Liu and M. P. Fitz, "Low complexity affine MMSE detector for iterative detection-decoding MIMO OFDM systems," *IEEE Transactions on Communications*, vol. 56, no. 1, pp. 150–158, January 2008.

[163] M. Caus and A. I. Prez-Neira, "Multi-Stream Transmission for Highly Frequency Selective Channels in MIMO-FBMC/OQAM Systems," *IEEE Transactions on Signal Processing*, vol. 62, no. 4, pp. 786–796, February 2014.

[164] Y. Cheng, P. Li, and M. Haardt, "Coordinated beamforming in MIMO FBMC/OQAM systems," in *2014 IEEE International Conference on Acoustics, Speech and Signal Processing (ICASSP), Florence, Italy*. IEEE, May 2014, pp. 484–488.

[165] A. Ikhlef and J. Louveaux, "Per subchannel equalization for MIMO FBMC/OQAM systems," in *2009 IEEE Pacific Rim Conference on Communications, Computers and Signal Processing, Victoria, BC, Canada*. IEEE, August 2009, pp. 559–564.

[166] T. Ihalainen, T. Hidalgo Stitz, and M. Renfors, "Efficient per-carrier channel equalizer for filter bank based multicarrier systems," in *2005 IEEE International Symposium on Circuits and Systems, Kobe, Japan*. IEEE, May 2005, pp. 3175–3178.

[167] T. Ihalainen, A. Ikhlef, J. Louveaux, and M. Renfors, "Channel equalization for multi-antenna FBMC/OQAM receivers," *IEEE Transactions on Vehicular Technology*, vol. 60, no. 5, pp. 2070–2085, June 2011.

[168] Y. Cheng and M. Haardt, "Widely linear processing in MIMO FBMC/OQAM systems," in *Proceedings of the Tenth International Symposium on Wireless Communication Systems (ISWCS 2013), Ilmenau, Germany*. VDE, August 2013, pp. 1–5.

[169] A. Lozano and N. Jindal, "Transmit diversity vs. spatial multiplexing in modern MIMO systems," *IEEE Transactions on Wireless Communications*, vol. 9, no. 1, pp. 186–197, January 2010.

[170] G. J. Foschini, "Layered space-time architecture for wireless communication in a fading environment when using multi-element antennas," *Bell Labs Technical Journal*, vol. 1, no. 2, pp. 41–59, Autumn 1996.

[171] L. Bai, J. Choi, and Q. Yu, *Low complexity MIMO receivers*, Springer Science & Business Media, 2014.

[172] J. F. Gerard, "Layered space-time architecture for wireless communication in a fading environment when using multi-element antennas," *Bell labs technical journal*, vol. 1, no. 2, pp. 41–59, 1996.

[173] P. W. Wolniansky, G. J. Foschini, G. D. Golden, and R. A. Valenzuela, "V-BLAST: an architecture for realizing very high data rates over the rich-scattering wireless channel," in *International Symposium on Signals, Systems, and Electronics (ISSSE 98) , Pisa, Italy*. IEEE, October 1998, pp. 295–300.

[174] W. H. Press, S. A. Teukolsky, W. T. Vetterling, and B. P. Flannery, *Numerical recipes in C: The Art of Scientific Computing*, Cambridge, Cambridge University Press, second edition, 1992.

[175] B. Hassibi, "An efficient square-root algorithm for BLAST," in *IEEE International Conference on Acoustics, Speech, and Signal Processing. Proceedings. ICASSP-2000 , Istanbul, Turkey*. IEEE, June 2000, vol. 2, pp. 11737–11740.

[176] H. Zhu, Z. Lei, and F. P. S. Chin, "An improved square-root algorithm for BLAST," *IEEE Signal Processing Letters*, vol. 11, no. 9, pp. 772–775, September 2004.

[177] H. Zhu, W. Chen, B. Li, and F. Gao, "An Improved Square-Root Algorithm for V-BLAST Based on Efficient Inverse Cholesky Factorization," *IEEE Transactions on Wireless Communications*, vol. 10, no. 1, pp. 43–48, January 2011.

[178] S. Ten Brink, "Convergence behavior of iteratively decoded parallel concatenated codes," *IEEE Transactions on Communications*, vol. 49, no. 10, pp. 1727–1737, October 2001.

[179] E. Zehavi, "8-PSK trellis codes for a Rayleigh channel," *IEEE Transactions on Communications*, vol. 40, no. 5, pp. 873–884, May 1992.

[180] G. Caire, G. Taricco, and E. Biglieri, "Bit-interleaved coded modulation," *IEEE Transactions on Information Theory*, vol. 44, no. 3, pp. 927–946, May 1998.

[181] X. Li and J. A. Ritcey, "Bit-interleaved coded modulation with iterative decoding," *IEEE Communications Letters*, vol. 1, no. 6, pp. 169–171, November 1997.

[182] S. Ten Brink and Ran-Hong Speidel, J.and Yan, "Iterative demapping and decoding for multilevel modulation," in *Global Telecommunications Conference GLOBE-*

COM 1998. The Bridge to Global Integration, Sydney, Australia. IEEE, November 1998, vol. 6, pp. 579–584.

[183] S. Ten Brink, "Designing iterative decoding schemes with the extrinsic information transfer chart," *AEÜ International Journal of Electronics and Communications*, vol. 54, no. 6, pp. 389–398, 2000.

[184] E. Akay and E. Ayanoglu, "Achieving full frequency and space diversity in wireless systems via BICM, OFDM, STBC, and Viterbi decoding," *IEEE Transactions on Communications*, vol. 54, no. 12, pp. 2164–2172, December 2006.

[185] M. Mohammadnia-Avval, C. Snow, and L. Lampe, "Error-rate analysis for bit-loaded coded MIMO-OFDM," *IEEE Transactions on Vehicular Technology*, vol. 59, no. 5, pp. 2340–2351, June 2010.

[186] H. Lin, N. Lahbabi, P. Siohan, and X. Jiang, "An efficient FTN implementation of the OFDM/OQAM system," in *IEEE International Conference on Communications (ICC 2015), London, UK*. IEEE, June 2015, pp. 4787–4792.

[187] S. Ten Brink, G. Kramer, and A. Ashikhmin, "Design of low-density parity-check codes for modulation and detection," *IEEE Transactions on Communications*, vol. 52, no. 4, pp. 670–678, April 2004.

[188] E. Sharon, A. Ashikhmin, and S. Litsyn, "Analysis of low-density parity-check codes based on EXIT functions," *IEEE Transactions on Communications*, vol. 54, no. 8, pp. 1407–1414, August 2006.

[189] M. Oh, M. Hyuck Kwon, D. Park, and Y. Hoon Lee, "Iterative channel estimation and LDPC decoding with encoded pilots," *IEEE Transactions on Vehicular Technology*, vol. 57, no. 1, pp. 273–285, January 2008.

[190] J. Hagenauer, "The EXIT chart-introduction to extrinsic information transfer in iterative processing," in *12th European Signal Processing Conference (EUSIPCO), Lake Buena Vista, Fla, USA*. Citeseer, September 2004, pp. 1541–1548.

[191] F. Brannstrom, K. Lars Rasmussen, and J. Alex Grant, "Convergence analysis and optimal scheduling for multiple concatenated codes," *IEEE Transactions on Information Theory*, vol. 51, no. 9, pp. 3354–3364, September 2005.

[192] F. Schreckenbach, N. Gortz, J. Hagenauer, and G. Bauch, "Optimization of symbol mappings for bit-interleaved coded Modulation with iterative decoding," *IEEE Communications Letters*, vol. 7, no. 12, pp. 593–595, December 2003.

[193] J. Tan and G. L. Stuber, "Analysis and design of interleaver mappings for iteratively decoded BICM," in *IEEE International Conference on Communications. Conference Proceedings. ICC 2002 , New York, NY, USA*. IEEE, April 2002, vol. 3, pp. 1403–1407.

Appendix A

A.1 Uncoded systems:

In the appendix, Frame Error Rate (FER) performance of the uncoded and coded OFDM, DWT/MCM, and FBMC/OQAM systems are provided.

In case of uncoded OFDM systems, Figures A.1 and A.2 illustrate the performance analysis of the all systems using MMSE equalizer with 4-QAM and 16-QAM respectively and over EVA-LTE channel. By contrast, these figures show that the FER performance of the DWT based MCM is significantly improved compared with OFDM and FBMC/OQAM systems. That means, the probability of successful frame error rate (FER) of the DWT-MCM can be significantly detected compared with other systems.

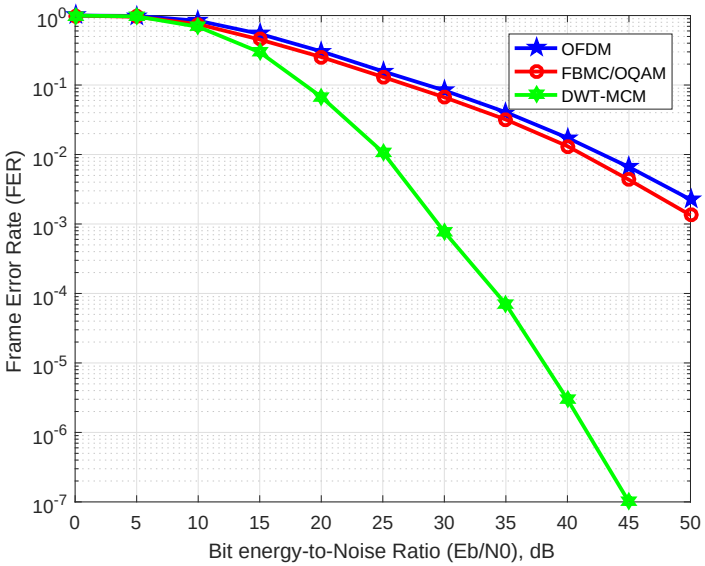

Figure A.1: Frame error probability curves for SISO-OFDM, SISO-FBMC/OQAM, and SISO-DWT-MCM systems using MMSE equalizer with 4-QAM modulation over (EVA) LTE channel.

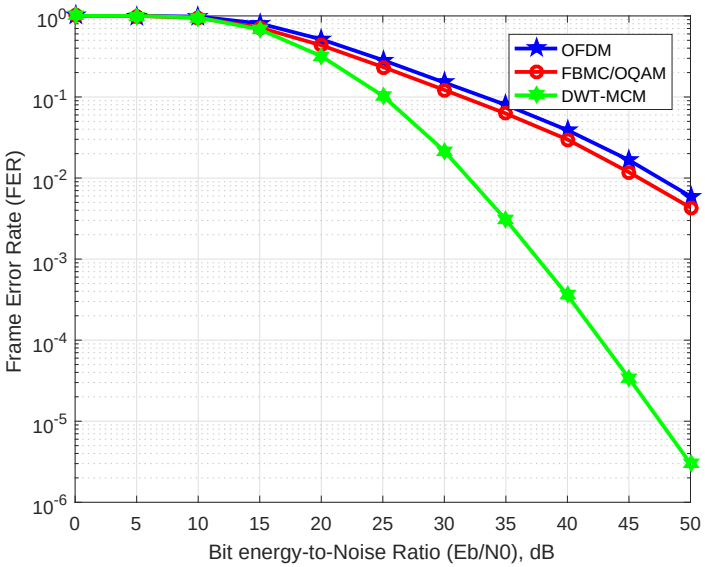

Figure A.2: Frame error probability curves for SISO-OFDM, SISO-FBMC/OQAM, and SISO-DWT-MCM systems using MMSE equalizer with 16-QAM modulation over (EVA) LTE channel.

Figure A.3 shows the simulation results of the bit error probability and frame error rate respectively using 16-QAM and 4-QAM modulation over EVA channel with wavelet

domain equalizer.

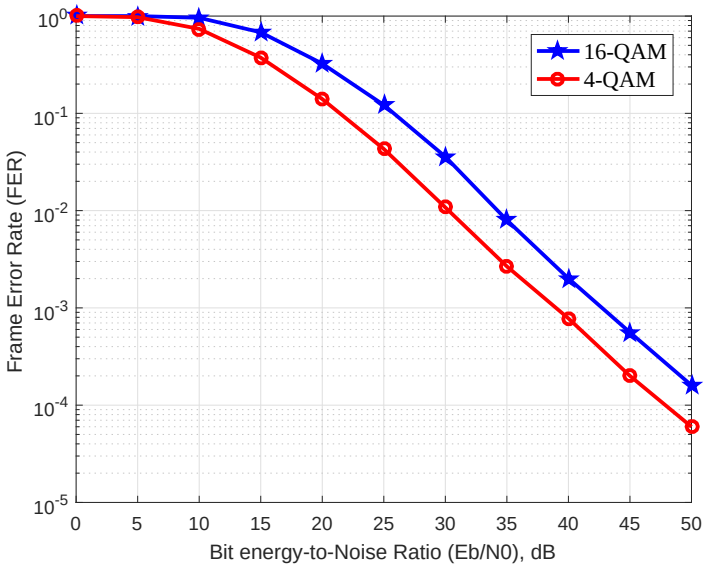

Figure A.3: Frame error probability curves for SISO-DWT-MCM system using wavelet domain equalizer with 16-QAM and 4-QAM modulation over (EVA) LTE channel.

Figure A.4 shows the FER simulation results for the SISO-OFDM system using QPSK modulation and 5 Hz Doppler frequency over the EVA-LTE channel with ZF and MMSE equalizers. Figure A.5 shows the FER performance for the SISO-OFDM system using 16-QAM modulation and 70 Hz Doppler frequency over the medium spread EVA-LTE channel with ZF and MMSE equalizers. Figure A.6 shows the FER performance analysis of the SISO-OFDM system using 16-QAM modulation and 70 Hz Doppler frequency over the ETU-LTE channel with ZF and MMSE equalizers. The FER simulation results are compared with the result of the perfect channel state information (PCSI). However, due to the Doppler shift, the resulting time-variant channel is not perfectly known at the receiver. That means an error floor will appears at high $Eb/N0$ when Doppler frequency is 70 Hz.

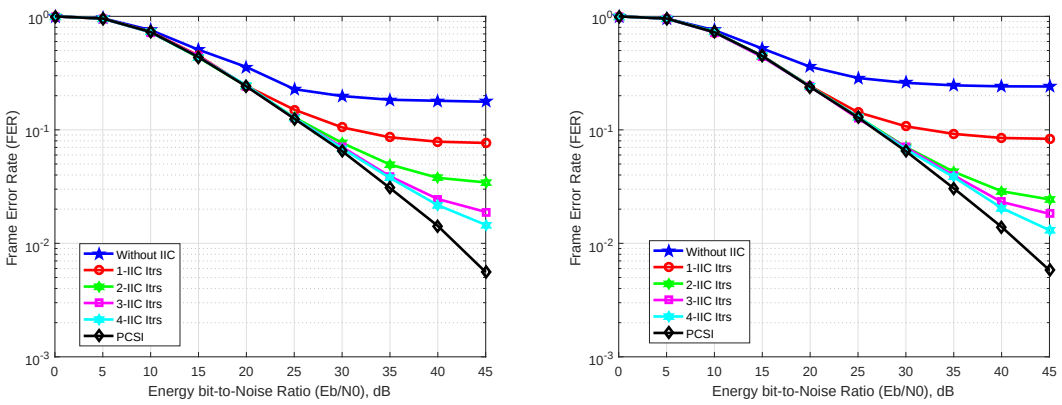

(a) ZF-Equalizer

(b) MMSE-Equalizer

Figure A.4: Frame error probability curves for SISO-OFDM system using QPSK modulation and 5Hz Doppler shift over (EVA) LTE channel (a) ZF-Equalizer (b) MMSE-Equalizer.

Its clear from these figures that the FER performance have improved after some IIC iterations. The error floor is reduced but not completely removed. The improvements of the FER simulation results of the OFDM system are reduced with the increasing of the modulation order, Doppler shift, and the spread of the channel. In the case of EVA channel with 5Hz Doppler and QPSK modulation, the error floor of the FER simulation is reduced by a factor R_k of approximately 2, 5, 7 and 8 and by a factor 3, 8, 10, and 12 after one, two, three, and four IIC iterations with ZF and MMSE equalisation respectively, measured at 40 dB $Eb/N0$ as shown in Figure A.4.

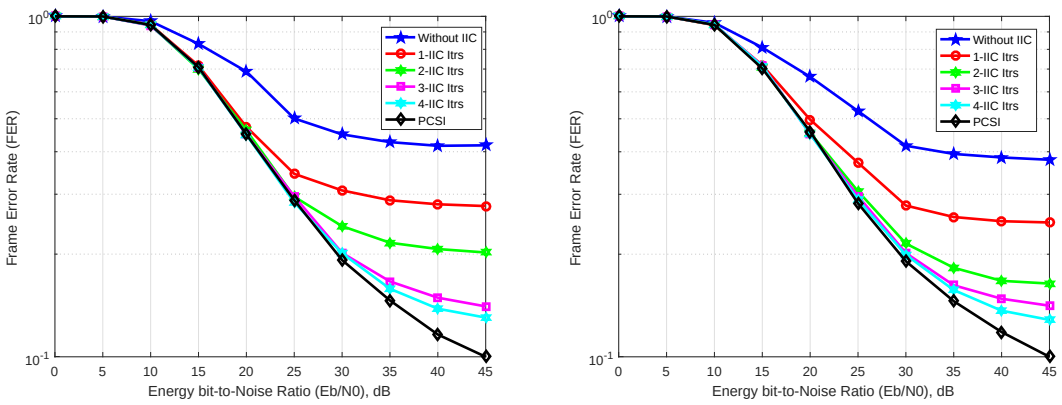

(a) ZF-Equalizer (b) MMSE-Equalizer

Figure A.5: Frame error probability curves for SISO-OFDM system using 16-QAM modulation and 70Hz Doppler shift over (EVA) LTE channel (a) ZF-Equalizer (b) MMSE-Equalizer.

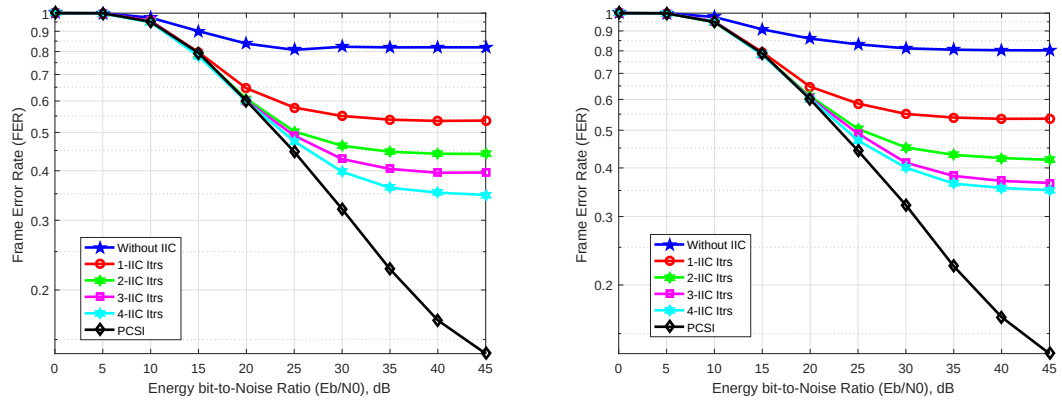

(a) ZF-Equalizer (b) MMSE-Equalizer

Figure A.6: Frame error probability curves for SISO-OFDM system using 16-QAM modulation and 70Hz Doppler shift over (ETU) LTE channel (a) ZF-Equalizer (b) MMSE-Equalizer.

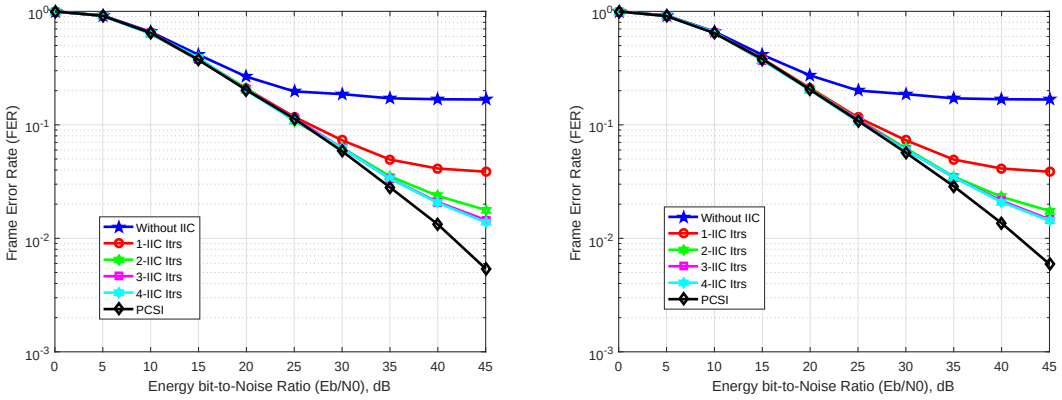

(a) ZF-Equalizer (b) MMSE-Equalizer

Figure A.7: Frame error probability curves for SISO-FBMC/OQAM system using QPSK modulation and 5Hz Doppler shift over (EVA) LTE channel (a) ZF-Equalizer (b) MMSE-Equalizer.

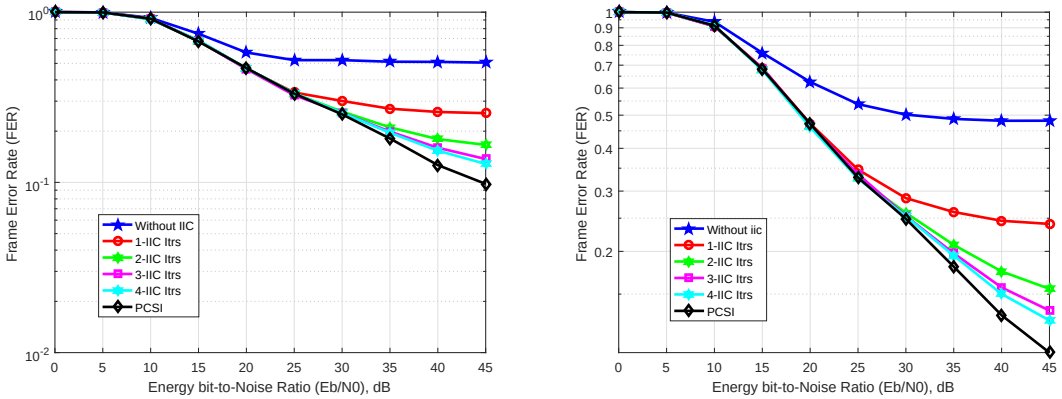

(a) ZF-Equalizer (b) MMSE-Equalizer

Figure A.8: Frame error probability curves for SISO-FBMC/OQAM system using 16-QAM modulation and 70Hz Doppler shift over (EVA) LTE channel (a) ZF-Equalizer (b) MMSE-Equalizer.

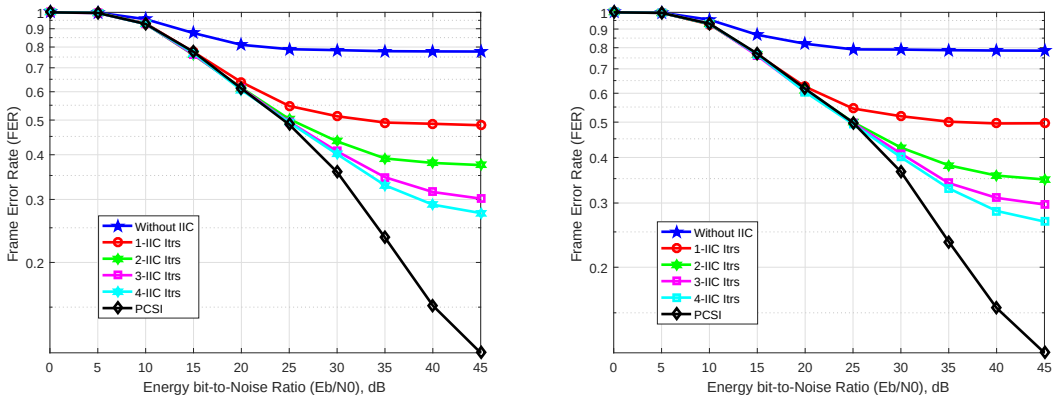

(a) ZF-Equalizer (b) MMSE-Equalizer

Figure A.9: Frame error probability curves for SISO-FBMC/OQAM system using 16-QAM modulation and 70Hz Doppler shift over (ETU) LTE channel (a) ZF-Equalizer (b) MMSE-Equalizer.

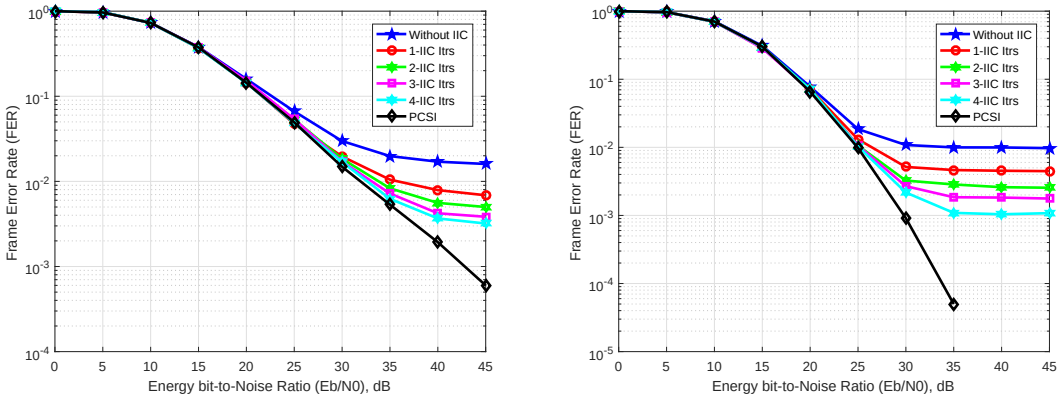

(a) ZF-Equalizer (b) MMSE-Equalizer

Figure A.10: Frame error probability curves for SISO-DWT-MCM system using Daubechies (db4) wavelet with L=1, QPSK modulation and 5Hz Doppler shift over (EVA) LTE channel (a) ZF-Equalizer (b) MMSE-Equalizer.

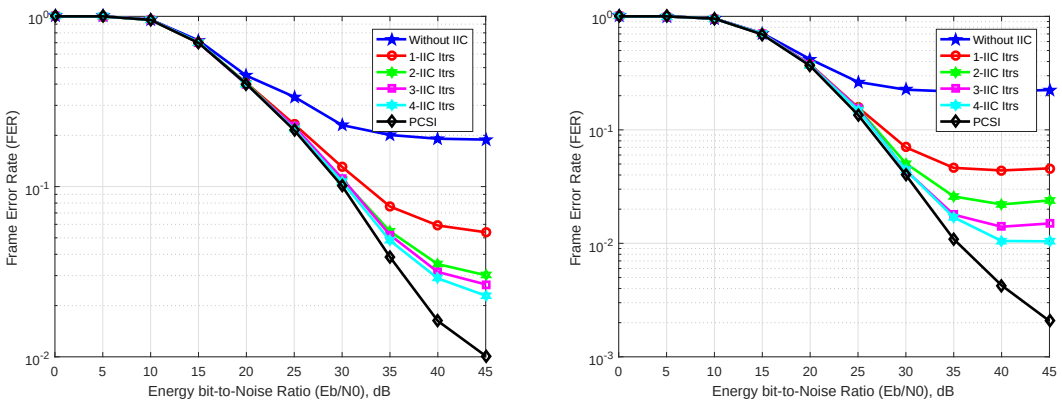

(a) ZF-Equalizer (b) MMSE-Equalizer

Figure A.11: Frame error probability curves for SISO-DWT-MCM system using Daubechies (db4) wavelet with L=1, 16-QAM modulation and 70Hz Doppler shift over (EVA) LTE channel (a) ZF-Equalizer (b) MMSE-Equalizer.

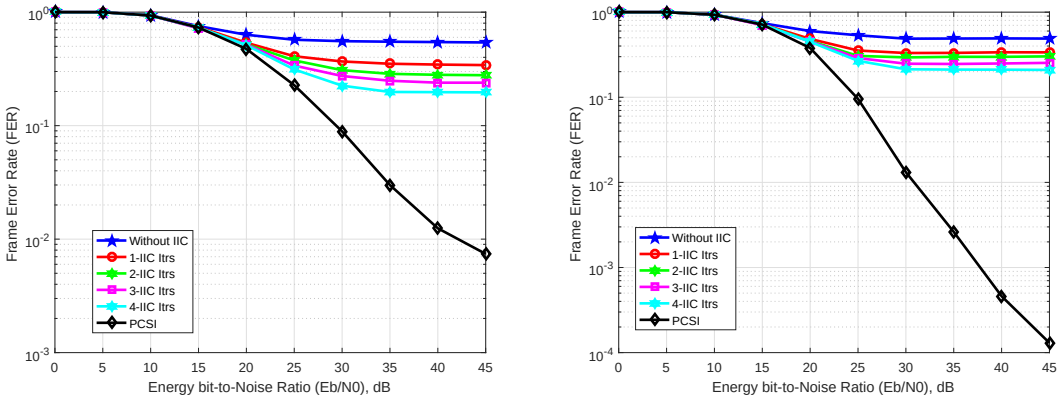

(a) ZF-Equalizer (b) MMSE-Equalizer

Figure A.12: Frame error probability curves for SISO-DWT-MCM system using Daubechies (db4) wavelet with L=1, 16-QAM modulation and 70Hz Doppler shift over (ETU) LTE channel (a) ZF-Equalizer (b) MMSE-Equalizer.

The simulation results of the FER for different cases is summarized in Table A.1.

Table A.1: FER simulation results for MCM systems

System	N_{Fig}	Eq.	IIC-Itrs	R_k	$Eb/N0$ dB	Channel	Doppler Hz	M-QAM
OFDM	A.5	ZF	4	3	45	EVA	70	16-QAM
		MMSE	4	3	45	EVA	70	16-QAM
OFDM	A.6	ZF	4	2.3	45	ETU	70	16-QAM
		MMSE	4	2.3	45	ETU	70	16-QAM
FBMC/	A.7	ZF	4	8	45	EVA	5	4-QAM
OQAM		MMSE	4	8	45	EVA	5	4-QAM
FBMC/	A.8	ZF	4	3.3	45	EVA	70	16-QAM
OQAM		MMSE	4	3.3	45	EVA	70	16-QAM
FBMC/	A.9	ZF	4	2.7	45	ETU	70	16-QAM
OQAM		MMSE	4	2.7	45	ETU	70	16-QAM
DWT/	A.10	ZF	4	4.6	45	EVA	5	4-QAM
MCM		MMSE	4	9.6	45	EVA	5	4-QAM
DWT/	A.11	ZF	4	6.6	45	EVA	70	16-QAM
MCM		MMSE	4	2.1	45	EVA	70	16-QAM
DWT/	A.12	ZF	4	2.8	45	ETU	70	16-QAM
MCM		MMSE	4	2.3	45	ETU	70	16-QAM